



---

# Critical Design Review

## New Short-Range Airliner Family

### AERO 5 - ENG3162

#### Version 1.0

17/03/2019



---

#### GROUP MEMBERS

Youssef Abouelmagd  
Barney Green  
Salman Habib  
Megan Keeping  
Tak Li  
Luca Moscattini

Aanantha Murugavel  
Kusha Oza  
Preeti Singh  
Andre Sunaryo  
Tomas Webster

We confirm that the submitted work is our own work. No element has been previously submitted for assessment, or where it has, it has been correctly referenced. We have also clearly identified and fully acknowledged all material that is entitled to be attributed to others (whether published or unpublished) using the referencing system set out in the programme handbook. We agree that the University may submit our work to means of checking this, such as the plagiarism detection service Turnitin® UK. We confirm that we understand that assessed work that has been shown to have been plagiarised will be penalised.

## **Document History**

| <b>Document Version</b> | <b>Document Editor</b> | <b>Date</b> |
|-------------------------|------------------------|-------------|
| DRAFT 1.0               | BG                     | 15/03/2019  |
| DRAFT 1.1               | BG                     | 16/03/2019  |
| DRAFT 1.2               | BG                     | 17/03/2019  |
| Version 1.0             | BG, SH, PS, KO         | 17/03/2019  |

## **Executive Summary – KO**

An aircraft is designed to prioritise safety and meet top level aircraft requirements. However, there are a number of potential designs that agree with those specifications, so along with these, it was the goal of Aero 5 to maximise the amount of profit, as well as incorporate new levels of possible innovation wherever advantageous. This Critical Design Review document builds on the initial concept presented by the team in the Preliminary Design Review. In this report, the team continue to justify their design choices with credible sources, engineering knowledge and extensive calculations.

The first section of the document updates the position of the aircraft in the higher end the short-range airline market and the market forecast for the next 10 years. It presents the calculations carried out (using the method set forward by the Association of European Airlines) to show an 18.8% Direct Operating Cost reduction in comparison to 2015-state-of-the-art technology. The aircraft is set to enter into service in 2027 with a selling price of \$108 million, which sits between the higher and lower price points that market.

All top-level requirements that the aircraft design is affected by were analysed and verified, based on a verification matrix, in Section 3 of this document. Their functional and design relationships have been explained and referenced to industry requirements, allowing the aircraft in later stages to become certified.

The engine, after extensive consideration in the Preliminary Design Review, was confirmed as the LEAP-1C, which was initially a placeholder engine while the team awaited relevant data needed to carry out calculations on an engine still in its final design and manufacturing stages. Due to this, the team has laid out a suitable future plan for further development in the aircraft life cycle.

The structure of the aircraft was considered methodically, with sections focusing on the fuselage, the wings and the tail plane. With essential requirements highlighted throughout the sections, they focus on calculating the bending moment and shear force diagrams. The process to obtaining these results, including analysis of various load cases, is explained thoroughly, and the results from these diagrams were used to determine the sizing of factors such as the spar dimensions. The sizing of the empennage was considered, based on calculations for the tail scrape angle and control surface sizing, with room for development at further stages of design, and CAD of the fuselage and wing structure is presented, with accurately scaled individual components for each part.

When evaluating the internal structural components, boom idealisation studies and buckling analysis was carried out, providing the dimensions for the stringers and frames in different sections of the fuselage, based on the loads each section was supporting. At each stage, development options were highlighted, and manufacture and maintenance processes were considered. A similar process was carried out for the wings, with an acceptable level of accuracy. Shear force and bending moment diagrams were presented as a result of static loading and gust loading cases and a rib boom idealisation analysis was carried out, from which stringer and spar shapes were determined.

High lift devices and wing control surface sizing, as well as tail plane sizing were determined from researching historical precedents and evaluated to ensure that stability criteria was satisfied. From this hinge moments and actuator loads were analysed to validate that the control surfaces are suitably sized for all operable cases.

The interfaces between different components of the aircraft were detailed, with the mounting of the engine and the wing root joints being physically and technically analysed. This resulted in wing and fuselage being attached using a traditional lugs technique and the engine being mounted using pylons. Assembly CAD models of the final completed Aero 5 aircraft can be found in this report, with a representation of the cabin layout in a 3D configuration.

This document presents in detail the aircraft systems used in this project, with justification, where multiple failure modes were analysed and development considerations. Avionics systems, flight data recorders, environmental control systems, ice and fire protection systems and fuel and hydraulics systems were all evaluated, with a suitable solution to be implemented. New technology such as carbon

nanotubes for anti-icing have been implemented, and a fault tree analysis was carried out for the electrical systems, with a physical representation of its architecture.

Project management tasks were carried out to ensure efficient resource allocation. The work breakdown structure allowed for Aero 5 team members to maximise their contribution to the design and meet internal and external deadlines. The risk management section allowed for project risks to be mitigated and the interface list detailed the assembly of the aircraft to meet current design specifications, as well as any future considerations. Configuration management allowed for the project changes and procedures to be tracked. The array of steps taken ensure an efficient and accurate report and design, minimising the impact any potential project risks.

Overall in this document, Aero 5 strived to produce a design suitable for a Critical Design Review, with sufficient development options and room for realistic growth, whilst remaining within an appropriate price range and aiming for low Direct Operating Costs.

## Acronyms

Throughout this document the Aero 5 team members have been referred to using the following acronyms:

|    |                    |
|----|--------------------|
| AM | Aanantha Murugavel |
| AS | Andre Sunaryo      |
| BG | Barney Green       |
| KO | Kusha Oza          |
| LM | Luca Moscattini    |
| MK | Megan Keeping      |
| PS | Preeti Singh       |
| SH | Salman Habib       |
| TL | Tak Li             |
| TW | Tomas Webster      |
| YA | Youssef Abouelmagd |

The following list details all the acronyms that appear throughout this document:

|       |  |
|-------|--|
| ABO   | Aviators Grade Breathing Oxygen                |
| AC    | Aerodynamic Centre                             |
| AC    | Alternating Current                            |
| AEA   | Association of European Airlines               |
| AFCS  | Automatic Flight Control System                |
| AMC   | Acceptable Means of Compliance                 |
| APU   | Auxiliary Power Unit                           |
| AR    | Aspect Ratio                                   |
| BMD   | Bending Moment Diagram                         |
| BPR   | Bypass Ratio                                   |
| CAD   | Computer Aided Design                          |
| CDB   | Customer Design Brief                          |
| CDR   | Critical Design Review                         |
| CFRP  | Carbon Fibre Reinforced Polymer                |
| CG    | Centre of Gravity                              |
| COC   | Cash Operating Cost                            |
| CR    | Change Request                                 |
| CVR   | Cockpit Voice Recorder                         |
| DC    | Direct Current                                 |
| DOC   | Direct Operating Cost                          |
| EASA  | European Union Aviation Safety Agency          |
| ECS   | Environmental Control System                   |
| EFIS  | Electronic Flight Instrument System            |
| EGPWS | Enhanced Ground Proximity Warning System       |
| EHA   | Electro-Hydraulic Actuators                    |
| FAA   | Federal Aviation Authority                     |
| FDR   | Flight Data Recorder                           |
| FMC   | Flight Management Computer                     |
| FMECA | Failure Mode, Effects and Criticality Analysis |
| FOD   | Foreign Object Damage                          |

|        |   |
|--------|---|
| GMC    | General Means of Compliance                   |
| GPS    | Global Positioning System                     |
| ICAO   | International Civil Aviation Organisation     |
| IOC    | Indirect Operating Cost                       |
| IRS    | Inertial Reference System                     |
| ISA    | International Standard Atmosphere             |
| MAC    | Mean Aerodynamic Chord                        |
| MSP    | Manufacturer's Study Price                    |
| MTBF   | Mean Time Between Failure                     |
| MTOW   | Maximum Take-Off Weight                       |
| N/A    | Not Applicable                                |
| NASA   | National Aeronautics and Space Administration |
| NDT    | Non-Destructive Techniques                    |
| OEI    | One Engine Inoperable                         |
| PDR    | Preliminary Design Review                     |
| PDS    | Product Design Specification                  |
| PFD    | Primary Flight Display                        |
| PL     | Point Load                                    |
| QFD    | Quality Function Deployment                   |
| RRF    | Risk Reduction Factor                         |
| SF     | Safety Factor                                 |
| SFC    | Specific Fuel Consumption                     |
| SFD    | Shear Force Diagram                           |
| SIL    | Safety Integrity Level                        |
| TCAS   | Traffic Collision Avoidance System            |
| TOC    | Total Operating Cost                          |
| TRU    | Transformer Rectifier Unit                    |
| TSFC   | Thrust Specific Fuel Consumption              |
| UHMWPE | Ultra-High Molecular Weight Polyethylene      |
| WBS    | Work Breakdown Structure                      |
| WMTOW  | Maximum Take-Off Weight                       |
| WXR    | Airborne Weather Radar                        |

## Contents

|        |  |    |
|--------|--|----|
| 1.     | Introduction – SH.....   | 1  |
| 2.     | Business Case – PS, KO .....   | 1  |
| 2.1    | Updated Market Research – KO .....                                       | 1  |
| 2.2    | Direct Operating Cost Calculations – KO.....                             | 1  |
| 2.3    | DOC Reduction – PS .....   | 3  |
| 2.4    | Profit Margin – PS .....   | 4  |
| 3.     | Requirement Analysis & Verification – SH, LM.....                        | 4  |
| 3.1    | Verification Planning for Risk Assessment Requirements – SH, LM .....    | 5  |
| 4.     | Powerplant Selection – SH .....  | 8  |
| 4.1    | TSFC Targets – SH.....   | 8  |
| 4.2    | Derivative Projected Engine – SH .....                                   | 8  |
| 5.     | Aircraft Structure and Performance – LM, PS, KO, BG, AM, SH, AS, TL..... | 8  |
| 5.1    | Introduction – LM.....   | 8  |
| 5.2    | Fuselage – LM, KO, PS .....  | 9  |
| 5.2.1  | Fuselage Design Considerations – KO .....                                | 9  |
| 5.2.2  | Fuselage Structure – LM, KO, PS.....                                     | 12 |
| 5.2.3  | Fuselage Manufacture and Maintenance – KO .....                          | 22 |
| 5.2.4  | Wing – Fuselage Interface – KO.....                                      | 23 |
| 5.3    | Wings – SH, AS, AM .....   | 24 |
| 5.3.1  | Static Loading Case – SH .....   | 24 |
| 5.3.2  | Gust Loading Case – SH.....  | 27 |
| 5.3.3  | Wing Structure Overview – AS .....                                       | 29 |
| 5.3.4  | Spar Sizing – SH.....  | 30 |
| 5.3.5  | Rib Boom Idealisation Analysis – SH .....                                | 31 |
| 5.3.6  | Stringer Boom Idealisation Analysis – AS .....                           | 33 |
| 5.3.7  | Wing Structure CAD – TL.....   | 36 |
| 5.3.8  | Wing Structure – Further Improvements – SH .....                         | 36 |
| 5.3.9  | Wing Box – AM.....   | 37 |
| 5.3.10 | Wing Fuel Tanks – AM .....   | 38 |
| 5.3.11 | Engine Mounting – AM .....   | 39 |
| 5.3.12 | Wing CAD – TL .....  | 40 |
| 5.4    | Horizontal Tail Plane – BG.....  | 42 |
| 5.4.1  | Horizontal Tail Plane Considerations – BG.....                           | 42 |
| 5.5    | Control Surface Sizing – PS.....   | 43 |
| 5.5.1  | Elevator Sizing – PS .....   | 45 |
| 5.5.2  | Rudder Sizing – PS .....   | 46 |
| 5.5.3  | Wing Control Surface Sizing – PS.....                                    | 48 |
| 5.5.4  | Further Development and Improvements – PS .....                          | 51 |

|       |  |    |
|-------|--|----|
| 5.5.5 | Tail Plane CAD – PS .....                        | 51 |
| 5.6   | Hinge Moments – BG .....                         | 52 |
| 5.6.1 | Process for Calculating Hinge Moments – BG ..... | 53 |
| 5.6.2 | Actuator Loads – BG .....                        | 55 |
| 5.7   | Take-off and Landing Considerations – BG .....   | 56 |
| 5.7.1 | Take-off Considerations – BG .....               | 56 |
| 5.7.2 | Drag at Take-off – BG .....                      | 56 |
| 5.7.3 | Rate of Climb – BG .....                         | 57 |
| 5.7.4 | Landing Considerations – BG.....                 | 59 |
| 5.8   | Aero 5 Aircraft Flight Envelope – SH .....       | 60 |
| 5.9   | Additional CAD Components – TL, AM.....          | 61 |
| 5.9.1 | Nacelle – AM.....                                | 61 |
| 5.9.2 | Passenger Seats – TL .....                       | 61 |
| 5.9.3 | Aircraft Cabin – TL, KO.....                     | 61 |
| 5.9.4 | Pilot Seat and Attendant Seat – TL.....          | 62 |
| 5.10  | Full Aircraft CAD – TL, PS, KO .....             | 62 |
| 5.11  | Aircraft Centre of Gravity – SH.....             | 64 |
| 6.    | Aircraft Systems – YA, MK .....                  | 66 |
| 6.1   | Avionics Systems – YA, MK.....                   | 66 |
| 6.1.1 | Navigation Systems – YA.....                     | 66 |
| 6.1.2 | Flight Management System – YA.....               | 70 |
| 6.1.3 | Communications Systems – MK.....                 | 71 |
| 6.1.4 | Weather and Traffic Systems – MK.....            | 72 |
| 6.2   | Flight Data Recorder – YA .....                  | 72 |
| 6.3   | Environmental Control System – YA .....          | 74 |
| 6.4   | Ice Protection System – YA.....                  | 76 |
| 6.5   | Fuel Systems – MK.....                           | 77 |
| 6.6   | Hydraulics Systems – MK .....                    | 78 |
| 6.7   | Fire Protection System – MK.....                 | 78 |
| 6.8   | Electrical Systems – YA .....                    | 79 |
| 6.8.1 | Electrical Systems Architecture – MK.....        | 82 |
| 7.    | Interface List – TL .....                        | 84 |
| 8.    | Risk Management – YA, AS, AM .....               | 86 |
| 8.1   | Risk identification – YA .....                   | 86 |
| 8.1.1 | Human Safety – AM .....                          | 86 |
| 8.1.2 | Foreign Object Damage (FOD) – AS.....            | 86 |
| 8.1.3 | Accuracy of Installation – AM.....               | 87 |
| 8.1.4 | Structural Failure – AS .....                    | 87 |
| 8.1.5 | Engine Failure – AM.....                         | 88 |

|        |  |     |
|--------|--|-----|
| 8.1.6  | Aircraft Systems Failure – YA.....                           | 88  |
| 8.2    | Qualitative Risk Assessment – YA.....                        | 88  |
| 8.3    | Mitigation and Contingency – YA, AS, AM .....                | 89  |
| 8.3.1  | Human Safety – AM .....                                      | 89  |
| 8.3.2  | FOD – AS .....   | 89  |
| 8.3.3  | Accuracy of Installation – AM.....                           | 89  |
| 8.3.4  | Structural Failure – AS .....                                | 90  |
| 8.3.5  | Engine failure – AM .....                                    | 90  |
| 8.3.6  | Aircraft Systems Failure – YA.....                           | 90  |
| 9.     | Work Breakdown Structure and Schedule – BG, MK .....         | 91  |
| 9.1    | Work Breakdown Structure (WBS) – BG, MK .....                | 91  |
| 9.2    | Schedule – BG, MK.....                                       | 91  |
| 10.    | Configuration Management – BG.....                           | 94  |
| 11.    | Conclusions and Further Improvements – BG.....               | 95  |
| 11.1   | Design Conclusions – BG .....                                | 95  |
| 11.2   | Project Conclusions – BG.....                                | 95  |
| 12.    | References.....  | 97  |
| 13.    | Appendices.....  | 101 |
| 13.1   | Change Requests .....  | 101 |
| 13.1.1 | Change to Horizontal and Vertical Tail Plane Areas – PS..... | 101 |
| 13.1.2 | Moveable Tail Plane – BG.....                                | 102 |
| 13.1.3 | Addition of Spoilers – PS.....                               | 103 |
| 13.1.4 | Updated Engine Mounting Location – AM .....                  | 104 |
| 13.2   | Aero 5 Action Tracker Extract – BG .....                     | 105 |
| 13.3   | DOC – PS, KO.....  | 106 |
| 13.4   | Project Cost – PS, KO.....                                   | 108 |
| 13.5   | Fuselage Structure – LM.....                                 | 109 |
| 13.5.1 | Fuselage Weight Distribution – LM .....                      | 109 |
| 13.5.2 | Bending Moment Diagram (Iteration 1) – LM .....              | 110 |
| 13.5.3 | Shear Force Diagram (Iteration 1) – LM .....                 | 110 |
| 13.5.4 | Initial Boom Area Calculations – LM.....                     | 110 |
| 13.5.5 | Initial Buckling Length Data – LM.....                       | 111 |
| 13.6   | Wing Design Material Data – SH .....                         | 111 |
| 13.7   | MATLAB Code for Fuel Tank Dimension Calculations – AM.....   | 112 |
| 13.8   | CDR Mass Fraction Iterations – SH .....                      | 113 |
| 13.9   | Pitching Moment Coefficient Calculation – PS .....           | 114 |
| 13.10  | Yawing Moment Coefficient Calculation – PS.....              | 114 |
| 13.11  | Rolling Moment Calculation – PS .....                        | 115 |
| 13.12  | Roll Contribution of Spoilers – PS .....                     | 116 |

|       |   |     |
|-------|---|-----|
| 13.13 | Rolling Moment Coefficient Calculation – PS ..... | 116 |
| 13.14 | Updated Risk Matrix – YA .....                    | 117 |
| 13.15 | Team Member Contributions – All .....             | 117 |
| 13.16 | Rendered CAD Images .....                         | 120 |

## List of Figures

|   |    |
|---|----|
| Figure 1 - Estimated Contribution of the Take-Off Weight of a Large Passenger Commercial Airliner (Mouritz, 2012) .....                     | 9  |
| Figure 2 - Dimensions for APU used by Aero 5 (Honeywell, 2008).....   | 9  |
| Figure 3 - Design Considerations for Empennage .....  | 10 |
| Figure 4 - Final Empennage CAD Design .....   | 10 |
| Figure 5 - Nose Cone CAD Design (Left) .....  | 10 |
| Figure 6 - Alternative Empennage CAD Design (Right).....  | 10 |
| Figure 7 - Fuselage Structure Cut-Away 1 .....  | 11 |
| Figure 8 - Fuselage Structure Cut-Away 2 .....  | 11 |
| Figure 9 - External Fuselage CAD.....   | 12 |
| Figure 10 (a and b) - Aircraft Sections used for BMD and SFD, shown on a Fuselage Cut-Away and on Fuselage Plan View Respectively (KO)..... | 13 |
| Figure 11 - Stringer locations along the fuselage cross-section (KO) .....  | 15 |
| Figure 12 - Updated Bending Moment Diagram (Including Structural Masses).....   | 16 |
| Figure 13 - Updated Shear Force Diagram (Including Structural Masses).....  | 16 |
| Figure 14 - Frames Cross-Section Labels .....   | 20 |
| Figure 15 - Wing Lug Design and Comparison (Niu, 1995) .....  | 23 |
| Figure 16 - Static Loading Cantilever Beam Force Balance Diagram.....   | 25 |
| Figure 17 - Shear Force Diagram for Static Loading Case .....   | 26 |
| Figure 18 - Bending Moment Diagram for Static Loading Case .....  | 26 |
| Figure 19 - Shear Force Diagram for Gust Loading Case .....   | 27 |
| Figure 20 - Bending Moment Diagram for Gust Load Case.....  | 28 |
| Figure 21 - Design Gust Velocity Profiles.....  | 29 |
| Figure 22 - I-Beam Stress Distribution (Tiwary, 2018).....  | 29 |
| Figure 23 - Half-Wing Rib Distribution .....  | 31 |
| Figure 24 - Stringer Dimensions for Root and Tip Chord .....  | 33 |
| Figure 25 - Simplified Wing Sketch .....  | 33 |
| Figure 26 - Sketch of Boom Allocation .....   | 34 |
| Figure 27 - Wing Ribs and Spars configuration. Plan View (Left), Side View (Top Right) and Isometric View (Bottom Right) .....              | 36 |
| Figure 28 - Wing Box Dimensions .....   | 37 |
| Figure 29 - Shear Flow along the Wing Skin.....   | 38 |
| Figure 30 - Cut Away of a Wing Fuel Section.....  | 39 |
| Figure 31 - Pylon Truss Structure .....   | 39 |
| Figure 32 - Identity and Dimensions of the Truss Members .....  | 40 |
| Figure 33 - Plan View of Aero 5 Wing .....  | 41 |
| Figure 34 - Side View of Aero 5 Wing .....  | 41 |
| Figure 35 - Isometric View of Assembled Aero 5 Wing and Nacelle .....   | 41 |
| Figure 36 - Location of Minimum Suction (Robins, 2018) .....  | 42 |
| Figure 37 - Diagrammatic Representation of an Overhung Aerodynamic Balance .....  | 45 |
| Figure 38 - Graphical Representation of Input Values for ESDU 87008 .....   | 47 |
| Figure 39 - Historical Guideline for Aileron Span and Chord Ratios (Raymer, 2012) .....   | 49 |
| Figure 40 - Planform Diagram of Final Control Surfaces Placement .....  | 51 |
| Figure 41 - Dimensioned and 3-D Model of the Vertical Tail.....   | 51 |
| Figure 42 - Dimensioned and 3-D Model of the Horizontal Tail .....  | 52 |
| Figure 43 - Typical Control Surface Planform (Gilbey, 1989) .....   | 52 |

|   |     |
|---|-----|
| Figure 44 - Typical Hinge Moment Coefficient vs. $\delta$ Curve (Gilbey, 1989).....   | 54  |
| Figure 45 - Drag vs. Velocity at Take-Off.....  | 57  |
| Figure 46 - $V_v$ vs. $V_H$ (OEI Case).....   | 58  |
| Figure 47 - Aero 5 Aircraft Flight Envelope.....                                      | 60  |
| Figure 48 - Front and Side View of Aero 5 Nacelle .....                               | 61  |
| Figure 49 - Front and Rear Isometric View of the Aero 5 Passenger Seats.....          | 61  |
| Figure 50 - Isometric View of Cabin Assembly .....                                    | 62  |
| Figure 51 - Isometric View of Pilot Seat (Left) and Attendant Seat (Right) .....      | 62  |
| Figure 52 - Plan View of Aero 5 Aircraft Assembly .....                               | 63  |
| Figure 53 - Isometric View of Aero 5 Aircraft .....                                   | 63  |
| Figure 54 - Isometric View of Aero 5 Aircraft (with Cabin Shown).....                 | 64  |
| Figure 55 - Aero 5 Aircraft Plan View (with CG and AC).....                           | 65  |
| Figure 56 - Navigation System Fault Tree Analysis.....                                | 68  |
| Figure 57 - Electrical System Fault Tree Analysis .....                               | 80  |
| Figure 58 - Systems Architecture Map .....  | 83  |
| Figure 59 - FOD Probability Association with Consequence Assessment (NASA, 2010)..... | 89  |
| Figure 60 - Aero 5 Work Breakdown Structure.....                                      | 92  |
| Figure 61 - Top Level Schedule Extract .....  | 93  |
| Figure 62 - Bending Moment Diagram after First Iteration.....                         | 110 |
| Figure 63 - Shear Force Diagram after First Iteration.....                            | 110 |
| Figure 64 - "Soar to the Sky" .....   | 120 |
| Figure 65 - "Beyond the Clouds" .....   | 121 |
| Figure 66 - "Over the City" .....   | 122 |

## List of Tables

|  |    |
|--|----|
| Table 1 - Final Input Values for DOC Calculations .....  | 2  |
| Table 2 - Final Cost Estimates .....   | 3  |
| Table 3 - Input Values for Airbus A320ceo DOC Calculation .....  | 3  |
| Table 4 - Total DOC of A320ceo (2015 Aircraft) .....   | 4  |
| Table 5 - Aero 5 Total Operating Cost .....  | 4  |
| Table 6 - Verification Matrix from JSSG-2001B .....  | 5  |
| Table 7 - CDR Functional Design Requirements Matrix.....   | 5  |
| Table 8 - CDR Business Case and Environmental Requirements Matrix.....                                   | 7  |
| Table 9 - LEAP-1C Powerplant Data Summary (Safran Aircraft Engines, 2018), (International, 2016). .....  | 8  |
| Table 10 - Structural Weight Breakdown as a Percentage of Total Weight (Mouritz, 2012).....              | 9  |
| Table 11 - Mechanical Properties of M55J 6k/954-3 Unidirectional Tape (DEPARTMENT OF DEFENSE, 2019)..... | 12 |
| Table 12 - Comparison of Different Stringer Types (Kaur, 2014) .....                                     | 14 |
| Table 13 - Updated Boom Areas of Each Section .....  | 17 |
| Table 14 - Stringer Dimensions (KO).....   | 17 |
| Table 15 - Updated Stringer Buckling Analysis per Section .....  | 18 |
| Table 16 - Shear Flow Distribution for each Fuselage Section of the Fuselage .....                       | 19 |
| Table 17 - Dimensioning of Single Frames in each Fuselage Section.....                                   | 20 |
| Table 18 - Cross-Section Dimensions of Frames in each Fuselage Section .....                             | 21 |
| Table 19 - Frame Dimensions (KO) .....   | 21 |
| Table 20 - Summary of Static Loading Force Balance .....   | 25 |
| Table 21 - Limit Point Load Safety Factor for Rib Mounting .....   | 28 |
| Table 22 - Extract from Spar Sizing Spreadsheet with Final Spar Dimensions at the Root Chord .....       | 30 |
| Table 23 - SF Table for Critical Buckling Loads for Rib Sections.....                                    | 33 |
| Table 24 - Boom Initial Spacing Across Perimeter .....   | 34 |
| Table 25 - Boom Allocation with Regard to the Geometry .....   | 34 |
| Table 26 - New Boom Quantity on Hypotenuse Section .....   | 34 |

|   |     |
|---|-----|
| Table 27 - Ratio of Spacing from the Boom Point to the Neutral Axis in Hypotenuse Section ..... | 34  |
| Table 28 - Total Second Moment of Area and Applicable Bending Moment .....                      | 35  |
| Table 29 - Stringer Material Properties (Honeywell, 2019) .....                                 | 35  |
| Table 30 - Final Result of Safety Factor Analysis .....   | 36  |
| Table 31 - Iteration between the Thickness and the Safety Factor .....                          | 38  |
| Table 32 - Forces and Thickness of the Truss Members .....                                      | 40  |
| Table 33 - Prandtl-Glauert Theory .....   | 43  |
| Table 34 - Final Empennage Dimensions .....   | 44  |
| Table 35 - List of ESDU Data Sheets and Tools Used .....  | 44  |
| Table 36 - Initial Elevator Dimensions .....  | 45  |
| Table 37 - Final Elevator Dimensions .....  | 46  |
| Table 38 - Input and Output Data for ESDU AERO C.08.01.01 .....                                 | 46  |
| Table 39 - Initial Rudder Dimensions .....  | 47  |
| Table 40 - Final Rudder Dimensions .....  | 47  |
| Table 41 - Input and Output Data for ESDU 87008 .....   | 48  |
| Table 42 - Wing Control Surface Dimensions .....  | 49  |
| Table 43 - Input and Output Data for ESDU 70011 and ESDU 88040 .....                            | 50  |
| Table 44 - Values of K .....  | 53  |
| Table 45 - Hinge Moment Coefficient Derivatives .....   | 54  |
| Table 46 - $C_H$ Values .....   | 55  |
| Table 47 - Comparison of $H$ and $H_0$ .....  | 55  |
| Table 48 - Maximum Hinge Moments .....  | 55  |
| Table 49 - Angle of Climb and Gradient of Climb .....   | 59  |
| Table 44 - Summary of CG Data and other Dimensional Data .....                                  | 64  |
| Table 51 - SIL as a Function of RRF (Yoset, 2017) .....   | 69  |
| Table 52 - Failure Rates for IRS Failure Modes (Air Force Avionics Laboratory, 1973) .....      | 69  |
| Table 53 - Oxygen Emergency System Considerations .....   | 75  |
| Table 54 - Heat Exchanger Parameters Indications (Lu, 2015) .....                               | 76  |
| Table 55 - Effect of Insufficient Power on Aircraft .....                                       | 76  |
| Table 56 - Systems and Subsystems as Labelled on Figure 58 .....                                | 82  |
| Table 57 - Interface List .....   | 84  |
| Table 58 - Sources of FOD (FAA, 2010) .....   | 86  |
| Table 59 - Turbine Blade Severity Level Indicator (Maragakis, 2008) .....                       | 87  |
| Table 60 - Distribution of the Random Variables (White, 2006) .....                             | 88  |
| Table 61 - Updated Risk Register .....  | 88  |
| Table 62 - Aero 5 Action Tracker Extract .....  | 105 |
| Table 63 - DOC Spreadsheet Sheet 1 .....  | 106 |
| Table 64 - DOC Spreadsheet Sheet 2 .....  | 106 |
| Table 65 - DOC Spreadsheet Sheet 3 .....  | 106 |
| Table 66 - Project Cost Calculation .....   | 108 |
| Table 67 - Fuselage Weight Distribution .....   | 109 |
| Table 68 - Initial Boom Area Calculations .....   | 110 |
| Table 69 - Initial Buckling Length Data .....   | 111 |
| Table 70 - Wing Design Material Data .....  | 111 |
| Table 71 - Mass Fraction Iterations .....   | 113 |
| Table 72 - Updated Risk Matrix .....  | 117 |
| Table 73 - Team Member Contributions .....  | 117 |

## **1. Introduction – SH**

The Critical Design Review (CDR) is the culmination of the analysis conducted by Aero 5 over two academic semesters. It aims to present a detailed design description supported by technical analysis for a short-range single aircraft design with 190 and 240 passenger interior cabin layout configuration, to occupy a market gap and provide a competitive design solution. The key driving requirement for the design was a 15% reduction in Direct Operating Cost (DOC) when compared to the 2015 state of the art competitors with a 2027 entry into service date. To facilitate the viability and certification of the proposed aircraft design, a comprehensive research and requirement analysis was undertaken to ensure the final qualifying implicit design choices have sound merit and respond to all the customer needs stated in the Customer Design Brief (CDB).

The technical sections of this report focus on the structure and systems of the aircraft. The engineering process is supported with approved methods of theoretical analysis and concluding statements. Principal results have been presented in tables and figures for precision and succinctness. The product of this analysis informed the detailed CAD designs presented in this report for significant structural members as well as for the complete aircraft assembly. Any underlying assumptions in the design process and constraints have been addressed in the relevant sections of the report. The CDR also presents a refined cost model scheme to support the long-term operation and maintenance of the Aero 5 aircraft during service. The latter part of this report addresses the engineering management aspect of the design project and the measures taken to enforce healthy management practice and preserving traceability as well as an updated risk management database for the matured design.

## **2. Business Case – PS, KO**

### **2.1 Updated Market Research – KO**

The Aero 5 aircraft, which fits into the short-range airline market, has two main competitors; the Airbus A320neo family and the Boeing 737Max family. The market forecast remains unchanged from the PDR document. However, the pricing strategy of the aircraft has been updated.

It was initially decided that, solely based on market research and the predicted rise in demand within the particular market, if Aero 5 wanted to acquire 1/6<sup>th</sup> of the market, with an expected 37.4% backlog, then by 2027, a maximum of 2,443 aircraft would have to be sold and 1,529 of those would need to be delivered. In the PDR (Section 6.1), it is explained that in comparison with the A321neo and 737 Max 10, the aircraft may be priced at around \$129 million. However, in Section 6.6.3 of the PDR, it can be seen that the DOC reduction target could be met with a lower market price of \$88.7 million.

After implementing a new method of DOC calculation, seen in Section 2.3 and a comparison with 2015 state-of-the-art technology, the A321ceo, the final cost of the aircraft was set to \$108 million. This comes from exploring how the Direct Operating Costs and Total Operating Costs change as the Manufacturer's Study Price is changed. It allows for a 18.8% DOC reduction and takes into account the increased price of manufacturing due to the incorporation of new technologies and major inclusion of composite parts in a high percentage of the aircraft structure, which increases cost due to its expensive manufacturing process. This also takes into consideration the cost of the aircraft determined using the Jenkinson method, with 1995 US Dollars adjusted for inflation, however this estimation was taken lightly due to the lack of inclusion of new developments.

### **2.2 Direct Operating Cost Calculations – KO**

The Aero 5 team, which took the role of aircraft manufacturer, aim to maximise profit by selling a high number of aircraft at a premium price, whilst keeping manufacturing costs as low as possible.

The costs and economics for this aircraft were analysed using the typical Direct Operating Costs method, as it allowed for the best results with the data available at this stage of design. Life cycle costs were not analysed as this technique requires complex models. The method followed is from Association of European Airlines (AEA) and has been reinforced by Airbus (Leoviriyakit, 2019). The DOC is made up of the financial costs and the Cash Operating Costs (COC) of the aircraft. The COC is useful in comparing aircraft operation costs, however, as the market grows to become more competitive, manufacturers are driven to design aircraft with better technology, which in turn increases the cost. Therefore, it is better to use DOC as the financial costs include depreciation, interest and insurance. The Indirect Operating Costs (IOC) include factors such as the ground property, equipment, administration fees, sales and servicing, where the IOC and the DOC make up the Total Operating Cost (TOC) of the aircraft. In this method, the IOC was not calculated, as it is heavily dependent on airline operations, however an initial cost estimation was provided in the PDR Section 6.5.

A Microsoft Excel spreadsheet was used when carrying out this method, as this allowed the technique to be clearly followed and tracked, both during the calculations and for analysing the results. From the AEA method, the cost calculations can be split into three sections; inputs, assumptions and results. This technique was followed when creating the spreadsheet. Table 1 shows the final inputs used.

*Table 1 - Final Input Values for DOC Calculations*

| <b>Input</b>                         | <b>Value</b> |
|--------------------------------------|--------------|
| <b>Mission Data</b>                  |              |
| Stage Length (NM)                    | 500          |
| Block Fuel (lbs)                     | 2040         |
| Block Time (hr)                      | 2.13         |
| Passengers (Pax)                     | 240          |
| <b>Weight Data</b>                   |              |
| MTOW (tonnes)                        | 106          |
| MWE (tonnes)                         | 38.3         |
| <b>Engine Parameters</b>             |              |
| Number of Engines                    | 2.00         |
| Bypass Ratio                         | 11:1         |
| Overall Pressure Ratio               | 40:1         |
| No. of Compressor Stages             | 3            |
| <b>Price Data</b>                    |              |
| Engine Price (\$)                    | 1.5 million  |
| Manufacturers Study Price (MSP) (\$) | 108 million  |
| Airframe Cost (\$)                   | 10.5 million |
| Fuel Price (\$/USgal)                | 1.50         |

The following approach was taken to most efficiently determine the final DOC:

- Primarily, the input values were split into sections, the first one being mission data, which is the information related to the study mission. The Stage Length was obtained from the Customer Design Brief (CDB), as were the number of passengers required. The Block Time was calculated in the PDR and does not include the turnaround time. This allowed the Block Fuel to be calculated by dividing Engine Specific Fuel Consumption (SFC) by Block Time.
- The Manufacturer's Study Price (MSP) is a major factor in the DOC calculations and is used in multiple sections. It is defined as a sum of the Airframe Price and the Engine Price, or a sum of the Aircraft Cost and the Manufacturer's Profit. This value was set to \$108 million, as this is what Aero 5 aim to market the final aircraft for (as seen in Section 2.4).
- The financial costs were then calculated. The method, shown below, estimated that total financial overheads will be approximately \$7550 per trip for a 25-year period.
  - The depreciation of the aircraft value was calculated using Equation (1). For this, total investment and utilisation values were needed. The value of depreciation is \$3045 per trip for a 25-year period.

$$\frac{\text{Total Investment}}{14 \times \text{Utilisation}} \quad (1)$$

- Interest is the payment of aircraft financing and was determined using Equation (2) giving a result of \$3810 per trip.

$$0.05 \times \frac{\text{Total Investment}}{\text{Utilisation}} \quad (2)$$

- The cost of insuring the aircraft was computed using Equation (3) and was determined to be \$413 per trip.

$$0.006 \times \frac{\text{MSP}}{\text{Utilisation}} \quad (3)$$

- Utilisation, which is the number of trips in a year, was found by using 4,000 available hours per year and the values for calculated block time and turn-around time. This gave a result of 1,569 trips per year.
  - The total investment was calculated as a sum of MSP, airframe spares cost and spare propulsion unit costs. Following the recommended calculation method, airframe spares costs amounted to \$8.0 million and spare propulsion units accounted for \$8.40 million. Therefore, total investment is \$124 million.
4. Then, Maintenance Costs were calculated. This is analysed as a sum of Airframe Materials and Airframe Labour. To obtain these values, inputs such as Airframe Price, Airframe Weight, Labour Rate, Manufacturers Empty Weight and Block Time were needed. The equations for these, and all other calculations are not included, however can be found in Appendix 13.3. Many of these input values were obtained from the PDR document and have not changed. Airframe Maintenance Costs accounted to \$66.7 million and the Engine Maintenance Costs came to \$436 per flight, leaving final maintenance costs to amount to slightly higher than \$66.7 million.
5. Flight costs, which, along with the maintenance costs make up the COC, were then considered. These are a summation of total Crew Costs, Navigation Charges, Landing Fees and Fuel. This section assumes that the cost of a 2-person flight crew is \$380 per block hour and a cabin crew member is paid \$60 per block hour. The Number of Cabin Crew (NCAB) was assumed to be 1 per 35 passengers. The total Flight Costs were forecasted around \$3470 per block hour, where total Crew Costs are \$1704, Navigation Charges are \$674, and the Landing Fees are \$636. The breakdown of these calculations, as well as the rest of the cost calculations, can be seen in Appendix 13.3.
6. Therefore, the final DOC value was estimated around \$667 million, to 3 significant figures, where COC makes up 99% of the total DOC. The final costs can be seen in Table 2.

*Table 2 - Final Cost Estimates*

|                                     |                      |
|-------------------------------------|----------------------|
| Total Financial Costs               | \$7550               |
| Total Cash Operating Costs          | \$667 million        |
| <b>Total Direct Operating Costs</b> | <b>\$667 million</b> |

### 2.3 DOC Reduction – PS

Once Aero 5 had confirmed the DOC for the design, it was possible to compare the reduction in DOC achieved. In the PDR, Aero 5 compared most of its reduction with the competitor aircraft, the A320ceo, a 2015 state-of-the-art technology. It was decided that the most accurate comparison would result from producing the DOC for the A320ceo using the AEA method used in Section 2.1. The comparison input values are shown in Table 3.

*Table 3 - Input Values for Airbus A320ceo DOC Calculation*

| Input                                | Value        |
|--------------------------------------|--------------|
| <b>Mission Data</b>                  |              |
| Stage Length (NM)                    | 500          |
| Block Fuel (lbs)                     | 4350         |
| Block Time (hr)                      | 2.13         |
| Passengers (Pax)                     | 150          |
| <b>Weight Data</b>                   |              |
| MTOW (tonnes)                        | 78.0         |
| MWE (tonnes)                         | 42.6         |
| <b>Engine Parameters</b>             |              |
| Number of Engines                    | 2.00         |
| Bypass Ratio                         | 5.7:1        |
| Overall Pressure Ratio               | 40:1         |
| No. of Compressor Stages             | 3            |
| <b>Price Data</b>                    |              |
| Engine Price (\$)                    | 10.0 million |
| Manufacturers Study Price (MSP) (\$) | 118 million  |

|                       |              |
|-----------------------|--------------|
| Airframe Cost (\$)    | 98.3 million |
| Fuel Price (\$/USgal) | 1.50         |

The main difference between the Aero 5 design and the 2015 A320ceo that had a significant impact was the choice of engine. The A320ceo uses the CFM56 5 series, specifically the CFM56-5B4 therefore properties and characteristics of this engine were used. The SFC of the CFM engine was much larger than that of the LEAP-1C used in the Aero 5 aircraft, which resulted in a higher block fuel (Meier, 2005). This was expected due to a newer engine choice with better fuel consumption as justified in Section 4.

The price of the CFM56 engine was lower than the LEAP-1C (CFM, 2015), however the higher MSP of the A320ceo led to a decrease in the total investment cost. This was due to a higher ownership cost and depreciation due to the lifespan of the A320ceo which is assumed to be 15 years as mentioned in the PDR (Section 6.5.4).

All of the AEA assumptions and calculations have been carried out following the same steps as stated above, from which the resulting DOC of the A320ceo can be found below in Table 4. The spreadsheet data and input values can be found in Appendix 13.4.

Table 4 - Total DOC of A320ceo (2015 Aircraft)

|                                     |                      |
|-------------------------------------|----------------------|
| Total Financial Costs               | \$10400              |
| Total Cash Operating Costs          | \$821 million        |
| <b>Total Direct Operating Costs</b> | <b>\$821 million</b> |

From the AEA DOC analysis of both the Aero 5 design and the A320ceo which represents the 2015 state-of-the-art technology, the relative reduction of DOC was determined, using Equation (4). From this, it can be seen the Aero 5 design has achieved the 15% DOC reduction target set for the design.

$$DOC \% reduction = \frac{A320ceo DOC - Aero 5 Design DOC}{A320ceo DOC} \times 100 \quad (4)$$

$$DOC reduction = 18.8\%$$

## 2.4 Profit Margin – PS

To determine the required sale price of Aero 5's design, it was required to combine the DOC and IOC of the design. From the PDR (Section 6.2), it was calculated that the total ground operation cost would accumulate to around \$8950 per trip, representative of around 30% of the IOC. This value was multiplied by the utilisation and 25-year life to give the total ground operation cost as \$356 Million.

The remainder of the IOC lies with the system operating cost as discussed in PDR Section 6.3. This 20% was difficult to assume as it relied heavily on the service provided by the airline. It was therefore assumed that the total IOC would be equivalent to the DOC (Raymer, 2012), however Aero 5 were aware this would result in an estimated TOC. This approach would give the total system operating cost as \$1.33 Billion.

The TOC can be found below in Table 5. Once this was calculated, Aero 5 could determine the number of aircrafts required to break-even with pricing of Aero 5's design at \$108 million.

Table 5 - Aero 5 Total Operating Cost

|            |                       |
|------------|-----------------------|
| DOC        | \$667 million         |
| IOC        | \$667 million         |
| <b>TOC</b> | <b>\$1.33 billion</b> |

It was determined by Aero 5 that to break-even, 13 aircraft would be required to be sold at the list price of \$108 million.

## 3. Requirement Analysis & Verification – SH, LM

The CDR delves into high fidelity design and technical analysis, a multitude of governing design drivers had to be accounted for in the design process that was driven by framework regulations and compliance criteria. Continuing from the PDR, the requirement capture for the CDR will address any newly emerged top-level functional requirements that influenced the technical analysis. The lower level requirements that do not directly affect technical design were superseded by the top-level requirements. This was deemed appropriate because

they did not contribute in a noteworthy manner to the technical analysis and design process. However, these requirements have been mentioned in relevant sections by the responsible Aero 5 Engineer when applicable.

*Table 6 - Verification Matrix from JSSG-2001B*

| Approved Verification Methods |               |
|-------------------------------|---------------|
| Method Shorthand              | Description   |
| I                             | Inspection    |
| A                             | Analysis      |
| S                             | Simulation    |
| D                             | Demonstration |
| T                             | Test          |

### **3.1 Verification Planning for Risk Assessment Requirements – SH, LM**

The requirements listed in Table 7 have been related to their relevant risk management section in order to see the direct effect of each requirement. The risks that have been shown to pose the most threat and deemed severe are structural failure and systems failure. For this reason, the requirements were closely followed and their compliance criteria was adhered to which provided Aero 5 with confidence in the reliability of the aircraft and its purpose. JSSG-2001B was the method used for the verification matrix which is consistent with the PDS and PDR, where the most suitable verification methods are indicated for the most prevalent requirements which directly impacted the technical design.

*Table 7 - CDR Functional Design Requirements Matrix*

| Aircraft Functional Design Requirements |                      |                                   |                     |   |                         |
|---|----------------------|-----------------------------------|---------------------|---|-------------------------|
| Requirement(s) description              | Regulatory Framework | Compliance criteria/ Verification | Associated Engineer | Functional/design Relationship  | Risk assessment section |
| Stall Speed                             | CS 25.103            | AMC 25.103(b)-(d)/ A, T, D        | BG, SH              | Stall speed was used in the gust modelling case which effected the point loads used for sizing the control surfaces   | 8.1.6                   |
| Take-off speed                          | CS 25.107            | AMC 25.107(d)-(e)(4)/ A, T, D     | BG                  | Influenced control surface sizing and used in flight envelope construction  | 8.1.6                   |
| Take-off path                           | CS 25.111            | AMC 25.111/A, D, T                | BG                  | Defines the conditions for three separate take-off stage phases and the minimum gradients required and thus affected control surface sizing to support these needs. | 8.1.6                   |
| Climb: one-engine-inoperative           | CS 25.121            | AMC 25.121/A,T,S                  | BG                  | The critical engine inoperative case determined the climb rate needed, which was specified in the requirement   | 8.1.5                   |
| Static longitudinal stability           | CS 25.173            | AMC 25.173(c)/ I, A, D            | PS                  | Directly influence the sizing of the elevator control surface.  | 8.1.4                   |
| Loads                                   | CS 25.301            | AMC 25.301 (1)-(2)/A              | SH, AS, LM          | Strength requirements had to be identified for the maximum loads expected in service, hence structural members were sized to meet such conditions.                  | 8.1.4                   |

|  |           |                               |                    |  |              |
|--|-----------|-------------------------------|--------------------|--|--------------|
| Interaction of systems and structures  | CS 25.302 | Appendix K/ S, T, D           | YA, MK             | Impact of systems integration that affect structural performance had to be accounted for and shared with the structural team.  | 8.1.6, 8.1.4 |
| Factor of safety                       | CS 25.303 | Satisfied by demonstration/ D | SH, AS, LM, AM     | All structural members being designed had to adequately meet safety requirements. As a result, dimensions and material selection had to adjust accordingly.                                    | 8.1.4        |
| Proof of structure                     | CS 25.307 | Satisfied by demonstration/ D | SH, LM             | Force modelling diagrams need to be placed in equilibrium ‘in a rational and conservative manner’ this directly affected point load placements and total bending moments.                      | 8.1.4        |
| Flight manoeuvring envelope            | CS 25.333 | Satisfied by demonstration/D  | PS, BG, SH, AS, LM | The flight envelope details the external loads experienced by the aircraft during flight and must be designed for various sections within the envelope.  | 8.1.4        |
| Limit manoeuvring load factors         | CS 25.337 | AMC 25.337/ A, S, T           | SH, BG, PS, LM     | Aircraft had to be designed to operate between a minimum and maximum expected load factor up to the dive speed.  | 8.1.4        |
| Gust and turbulence loads              | CS 25.341 | AMC 25.341/ A, S, T, D        | SH                 | Rib structure had to withstand point limit loads caused by critical gust velocities.   | 8.1.4        |
| Design fuel and oil loads              | CS 25.343 | Satisfied by demonstration/ D | SH                 | The aircraft static and gust loading cases were modelled with an empty fuel reservoir and this reduced the available bending relief on the spar.   | 8.1.4, 8.1.6 |
| High lift devices                      | CS 25.345 | Satisfied by demonstration/ D | BG, PS             | The design of high lift devices had to operate against gust load conditions prescribed in the requirement.   | 8.1.6        |
| Yaw manoeuvre conditions               | CS 25.351 | Satisfied by demonstration/D  | PS                 | Design loads resulting from yaw maneuver conditions influenced the sizing of control surfaces  | 8.1.6        |
| Engine and auxiliary power unit torque | CS 25.361 | AMC 25.361/ A, T, D           | AM                 | Engine installations and their supporting structural frames had to be designed for the effects of engine torque corresponding to maximum thrust output. Directly impacting wing box internals. | 8.1.4, 8.1.5 |
| Ground gust conditions                 | CS 25.415 | Satisfied by demonstration/ D | BG                 | Flight control systems and surfaces had to be designed for the limit loads for specific ground gust velocities.  | 8.1.4        |

|   |            |                                |                          |  |              |
|---|------------|--------------------------------|--------------------------|--|--------------|
| Material strength properties and Material Design Values | CS 25.613  | AMC 25.613/<br>A, S, I         | SH, LM,<br>AS, KO,<br>Tl | Using materials with approved specifications meant that structural design materials had to be chosen based on certain approved catalogues of materials.                        | 8.1.4        |
| Aeroelastic stability requirements                      | CS 25.629  | AMC 25.629/<br>A, T            | AM                       | Design criteria for engine placement directly related to point load placement for static and gust loading analysis. Also regulating engine mounting structural considerations. | 8.1.4,8.1.5  |
| Lift and drag devices, controls                         | CS 25.697  | Satisfied by demonstration / D | BG, PS                   | Designing the control surfaces to meet the control conditions described in the requirement, detailing ranges of motion and certain stages of flight.                           | 8.1.3, 8.1.4 |
| Flight recorders  | CS 25.1459 | Satisfied by demonstration/D   | YA                       | The location of the flight recorder influences the electrical architecture and its interaction with the structure.   | 8.1.6        |

Table 8 - CDR Business Case and Environmental Requirements Matrix

| Commercial & Environmental Requirements |                                    |   |                     |  |              |
|---|------------------------------------|---|---------------------|--|--------------|
| Requirement(s)                          | Regulatory Framework               | Compliance Criteria/<br>Verification                                    | Associated Engineer | Functional/design Relationship   | Risk Section |
| Weight optimisation                     | ICAO-Annex 6                       | Annex 6-Part 1- Chapter 4.3.6. 3 (a)-(e), CS 25.857, CS 25.858/ A,D,T,S | SH, LM, AS          | Economical design achieved with effective structural analysis  | 8.1.4        |
| Economical maintenance cycle            | CS 25.71, CS 25.901 (b) CS.25.1529 | CS 25.71, CS 25.901 (b)-2 , CS.25.1529, Appendix H/ A,S,D               | PS, KO, TW          | 15% reduction in DOC for extended aircraft use and maintenance   | 8.1.4, 8.16  |
| Airport infrastructure compatibility    | CS 25.783                          | CS 25.783/ A,S,T,D  | MK, BG, SH, LM, PS  | Aircraft design must be compatible with ICAO aerodrome requirements  | 8.1.2,8.1.5, |
| Turn-Around Time                        | CS-25.143, CDB                     | CS 25.143/ T,D  | PS                  | Must have a turnaround time at least equal to that of 2015 state of the art competitors                      | N/A          |
| DOC Target                              | CDB                                | CDB/D,T   | Aero 5              | 2015 State of the art minus 15%  | N/A          |
| Expected Entry into Service             | CDB                                | CDB/ A,S,I,T,D  | Aero 5              | All design aspects must consider uphold a certain level of realism and be achievable in the given time frame | 8.1.1        |
| Aircraft Noise                          | CS 36                              | AMC 36.1, GMC 36.1/T,D  | SH, PS, AM, TW      | Powerplant selection cannot exceed the ICAO noise limits   | 8.1.1        |

|  |       |                        |                |  |             |
|--|-------|------------------------|----------------|--|-------------|
| Aircraft Engine Emissions and Fuel Venting | CS 34 | AMC 34.2, GMC 34.2/T,D | SH, PS, AM, TW | Aircraft selection and installation had to provide means of fuel venting and emission regulation | 8.1.1,8.1.5 |
|--|-------|------------------------|----------------|--|-------------|

## 4. Powerplant Selection – SH

### 4.1 TSFC Targets – SH

Upon the delivery of the Preliminary Design Report (PDR), the LEAP-1C was incorporated as a placeholder design engine. The analysis presented in the PDR already introduced preparatory calculations and analysis to justify its transition into the final implicit design. As a result, the impact of the LEAP-1C dispersed into many aspects of the PDR analysis and streamlined the design alternatives to other areas. Regarding the specifications of the powerplant selection, the LEAP-1C engine thrust rating was already proved to be capable of meeting OEI certification criteria. The justification and the calculation process for discovering thrust requirements can be found in Section 4.6.9 of the PDR. This analysis supports that only a two-engine set up is needed to meet all thrust and power needs of the proposed aircraft design. The preceding PDR analysis has already accounted for the LEAP-1C in the sizing process, and the forthcoming Critical Design Report (CDR), supplements the powerplant selection.

Table 9 - LEAP-1C Powerplant Data Summary (Safran Aircraft Engines, 2018), (International, 2016).

| LEAP-1C Dimensions             |                             |               |                |                         |
|--------------------------------|-----------------------------|---------------|----------------|-------------------------|
| Fan Diameter (m)               | Length (m)                  | Max Width (m) | Max Height (m) | Weight (kg)             |
| 1.96                           | 4.51                        | 2.66          | 2.71           | 3950                    |
| LEAP-1C Engine Characteristics |                             |               |                |                         |
| Max Take-off thrust (lbf)      | Max Continuous Thrust (lbf) | Bypass Ratio  | SFC (kg/Hr)    | TSFC Targets (kg/Hr. N) |
| 30800                          | 30000                       | 11:01         | 1970.0         | 0.0655                  |

### 4.2 Derivative Projected Engine – SH

The primary research and analysis for the powerplant was confirmed in the PDR and the sizing and iteration process conducted with the placeholder LEAP-1C engine provided satisfactory stability and thrust outputs for the tested configurations. As it stands it is a viable commercial offering that will integrate into the CDR design process. For a future engine alternative, a promising option providing improved bypass ratios, fuel burn and reduced CO<sub>2</sub> emissions were discussed in section 3.2.5 of the PDR (Future Engine Options). The integration of the Advance3 Rolls Royce engine claiming a 15:1 Bypass ratio (BPR) and a further 25% reduction in fuel burn compared to the Trent 800 engine series with a comparative 10% fuel improvement when compared to the LEAP-1C and other 2015 state of the art engines, significantly boosting performance and efficiency.

## 5. Aircraft Structure and Performance – LM, PS, KO, BG, AM, SH, AS, TL

### 5.1 Introduction – LM

The fuselage and wing will have a semi-monocoque structural design which will be the same for both aircraft families allowing for ease of interchangeability between the two separate layouts, making repair easier due to a consistent structural arrangement. The design is of extreme importance as the fuselage contains the passengers and is subject to various point and continuous loads whether on the ground or airborne, so structural integrity is vital for passenger safety. The wings are responsible for the main attributes of aerodynamics of the aircraft, so maintaining their shape and form is imperative for flight efficiency.

The main requirements of the aircraft structural components are that they need to have suitable mechanical properties such as strength, stiffness and fatigue resistance. Strength is needed to withstand the operational loads that the aircraft will be subject to in the extremities of the flight envelope, in conjunction with an appropriate stiffness to ensure that the deflections that occur are not detrimental to the design. Finally, fatigue is important with regard to the business case as this is what will determine the life time of the airframe. The weight is also a driving factor in the design of the structure as this will directly influence aerodynamic effects. A breakdown of the weight of a passenger aircraft is shown in Figure 1.

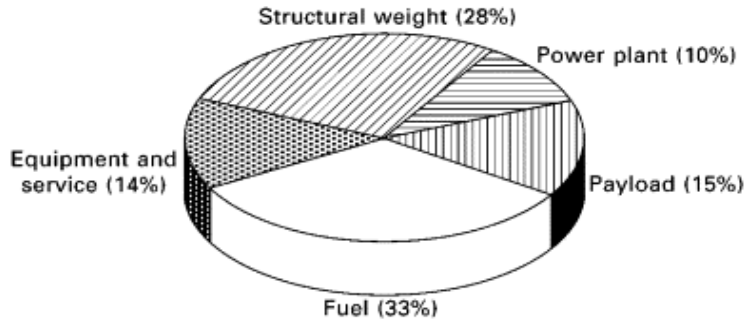


Figure 1 - Estimated Contribution of the Take-Off Weight of a Large Passenger Commercial Airliner (Mouritz, 2012)

A more in depth table below shows a breakdown of the contribution of various structural sections to the total structural mass.

Table 10 - Structural Weight Breakdown as a Percentage of Total Weight (Mouritz, 2012)

| Structural Component | Subsonic Airliner |
|----------------------|-------------------|
| Fuselage             | 7                 |
| Wing                 | 8                 |
| Stabilisers          | 4                 |
| Undercarriage        | 4                 |
| <b>Total %</b>       | <b>23</b>         |

Figure 1 shows that the structural weight of an aircraft roughly accounts for 28% of the take-off weight of the aircraft, so by use of composite materials and geometric design, reducing the weight of the structure of the fuselage and wings which accounts for roughly 15% of the total aircraft weight, this could increase efficiency and reduce cash operating costs by reducing fuel-burn.

## 5.2 Fuselage – LM, KO, PS

### 5.2.1 Fuselage Design Considerations – KO

The final fuselage structure was designed to meet the requirements set forward by Aero 5 in the PDR document as a result of the drag and lift analysis. Due to this, the length of the fuselage and the cabin floor were defined as 45.9m and around 40m, respectively. In order to integrate the empennage and the nose cone into the fuselage, the tail scrape angle, auxiliary power unit (APU) dimensions and height requirements for some parts of the cabin and cockpit had to be considered, as well as the dimensions required to maintain stability due the size of the empennage affecting the force required by the rudder to function effectively.

When considering the design for the empennage the following constraints had to be satisfied:

- The empennage was designed to accommodate the Honeywell 131-9A APU. The dimensions for this can be seen in Figure 2 (Honeywell, 2008).

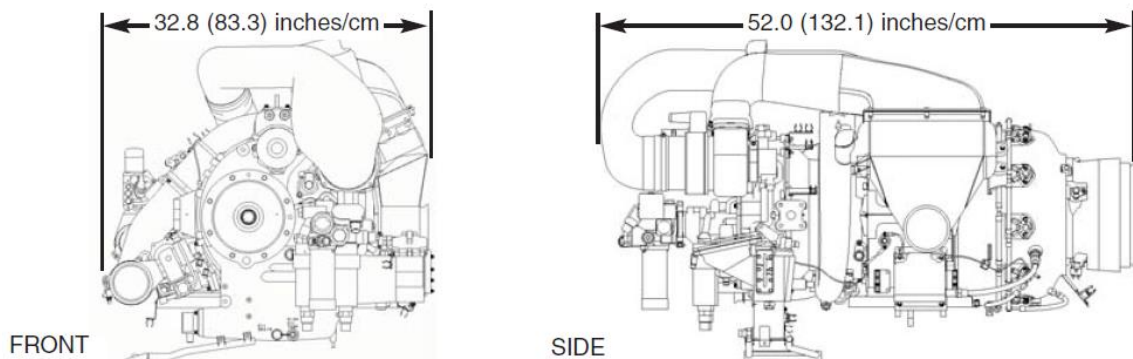


Figure 2 - Dimensions for APU used by Aero 5 (Honeywell, 2008)

- The tail scrape angle, as can be seen in Section 5.7.4 was initially calculated as  $13^\circ$  and then updated to  $15^\circ$  as the project progressed. This was adapted into the empennage and nose cone design calculations and CAD. Figure 3 shows the different layouts considered for the empennage section. The

$15^\circ$  tail scrape angle was met initially at the front, however had to be gradually increased to avoid having to extend the length of the fuselage determined in the PDR.

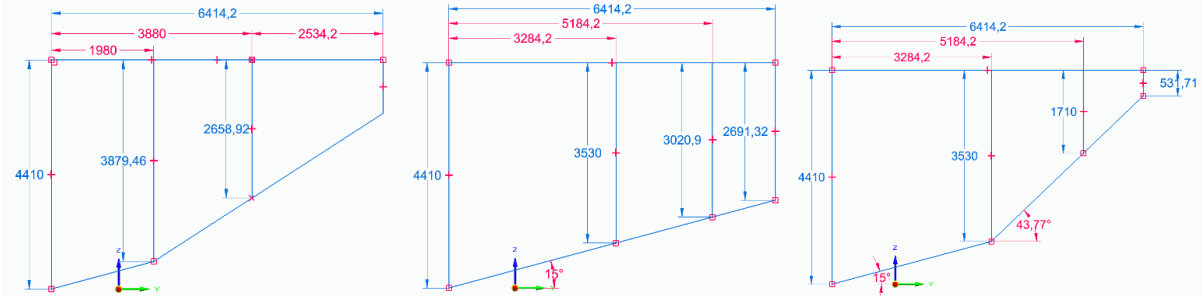


Figure 3 - Design Considerations for Empennage

- The dimensions shown in Table 34 were to be implemented as these were used for stability calculations seen in Section 5.5. However, these dimensions were modified in the design to incorporate the tail scrape angle, and another iteration of stability calculations were performed to determine if these were suitable.

Figure 4 and Figure 5 show the final CAD models of the empennage and nose cone, which were used in the compilation for the final aircraft CAD assembly, seen in Section 5.10. An implicit decision was made, based on general aircraft precedents, to use the empennage sections shown in Figure 3 with a gradual change in the angles and cross sections, instead of the one shown in Figure 6 with a sharper transition. However, the dimensions remain unchanged.

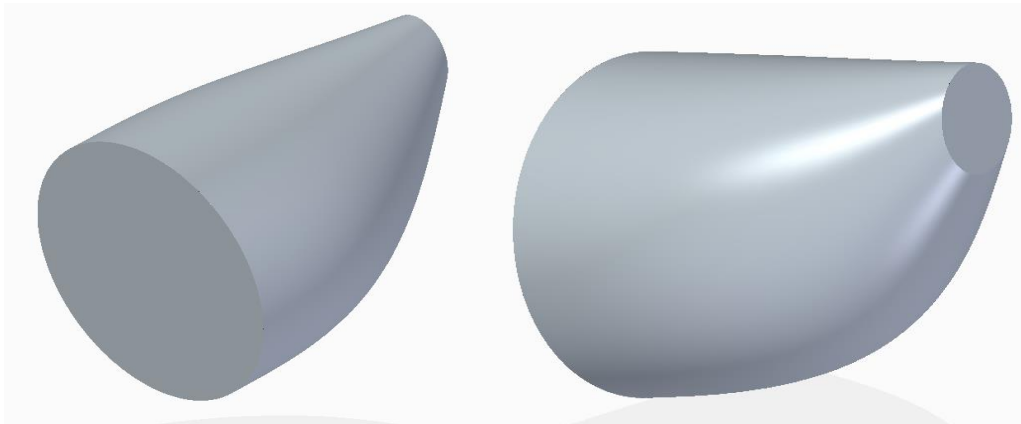


Figure 4 - Final Empennage CAD Design

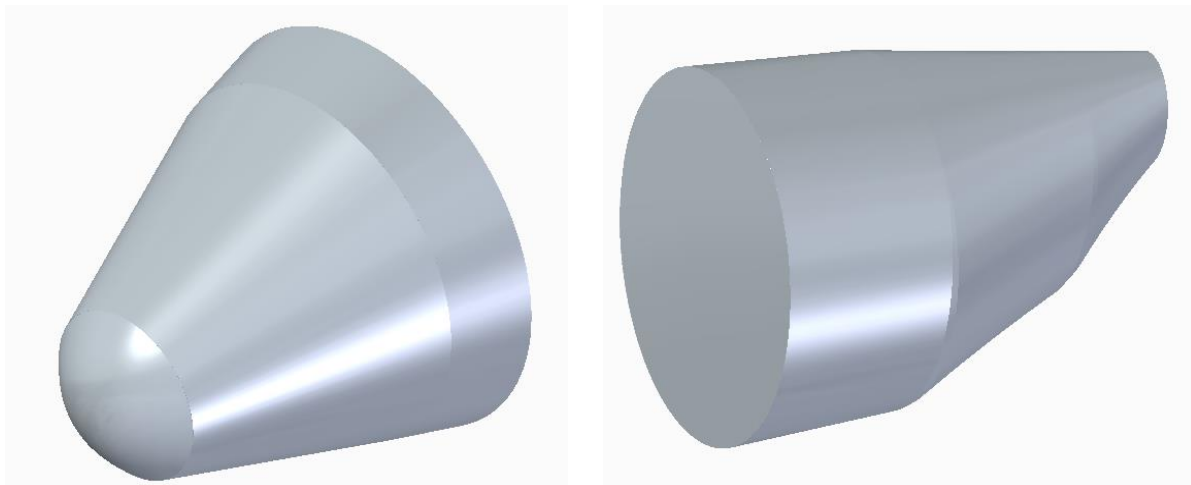


Figure 5 - Nose Cone CAD Design (Left)

Figure 6 - Alternative Empennage CAD Design (Right)

The structure of the fuselage was designed multiple times due to a change in dimensions of skin thickness, stringers and frames. This can be seen in Section 5.2.2.4 and Section 5.2.2.5. The final dimensions and designs of the stringers and frames can be seen in Table 14 and Table 19 respectively. An exterior was created for the fuselage for the assembly shown in Figure 7, Figure 8 and Figure 9. The ends of the fuselage are supported by bulkheads, not sized or demonstrated in the figures. The internal structure of the fuselage can be seen in Figure 7 and Figure 8 in cut-away form. The frames and stringers are shown to size for each separate section of the fuselage. Section 6 of the fuselage was focused on to demonstrate the number of stringers and frames required.

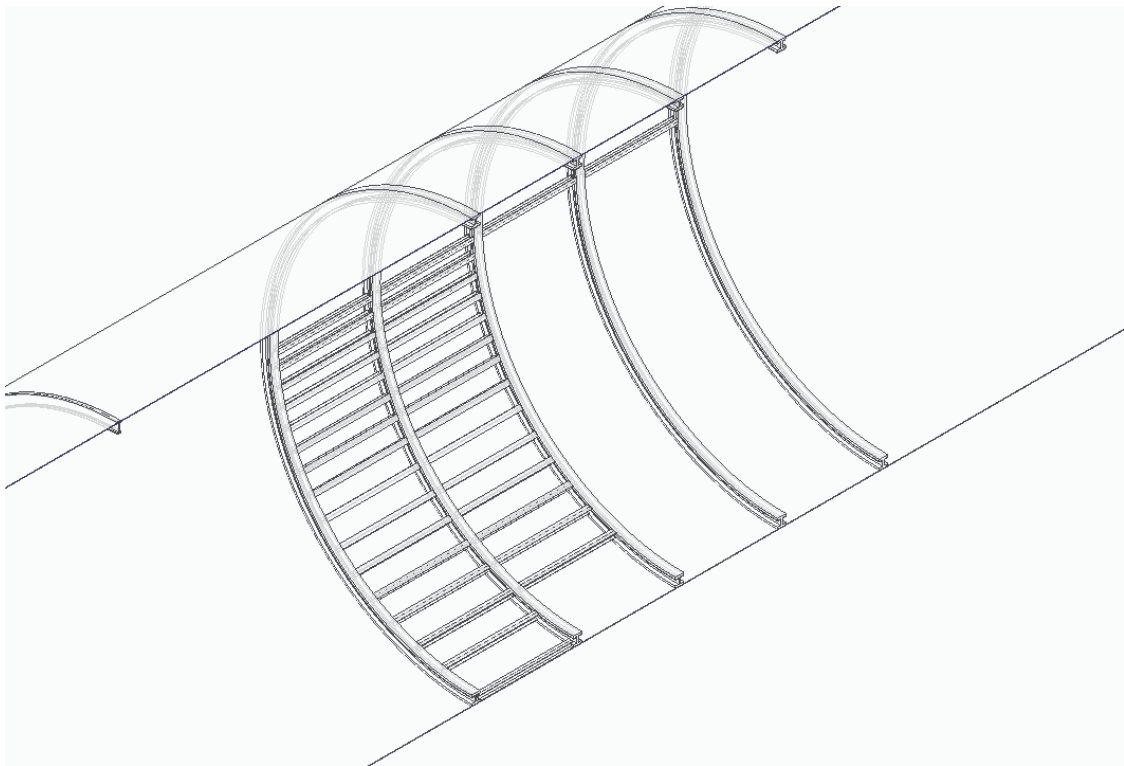


Figure 7 - Fuselage Structure Cut-Away 1

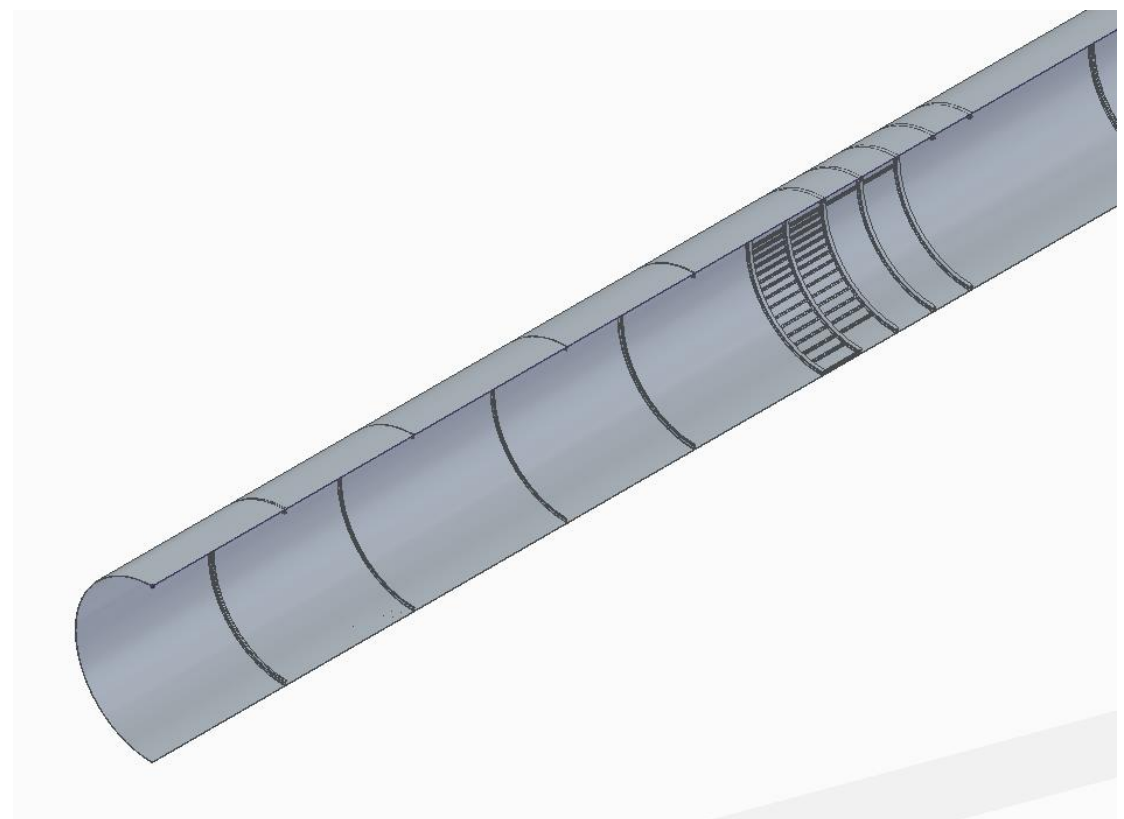


Figure 8 - Fuselage Structure Cut-Away 2



*Figure 9 - External Fuselage CAD*

### 5.2.2 Fuselage Structure – LM, KO, PS

#### 5.2.2.1 Fuselage structure – LM

The main structural components which make up the fuselage are the Skin, Bulkheads, Frames and Stringers (longerons).

The skin acts to resist the shear and pressure forces from the cabin. Stringers act in the longitudinal direction and carry the compressive and tensile forces due to the bending of the fuselage, whereas longerons are simply larger and heavier stringers that span across multiple sections. Frames are used to maintain the shape of the fuselage, reduce the length of the stringers and provide end restraints for the panels of the skin, whereas bulkheads are used to separate different sections of the aircraft where their main priority is carrying concentrated loads (Mouritz, 2012).

As proposed in the PDR, composites will be extensively used in the aircraft fuselage structure in order to minimise weight. Based on the materials QFD (Aero 5, 2018) CFRP will be used for the skin, stringers and frame. The specific composition is a M55J 6k/954-3 unidirectional tape which consists of a Toray M55J 6k, surface treated Type 5, no twist fibre in a Hexcel 954-3 matrix, with the mechanical properties indicated below in Table 11.

*Table 11 - Mechanical Properties of M55J 6k/954-3 Unidirectional Tape (DEPARTMENT OF DEFENSE, 2019)*

| Property                | Value                         |
|-------------------------|-------------------------------|
| Resin Content           | 22.3 - 24.1 wt%               |
| Fibre Volume            | 53.1 - 65.4 %                 |
| Composite Density       | 1.66 - 1.67 g/cm <sup>3</sup> |
| Lay-up                  | [0] <sub>16</sub>             |
| Tensile Strength (mean) | 320 GPa                       |
| Young's Modulus (mean)  | 47 GPa                        |

When designing the structural components of the fuselage the main focus is the stress in each component which is dictated by the allowable strain of the structure. In general for aircraft using a composite structure the allowable strain is between 3000 and 5000 $\mu\epsilon$  (Wencheng, 2011). As the CFRP composite was only tested between 1000-3000 $\mu\epsilon$  therefore the allowable strain that Aero 5 will conform to will be 3000 $\mu\epsilon$  as extrapolating the composite materials properties could prove unreliable.

### 5.2.2.2 Pressurisation – LM

Large commercial aircraft are pressurised twice per flight in order to allow for passenger comfort at high altitudes. In order to obtain a first estimate for the skin thickness of the aircraft, the pressurisation case was analysed.

The pressurisation stress was assumed to be taken fully by the skin in order to calculate an initial skin thickness. As the fuselage is cylindrical in design, then the maximum stress that the fuselage will be subject due to pressurisation will be the hoop stress. The equation linking the hoop stress to the thickness is detailed below.

$$\sigma_H = \frac{Pd}{2t} \quad (5)$$

In Equation (5)  $P$  indicates the difference in pressure across the fuselage at cruise altitude which came out to be 56.6kPa;  $d$  is the fuselage diameter which was 4.37m and  $t$  is the thickness which is to be calculated. The hoop stress  $\sigma_H$  was determined from the allowable strain of  $3000\mu\epsilon$  which, based on the material properties of the CFRP composite gave 141MPa, which was then divided by a factor of safety of 1.5 (as described by CS 25.303) to obtain the maximum allowable hoop stress of 94MPa. Equation (5) was manipulated to make  $t$  the subject which yielded an initial thickness of 1.32mm. This appears to be an appropriate initial estimate as for a narrow-body pressurised thin aircraft; the fuselage skin thickness typically ranges from 1-1.6mm (Lindeman 2006, ARFF website 2006).

### 5.2.2.3 Load Case – LM

As Aero 5 have opted for one constant structural layout that encompasses both cabin layouts to allow for ease of repair, it is therefore known that the heavier aircraft (i.e. the 240 passenger configuration) will acquire higher bending and shear loads, and therefore the structural analysis has been based off the load cases for this aircraft.

The fuselage was analysed as two separate cantilever beams supported by the frames that take the main load from the wing, one in the direction of the nose and the other in the tail direction. The fuselage was then split into smaller sections and it was assumed that all the loads in each section act as one point load in the centre of the section. The way in which the aircraft is split up is indicated below in Figure 10.

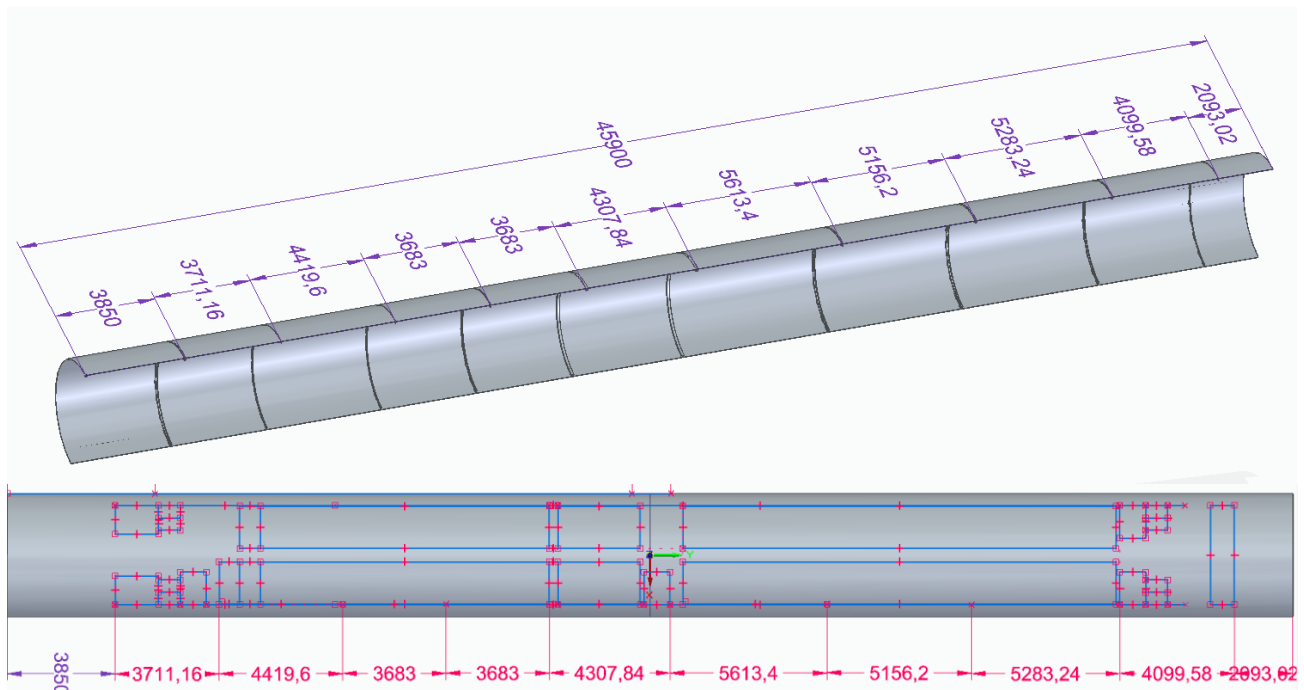


Figure 10 (a and b) - Aircraft Sections used for BMD and SFD, shown on a Fuselage Cut-Away and on Fuselage Plan View Respectively (KO)

The total mass of each section and their constituent components and respective masses can be seen in Appendix 13.5.1 where the mass of the nose has been approximated using length and mass ratios for Aero 5's main competitor aircraft, the Airbus A321 (Airbus, 2019), leading to a nose mass of 10.7 tonnes. The mass of the empennage was approximated using the same process which gave a mass of 16.7 tonnes. Another key assumption was that there is enough toilet rinse for each passenger to go toilet twice, split between four lavatories which meant that each toilet had half the maximum toilet rinse for 240 passengers. Also, it was

assumed, based off the Customer Design Brief (CDB), that the mass of a passenger included their baggage mass at each point. The nose gear was assumed to have a mass equal to half the mass of the main landing gear which is 4.5% of the WMTOW (Kundu, 2010) leading to a mass of 954kg. This approach does not include any structural supports as the masses and geometries are yet to be found and hence this process will be iterative. The initial bending moment diagram can be seen in Appendix 13.5.2.

This bending moment diagram indicates the magnitude of various bending moments that the aircraft will experience during flight, with the negative sign indicating a counter-clockwise bending direction for the first cantilever beam (from the nose to the A.C) and a clockwise bending moment direction for the second cantilever beam (from the A.C to the tail).

Appendix 13.5.2 then allows the understanding of the maximum bending moment occurring in each fuselage section, such that the stringers can be sized for each individual section. This optimises the structural stability for each section whilst still keeping the weight to a minimum.

A shear force diagram was created to assist with the optimisation of the frame geometry which used the same cantilever analysis and can be seen in Appendix 13.5.3.

The main assumption in the shear force diagram is that the shear force is constant in each section which can be seen by the various zero gradient sections. This assisted in the calculation of the frame geometry. The maximum shear occurred in section seven which is reasonable as this is where the shear load from the wing comes into the fuselage.

#### 5.2.2.4 Fuselage Stringer Design and Lay-Up – LM

The stringer geometry, location and amount was determined such that it could carry the tensile and compressive forces acting on the aircraft throughout the flight path and to resist buckling along with the skin.

Four stringer designs were compared and contrasted to find out which one would be optimal for the Aero 5 design by using a QFD matrix with ranked requirements. The stringer requirements are seen below in Table 12 where the most important requirements were chosen to be ‘fail-safe’ which is related to the way in which the stringers are attached to the panels, and ‘structural efficiency’. ‘Cost of manufacture’ was thought to be of the least importance, as with respect to the total cost of the aircraft, changes in stringer cost are minimal. Furthermore, a more resistant and redundant design could reduce maintenance costs despite being more expensive as an initial investment. The Stringer types were rated high, medium or low (H, M, L) based on how well they fit the criteria.

*Table 12 - Comparison of Different Stringer Types (Kaur, 2014)*

| Properties                 | Importance | Stringer Type |        |        |        |
|----------------------------|------------|---------------|--------|--------|--------|
|                            |            | J             | -      | Hat    | N      |
| Structural Efficiency      | 4          | H             | M      | M      | H      |
| Low Cost of Manufacture    | 1          | L             | H      | L      | H      |
| Corrosion Resistance       | 3          | M             | M      | L      | M      |
| Ease of Assembly           | 3          | M             | L      | L      | H      |
| Fail-safe                  | 5          | H             | H      | H      | M      |
| Total                      |            | 100           | 78     | 64     | 96     |
| Relative Weight (Priority) |            | 29.59%        | 23.08% | 18.93% | 28.40% |

From the ‘Relative Weight’ it can be seen that the most suitable stringer design for Aero 5 is the ‘J’ configuration, mainly due to its effectiveness at joining panels and its high second moment of area.

Next, a set amount of stringers needed to be chosen which was based off historical data. A generic stringer pitch for commercial aircraft is usually in the range of 150-250mm (EASA, 2012) with the only publicly available stringer spacing for a composite commercial aircraft being the Boeing 787 with a larger fuselage diameter of 5.77m (Wide-body aircraft, 2011). Each barrel section contains 80 stringers (Ostrower, 2009) which produced a stringer pitch of roughly 227mm. As this aircraft is much larger in size and weight it was

thought that a suitable stringer pitch of 230mm would be used for Aero 5. This gives Aero 5 60 stringers per frame which can be seen below in Figure 11.

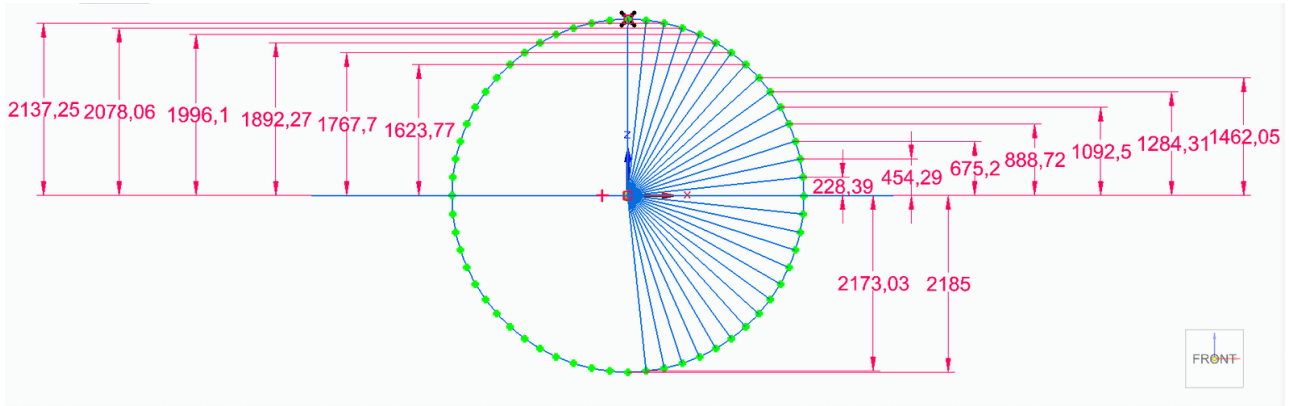


Figure 11 - Stringer locations along the fuselage cross-section (KO)

The stringer locations shown in Figure 11 formed the basis for the stiffened skin and boom idealisation which was used to calculate the area needed for each stringer in each fuselage section to maintain the maximum bending moment in that section.

The direct stress in each stringer is related to the bending moments produced by Equation (6).

$$\sigma_z = \frac{M_x}{I_{xx}} y \quad (6)$$

Where  $\sigma_z$  is the direct stress in the stringer,  $M_x$  is the bending moment producing the direct stress,  $I_{xx}$  is the total second moment of inertia of the section and  $y$  is the vertical distance from the stringer to the centroid.

$I_{xx}$  of Figure 11 was found using Equation (7) below, which came out to be  $173\text{Bm}^4$ , where  $B$  indicates the boom area.

$$I_{xx} = \sum B_i y_i^2 \quad (7)$$

From Equation (6) it was deduced that the boom containing the maximum direct stress was located furthest from the centroid ( $\pm 2.185\text{m}$ ). Therefore, the maximum direct stress in each section is shown in Appendix 13.5.4 along with the necessary boom area to withstand the maximum stress in each section which was calculated using Equation (6).

The allowable stress in the section was dictated by the material properties of M55J 6k/954-3 unidirectional tape which includes the 1.5 factor of safety. Then by equating the maximum stress in the section as a function of  $B$  to the allowable stress allows the calculation of the Boom areas above.

It is understood that one of the most prevalent modes of failure of a stringer is failure by buckling, therefore a buckling analysis was undertaken for the stringers in each section to find out the appropriate length before buckling can occur. This gave an indication to the frame spacing and in turn the quantity of frames needed for the total fuselage section.

Euler's buckling formula is detailed in Equation (8).

$$P_{cr} = \frac{\pi^2 EI}{L^2} \quad (8)$$

Where  $P_{cr}$  is the critical load. However, for this calculation it was substituted in as the maximum load experienced in the respective sections multiplied by the 1.5 factor of safety,  $E$  is the materials Young's modulus,  $I$  is the lowest second moment of area of the beam (as it will fail in that direction first) and  $L$  is the beams effective length, which will be equal to  $2L$  as the beam is supported on both ends via a fixed support. Each individual stringer had to be sized at this point to obtain the  $I_{xx}$  and  $I_{yy}$  values, this was done on an Excel spreadsheet by picking a suitable thickness which ranged from 1mm for the smallest stringer to 4.5mm for the largest stringer and then setting the flange width, web height and crown width to be a function of  $x$  which were three, five and one respectively. Equation (8) was then rearranged to make  $L$  the subject to find the

appropriate length of the stringers before buckling occurs for each section. The lengths obtained are indicated in the Appendix 13.5.5.

Sections 1 and 11 represent the nose and empennage sections respectively and hence are not designed, so these results are already incorporated in the previous assumptions of the nose and empennage mass and the rest will be used to update the fidelity of the bending moment diagram.

This information was used to obtain the stringers mass which then updated Appendix 13.5.1. Furthermore, this gave information on how many frames were needed per section (by dividing the section length by the buckling length of the stringer) which came out to be; 16 frames in section two, 14 frames in section three, nine frames in section four, seven frames in section five, six frames in section 6, eight frames in section 7, nine frames in section 8, 11 frames in section 9 and 11 frames in section 10. Taking into account the overlapping frames, this produced a total of 84 frames from the nose to the empennage section which on average is a frame pitch of 481mm which fits in well with current aircraft which have frame pitches in the range 457.2mm – 533.4mm (EASA, 2012).

This point marks the end of the initial estimates, where the masses of the stringers were added to their relevant fuselage sections and then the whole process was iterated again to include the structural mass of the stringers in the process to determine the finalised parameters such as stringer sizing, stringer length and frame pitch.

After the introduction of the stringer masses to the fuselage sections, this produced the bending moment diagram and shear force diagram below.

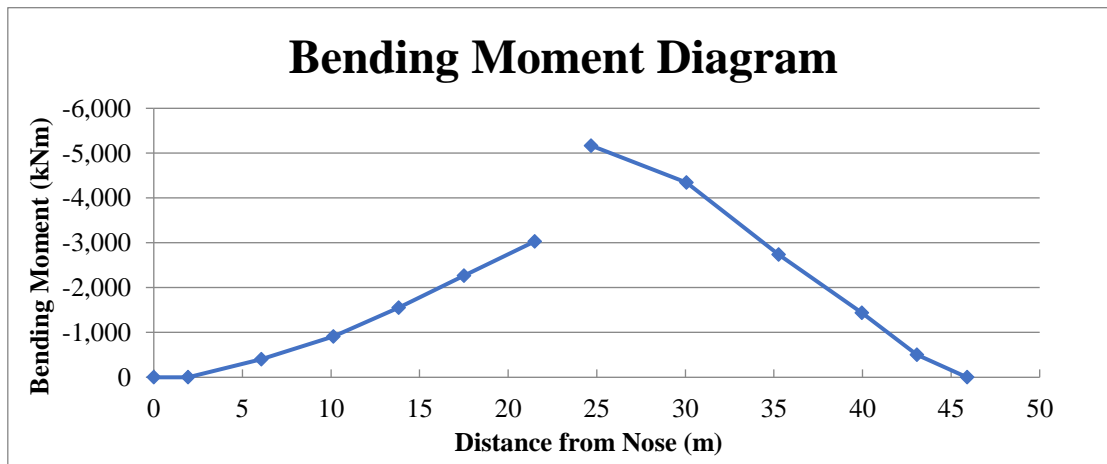


Figure 12 - Updated Bending Moment Diagram (Including Structural Masses)

The bending moment diagram remained largely the same, except the maximum bending moment increased by approximately 60kNm at the frame support for the rear cantilever section (section seven). This is reasonable as this is where the heaviest stringers are located. The updated shear force diagram can be seen below where the maximum increase in shear force can also be seen in section seven and increased by approximately 10kN which is roughly a 3% increase.

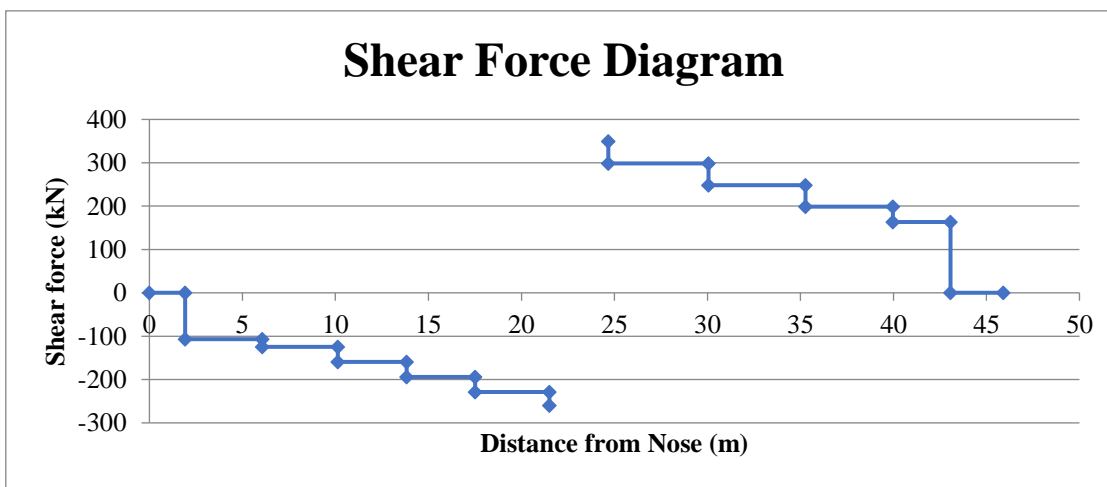


Figure 13 - Updated Shear Force Diagram (Including Structural Masses)

Then using Figure 12 and Equation (6) the new boom areas have been updated per section and can be seen below in Table 13.

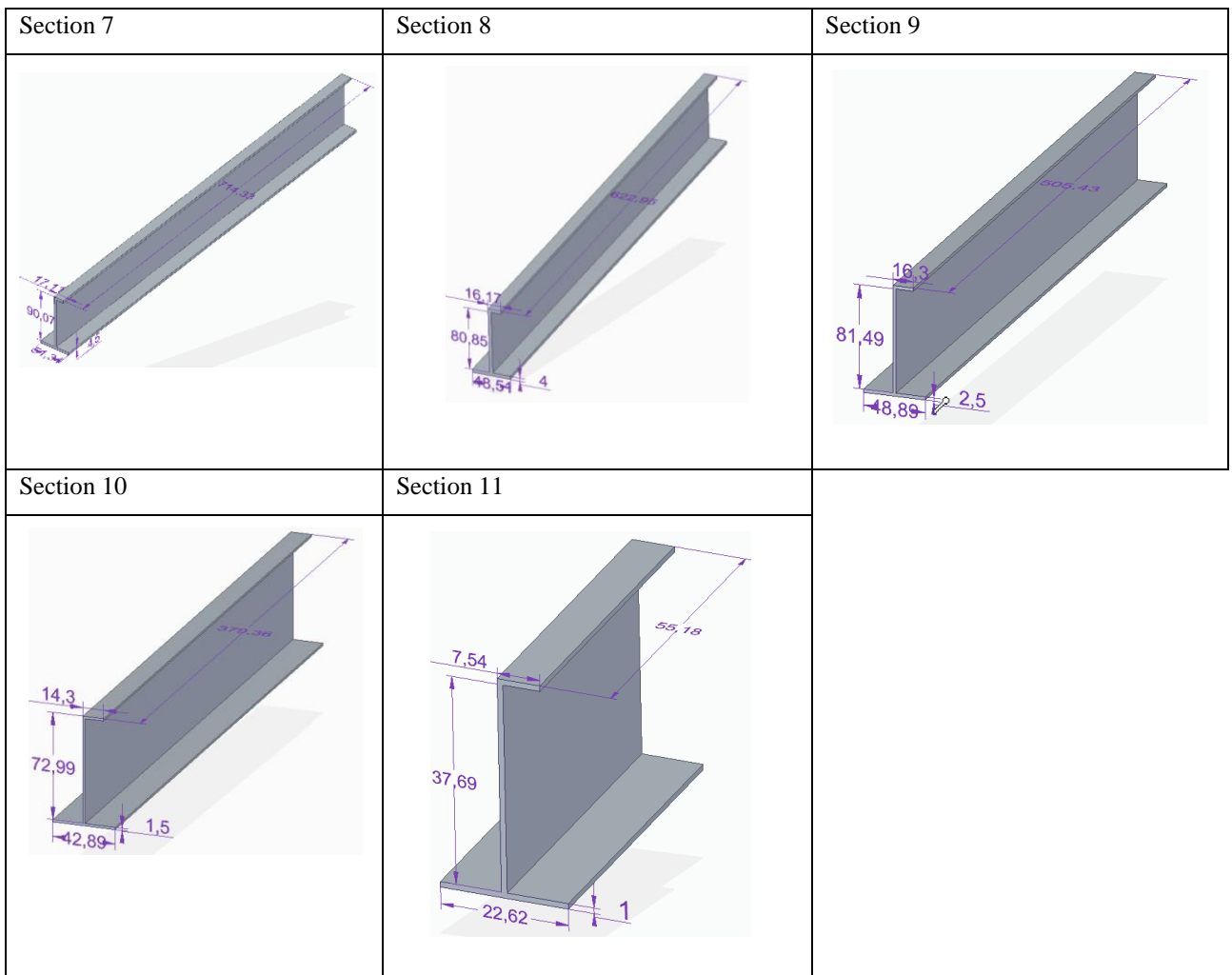
Table 13 - Updated Boom Areas of Each Section

| Section | $\pm$ Max y (m) | Total $I_{xx}$ ( $m^4$ ) | Max $M(x)$ (kNm) | $\pm$ Max Stress (MPa) | Allowable stress (MPa) | Boom area, B ( $mm^2$ ) |
|---------|-----------------|--------------------------|------------------|------------------------|------------------------|-------------------------|
| 1       | 2.19            | 173B                     | -205             | -2590/B                | 94.0                   | 27.0                    |
| 2       | 2.19            | 173B                     | -634             | -7990/B                | 94.0                   | 85.0                    |
| 3       | 2.19            | 173B                     | -1260            | -15900/B               | 94.0                   | 169                     |
| 4       | 2.19            | 173B                     | -1910            | -24100/B               | 94.0                   | 256                     |
| 5       | 2.19            | 173B                     | -2690            | -33900/B               | 94.0                   | 361                     |
| 6       | 2.19            | 173B                     | -3410            | -43000/B               | 94.0                   | 457                     |
| 7       | 2.19            | 173B                     | -5170            | -65200/B               | 94.0                   | 693                     |
| 8       | 2.19            | 173B                     | -4340            | -54700/B               | 94.0                   | 582                     |
| 9       | 2.19            | 173B                     | -2740            | -34500/B               | 94.0                   | 367                     |
| 10      | 2.19            | 173B                     | -1440            | -18100/B               | 94.0                   | 193                     |
| 11      | 2.19            | 173B                     | -506             | -6380/B                | 94.0                   | 68.0                    |

The boom areas can be seen to increase slightly in the more highly stressed regions, in and around section seven. These were then used to size the stringer geometry based on the method outlined previously. The largest change in stringer area is  $9mm^2$  which occurred in section seven and produced a 1.3% change which is minuscule and therefore the process does not need to be iterated through again. The final stringer sizing per section can be seen below.

Table 14 - Stringer Dimensions (KO)

|           |           |           |
|-----------|-----------|-----------|
| Section 1 | Section 2 | Section 3 |
|           |           |           |
| Section 4 | Section 5 | Section 6 |
|           |           |           |



The buckling analysis was then completed for the updated stringer designs using Equation (8) after calculating the lowest second moment of area per section which can be seen below.

Table 15 - Updated Stringer Buckling Analysis per Section

| Section | Buckling length (mm) |
|---------|----------------------|
| 1       | 17.0                 |
| 2       | 232                  |
| 3       | 315                  |
| 4       | 439                  |
| 5       | 583                  |
| 6       | 741                  |
| 7       | 714                  |
| 8       | 622                  |
| 9       | 505                  |
| 10      | 379                  |
| 11      | 55.0                 |

By comparing Appendix 13.5.5 and Table 15, it can be seen that whilst designing some of the stringers slightly larger in cross-sectional area, this led to a very acute decrease in buckling length. Overall, neglecting section 1 and 11 for the reasons mentioned previously, this led to 16 frames in section 2, 15 frames in section 3, nine frames in section 4, seven frames in section 5, six frames in section 6, eight frames in section 7, nine frames in section 8, and 11 frames in section 9 and 10. Once again, accounting for the overlapping frames of adjacent sections, this produces 85 frames with a frame pitch of 476mm for the whole aircraft.

### 5.2.2.5 Frames – PS

The semi-monocoque fuselage structure was required to be supported by integration of transverse frames as mentioned earlier in Section 5.2.2.1. Frames are an essential structural component to hold the aerodynamic shape of the fuselage and also work against buckling of stiffeners and support the skin (Megson, 2011). At locations of concentrated loads, the frames were sized to carry the shear load from the skin and the stiffeners sized earlier would be supported longitudinally (Megson, 2011). This required the frames to be placed at the start of every new fuselage section.

To start the sizing of the frames, it was idealized that the skin of the fuselage is effective only in shear. The fuselage shell was treated as a closed cell structure to perform shear flow analysis. From Section 5.2.2.3, the shear flow distribution on the fuselage skin was calculated for each fuselage section. The second moment of area of the fuselage,  $I_{xx}$ , was calculated to be  $17.9\text{m}^4$ . Skin thickness of the fuselage to be  $0.013\text{m}$  and the shear force was assumed acting through the shear centre and substituted into Equation (13) to give the open section shear flow distribution (Viquerat and Crocombe, 2019).

$$q_s - q_{s,0} = - \left( \frac{S_x I_{xx} - S_y I_{xy}}{I_{xx} I_{yy} - I_{xy}^2} \right) \int_0^s t x \, ds - \left( \frac{S_y I_{yy} - S_x I_{xy}}{I_{xx} I_{yy} - I_{xy}^2} \right) \int_0^s t y \, ds$$

As the shear load was vertically loaded, the x axis contribution was taken out as  $S_x = 0$ . As the fuselage had a circle cross-section,  $I_{xy} = 0$ , which results in the simplification below. Where  $q_s - q_{s,0}$  is the shear flow across two points of the open cross-section,  $S_y$  is the shear force acting in the fuselage section found in Table 16 were taken from calculations carried out in Section 5.2.2.4,  $t$  is the skin thickness and  $y$  is the distance from the shear centre to the cross-section.

$$q_s - q_{s,0} = - \left( \frac{S_y}{I_{xx}} \right) \int_0^s t y \, ds \quad (9)$$

Equation (10) was used to calculate the constant shear flow contribution (Viquerat and Crocombe, 2019) hence the total shear flow acting in each fuselage section was calculated using Equation (11) (Viquerat and Crocombe, 2019).

$$q_c = \frac{-\phi \frac{q_{os}}{t} ds}{\phi \frac{ds}{t}} \quad (10)$$

$$q_s = q_{os} + q_c \quad (11)$$

The results of the shear flow distribution in each fuselage section can be found presented in Table 16.

*Table 16 - Shear Flow Distribution for each Fuselage Section of the Fuselage*

| Fuselage Sections | $S_y (\text{N})$ | $I_{xx} (\text{m}^4)$ | T (m) | s (m) | $q_{os} (\text{N/m})$ | $q_c (\text{N/m})$ | $q_s (\text{N/m})$ |
|-------------------|------------------|-----------------------|-------|-------|-----------------------|--------------------|--------------------|
| 1                 | -107000          | 17.9                  | 0.013 | 2.19  | 369                   | -169               | 200                |
| 2                 | -115000          | 17.9                  | 0.013 | 2.19  | 399                   | -182               | 216                |
| 3                 | -149000          | 17.9                  | 0.013 | 2.19  | 516                   | -236               | 280                |
| 4                 | -183000          | 17.9                  | 0.013 | 2.19  | 633                   | -290               | 343                |
| 5                 | -217000          | 17.9                  | 0.013 | 2.19  | 751                   | -344               | 407                |
| 6                 | -245000          | 17.9                  | 0.013 | 2.19  | 851                   | -389               | 462                |
| 7                 | 340000           | 17.9                  | 0.013 | 2.19  | -1180                 | 540                | -640               |
| 8                 | 293000           | 17.9                  | 0.013 | 2.19  | -1020                 | 465                | -551               |
| 9                 | 246000           | 17.9                  | 0.013 | 2.19  | -852                  | 390                | -462               |
| 10                | 198000           | 17.9                  | 0.013 | 2.19  | -687                  | 315                | -373               |
| 11                | 163000           | 17.9                  | 0.013 | 2.19  | -567                  | 259                | -307               |

Once the shear flow for each fuselage section was calculated, Equation (16) was used to calculate the shear flow transmitted to the periphery of the frames from the start of one section to the start of the next one (Megson, 2011).

$$q_f = q_1 - q_2 \quad (12)$$

Where  $q_f$  is the shear flow at the frames,  $q_1$  and  $q_2$  is the shear flow of the previous fuselage section to the next, respectively.

It was suggested by Raymer (2012), that the clearance required for the cabin aisle height and headroom should be 1.93m and 1.65m respectively. It was decided by Aero 5 that the thickness of the frames would be around 0.1m. This gives enough clearance between the fuselage skin and the interior cabin walls, which is also the value that is typical for transport aircrafts (Raymer, 2012).

Using the thickness of the frames,  $t_f$  to be 0.1m, the shear stress at the frames,  $\tau$  was calculated by  $\frac{q_f}{t_f}$ . The material of the frames was decided to be the same as the stringers due to the benefits of joining the same composite, M55J 6k/954-3 as mentioned in Section 5.2.2.1. The shear stress was divided by the allowable stress of the material to calculate the cross-sectional area of the frames in each fuselage section.

The number of frames required in each fuselage section determined the frame area and hence the dimensions required for each frame in the fuselage section. The dimensions were calculated for an I cross-section frame due to the symmetry provided by the shape.

The required area of each frame is presented in Table 17 below. It was decided by Aero 5 that for fuselage sections 1 and 11, bulkheads would be used at the start and end of the sections respectively. Fuselage section 1 to 2 represents frames from the start of section 1 to the start of section 2. For example the one frame allocated to section 1 to 2, would be placed at the start of section 2 as a bulkhead was placed at the start of section 1. Table 17 shows the cross-section dimensions of each fuselage section frame and Table 18 provides a diagram of the frame cross-section.

Table 17 - Dimensioning of Single Frames in each Fuselage Section

| Section     | $q_f$<br>(N/m) | Frame<br>Height/<br>Clearanc<br>e (m) | Shear Stress<br>$\tau$ on Frames<br>(N) | Allowable<br>Stress (N) | Cross-Section<br>Area of<br>Frames<br>(mm <sup>2</sup> ) | Number<br>of<br>Frames<br>in<br>Section | Required<br>Area of<br>Each Frame |
|-------------|----------------|---------------------------------------|---|-------------------------|--|---|-----------------------------------|
| 1 to 2      | -15.8          | 0.100                                 | -158                                    | 94000                   | 1690   | 1                                       | 1690                              |
| 2 to 3      | -63.6          | 0.100                                 | -636                                    | 94000                   | 6770   | 15                                      | 451                               |
| 3 to 4      | -63.6          | 0.100                                 | -636                                    | 94000                   | 6770   | 14                                      | 484                               |
| 4 to 5      | -63.6          | 0.100                                 | -636                                    | 94000                   | 6770   | 8                                       | 846                               |
| 5 to 6      | -54.4          | 0.100                                 | -544                                    | 94000                   | 5790   | 6                                       | 965                               |
| 6 to 7      | -179           | 0.100                                 | -1790                                   | 94000                   | 19000  | 4                                       | 4760                              |
| 7 to 8      | -89.1          | 0.100                                 | -891                                    | 94000                   | 9480   | 7                                       | 1350                              |
| 8 to 9      | -89.1          | 0.100                                 | -891                                    | 94000                   | 9480   | 8                                       | 1180                              |
| 9 to 10     | -89.1          | 0.100                                 | -891                                    | 94000                   | 9480   | 10                                      | 948                               |
| 10 to<br>11 | -65.5          | 0.100                                 | -655                                    | 94000                   | 6970   | 11                                      | 634                               |

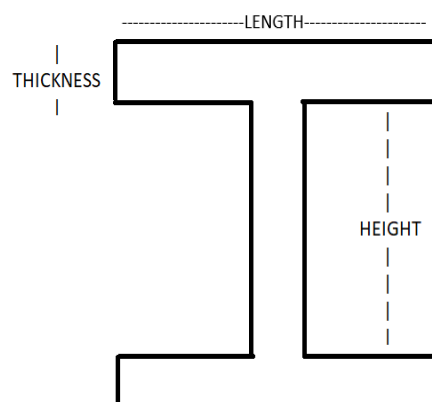


Figure 14 - Frames Cross-Section Labels

Table 18 - Cross-Section Dimensions of Frames in each Fuselage Section

| Fuselage Section | Cross-section thickness (mm) | Cross-section Height (mm) | Cross-section Length (mm) |
|------------------|------------------------------|---------------------------|---------------------------|
| 1 to 2           | 8                            | 84                        | 63.4                      |
| 2 to 3           | 5                            | 70                        | 25.0                      |
| 3 to 4           | 5                            | 70                        | 25.0                      |
| 4 to 5           | 5                            | 90                        | 39.6                      |
| 5 to 6           | 5                            | 90                        | 51.5                      |
| 6 to 7           | 20                           | 60                        | 88.7                      |
| 7 to 8           | 6                            | 88                        | 68.8                      |
| 8 to 9           | 5                            | 90                        | 73.5                      |
| 9 to 10          | 5                            | 90                        | 49.8                      |
| 10 to 11         | 5                            | 90                        | 18.4                      |

It was noted by Aero 5 that for the frames in fuselage sections 2 to 3 and 3 to 4, the frame cross-sectional areas would be larger than is required. This was decided due to the assumed frame height of 0.1m which resulted in small cross-section thickness and length. Therefore, it was decided to keep a minimum thickness of 5 mm and minimum length of 25 mm for fuselage sections 2 to 3 and 3 to 4.

Table 19 - Frame Dimensions (KO)



### **5.2.2.6 Conflicting Requirements – LM**

After the frames were sized, it was made apparent that in section 6 there was a mismatch between the total stringer height and the frame web height where the stringer attaches. Therefore, the ratio to determine the stringer heights had to be altered for section 6 to three, three, and two, which related to the flange width, web height and the crown width respectively. The thickness of the section was also increased to 3.5mm. All of this was done to make the total height of the stringer less than 6cm such that the stringer was small enough to successfully be attached to the frame web. This produced a greater  $I_{yy}$  of 63000mm<sup>4</sup>. This therefore produced a buckling length of 967mm according to Equation (8), which meant that section 6 of the fuselage would only need five frames. This reduced the total number of frames to 84 which produced a frame pitch of 481mm.

### **5.2.2.7 Further Development – LM**

Having been given more time to improve the design process, the weight of the frames would have been introduced back into Appendix 13.5.1, which would then go to update the bending moment diagram. This would have then been followed for another iteration to increase the fidelity of the model and this would continue until there was less than a 1% change in the bending moments produced for the aircraft. Furthermore, in order to better the structural design, the actual stringer cross-section design could have been developed in such a way to maximise the minimum second moment of inertia such that the buckling length could be increased, however, due to time constraints a ratio approach was used.

### **5.2.3 Fuselage Manufacture and Maintenance – KO**

It was concluded by Aero 5 in the PDR that a large percentage of the aircraft, including the fuselage would be manufactured using composite materials such as aramid fibre, glass fibre and carbon fibre reinforced plastics instead of metallic alloys. This allows for a lighter aircraft and lower fuel burn, which contributes towards the critical reduction in DOC.

Aero 5 considered two composite manufacturing techniques for the fuselage structure; a structure comprising of composite tape winding barrel sections and a structure assembled using composite panels. When finalising the assembly technique of the structure, lifecycle maintenance costs were an important factor as well as the manufacturing costs. Major maintenance considerations included the D check, also known as a heavy maintenance visit, which is a comprehensive check that inspects the entire aircraft and usually takes up to 50,000 man-hours and 2 months to complete. The cost of such a check is estimated around \$1.25-1.50 million. C checks were also considered, which is a maintenance check that requires a large majority of the aircraft's components to be inspected and usually takes up to 6,000 man-hours and at least 1-2 weeks. Being able to minimise the frequency of required maintenance checks allows the aircraft to stay in service for a longer period of time and limits time out of service, in turn promising higher revenue (Nickles, Him, Koenig, Gramopadhye, & Melloy, 2001).

The semi-monolithic structure, as seen in the Boeing 787 Dreamliner, combines an automated fibre or tape placement process with co-cured stringers to form a one-piece barrel. The stringers are combined with fibre-reinforced skin to enable a co-cured structure, and eventually interior structures are attached to the fuselage skin or the stringers. (Hale, 2006)

This manufacturing technique, which essentially optimises a large mandrel, was first used in 2009 and is therefore considered slightly dated, as well as having little room for development as the ability to upgrade materials and equipment is limited. The next significant development in this composite manufacturing technique is expected for the Boeing 797 and its rival aircraft, an upgrade of the Airbus 350.

Following historical trends, this method of manufacture means that the aircraft will not require heavy maintenance D checks until the 12<sup>th</sup> year in service, and the first base maintenance check would be 36 months after first use. This also means two fewer base checks, C checks, and one less structural check will be required.

The composite panels manufacturing technique can be currently seen in the Airbus A350 XWB aircraft, where carbon fibre composite panels are used in 53% of the overall aircraft structure, whereas titanium is used in 14% of the structure. The panels comprise of sheets, made of thin carbon threads and held by a resin, laid on top of each other and bonded in an autoclave. Usually, the outer skin panels of the fuselage, as well as the frames, are carbon fibre, with the largest panel created so far being 93.0m<sup>2</sup>. This resonates with the final material chosen by Aero 5 (Airbus Newsroom, 2011).

The supporting cross beams in the fuselage, however, are metallic. As analysed in the Aero 5 PDR document, using composites in the structure proves to be more expensive during the construction phase; mainly due to the precise engineering required when fabricating the tools to produce the parts as the composite parts are

made the correct size from the start, however this technique allows 50% fewer structural maintenance tasks to be carried out, also making the threshold for airframe checks around 12 years. (Airbus, Aircraft Characteristics: Airport and Maintenance planning A350, 2018)

The decrease in the need of maintenance checks is similar to that of the former technique, however the task would require significantly less manpower, time and tools with this technique, making each maintenance cost more economical.

### 5.2.4 Wing – Fuselage Interface – KO

Manufacturing joint requirements and wing sweep make the joint at the side of the fuselage necessary. When investigating the joints between the wings and the fuselage, two options were considered; a whole wing which connects in the middle through the fuselage, or two separate wings connecting to a central fuselage attachment point. For a better understanding of the whole wing, aircraft such as the 737-800, 737-900 and the B757 were researched. The final decision was taken based on the amount of information that was available.

When considering the whole wing configuration, there were constraints on the information available for the level of detail that was required to confidently choose this technique. It is understood that opting for this approach would have enabled higher structural stability for the wings and would be the best design in terms of resisting fatigue failure. However, this was outweighed by the case that the wing would not have been able to slide through the fuselage with the final diameter chosen in the PDR. This would mean that to accommodate for this configuration, the size of the fuselage would have to be changed, or an increase in volume according to the required shape would have to be added to at the bottom of the fuselage. This would result in an increase of the form drag calculated in the PDR and therefore a change in fuselage drag, lift estimation and their dependants. At this stage of design, the advantages of this technique are counterbalanced by the disadvantages.

Therefore, Aero 5 decided to use two separate wings and join them to the fuselage using bolts within an extruding wing box. As can be seen from Section 5.3.4, the spars of the wings will be constructed using aluminium, which allows the joints to be carried out using the techniques described by Niu (1995). Even though the skin of the fuselage is set to be manufactured using composites, the wing box, which will be slightly extruding from the fuselage and will contain the protrusions through which the wing will connect, will also be made using Aluminium. When evaluating wing root joints, it was understood that the joint should be kept short and two-row fastener joints should be used wherever possible. At the ends of the stringers, the local skin sections should be padded to reduce bearing and tension stress around the fastener holes.

The methods of joints that were analysed were all wing root fixed joints: spliced plates, tension bolts, lugs and a combination of spliced plates and tension bolts. The spliced plates method is widely used because of its light weight fail safe feature, however, are pricier than using tension bolts. Using tension bolts would mean that assembly would be slightly easier, and the wings would be easier to remove for maintenance or repair, however these are heavier than the spliced plates. A combination of both would allow for fail-safe design features and would also benefit from lower manufacturing fitness but would include both their disadvantages of being expensive and weighty.

In order to keep maintenance costs and manufacturing costs low, the lugs technique seemed appropriate. It carries the same advantages and disadvantages as the tension bolts technique, however it is widely considered for use with commercial aircraft, whereas the tension bolts method is usually more economical for military fighters. This method is summarised in Figure 15.

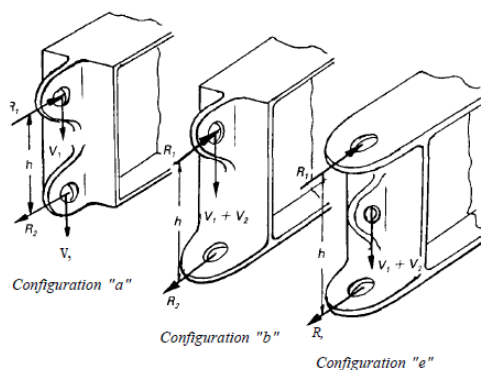


Figure 15 - Wing Lug Design and Comparison (Niu, 1995)

The connections shown are applied between the fuselage and the front spar of the wing as well as the rear spar. Each joint is attached using a typical double shear lug design (to ensure fatigue life) consisting of steel bushings, a bolt, a retainer washer and a hollow tube. Each configuration shown in the figure has various advantages and disadvantages, however Aero 5 decided to opt with the ‘e’ lug configuration due to the simplicity in installing it and as it provides a clear load distribution. In this set up, the upper and lower lugs carry axial load and the centre lug takes all of the vertical load. This allows it to produce the smallest lug load compared to the other designs. However, it can be heavy weight due to the third lug required, and it does carry the highest machining cost.

At a later design stage with a more detailed calculation, Aero 5 could analyse how many joints are required, and perform a trade-off between the methods with more in-depth considerations.

## 5.3 Wings – SH, AS, AM

### 5.3.1 Static Loading Case – SH

The structural analysis for the wing section of the proposed aircraft design uses the wing planform defined in the Preliminary Design Report (PDR) as the starting point. To sufficiently show the structural capabilities of the wing, it was modelled under a static loading and gust loading scenario, under dive speed and critical gust speeds respectively. The wing geometry was simplified to a uniform cantilever beam with a constant uniform lift distribution determined by the Maximum Take-Off Weight (MTOW) of the aircraft. Depending on the loading case, the appropriate load factor was integrated into the force model. The load factor value selected was informed by the CS-25 (EASA, 2011) regulations for the aforementioned dive and critical gust speed conditions.

The force model in each loading case had to account for the point load contributions of the engine mounting and the associated thrust loads that were decomposed into component directions. Both force modelling cases have omitted the fuel tank reservoirs as a point load since fuel mass reservoirs act as bending moment relief; alleviating the structural demands on the spar and other derivative strengthening members. As a result, the aircraft loading conditions assumed the aircraft had exhausted its fuel resources. Additionally, a point load has been implemented into the force model for the structural mass of the aircraft wing. This analytical approximation of the structural weight is rooted in the same theory employed for the mass forecast calculations in the PDR. As the force model analysis provides dimensional data, and the CAD model was being developed in parallel, an internal refinement process was introduced into the wing structural weight approximation.

Defining the aircraft dive speed from the structural flight envelope prescribed in the task specification, the dive velocity is a function of the cruise Mach speed. The succeeding step was to identify the atmospheric conditions under which the aircraft wings would be subjected to when performing a dive manoeuvre. Referring to CS 25.335 Design airspeeds (EASA, 2011), the diving flight profile is specified as ‘from an initial stable flight condition, the aircraft assumes an upset angle of 7.5° below the initial flight stable flight path at cruise’. Therefore, under the presumption that the aircraft was to begin a dive manoeuvre initiating at cruise altitude and lasting for the entire duration of the 1<sup>st</sup> step-down descent flight profile specified in the task specification extending to ISA sea level conditions; which would identify the upper limitations and capabilities of the design. This allows for clear safety margins to be identified. Using the precursory competitive aircraft design assumptions in the aircraft sizing process introduced in the PDR, a new thrust value was determined under the prescribed conditions.

$$\left(\frac{L}{D}\right)_{max} = \left(\frac{C_L}{C_D}\right)_{max} = \frac{1}{2} \sqrt{\frac{\pi AR}{k_1 C_{D0}}} = 20 \quad (13)$$

$$C_D = \frac{C_L}{20} : D = \frac{1}{2} * \rho * V_D^2 * S_w * C_D \quad (14)$$

$$\frac{D}{2} = P: Psin(\alpha) \quad (15)$$

Equations (13) and (14) were used to calculate the thrust requirement for the dive speed manoeuvre. The drag was then split in half and its vector components identified with Equation (15) corresponding to the vertical thrust contribution for a singular engine. The values for the variables in the equations were extracted from the aircraft sizing and refinement cycles used in the PDR.

Constructing the force model diagram, began with using the aerofoil cross-section, the lift force positioned at the aerodynamic centre (AC), and the engine and wing structural mass point loads were assumed to be perfectly positioned on the aerofoil AC. In addition to this, the aerofoil was orientated at an upset angle of  $7.5^\circ$  as prescribed in the CS-25 (EASA, 2011) requirements for dive-speed conditions. Consequently, the thrust vector at this angle has directional components that need to be accounted for in the point load modelling case. For the wing loading case, these were the following point load cases, the engine, thrust contribution, wing structural mass and the lift distribution. It is worth noting that the initial wing structural mass was derived from the mass forecast calculation based on the Torenbeek 88 method (HOOU, 2019) which can be reviewed in PDR Section 4.4. Proceeding from here, the aerofoil cross-section was extrapolated into a uniform cantilever beam, with total thickness equalling the average thickness of the wing planforms root and tip chord dimensions. In addition to this, the cantilever beam was attached with fixed wall support at the root-chord; simulating wing-fuselage section connection. In theory, the lift distribution on the wing geometry should be portrayed as an elliptical distribution, with larger magnitudes of force further inboard the wing. However, the static and gust loading analysis was conducted under the assumption that the wing geometry was subjected to a uniform lift distribution.

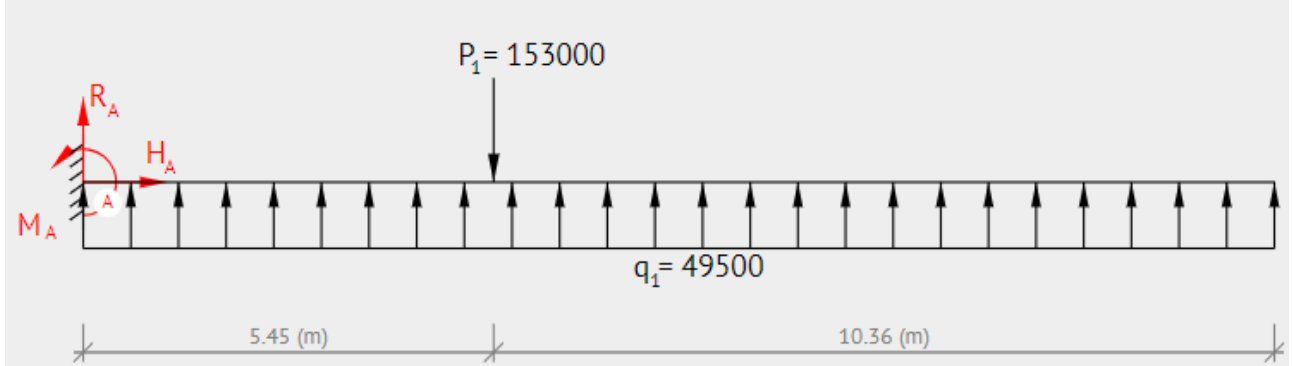


Figure 16 - Static Loading Cantilever Beam Force Balance Diagram

Figure 16 illustrates the cantilever beam for the static loading scenario where  $P_1$  is the combined point load accounting for the engine, thrust and structural mass contributions in Newtons ( $N$ ) positioned  $5.45\text{ (m)}$  from the root chord; which is the aerodynamic centre in the spanwise direction. The lift distribution given by  $q_1$ , was determined by the aircraft operating at its MTOW weight with an additional 1.5 load factor. At the root chord, reactional forces are attached with subscript A, the vertical and horizontal reaction forces are labelled  $R_A$  and  $H_A$  respectively. Finally, the bending moment reaction at the root chord is given as  $M_A$ . A conventional axis system was adopted, with vertical and horizontal forces being positive up and to the right of the axis origin (point A), and moments being positive in the anti-clockwise direction.

Table 20 - Summary of Static Loading Force Balance

| Force or Moment                      | Magnitude | Direction             | Units |
|--------------------------------------|-----------|-----------------------|-------|
| $q_1$ (Lift Distribution)            | 4.95E+04  | Positive              | N/m   |
| $P_1$ (Point Load Contribution)      | 1.53E+05  | Negative              | N     |
| $R_A$ (Fuselage Fixed Support)       | 6.30E+05  | Negative              | N     |
| $H_A$ (Horizontal Force)             | 0.00E+00  | Positive              | N     |
| $M_A$ (Fixed Support Bending Moment) | 5.36E+06  | Negative (Clock Wise) | Nm    |

Equation (16) through (21) divides the cantilever beam into two sections where shear and moment balance equations were derived. These equations were translated into Excel as functions to produce graphical plots for quantities of interest (shear & bending moment).

$$\Sigma F_y = 0: R_A + q_1 * 15.815 - P_1 \quad (16)$$

$$\Sigma M_A = 0: R_A + q_1 * 15.815 - P_1 \quad (17)$$

$$0 \leq x_1 < 5.45$$

$$\Sigma F_y = 0: Q(x_1) = -R_A + q_1 * (x_1 - 0) \quad (18)$$

$$\Sigma M_A = 0: M_X - R_A * (x_1) + M_A + q_1 * \left(\frac{x_1^2}{2}\right) \quad (19)$$

$$5.45 \leq x_2 < 15.815$$

$$\Sigma F_y = 0: Q(x_2) = -R_A + q_1 * (x_2 - 0) - P_1 \quad (20)$$

$$\Sigma M_A = 0: M_x = -R_A * (x_2) + M_A + q_1 * \left(\frac{x_1^2}{2}\right) - P_1 * (x_2 - 5.45) \quad (21)$$

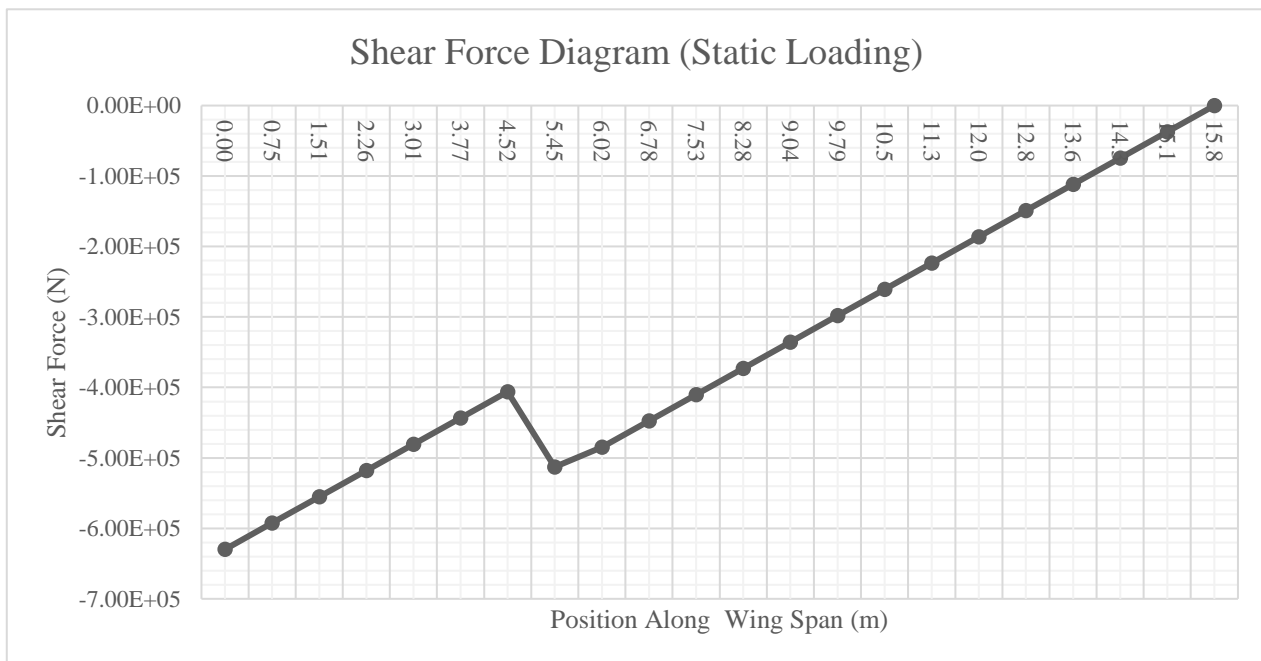


Figure 17 - Shear Force Diagram for Static Loading Case

Figure 17 supports the theoretical model and returns the largest shear force at the wing root chord with a magnitude of approximately 630kN. The graph exhibits a linear relationship as the shear force decreases at a set gradient. However, at the point load position, it was observed, a sharp increase in the shear force loading before returning to a new linear relationship. This was as expected, since the point load amassed the contributions from factors such as the engine, and consequently endures a predictable increase in shear loading.

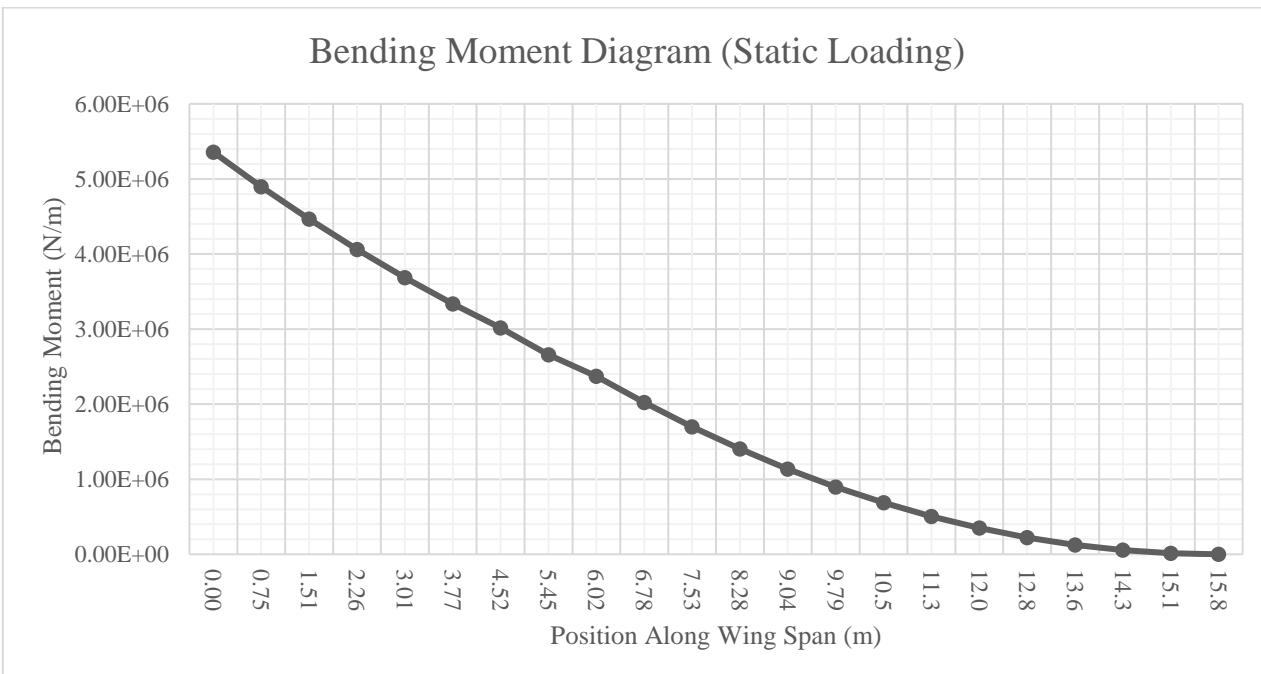


Figure 18 - Bending Moment Diagram for Static Loading Case

### 5.3.2 Gust Loading Case – SH

The atmospheric conditions under which the gust load analysis was conducted is assumed to be one dimensional with gust velocities ‘acting normal (either vertically or laterally) to the direction of aeroplane travel’. As described in CS 25 AMC 25.341 (EASA, 2011). Therefore, the one-dimensional assumption constrains the instantaneous vertical or lateral gust velocities to be equal at all points in planes normal to the direction of the aircraft travel path. The initial conditions for the following analysis will be based upon the Aero 5 aircraft operating at its cruising altitude and then instantaneously moving at its stall speed before penetrating a certain distance into the gust zone. To calculate the upper limit of the impact of gust velocities, the critical/maximum gust speed had to be solved for using the equation:

$$U_{ds} = U_{ref} F_g \left( \frac{H}{350} \right)^{\frac{1}{6}} \quad (22)$$

Where  $U_{ref}$  is a prescribed reference gust velocity found under CS 25.337 (5)(i) (EASA, 2011),  $H$  is the gust gradient distance and is a measure of how much the gust velocity increases up to its peak value against the distance. The flight profile alleviation factor  $F_g$ , quantifies the turbulence intensity as a function of altitude. This had to be separately determined by the following formula:

$$F_g = \frac{1}{2} * (F_{gz} + F_{gm}) \quad (23)$$

The flight alleviation factor is a function of  $F_{gz}$  and  $F_{gm}$  which are dependant on the maximum operating altitude and certain aircraft mass/fuel ratios. More detail can be found under CS 25.341 (a)(6) (EASA, 2011). Equations (22) and (23) together returned the maximum gust velocity ( $U_{ds}$ ) for a given  $H$ .

Using Equation (22) the maximum/critical gust velocity was found and transferred into the force modelling diagram. From here, the deflection in angle of attack from the regular flight path was calculated by using the inverse tangent function of the horizontal stall velocity and assumed perfectly vertical max gust velocity,  $U_{ds}$ . A new engine limit point load was calculated using Equation (24) (CS 25.341 (c)(2) (EASA, 2011) which would be used for updating the force model diagram (Figure 16) for a gust load version.

$$P_L = P_{L-1g} \pm 0.85\sqrt{(L_{Vi}^2 + L_{Li}^2)} \quad (24)$$

Equation (25) provides the maximum engine loads for a pair of discrete gusts acting vertically and laterally. The engine limit load,  $P_L$  is a function of its load factor at 1g ( $P_L$ ) and the sum of the square root of the peak incremental response loads squared for vertical and horizontal gust,  $L_{Vi}$  and  $L_{Li}$ . For the maximum/critical gust speed case, both the vertical and lateral incremental responses were assumed to equal in magnitude to  $U_{ds,Max}$ . Using a similar process described in the static loading case and using variations of Equation (16) to (21), the following graphs were produced:

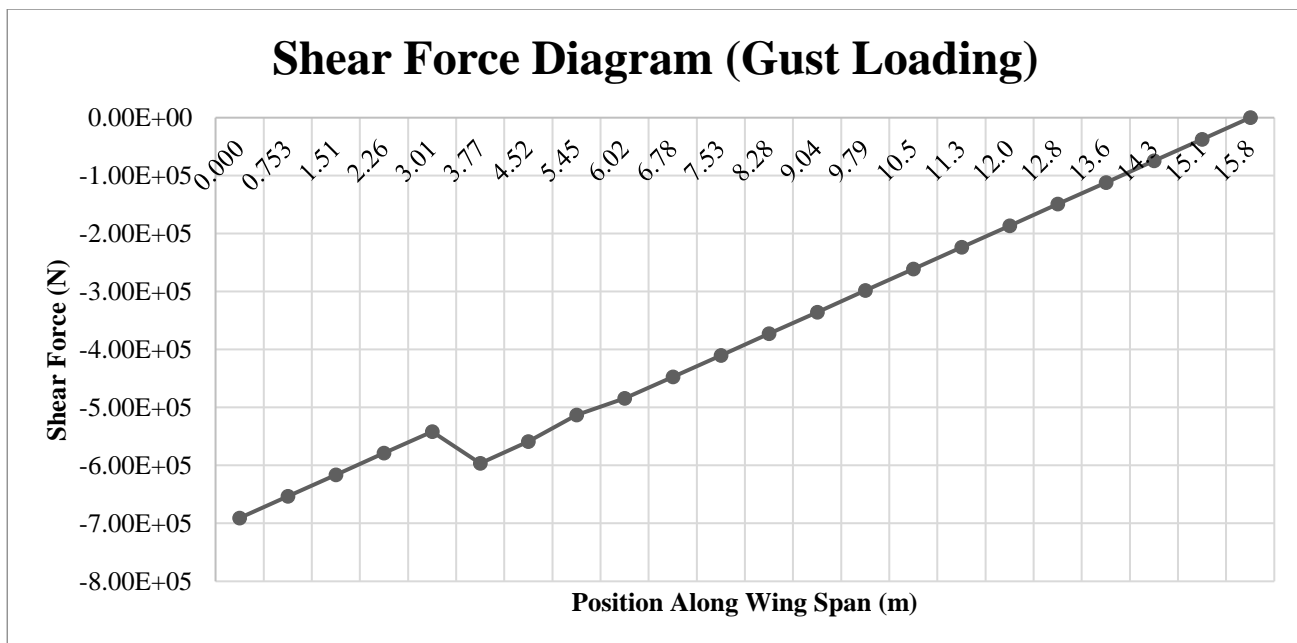


Figure 19 - Shear Force Diagram for Gust Loading Case

## Bending Moment Diagram (Gust Loading)

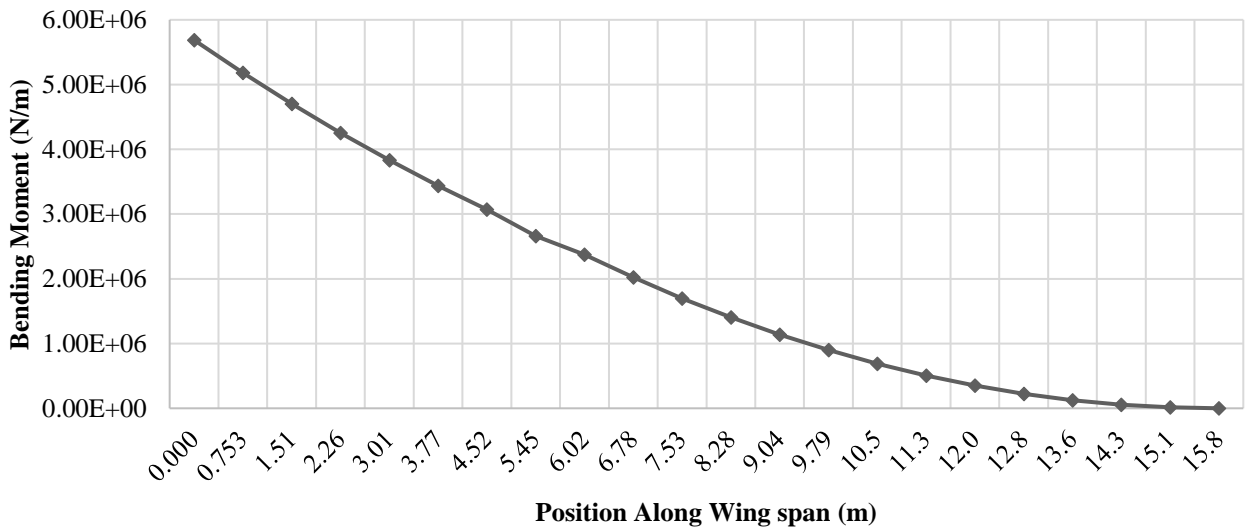


Figure 20 - Bending Moment Diagram for Gust Load Case

By identifying the critical point load acting on the engine, this analysis was later assimilated into the aircraft rib sizing analysis which is in the latter part of this technical write up. Being conscious of the fact that during gust load conditions, the ribs to which the engine will be mounted to will have to be considerably stronger to safely tolerate the greater loads under gusty/turbulent conditions. By relating the engine point load position assumed in the force modelling diagrams, the affiliated ribs across the wingspan were reviewed against the engine limit point load. Further detail is elaborated on in the separate rib analysis, but in summary ribs 7 & 8 were situated in closest proximity to the engine mounting positioning, so they were analytically tested to verify their structural integrity for the gust loading case. The following table revealed that using an Aluminium alloy proved unsuitable for the engine mounting at larger load factors, so a Titanium alloy more resistant to yielding had to be used for 2 of the ribs per wing.

Table 21 - Limit Point Load Safety Factor for Rib Mounting

| Load factor, n (g) | Limit Point Load, PL (N) | Stress on RIB 7 (MPa) | Stress on RIB 8 (MPa) | SF Al 2024-T4 (RIB 7) | SF Al 2024-T4 (RIB 8) | SF Ti-6Al-4V (RIB 7) | SF Ti-6Al-4V (RIB 8) |
|--------------------|--------------------------|-----------------------|-----------------------|-----------------------|-----------------------|----------------------|----------------------|
| 1                  | 9.22E+04                 | 73.2                  | 76.2                  | 4.43                  | 4.25                  | 11.75                | 11.28                |
| 1.5                | 1.38E+05                 | 110                   | 114                   | 2.96                  | 2.84                  | 7.85                 | 7.53                 |
| 2                  | 1.84E+05                 | 146                   | 152                   | 2.22                  | 2.13                  | 5.89                 | 5.66                 |
| 2.5                | 2.30E+05                 | 182                   | 190                   | 1.78                  | 1.71                  | 4.71                 | 4.53                 |
| 3                  | 2.76E+05                 | 219                   | 228                   | 1.48                  | 1.42                  | 3.93                 | 3.77                 |
| 3.5                | 3.22E+05                 | 255                   | 266                   | 1.27                  | 1.22                  | 3.37                 | 3.23                 |
| 3.6                | 3.31E+05                 | 263                   | 273                   | 1.23                  | 1.18                  | 3.28                 | 3.15                 |
| 3.7                | 3.40E+05                 | 270                   | 281                   | 1.20                  | 1.15                  | 3.19                 | 3.06                 |
| 3.8                | 3.49E+05                 | 277                   | 289                   | 1.17                  | 1.12                  | 3.10                 | 2.98                 |

The ribs have been certified for the positive limit manoeuvring load factors for the range  $2.5 < n < 3.8$  referenced from CS 25.337 (b) (EASA, 2011). The red cells in the table indicate the failure of the Aluminium alloy to provide a minimum SF of 1.5, hence the justification of a Titanium alloy, Ti-6AL-4V (Appendix 13.6) for ribs 7 and 8. The remainder of the rib material selection is discussed in the rib analysis section of this write-up.

Additionally, to analytically determine the expected behaviour of the Aero 5 aircraft in gust zones, the gust shape/velocity,  $U$  was determined across the whole spectrum of the gust penetration zone described in CS 25 AMC 25.341 (EASA, 2011) for cruising altitude from Equation (25).

$$U = \frac{U_{ds}}{2} [1 - \cos(\frac{\pi s}{H})] \quad (25)$$

The equations were formulated into a spreadsheet, and Figure 21 describes the (1-cosine) Design Gust Velocity Profiles that the proposed aircraft design can expect. This graph acts as an advisory piece of content that can be used to inform the aircraft piloting crew and quantifies the typical operational boundaries under normal aircraft operation.

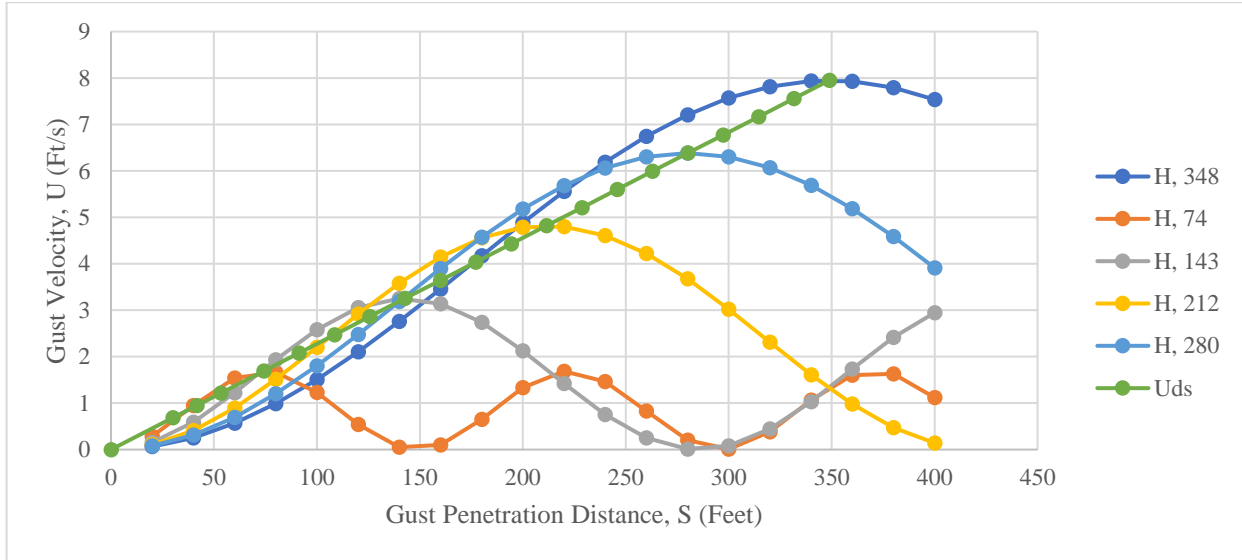


Figure 21 - Design Gust Velocity Profiles

### 5.3.3 Wing Structure Overview – AS

#### 5.3.3.1 Spars and Ribs – AS

Spars are the main structural foundation and attachment point for sub structural members. They are secured by bolts between the wing box and fuselage section and are responsible for resisting bending and axial loads longitudinally. The spars provide stability and overcome torsional forces.

Spars act as an attachment, that works in tandem with the ribs to support heavy point load installations such as the engine mounting (pylon), high-lift devices, spoilers and landing gear, whilst also supporting the ribs. Consequently, the spars carry the maximum bending moment at the wing root caused by the lift forces and point load contributions.

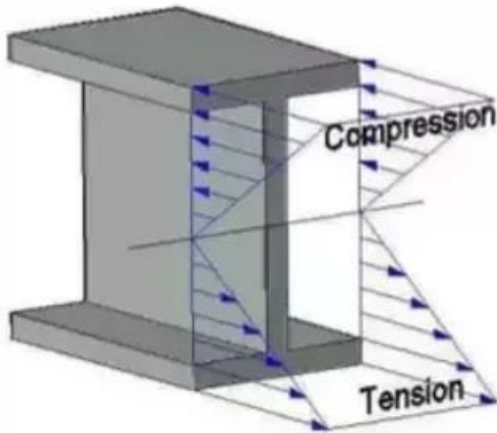


Figure 22 - I-Beam Stress Distribution (Tiwary, 2018)

An I-Beam has been chosen because it resists bending stress according to the uniaxial stress distribution between tension and compression, as shown in Figure 22. From the neutral axis point the maximum stress occurs at the top of the flange width and decreases as it moves towards the neutral axis. This indicates that the I-Beam has a well-balanced stress distribution.

In the longitudinal axis, ribs play the role of forming the shape of the aerofoil section for aerodynamic performance efficiency, since the aerodynamic force transfer starts from the skin and is transmitted to the ribs and consequently the spars.

### 5.3.3.2 Stringers – AS

The stringer's role is to primarily fasten the skin segments. It tends to divide the skin into small partial panels to decrease its buckling and compressive failure against the direct stress. Stringers also prevent crack growth from the tensile loads.

A T-Beam profile was chosen due to advantages based on the specific position on the wing, which is located in the internal structure to resist bending and axial load with the skin. In this case, the flanges take up the compressive stresses to resist sagging moments.

It is also effective to fasten and support the skin against the applied bending and axial load acting on it. Moreover, there is a maintenance benefit for stringer corrosion checks, as corrosion becomes easier to identify on the spar web and the bottom part of the flange.

### 5.3.3.3 Skin – AS

The skin covers the whole wing, acting as the first medium for transmitting the aerodynamic force to the other supporting members. Since the skin has been fastened by the stringers, the skin shear stress develops because of the torsional moment which results from the aerodynamic loads, engine thrust and static shear which is a result of wing mass and static load.

### 5.3.4 Spar Sizing – SH

The wing geometry exhibits its largest bending moment at the root chord (as shown by Figure 18) at an approximate value of 5.36MNm. Due to the fact that this is the largest magnitude bending moment the wing structure will be exposed to, the subsequent analysis was done to determine the required spar sizing. Supporting structural members sizing was influenced by the bending resistance required to withstand the calculated moments. Moreover, since the wing-box cross-section will be comprised of two spars placed at pre-defined positions of 12% and 71% of the chord length for leading and trailing edge spars respectively (Stanford, 2014). The two spars will need to collectively provide the minimum second moment of area,  $I_{xx}$  to sufficiently support the structural expectations.

#### 5.3.4.1 Defining spar dimensions – SH

From the bending moment analysis conducted on the cantilever beam static loading case, it is mandatory for the wing structure spar cross-sectional areas to provide the structural competency expected of them for safe operation. Using conventional, proven I beam sections for the two-spar wing configuration, the second moment of area can be deduced from Equation (26).

$$\sigma_b = \frac{My}{I_{xx}} \quad (26)$$

Where  $\sigma_b$  is the bending stress,  $M$  is the maximum bending moment,  $y$  is the vertical distance to the neutral axis and  $I_{xx}$  is the second moment of area about the neutral axis. For the spar to provide satisfactory performance, under the already presumed 1.5g load factor from which the calculated values are derived, the bending stresses returned from Equation (26) needs to be lower than the yield strength limit of the material by a reasonable margin otherwise the spar will undergo plastic deformation; leading to structural failure by yield.

To streamline the design process, a forced factor of safety was mathematically introduced into the bending stress capabilities of the spar by simply adjusting the old bending stress to a lower value, where  $\sigma_{b(new)} = \frac{\sigma_b}{1.5}$ . This forced relationship diminishes the material properties of the spar to resist the bending moment. Consequently, the second moment of area (which is inversely proportional to the bending stress) must increase to recover the deficit.

The scope of this methodology was to ensure that the procedure of analytically determining  $I_{xx}$  for the spar was confined to a safety factor of 1.5. This prevented excessive or over economical spar sizing. This blocked any over engineering and proved to be a valuable mass optimisation tool. Table 22 summarises the outcomes of the spar sizing with the final I-beam cross sectional dimensions at the wing root-chord. The tip chord dimensions were solved by using taper ratios. The material assigned for the spar is Aluminium 7075-T6 and its properties can be found in Appendix 13.6.

Table 22 - Extract from Spar Sizing Spreadsheet with Final Spar Dimensions at the Root Chord

| Spar          | Web Width, a (m) | Spar Height (m) | $I_{xx}$ (m^4) | Flange Width (m) |
|---------------|------------------|-----------------|----------------|------------------|
| Leading Edge  | 3.00E-02         | 0.664           | 2.10E-03       | 2.57E-01         |
| Trailing Edge | 6.00E-02         | 0.219           | 7.00E-04       | 8.77E-01         |

### 5.3.5 Rib Boom Idealisation Analysis – SH

The rib structural members are placed transversely across the leading and trailing edge spar members. The ribs are confined within the internal area of the wing-box dimensions and are placed at recurring intervals, with rib sizing trending from larger to smaller dimensions from inboard to outboard of the wingspan. They act to enforce and maintain the aerodynamic profile that extends through the wing and additionally transmit aerodynamic and fuel loads via the skin to the internal structure through the mechanism of a mounting interface between the ribs and the adjoining stringer and wing skin contact points.

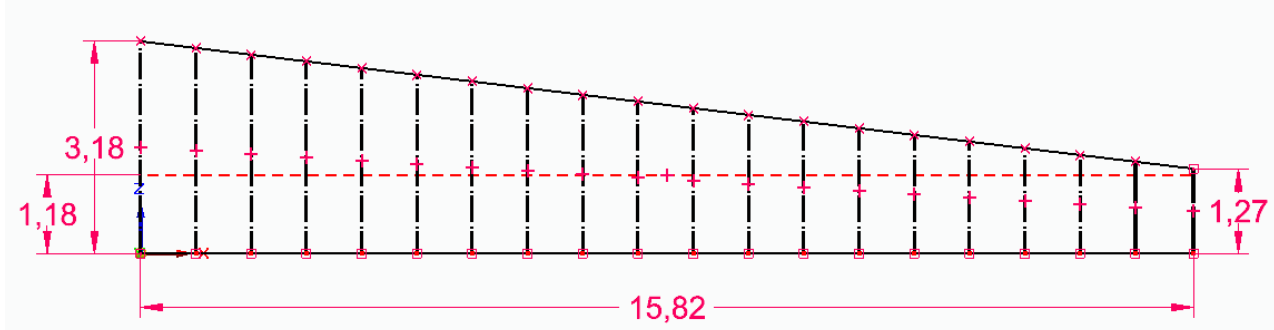


Figure 23 - Half-Wing Rib Distribution

Determining the number of ribs required to adequately withstand the aerodynamic forces being transmitted, a boom idealisation process was undertaken, to define the locations of the ribs and geometrical dimensions using a cartesian coordinate system. Figure 23 displays the rib distribution for the last iteration cycle. The analytical analysis concluded in a 20-rib configuration with the lowest factor of safety of 1.7 which was evaluated for critical shear buckling failure.

Conducting the boom analysis (Foreman, 2016), required the definition of boom points on the wing planform geometry, as seen in Figure 23. The circular and crossed markers positioned at alternate sides of the dashed red line (neutral axis) represent a concentrated boom area and its parallel opposing boom. Therefore, to construct a 20-rib configuration, the model demands 40 idealised boom areas; each with their unique boom areas correlating to their position along the wingspan and associated wing box length.

The first step was to determine an increment ratio for the spacing interval between ribs. This was calculated by:

$$I_{ratio} = (L_{tip} - L_{root}) / (n_{ribs} - 1) \quad (27)$$

This equation compares the tip and root length of the rib sections  $L$  and returns a balanced distribution for rib spacing as a function of rib number  $n_{ribs}$ ; giving a spacing ratio ( $I_{ratio}$ ). Identifying the neutral axis of the wing planform was done by decomposing the wing geometry into a triangle and rectangular compound shape and taking the average of their areas and individual centroids:

$$(x_c, y_c) = \frac{(\sum A_i \cdot (x_i, y_i))}{A_t} : \quad (28)$$

$$\text{Neutral Axis, NA} = y_c$$

The coordinates  $x, y$  with subscript  $i$  or  $c$  represent the coordinate placement for the constituent compound shapes and combined geometry respectively, with the area, symbol  $A$  adhering to the same notation. After this, the previously defined spar cross-sectional dimensions were referenced to be accounted for their thickness contributions for booms situated at the leading and trailing edge spars.

Generating the cartesian coordinate system for defining rib locations led to the derivation of the following equations, based upon the frozen wing planform in the PDR:

$$x_{no} = \frac{S_{wing-span}}{n_{ribs} - 1} * (R_{no} - 1) \quad (29)$$

$$y_{no} = C_{Root} + (R_{no} * I_{ratio}) \quad (30)$$

$$R_{depth} = \frac{t}{c} * y_{no} = 0.14(y_{no}) \quad (31)$$

Equation (29) uses the wingspan from the root to tip chord  $S_{wing-span}$ , which is the ratio between the total number of ribs subtract 1, and for every rib number  $R_{no}$ : (1,2,3, ...,  $n_{ribs}$ ) the longitudinal position,  $x_{no}$  across the span was found, with root and tip chord ribs being the preliminary and concluding rib members. Similarly, for the transverse position, Equation (30) uses the previously defined variables and solves for rib length as a function of the root chord length,  $C_{Root}$ . Equation (31) uses the wing thickness to chord ratio  $\frac{t}{c}$  and defines the rib thickness,  $R_{depth} = \frac{t}{c} * y_{no}$  for the affiliated chord length. Finally rib thickness was initially assumed, and iterated until design and load criteria were satisfied,  $t_{rib,no} = Initial\ assumption, iteration\ 1,2,3\dots$

Once these steps were completed, all 40 idealised boom cross-sectional areas were calculated for their individual points in accordance with their unique dimensions; using Equations (25), (26) and (27).

The boom areas for the 40 boom points were given by:

$$B_{(1:1:n)} = \frac{t_D \cdot b}{6} \cdot (2 + \frac{\sigma_1}{\sigma_2}) \quad (32)$$

The idealised boom points are summations of their individual boom areas and the boom area contributions from adjoining boom points. Hence for booms with multiple connections, their direct stress which can be assumed to be equal in ratio to the distance to the neutral axis had to be identified, e.g.  $\sigma_1$  and  $\sigma_2$ . The thickness of the adjoining lines between booms across the spars equalled the spar thickness at either the leading and trailing edge, and for adjoining rib booms, the thickness equated to  $t_D = t_{rib,no}$ .

The measure of space separating the ribs at the trailing edge in Figure 23 were of the same magnitude and frequency. For boom placements, separated by a hypotenuse section, Pythagoras theorem was employed to solve for the length  $b$ . Since the vertical and horizontal rib segments decreased in uniform increments, once one length was solved they were equivalent for every successive rib placement. In general, boom points placed at corners had to account for 2 additional boom contributions, whereas all other booms accounted for 3 boom contributions - 2 positioned laterally and 1 vertical boom that was its opposite pair.

Subsequently, once all boom areas were tabulated in an Excel spreadsheet, the individual and summated second moment of areas,  $I_{xx}$  were calculated. The bending stress formula, Equation (26) where the bending moment for each individual rib was inferred from Equations (19) and (21) as a function of their longitudinal position along the wing span was used, and stresses for each boom were used to evaluate the structural confidence of the rib geometries.

The technical analysis showed that the SF of all the ribs was lowest at the root chord with a minimum SF of 1.9 with a material selection of Aluminium 2024-T4 (Appendix 13.6). Rib stresses were also acknowledged at the engine point load/attachment point, 5.45m from the root chord and were evaluated to provide a more than capable SF with an average of approximately 8. The rib structural members analytically performed as predicted under stress and typically fare well against yielding. The primary structural consideration for the rib dimensions and number was driven by its ability to withstand failure by critical shear buckling. To substantiate a minimum of 1.5 SF against critical shear buckling, the critical buckling load was calculated and contrasted against the shear force present on the rib due to the lift distribution.

$$P_{cr} = \frac{\pi^2 \cdot E \cdot A}{\left(\frac{KL}{r}\right)^2}, K_{x,y} = 0.7L \quad (33)$$

The critical buckling load  $P_{cr}$  (Engineering ToolBox, 2012), was a function of  $E$ , the Elastic Modulus of the material, the cross-sectional area,  $A$ , under which the load is being transmitted, effective length factor  $K$  and the slenderness ratio,  $\frac{KL}{r}$ . Where  $L$  is the rib/column length and  $r$  is the square root of the second moment of area over cross-sectional area. Note for critical buckling,  $K = 0.7$  for critical failure. To adequately support the critical buckling loads, Aluminium 2024-T4 (Appendix 13.6) provided a minimum SF of 2.05 for a critical

buckling load failure of 84.4kN. The SF calculation in Table 23 compares the critical buckling load versus the shear force present on the respective rib.

Table 23 - SF Table for Critical Buckling Loads for Rib Sections

| Rib Number | Critical Buckling Load, Pcr (kN) | Safety Factor, SF |
|------------|----------------------------------|-------------------|
| 1          | 8.44E+01                         | 2.05              |
| 2          | 8.72E+01                         | 2.12              |
| 3          | 9.01E+01                         | 2.19              |

Upon completion of these validation criteria, the aircraft wing rib analysis and design requirements were fulfilled. The iterative process responsible for the data and numbers presented in this segment of the technical write up, simply cycled through the process until the driving design criteria were satisfied while enforcing an internal minimum target SF of 1.5 for the internal wing structural members; as required in CS 25.303 Factor of Safety (EASA, 2011). The iterative process involved adjusting the number of structural members and/or their geometrical dimensions and spacing. The directive of this exercise was to aim for the most effective balance between mass and safety. This design philosophy was true for all structural members and was reflected in all aspects of the wing structural analysis where possible was conducted for the ribs and spar sizing.

### 5.3.6 Stringer Boom Idealisation Analysis – AS

Boom idealisation was used on the wing section, to represent the relationship between stringers and the associated stress. This was completed using an iterative approach by taking the comparison for each boom quantity. The calculations were carried out for 60, 50 and 40 booms in order to compare the total average safety factor.

The skin thickness was fixed at 2.5mm with a material choice of the Spectra 900 series, a light composite with extreme moisture resistance. Figure 24 shows the stringer selection and dimensioning, and a T-Beam stringer had been selected. The stringer cross sectional area was obtained as 76mm<sup>2</sup> and 36mm<sup>2</sup> respectively for the wing root and tip chord and the boom idealisation was specifically analysed in the wing root chord.

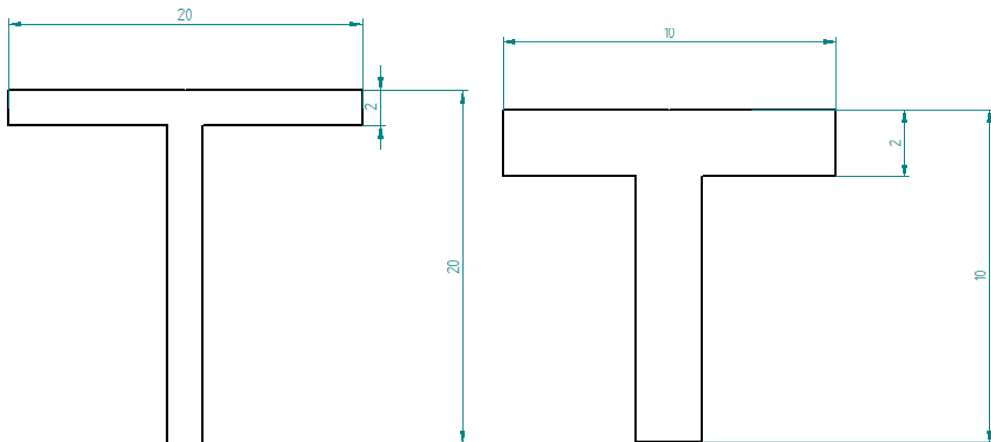


Figure 24 - Stringer Dimensions for Root and Tip Chord

The method began from the spacing calculation by stretching the wing drawing design into the straight line to get the total wing dimensions. The assumption was made on the leading and trailing edge part by re-shaping into vertical straight lines but without changing any dimension from the wing sizing.

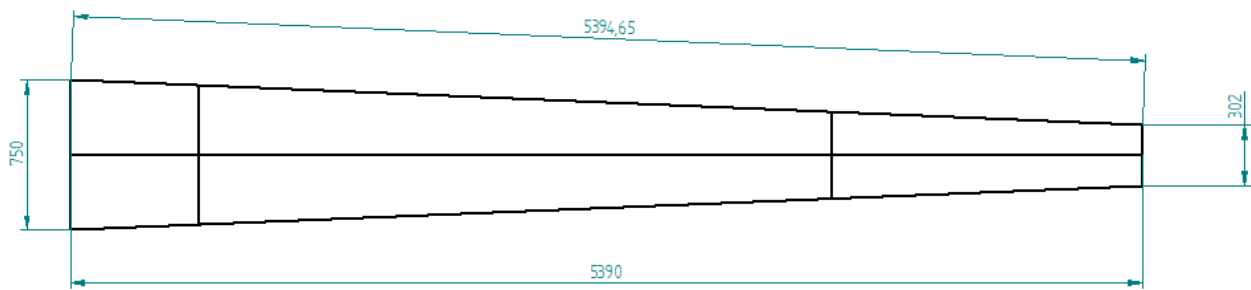


Figure 25 - Simplified Wing Sketch

It can be seen in Figure 25 that the leading edge and trailing edge height is 750mm and 302mm respectively and hence, by taking the whole wing root chord, 5.390m, the hypotenuse on the top and bottom were obtained using Pythagoras theorem which is 5.394m.

The total perimeter was calculated as 11.9m and therefore, the spacing can be obtained using Equation (34):

$$\text{Boom Parameter Spacing} = \frac{\text{Total Wing Parameter}}{\text{Number of Stringers} - 1} \quad (34)$$

Table 24 - Boom Initial Spacing Across Perimeter

| Boom No. | Boom Parameter Spacing (mm) |
|----------|-----------------------------|
| 60       | 201                         |
| 50       | 242                         |
| 40       | 304                         |

After the total perimeter is obtained, the boom allocation is available by taking the length from each position and dividing it by the boom spacing.

Table 25 - Boom Allocation with Regard to the Geometry

| Boom Iteration | Hypotenuse Section | Leading Edge Section | Trailing Edge Section |
|----------------|--------------------|----------------------|-----------------------|
| 60             | 26 booms           | 5 booms              | 5 booms               |
| 50             | 22 booms           | 3 booms              | 3 booms               |
| 40             | 17 booms           | 3 booms              | 3 booms               |

In the hypotenuse section calculation, an assumption was made because the result was rounded down. In other words, some booms were not accurately positioned at the edge of the geometry.

Table 26 - New Boom Quantity on Hypotenuse Section

| Boom Iteration | Hypotenuse Boom Quantity | New Hypotenuse Boom Quantity | New Spacing (mm) |
|----------------|--------------------------|------------------------------|------------------|
| 60             | 26.8                     | 26                           | 216              |
| 50             | 22.3                     | 22                           | 257              |
| 40             | 17.7                     | 17                           | 337              |

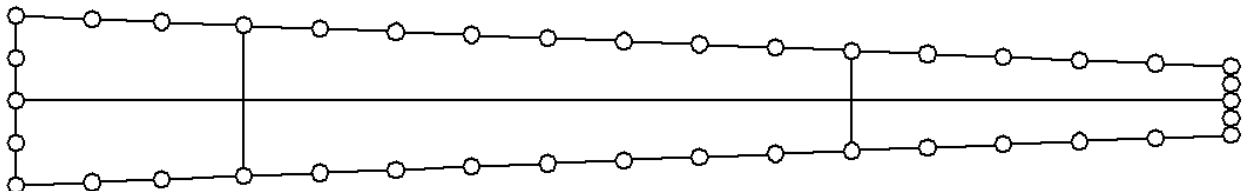


Figure 26 - Sketch of Boom Allocation

Since the geometry is symmetric, the neutral axis is located in the middle of the geometry representing a mirror image between top and bottom. The major role of this calculation was to solve the distance from each boom to the neutral axis using an arithmetic series on the hypotenuse section.

$$U_n = U_1 + (n - 1)d \quad (35)$$

Equation (35) was used to calculate the increment ratio ( $d$ ) and distance to neutral axis ( $U_n$ ) which is represented in Figure 26. The calculation was done separately for the top and bottom but still uses the same formula, by considering the first sequence on the vertical distance from the leading edge to the trailing edge.

Table 27 - Ratio of Spacing from the Boom Point to the Neutral Axis in Hypotenuse Section

| Boom Iteration | U1 (Leading edge Thickness) | Un (Trailing Edge Thickness) | Ratio |
|----------------|-----------------------------|------------------------------|-------|
| 60             | 750                         | 302 (U26)                    | 8.96  |
| 50             | 750                         | 302 (U22)                    | 10.7  |
| 40             | 750                         | 302 (U17)                    | 14.0  |

This consideration was made by measuring the exact position of allocated spars located at 0.12c and 0.71c from the chord respectively for the leading edge spar and trailing edge spar. This is where the special case was made for the boom calculation because the additional term was added which connects one boom from the top to the bottom boom by both spars.

Foreman (2016), has recommended some technical resources to calculate the boom area ( $B$ ), second moment of area ( $I_{xx}$ ), direct stress ( $\sigma_z$ ) and hence Equation (36), Equation (37) and Equation (38) were used.

$$B_i = \frac{td b}{6} \left( 2 + \frac{Y(i-1)}{Y_i} \right) \quad (36)$$

$$I_{xx} = \sum_{i=1}^n B_i Y_i^2 \quad (37)$$

$$\sigma_z = \frac{M_x Y_i}{I_{xx}} \quad (38)$$

After each individual boom area was calculated, the second moment of area was obtained for each boom. The total second moment area of each iteration process was found.

Furthermore, the applicable bending moment ( $M_x$ ) was purposely divided into the total number of stringers in order to withstand the load for each individual stringer. There was a consideration to be made due to the spars assumed as two cantilever beams instead of a realistic segmented beam which had a was spaced longitudinally from the root to the tip.

*Table 28 - Total Second Moment of Area and Applicable Bending Moment*

| Boom Iteration | Total $I_{xx}$ (mm <sup>4</sup> ) | Applicable $M_x$ (Nmm) |
|----------------|-----------------------------------|------------------------|
| 60             | $2.13 \times 10^9$                | $8.93 \times 10^7$     |
| 50             | $2.04 \times 10^9$                | $1.07 \times 10^8$     |
| 40             | $1.95 \times 10^9$                | $1.34 \times 10^8$     |

The lightest feasible material was selected for the stringers, since the total average applied stress ( $\sigma_z$ ) for each iteration was not more than 30 MPa. The Composite Material Handbook (2002), from the USA Department of Defence, published information about UHMWPE Spectra 900 fibre which is the lightest possible composite material with a density of 0.97g/cm<sup>3</sup>. This material is stronger than steel however it has poor high temperature performance which affects the ease of manufacture.

UHMWPE Spectra 900 fibre offers excellent chemical inertness and extreme moisture resistance to resist reactive chemical acids, indicating outstanding corrosion and abrasion resistance. This was an important consideration because stringers often have corrosion problems when placed inside the wing.

The allowable strain was referenced from the general airworthiness engineering centre article by Wencheng, (2011) that stated that typical short-range family have  $3200\mu\epsilon$  and hence, the allowable stress can be calculated from Equation (39).

$$\text{Allowable Stress} = \text{Young's Modulus} \times \text{Allowable Strain} \quad (39)$$

*Table 29 - Stringer Material Properties (Honeywell, 2019)*

| Material Properties          | Spectra Fibre 900 Series |
|------------------------------|--------------------------|
| Young's Modulus (GPa)        | 73.0                     |
| Allowable Stress (MPa)       | 233                      |
| Density (g/cm <sup>3</sup> ) | 0.970                    |
| Elongation (%)               | 3.90                     |

After material consideration, the final safety factor analysis can be done by finding the total average safety ratio between the material strength and each boom direct stress from Equation (40).

$$\text{Total Average Safety Factor} = \frac{\text{Allowable Stress}}{\sigma_z} \quad (40)$$

Table 30 - Final Result of Safety Factor Analysis

| Boom Iteration | Possible lowest safety factor | Possible highest safety factor | Total average safety factor |
|----------------|-------------------------------|--------------------------------|-----------------------------|
| 60             | 14.9                          | 72.9                           | 24.9                        |
| 50             | 11.9                          | 58.9                           | 20.4                        |
| 40             | 9.07                          | 45.0                           | 16.0                        |

To conclude, the final result of the safety factor has shown that it has achieved beyond the minimum safety factor (1.5). A comparison was also done between the lowest and highest safety factor which justified the decision for 40 booms due to the top-level goals based on the recommendation that the total wing mass be as light as possible to improve the fuel efficiency. As a result, this weight reduction would help to reduce the DOC and the cost of manufacture was reduced based on the material selection.

### 5.3.7 Wing Structure CAD – TL

Figure 27 shows the CAD model of the wing structure for the Aero 5 design.

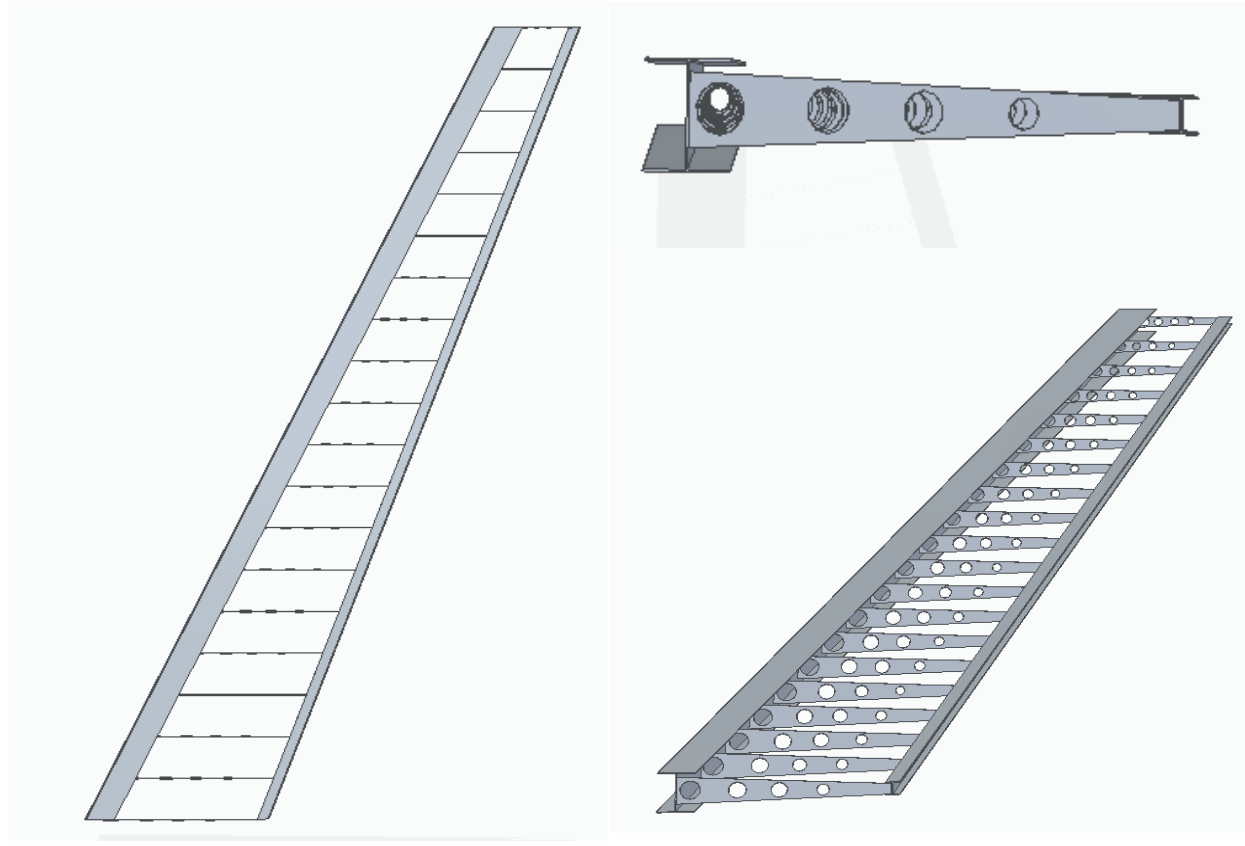


Figure 27 - Wing Ribs and Spars configuration. Plan View (Left), Side View (Top Right) and Isometric View (Bottom Right)

### 5.3.8 Wing Structure – Further Improvements – SH

To further optimise the analysis for favouring the aerodynamic performance of the aircraft, greater care and detail could have been given to the mass optimisation for the ribs, by better developing the spacing ratios and incorporate a changing spacing interval inboard the wing and the outboard sections of the wing. Moreover, the rib thickness could have been tailored individually rather than taking an assumed value for the whole array. This would have assisted in better engineering the individual ribs towards an SF that was not excessive, compared to the current approach which aimed to ensure that the minimum rib SF met the regulations. This could have led to substantial improvements in mass optimisation; reducing the material and resource needs.

The value of this analysis would benefit the DOC case because of lower manufacturing cost. For the shear force and bending moment diagrams, higher fidelity force models incorporating more accurate landing gear and wing mass loads would have strengthened the analysis and subsequent results. Gust load analysis could have also been completed for a larger range of altitudes to enrich the flight operation data of the aircraft design. This is also true for the static loading case where different operational variations could have been tested to create confidence in the design. Lastly, more creativity in the structural layout and material selection could have had

several positive effects. If there was more time, the exploration of design alternatives to a larger degree could have yielded better results than just using an iterative approach. This would have given valuable insight and lead to possible complete design overhauls.

### 5.3.9 Wing Box – AM

The wing box is an aircraft component which is designed to reinforce support and structural rigidity to the wing. The calculations around the wing commonly consist of the approximation that the loads acting upon the wing are distributed through the wing box; the booms carry direct stress and the skin carries shear stress. Hence, it is necessary to carry out analysis to ensure that the skin will be able to withstand the shear stress acting upon it without failure.

The wing box is enclosed by the front and rear spars in the chordwise dimension whereas in the vertical dimensions, the skin encloses the wing box. To reduce the complexity of the following calculations, the upper and lower surfaces of the wing is approximated as a straight line. To increase the accuracy, the length of the spars is approximated as the mean of the actual spar lengths and the maximum thickness of the aerofoil. As a result, the following wing box is obtained.

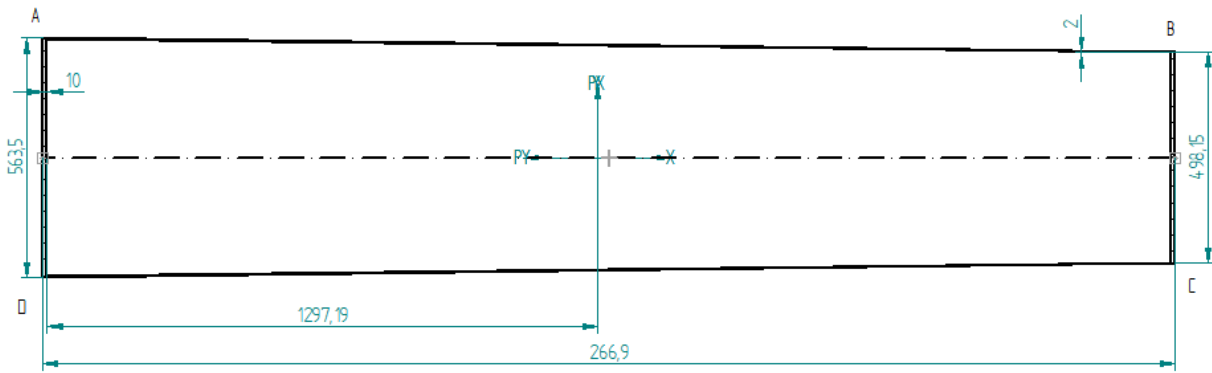


Figure 28 - Wing Box Dimensions

The shear flow of a closed section can be determined through Equations (41) and (42) (Viquerat, 2019).

$$q_s = q_{os,s} + q_c \quad (41)$$

Where  $q_c$ ,  $q_s$ ,  $q_{os,s}$  are the constant shear flow, shear flow in the closed section and shear flow in the open section respectively. The open section is obtained through cutting the closed section.

$$q_{os,s} = q_{s,o} + \frac{I_{xy}S_y - I_{xx}S_x}{I_{xy}I_{yy} - I_{xy}^2} \int_0^s t x ds + \frac{I_{xy}S_x - I_{yy}S_y}{I_{xy}I_{yy} - I_{xy}^2} \int_0^s t y ds \quad (42)$$

Where  $I_{xx}$  and  $I_{yy}$  are the second moment of area,  $I_{xy}$  is the product second moment of area,  $S_x$  and  $S_y$  are the vertical and horizontal shear forces acting on the wing box and  $t$  is the thickness of the section.

Due to the line of symmetry in the section,  $I_{xy}$  is zero. The thickness of the spars and the skin are 10mm and 1mm. The values for  $I_{xx}$  and  $I_{yy}$  are calculated to be  $6.12 \times 10^8 \text{ mm}^4$  and  $2.08 \times 10^{10} \text{ mm}^4$  with the centre of gravity to be at 1297mm from the leading-edge spar.  $S_x$  is -150,000N, which is the maximum thrust force from the engine, and  $S_y$  is -513,000N, which is the shear force acting upon the section.

The shear centre is located along the line of symmetry. Therefore, attaching the pylon about the symmetric axis provides zero twist in the wing box.

Substituting the values provides:

$$q_{os,s} = q_{s,o} + 7.21 \times 10^{-6} \int_0^s t x ds + 8.39 \times 10^{-4} \int_0^s t y ds$$

Solving the equation for section CB provides:  $q_{os,s} = 0.0996s + 4.195 \times 10^{-3}s^2$

Solving the equation for section BA provides:  $q_{os,s} = 280 + 0.217s - 3.605 \times 10^{-6}s^2$

Solving the equation for section AD provides:  $q_{os,s} = 834 - 2.26s - 4.195 \times 10^{-3}s^2$

$$q_c = -\frac{555.6N}{mm}$$

The section BA provides the shear slow in the skin plotting the equation provides the following graph.

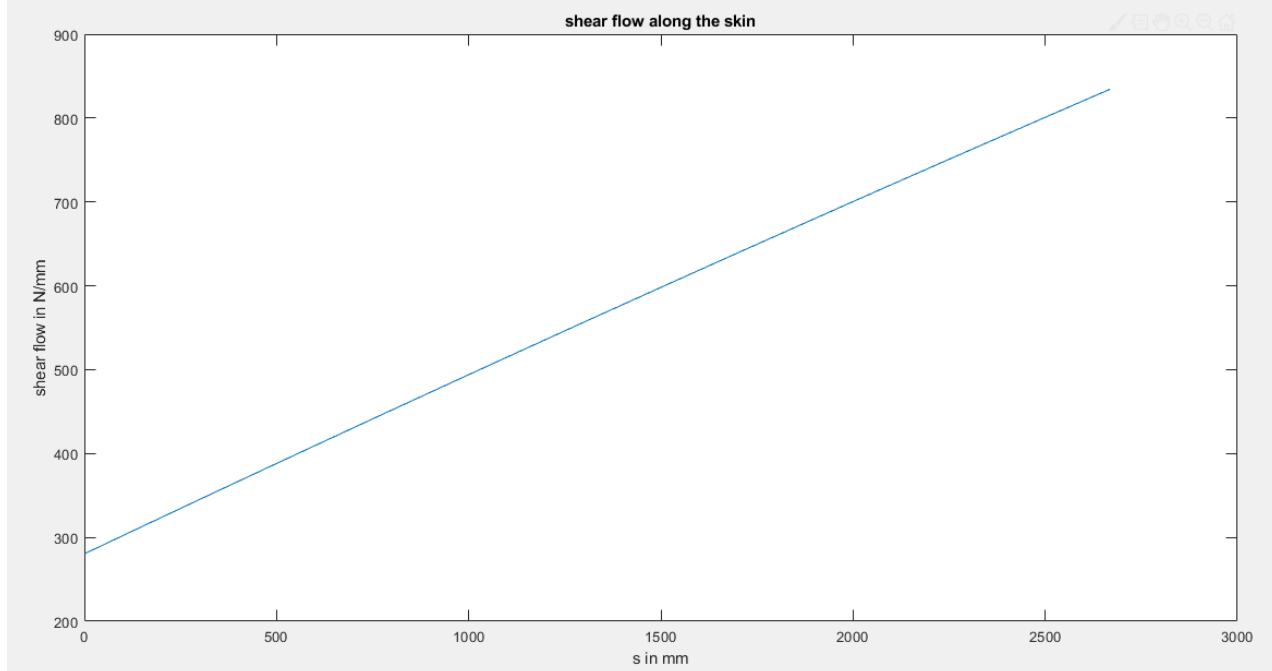


Figure 29 - Shear Flow along the Wing Skin

Figure 29, shows that the maximum shear flow is 834N/mm. Summing the maximum open section shear flow to the constant closed section shear flow equals to 279N/mm. Dividing the shear flow by the skin thickness provides the shear stress acting upon the skin. Thus, the maximum shear stress is 279MPa for the thickness of 1mm. The thickness is chosen through the historical precedence of the Boeing aircraft.

Through the materials research, the chosen material for the skin is a carbon composite. The shear modulus of carbon composite is 33GPa (Anon, 2019) and the with the historical data of allowable shear strain from Airbus is 5300 $\mu\epsilon$  (core.ac.uk, 2019). Thus, the calculated safety factor is 0.63. This design does not comply with the design requirements as the safety factor is less than 1.5. Therefore, the iterative process (shown in Table 31) is taken into consideration to find the skin thickness required to withstand the shear stress applied; which is 2.5mm.

Table 31 - Iteration between the Thickness and the Safety Factor

| Thickness (mm):     | 1     | 2    | 2.1  | 2.2  | 2.3  | 2.4  | 2.5  |
|---------------------|-------|------|------|------|------|------|------|
| Shear Stress (MPa): | 279   | 142  | 136  | 130  | 124  | 119  | 115  |
| Safety Factor       | 0.628 | 1.23 | 1.29 | 1.35 | 1.41 | 1.47 | 1.52 |

### 5.3.10 Wing Fuel Tanks – AM

Research based on the historical precedence of the wing fuel tanks has been carried out; the results show that wing fuel tanks are a conventional design used in almost all the modern-day aircrafts, from short range to long range aircrafts such as A320, A380 and Boeing 777. Such designs have several advantages, one of which is that the design is cost efficient as it reduces the work done to transport the fuel to the engine. Another major advantage is that, in case of a damage in the fuel tank, the debris would not affect the passengers as the fuel is stored away from the fuselage. The design also helps to reduce the bending moment on the wing by counteracting the lift force with the weight of the fuel.

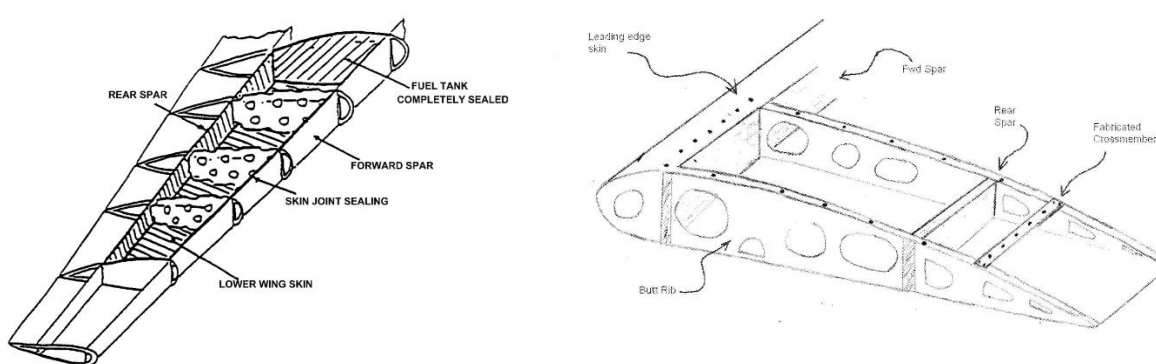


Figure 30 - Cut Away of a Wing Fuel Section

Considering historical precedence, wing fuel tanks are designed to be consistent with the geometry represented in Figure 30 (Pathirana, 2019). The fuel tank is enclosed by the front and rear spar in terms of the chord-wise direction, whereas the ribs are enclosing the tank in terms of the span-wise direction. The ribs are coated to reduce the contact with the fuel. The fuel tank consists of a pipe which connects the neighbouring fuel tank to transport the fuel across the ribs.

As specified in the PDR, one third of the entire fuel is stored in the wing; which is approximately  $6.67\text{m}^3$  of fuel. The calculations are carried out in the following manner for the span-wise dimension of the space occupied by the fuel. Initially, the aerofoil coordinates between the front and rear spars are collected for both the wing root and wing tip. Then using the MATLAB code provided in Appendix 13.7, the area enclosed by both the wing root and wing tip aerofoils are calculated to be  $2280000\text{mm}^2$  and  $345000\text{mm}^2$  respectively. The area enclosed from the wing root to the wing tip was approximated as a linear relationship. Equation (43) provides the area enclosed by the aerofoil as a function of the distance,  $x$ , from the wing root.

$$A = 2283611.61 - 129.23x \quad (43)$$

Thus, the volume occupied as a function of  $x$  was obtained from Equation (44):

$$V = \int_0^x 2283611.61 - 129.23x dx \quad (44)$$

Integrating Equation (44) and substituting  $6.67\text{m}^3$  as the volume occupied provides the span wise dimension of the fuel tank to be 3.21m. The approximations which reduce the accuracy of the calculation is that the volume occupied by the stringers and the skin is negligible. The wing fuel tanks were designed to comply with CS 25.969. Hence, according to CS 25.969, the fuel tank expansion space of 5% has been taken into consideration in calculating the dimension of the fuel tank.

### 5.3.11 Engine Mounting – AM

Prior to determining the engine mounting method, the engine mounting location was updated from the values presented in the PDR, as described in Appendix 13.1.4. Under wing engines are mounted with pylons. Pylons connect the engine to the wing and help to distribute the load from the engine through the wing box. Hence the analysis of a pylon truss structure is required to ensure that the pylon can withstand the loads it is subjected to.

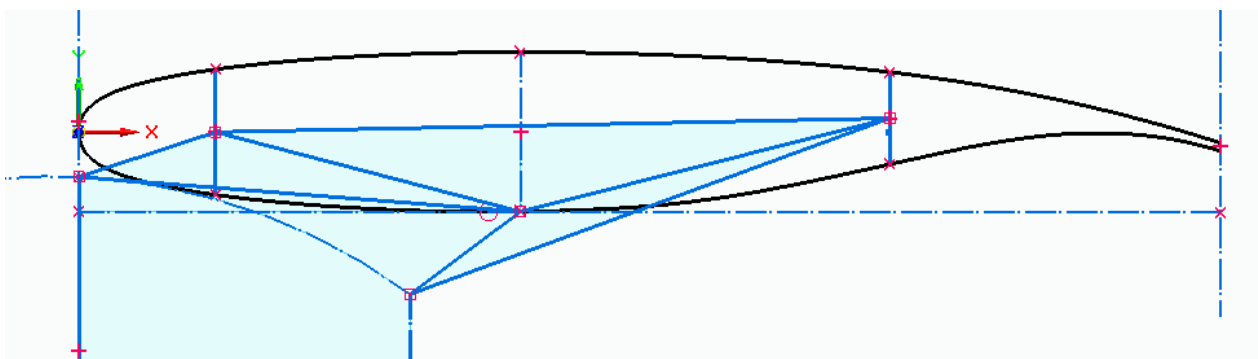


Figure 31 - Pylon Truss Structure

As the first step, the 2D CAD was created for the cross section of the wing at the point where the engine is located as presented in Figure 31. Following the initial step, the truss structure was created with the dimensions relating to that of the cross section. The truss must be able to withstand the engine thrust force of 137,000N in the horizontal direction and the weight of the engine, 38,600N, in the vertical direction. Analysing the truss joints and balancing the forces acting on the truss members provides the maximum compressive and tensile force experienced by a truss member, which are 110,000N and 97,300N respectively.

Next, the selection of material was taken into consideration. Considering historical precedence, the materials commonly chosen for the engine pylon structure are Titanium, Aluminium and Nickel alloys (Patents.google.com, 2019). The modulus of elasticity of Aluminium 7075 is 71.7GPa, whereas Titanium and Nickel have a modulus of elasticity of 114GPa and 200GPa respectively. Also considering their density, Titanium has been chosen.

From the allowable compression strain of  $3200\mu\epsilon$  (core.ac.uk, 2019), the maximum stress experienced by any truss member is 365MPa. To comply with the design requirements, the safety factor of 1.5 is taken into consideration. Hence, the truss member must be able to withstand the stress of 547MPa. Since stress is the ratio between the force and the cross-sectional area, the thickness of each truss member was calculated to be 16mm. The calculation was carried out for all the truss members and their thicknesses are listed in the Table 32.

*Table 32 - Forces and Thickness of the Truss Members*

| Truss Members | Force (N) | Thickness (mm) |
|---------------|-----------|----------------|
| AD            | 97300     | 15.0           |
| AC            | 109000    | 16.0           |
| BC            | 12900     | 5.50           |
| CE            | 20300     | 6.86           |
| BE            | 72700     | 13.0           |
| DC            | 82400     | 13.8           |

The dimensions and the truss members are annotated in Figure 32.

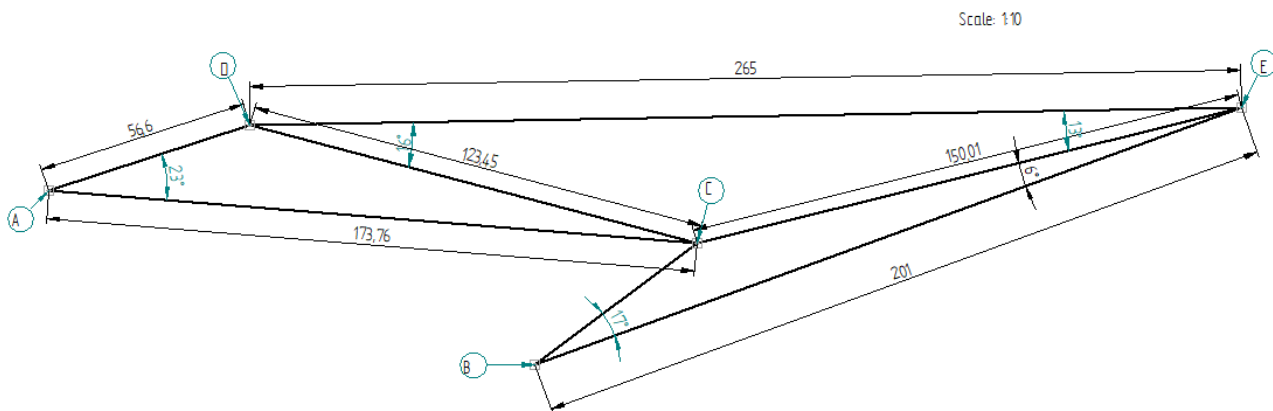


*Figure 32 - Identity and Dimensions of the Truss Members*

### 5.3.12 Wing CAD – TL

The CAD models of the wing and the control surfaces are shown in Figure 33 and Figure 34 respectively. Figure 35 shows an isometric view of the assembled wing and nacelle. The control surfaces for the wing are defined in Section 5.5 of this report. For the creation of the wings in Solid Edge, the aerofoil coordinates were obtained online as a .DAT file (airfoiltools.com, 2018) and once converted to a .txt file, imported in.

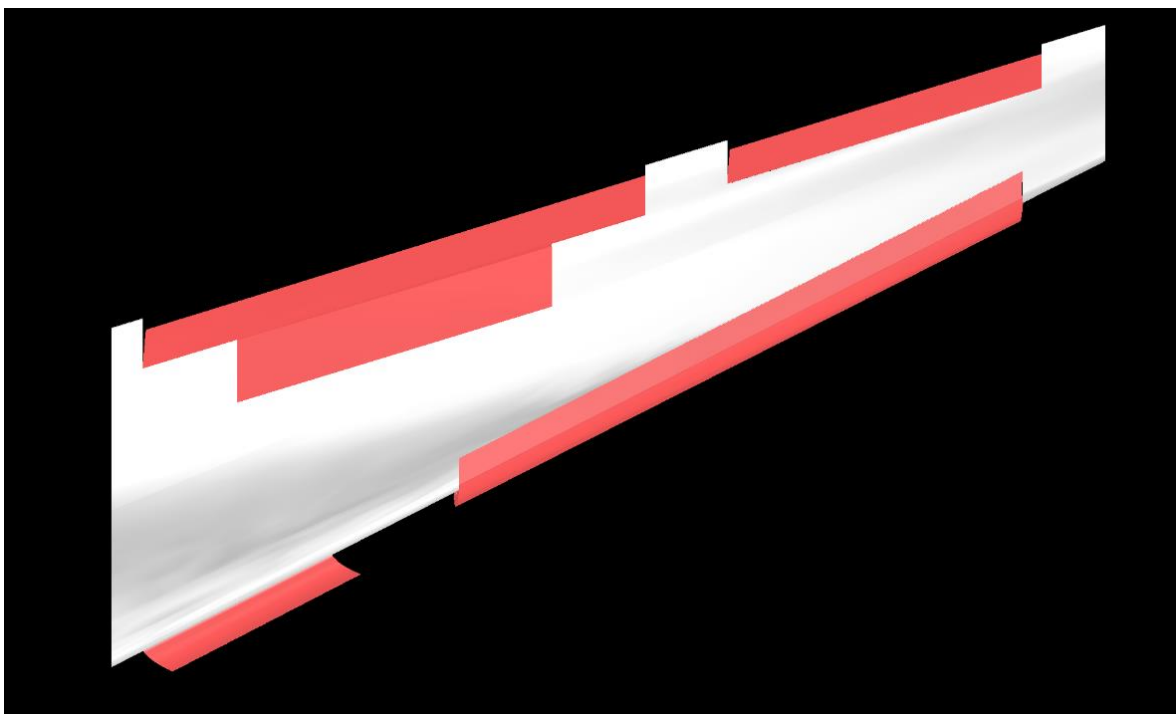


Figure 33 - Plan View of Aero 5 Wing

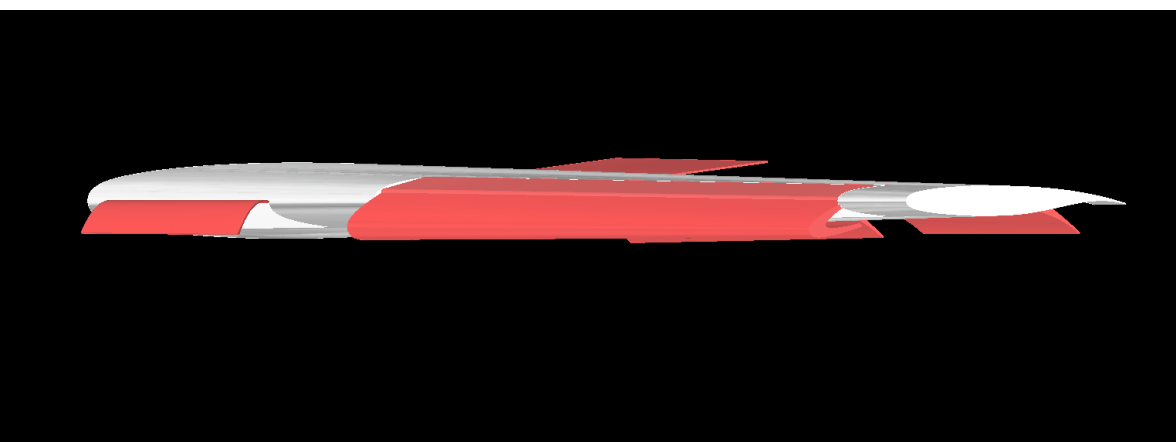


Figure 34 - Side View of Aero 5 Wing

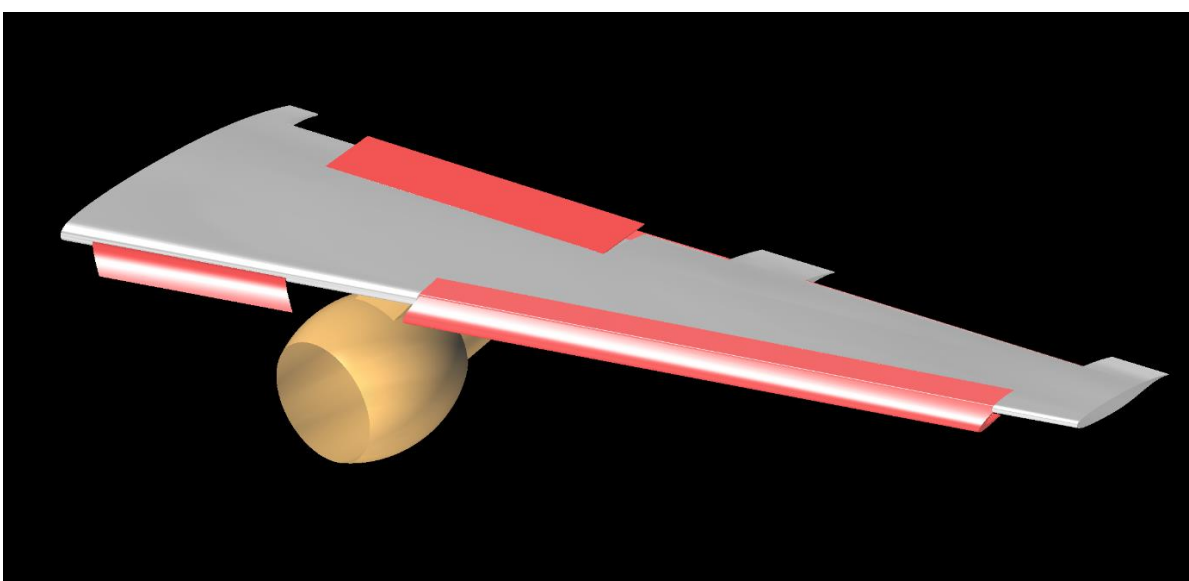


Figure 35 - Isometric View of Assembled Aero 5 Wing and Nacelle

## 5.4 Horizontal Tail Plane – BG

### 5.4.1 Horizontal Tail Plane Considerations – BG

During the conceptual design phase, an assumption was made to utilise a fixed tailplane in the design of the Aero 5 aircraft. For this CDR, it was determined that further analysis was required as to whether this was an appropriate assumption.

Throughout the design process, the Aero 5 aircraft has been sized and designed to fly at a Mach Number of  $M = 0.76$ , which could potentially fall in the transonic flow regime. A transonic flow contains regions of both subsonic and supersonic flow. The transonic regime begins when the free stream flow reaches the Critical Mach Number, which is defined as the free stream Mach Number at which the flow over the wing first reaches sonic conditions ( $M=1$ ). In the transonic flow regime, the interaction of the shocks that develop across a wing and the boundary layer lead to boundary layer transition and flow separation (Robins, 2018).

If the flow were to separate over the horizontal tailplane (due to being in the transonic regime), the effectiveness of the elevators would be diminished. A possible solution is to install a moveable tailplane to ensure that there is no flow separation, however this would result in a deviation from the proposed design in the Aero 5 Preliminary Design Review (PDR). To determine whether a moveable tailplane was required, the following analysis, based on Prandtl-Glauert theory (Robins, 2018) was carried out.

The analysis used Prandtl-Glauert theory to first determine the maximum Mach Number for the flow over the horizontal tailplane in the cruise configuration. It was also used to determine the Critical Mach Number for the horizontal tailplane. Equation (45) is based on Prandtl-Glauert theory and utilises Equation (46) to determine the pressure ratio at the point of minimum suction over a wing, as this is where sonic conditions would first occur (described by Figure 36).

$$\frac{C_p(M_1)}{C_p(M_{REF})} = \sqrt{\frac{1 - M_{REF}^2}{1 - M_1^2}} \quad (45)$$

$$\frac{p_s}{p_1} = 1 + \frac{\gamma C_p(M_1)}{2} M_1^2 \quad (46)$$

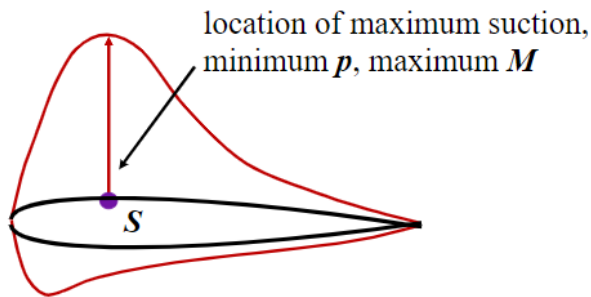


Figure 36 - Location of Minimum Suction (Robins, 2018)

Where, for this analysis,  $C_p(M)$  is the pressure coefficient for the flow at cruise conditions,  $M_1$  is the Mach Number at cruise and  $C_p(M_{REF})$  is the pressure coefficient for a reference Mach Number ( $M_{REF}$ ). These values were then used to calculate the pressure ratio at the point of minimum suction, which in turn was used, with the Isentropic Flow Tables (Robins, 2018), to calculate the Mach Number at that location.

Before using the Prandtl-Glauert relationship, the reference pressure coefficient was calculated. A reference Mach Number of 0.6 was selected as the starting point for this analysis, as typically the transonic regime is in the range  $0.8 < M < 1.2$  (Robins, 2018). Assuming the flow in cruise conditions is isentropic, the ratio of the local temperature ( $T_1$ ) to the free stream (stagnation) temperature ( $T_\infty$ ) was determined, using the Isentropic Flow Tables (Robins, 2018). This value was then used in Equation (47), to determine the ratio of the local pressure ( $p_1$ ) to the free stream (stagnation) pressure ( $p_\infty$ ).

$$\frac{p_1}{p_\infty} = \left( \frac{T_1}{T_\infty} \right)^{\frac{\gamma}{\gamma-1}} \quad (47)$$

Where  $\gamma$  is the ratio of specific heats (for air,  $\gamma = 1.4$ ). After calculating the pressure ratio, the local pressure for the reference Mach Number was determined by multiplying the pressure ratio by the free stream pressure. This enabled the calculation of the reference pressure coefficient  $C_p(M_{REF})$  using Equation (48).

$$C_p(M_{REF}) = \frac{p - p_\infty}{\frac{1}{2} \rho V^2} \quad (48)$$

Where  $\rho$  is the air density at cruise conditions and  $V$  is the aircraft velocity that corresponds to  $M = 0.6$ .  $V$  was calculated using the relationships formulated in Equation (49).

$$V = Ma = M\sqrt{\gamma RT_\infty} \quad (49)$$

Where  $a$  is the local speed of sound and  $R$  is the gas constant (for air,  $R = 287 \text{ J/kg K}$ ). Using the data obtained from Equations (47), (48) and (49), the value of  $C_p(M_1)$  was found using Equation (45). This value was used in Equation (46) to determine the pressure ratio at the point of minimum suction, which in turn was used to calculate the Mach Number at the same point, using Equation (50) (Robins, 2018). The Mach Number at the point of minimum suction ( $M_s$ ) was found using the Isentropic Flow Tables.

$$\frac{p_\infty}{p_s} = \frac{p_1}{p_s} \frac{p_\infty}{p_1} \quad (50)$$

In addition to calculating the value of  $M_s$  for a given free stream Mach Number, the Prandtl-Glauert theory and the process outlined in this section of the report can be used as an iterative process to calculate the critical Mach Number for a wing. Table 33 shows the values calculated using the Prandtl-Glauert theory. Note that the first row of the table details the reference values and all data is presented to three significant figures.

Table 33 - Prandtl-Glauert Theory

| $M_1$ | $p_\infty/p_1$ | $C_p(M_1)$ | $p_s/p_1$ | $p_\infty/p_s$ | $M_s$ |
|-------|----------------|------------|-----------|----------------|-------|
| 0.600 | 1.28           | -0.858     | -         | -              | -     |
| 0.650 | 1.33           | -0.908     | 0.731     | 1.81           | 0.96  |
| 0.660 | 1.34           | -0.918     | 0.720     | 1.86           | 0.98  |
| 0.670 | 1.35           | -0.929     | 0.708     | 1.91           | 1.00  |
| 0.760 | 1.47           | -1.06      | 0.571     | 2.57           | 1.25  |

Table 33 shows that, at the cruise Mach Number ( $M = 0.76$ ), there are regions of supersonic flow over the horizontal tailplane, as the value of  $M_s$  is 1.25. The critical Mach Number for the flow over the horizontal tailplane is  $M = 0.670$ , as this is the Mach Number at which the flow first becomes supersonic. Additionally, the calculations are supported by Abbott and von Doenhoff (1959), as the reference pressure calculated using Equation (48) is similar to the data provided in ‘Theory of Wing Sections’ for symmetrical NACA aerofoils.

This analysis indicates that a moveable tailplane is a more suitable design for the Aero 5 aircraft, to ensure that there is no flow separation and therefore ensuring elevator effectiveness for all flight conditions. This will be achieved in flight by modifying the effective incidence of the tailplane, in order to maintain a fully subsonic and attached flow in the cruise condition. This signifies that the flow will remain attached at the elevator, and hence the elevator retains its effectiveness. A Change Request (CR) (Appendix 13.1.1) was raised to incorporate this moveable tailplane design into the Aero 5 aircraft design in order to mitigate the risks associated with flow separation and loss of elevator effectiveness.

## 5.5 Control Surface Sizing – PS

In the PDR (Section 4.5), the tail plane surface areas were calculated based on the volume coefficient method. It was decided by Aero 5 that higher fidelity tail plane surface areas could be calculated to incorporate the moment arm from the wing AC instead of the ETOW CG location. Aero 5 completed the sizing iteration once more as laid out in PDR Section 4.7. This overcame the issue of a variable CG location and therefore provided a better area to then allow Aero 5 to size the control surfaces. A change request was raised to incorporate the new calculated area values and is detailed in Appendix 13.1.1. The new iteration provided updated dimensions for the horizontal and vertical tail planes presented in Table 34.

Table 34 - Final Empennage Dimensions

| Horizontal Tail        |       | Vertical Tail          |       |
|------------------------|-------|------------------------|-------|
| Area (m <sup>2</sup> ) | 26.1  | Area (m <sup>2</sup> ) | 22.0  |
| AR                     | 4.77  | AR                     | 1.72  |
| Span (m)               | 11.2  | Height (m)             | 6.14  |
| Half span (m)          | 5.60  | Taper                  | 0.400 |
| Taper                  | 0.400 | Root chord (m)         | 5.11  |
| Root chord (m)         | 3.34  | Tip chord (m)          | 2.05  |
| Tip chord (m)          | 1.34  | 1/4 c sweep (degrees)  | 40.0  |
| 1/4 c sweep (degrees)  | 30.0  | MAC (m)                | 3.80  |
| MAC (m)                | 2.48  | Ybar (m)               | 1.32  |
| Ybar (m)               | 2.39  | t/c                    | 0.126 |
| t/c                    | 0.126 |                        |       |

Once the new surface areas and dimensions of both of the tail planes were determined, the control surfaces could be sized.

The control surfaces were to be sized effectively to improve the dynamic stability and handling qualities of the aircraft. As an Automatic Flight Control System (AFCS) was equipped in the Aero 5 design, all analysis of control surfaces conducted through the ESDU data sheet method assumed an AFCS-equipped aircraft. For the ESDU data sheet analysis, the control surface deflection was taken to be  $\pm 20^\circ$ , apart from the spoiler deflection which was taken to be  $50^\circ$ . It was also assumed for simplicity that each control device would be modelled as a single surface.

It was required that the aircraft was designed to satisfy the requirements for manoeuvres and gusts set in CS 25.333 and CS 25.337, to also satisfy for yawing manoeuvres set in CS 25.351. Longitudinal stability requirements set by CS 25.173 and lateral stability set by CS 25.177 were also to be complied with during control surface sizing. For the stability criteria to be met, it is required for the aircraft and control surfaces to produce a positive yawing moment coefficient,  $C_n$ , a negative pitching moment coefficient,  $C_m$  and a negative rolling moment coefficient,  $C_l$ .

For the analysis of control surfaces, the ESDU Aerodynamics data sheets and tools were utilised, in Table 35 below, Aero 5 has listed all the key documents that were used.

Table 35 - List of ESDU Data Sheets and Tools Used

| ESDU SHEETS                            | Title  |
|--|--|
| ESDU AERO C.08.01.01 (Gilbey, 2015)    | Rate of change of pitching moment coefficient with control deflection for a plain control in incompressible two-dimensional flow, m0 |
| ESDU AERO C.08.01.03 (Gilbey, 1978)    | Rate of change of lift coefficient with control deflection in incompressible two-dimensional flow, (a2)0                             |
| ESDU 87008 (Gilbey and Wood 2014)      | Rudder side force, yawing moment and rolling moment control derivatives at low speeds: $Y_\zeta$ , $N_\zeta$ and $L_\zeta$           |
| ESDU 70011 (Allan, 1997)               | Rate of change of lift coefficient with control deflection for full-span plain controls.   |
| ESDU 88013 (Gilbey, 1992)              | Rolling moment derivative, $L_\xi$ for plain ailerons at subsonic speeds.  |
| ESDU 96003 (Dovey, 2003)               | Lift curve of wings with high-lift devices deployed at low speeds.   |
| ESDU 14004 Flower, (J. and Batt, 2014) | Lift and rolling moment due to spoilers on wings at subsonic speeds with trailing-edge flaps undeployed                              |
| ESDU 88040 (Gilbey, 1992)              | Program for the calculation of aileron rolling moment and yawing moment coefficients at subsonic speeds.                             |

### 5.5.1 Elevator Sizing – PS

The elevator surface on the horizontal tail plane is required to provide control in pitch of the aircraft as required by CS 25.173 for longitudinal stability. The elevator was initially sized based on the assumptions described in the PDR (Section 4.5.1).

It was decided by Aero 5 that the chord of the elevator was to be approximately 40% of the horizontal tail plane chord, the span of the elevator to be the whole span of the horizontal tail. It was decided that the taper ratio of the elevator was to be 0.4, which was the same as the taper ratio of the horizontal tail. The initial dimensions of the sized elevator is presented in Table 36.

*Table 36 - Initial Elevator Dimensions*

| Elevator Dimensions                                      | Value |
|--|-------|
| Elevator chord to horizontal tail chord ratio, $c_e/c_h$ | 0.500 |
| Elevator root chord (m)                                  | 1.67  |
| Elevator tip chord (m)                                   | 0.67  |
| Elevator span to horizontal tail span ratio, $b_e/b_h$   | 1.00  |
| Elevator span (m)  | 5.60  |
| Elevator taper ratio                                     | 0.40  |
| Elevator sweep (degrees)                                 | 20.0  |

The elevator dimensions from this estimate was interpreted through the ESDU data sheet tools to provide the surface loads and resulting stability derivatives. Aero 5 conducted analysis through EDSU AERO C.08.01.01 for the rate of change of pitching moment coefficient.

However, a second iteration was required as aerodynamic balance was taken into account. Control surfaces can suffer from flutter due to the high aerodynamic loads which can cause significant damage to the aircraft (Raymer, 2012). To reduce the flutter tendencies, the span was adjusted to only taken up around 85-90% of the vertical tail span. This would allow the hinge line to lie behind the leading edge of the control surface and provide an aerodynamic balance. The configuration of the tail due to this can be seen in Figure 37.

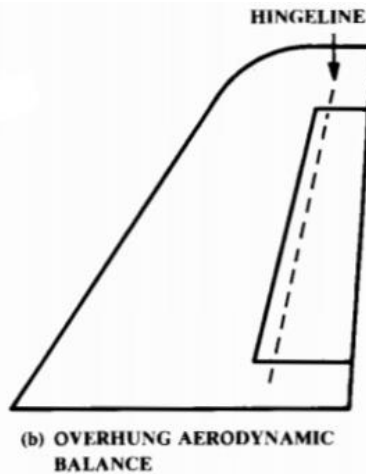


*Figure 37 - Diagrammatic Representation of an Overhung Aerodynamic Balance*

Due to this change in dimension, the ESDU analysis was conducted again for the dimensions shown below in Table 37.

Table 37 - Final Elevator Dimensions

| Elevator Dimensions                                      | Value |
|--|-------|
| Elevator chord to horizontal tail chord ratio, $c_e/c_h$ | 0.400 |
| Elevator root chord (m)                                  | 1.35  |
| Elevator tip chord (m)                                   | 0.58  |
| Elevator span to horizontal tail span ratio, $b_e/b_h$   | 0.87  |
| Elevator span (m)  | 4.89  |
| Elevator taper ratio                                     | 0.400 |
| Elevator sweep (degrees)                                 | 20.0  |

The input output data can be seen in Table 38.

Table 38 - Input and Output Data for ESDU AERO C.08.01.01

| ESDU AERO C.08.01.01 |                    |        |          |                         |       |
|----------------------|--------------------|--------|----------|-------------------------|-------|
| INPUTS:              | $C_e/C$            | 0.400  | OUTPUTS: | $M_0 (\text{rad}^{-1})$ | 0.624 |
|                      | $(t/c)_e$          | 0.126  |          |                         |       |
|                      | $\tan(\tau_a/2)_e$ | 0.0630 |          |                         |       |

Where  $\tan(\tau_a/2)_e$  was calculated by  $\frac{(t_{90}-t_{99})}{0.18c}$ , where  $t_{90}$  and  $t_{99}$  is the thickness of the elevator at 90% and 99% of the elevator chord respectively.

$M_0$  gives the rate of change in pitching moment coefficient as 0.624 per radian. Therefore the elevator deflected by  $\pm 20^\circ$  can provide a change in pitching moment coefficient of  $\pm 0.218$ .

This was evaluated using the method suggested by Raymer (2012), shown Equation (51) below. The equation has been simplified to assume the pitching moment due to engine thrust and normal force on the engine is negligible.

$$C_{m_{cg}} = C_L(\bar{X}_{cg} - \bar{X}_{acw}) + C_{m_w} + C_{m_{w\delta f}}\delta_f + C_{m_{fus}} - \eta_h \frac{S_h}{S_w} C_{L_h}(\bar{X}_{ach} - \bar{X}_{cg}) \quad (51)$$

Where the coefficient of the moment about the CG location  $C_{m_{cg}}$  is the sum of the coefficient of moments from the wing, flaps, fuselage, the coefficient of lift and the  $\eta_h \frac{S_h}{S_w} C_{L_h}(\bar{X}_{ach} - \bar{X}_{cg})$  term from the horizontal tail. Substituting values into the equation should result in a negative pitching moment for stability. The calculation of each term can be found in Appendix 13.9.

$$C_{m_{cg}} = -0.0335 - 0.0937 - 0.417 + 0.0482 + 0$$

$$C_{m_{cg}} = -0.496$$

As the pitching moment coefficient is -0.496, the aircraft is stable and with a deflected elevator the rate of pitching moment is low enough for the aircraft to be consistently stable.

Once the final dimensions of the elevator were sufficient, the hinge moment was calculated for the elevator as shown in Section 5.6.

### 5.5.2 Rudder Sizing – PS

The rudder is an essential control surface for sideslip control and the size was determined by cross-wind landing requirements defined in CS 25.237 and complied with CS 25.177 for directional stability. As mentioned in the PDR (Section 4.5.1), the rudder was initially sized with 40% of the vertical tail chord and the full height of the vertical tail plane whilst keeping the same taper of 0.4. The initial dimensions of the rudder can be below in Table 39.

Table 39 - Initial Rudder Dimensions

| Rudder Dimensions                                      | Value |
|--|-------|
| Rudder chord to vertical tail chord ratio, $c_r/c_v$   | 0.500 |
| Rudder root chord (m)                                  | 2.56  |
| Rudder tip chord (m)                                   | 1.03  |
| Rudder height to vertical tail height ratio, $b_r/b_v$ | 1.00  |
| Rudder height (m)                                      | 6.14  |
| Rudder taper ratio                                     | 0.400 |
| Rudder sweep (degrees)                                 | 40.0  |

However, as mentioned in Section 5.5.1, the aerodynamic balance required a change of the height of the rudder to reduce flutter tendencies. A change in tail cone dimensions occurred due to the area required to fit an APU, which changed some of the input values for the ESDU tool. It was decided by Aero 5 to size the rudder height to be 90% of the vertical tail height. This resulted in the following dimensions shown in Table 40.

Table 40 - Final Rudder Dimensions

| Rudder Dimensions                                      | Value |
|--|-------|
| Rudder chord to vertical tail chord ratio, $c_r/c_v$   | 0.400 |
| Rudder root chord (m)                                  | 1.84  |
| Rudder tip chord (m)                                   | 0.72  |
| Rudder height to vertical tail height ratio, $b_r/b_v$ | 0.900 |
| Rudder height (m)                                      | 5.53  |
| Rudder taper ratio                                     | 0.400 |
| Rudder sweep (degrees)                                 | 40.0  |

These dimensions were examined through the ESDU 87008 to provide the rudder side force, yawing moment and rolling moment derivatives. The input dimensions required are shown in Figure 38. The values of the input and the resulting derivatives can be found in Table 41.

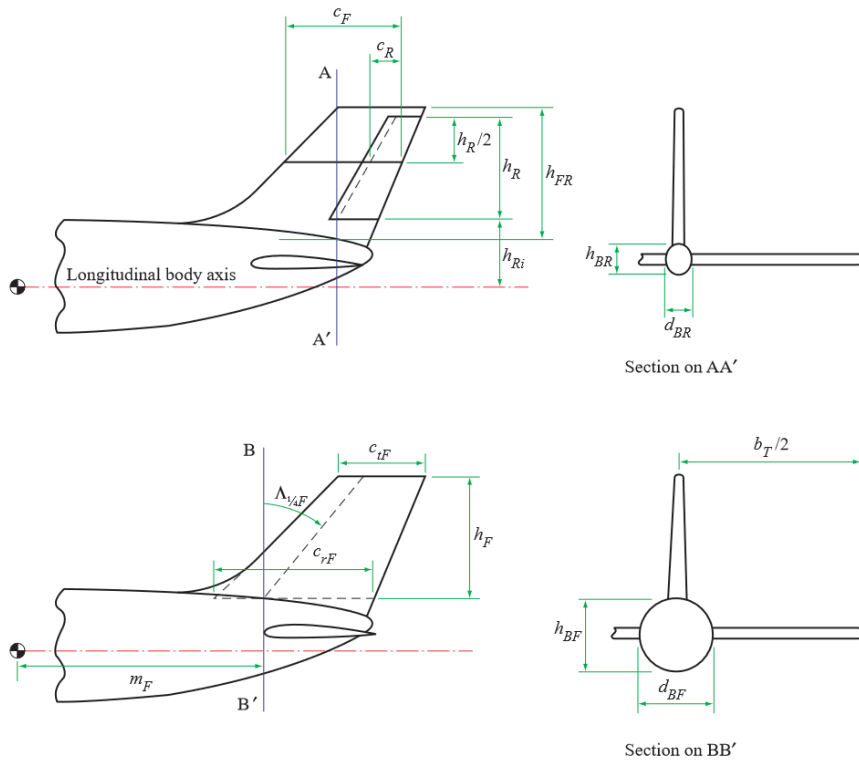


Figure 38 - Graphical Representation of Input Values for ESDU 87008

AA' represents the cross-section of the empennage at the start of the hinge line inboard and BB' represents the cross-section at the quarter-chord of the vertical tail root.

Table 41 - Input and Output Data for ESDU 87008

| ESDU 87008         |                |                  |                 |                                |                |      | OUTPUTS:       |        |   |
|--------------------|----------------|------------------|-----------------|--------------------------------|----------------|------|----------------|--------|---|
| INPUTS:            | S <sub>w</sub> | 136              | h <sub>Ri</sub> | 2.60                           | h <sub>F</sub> | 6.14 | OUTPUTS:       | α      | 0 |
| b                  | 36.0           | h <sub>FR</sub>  | 6.14            | h <sub>BR</sub>                | 3.88           |      | Y <sub>ζ</sub> | 0.288  |   |
| c <sub>F</sub>     | 3.80           | h <sub>BR</sub>  | 2.66            | b <sub>T</sub>                 | 11.2           |      | N <sub>ζ</sub> | -0.180 |   |
| c <sub>R</sub>     | 1.37           | d <sub>BR</sub>  | 1.68            | η <sub>i</sub> h <sub>FR</sub> | 0.410          |      | L <sub>ζ</sub> | 0.0384 |   |
| (t/c) <sub>F</sub> | 0.126          | l <sub>v</sub>   | 20.1            | η <sub>0</sub> h <sub>FR</sub> | 5.93           |      |                |        |   |
| τ <sub>F</sub>     | 7.21           | c <sub>rF</sub>  | 5.11            | α                              | 0              |      |                |        |   |
| R <sub>F</sub>     | 3.36E+07       | c <sub>tF</sub>  | 2.05            |                                |                |      |                |        |   |
| h <sub>R</sub>     | 5.53           | Λ <sub>1/4</sub> | 40.0            |                                |                |      |                |        |   |

The results calculated from the ESDU tools were compared for yaw control effectiveness as set out by Raymer (2012). It was assumed that through these calculations that one aircraft engine was inoperative, with a 11.5° sideslip angle and 20° deflection of the control surfaces (Raymer, 2012). Equation (52) was used to calculate the yawing moment derivative of the aircraft. It was simplified through the assumption that propwash would not be considered in this analysis and all angles included were converted to radians.

$$C_n = C_{n\beta_w} \beta + C_{n\delta_a} \delta_a + C_{n\beta_{fus}} \beta + C_{n\beta_v} \beta - \frac{\overline{TY_p}}{qS_w} - \frac{\overline{DY_p}}{qS_w} \quad (52)$$

Where  $C_{n\beta_w}$  is the wing yawing coefficient due to sideslip,  $C_{n\delta_a}$  is the yawing moment coefficient due to aileron deflection,  $C_{n\beta_{fus}}$  due to fuselage,  $C_{n\beta_v}$  due to the side force given by Equation (53) and  $\frac{\overline{TY_p}}{qS_w} - \frac{\overline{DY_p}}{qS_w}$  term represents the one engine inoperative case (Raymer, 2012).

$$C_{n\beta_v} = C_{F\beta_v} \frac{\partial \beta_v}{\partial \beta} \eta_v \frac{S_v}{S_w} (\overline{X_{acv}} - \overline{X_{cg}}) \quad (53)$$

Where  $C_{F\beta_v} = 0.288$  was assumed from the side force derivative given in Table 41,  $\frac{\partial \beta_v}{\partial \beta} \eta_v = 1.05$ ,  $\frac{S_v}{S_w}$  is the area ratio and  $\overline{X_{acv}} - \overline{X_{cg}}$  is the moment arm to the vertical tail AC. Each term can be found calculated in Appendix 13.10 using equations given by Raymer (2012), from which the yawing moment derivative,  $C_n$  was calculated. The sideslip angle,  $\beta$  and the aileron deflection angle,  $\delta_a$  have been converted to radians.

$$C_n = 0.0143 * 0.2 - 0.00823 * 0.349 - 0.183 * 0.2 + 0.978 * 0.2 - 0.0464 * 2$$

$$C_n = 0.0662$$

The resulting yawing moment coefficient with one engine inoperative in side slip can still be seen as positive. Therefore, an addition of the yawing moment derivative produced at a rudder deflection of ±20° would provide a 0.604 yawing moment coefficient that would be sufficient in the worst case scenario of one engine failure.

### 5.5.3 Wing Control Surface Sizing – PS

The wing required sizing of the primary control surface, the aileron, however the impact of the secondary control surfaces were also considered hence requiring the secondary control surfaces to be sized as well. The configuration of the control surfaces on the wing was based on the location of the engine and the available space, which played an important part for the effectiveness of the aileron.

The aileron is required to produce sufficient roll control and work in conjunction with the rudder for yaw control and manoeuvrability. High speed civil aircraft have the risk of producing rolling moment greater than that produced by aileron which results in roll in the opposite direction. This is due to aileron reversal which can cause the wing to twist as large air loads act on the deflected aileron surface (Raymer, 2012).

It was therefore decided by Aero 5 to include spoilers into the design of the wing. Spoilers can act to provide roll control that the ailerons may not be able to provide at high speeds and hence avoid uncontrollability of the aircraft. Spoilers can provide a large rolling moment that would be enough to keep control caused by deploying spoilers on one side of the wing (Raymer, 2012). As the Aero 5 design incorporates an AFCS, the nonlinear response characteristic of the spoilers shouldn't affect the implementation of roll control.

The initial size of the aileron control surface was based upon the guideline provided by Raymer (2012). Due to the location of the rear spar which is located at 71% wing chord (Section 5.3.4), the aileron chord was sized to be 0.7m which would allow the spar to lie before the aileron. Figure 39 shows the historical guidelines for sizing the aileron. From which, for an aileron chord to wing (tip) chord ratio of 0.32 the aileron span to wing span ratio was determined to be approximately 0.3. This provides the spanwise dimension of the aileron to be 5m.

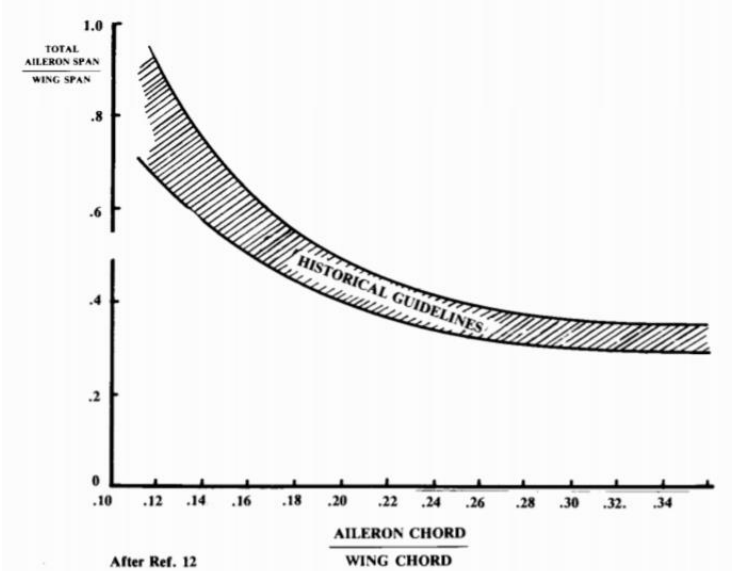


Figure 39 - Historical Guideline for Aileron Span and Chord Ratios (Raymer, 2012)

To evaluate the effectiveness of the ailerons through the ESDU tools, it was required to size the high lift devices and include the contribution of spoilers to the roll control.

It was decided by Aero 5 that the design would incorporate Fowler flaps at the trailing edge and Krueger flaps with a single slotted slat at the leading edge (Section 3.4 of the Aero 5 PDR). To maximise the lift coefficient, the Fowler flaps were sized based on the space available after including the aileron. This resulted in the spanwise direction of the Fowler flap to be 8m and the chord to be 0.8m.

The leading edge high lift devices were sized and placed based on the location of the engine so that there would be sufficient clearance for deployment. The Krueger flap was placed inboard and due to the engine location lying 4.19m from the wing root as mentioned in Change Request 3 (Appendix 13.1.3), the span was sized to be 3m and chord to be 0.6m due to the leading edge spar placed at 12% of the wing chord (from Section 5.3.4). Similarly, the single slotted slat was sized due to the availability on the leading edge of the wing and spar location, which yielded the dimensions for the slotted slat to have 9m span and chord 0.5m. The control surface dimensions are presented in Table 42.

The contribution of roll control by spoilers was required to be added to the ailerons to get a final derivative for roll. The sizing of the spoilers was primarily based on the Fowler flaps sizing and available space forward of the flaps. Flap type spoilers were chosen, as they only occupy the top surface of the wing and have minimal impact on the internal wing structure. Spoilers are typically located aft of the thickest point of the wing (Raymer, 2012), hence, the available space between the thickest point and the leading edge of the Fowler flap resulted in the spoiler to have a chord of 1m and a span of 5m, as shown in Table 42 below.

Table 42 - Wing Control Surface Dimensions

| Wing Control Surface Dimensions | Chord (m) | Span (m) | Mid-point Location from Wing Root (m) |
|---------------------------------|-----------|----------|---------------------------------------|
| Aileron                         | 0.700     | 5.00     | 12.3                                  |
| Fowler Flap                     | 0.800     | 8.00     | 4.50                                  |
| Krueger Flap                    | 0.600     | 3.00     | 2.00                                  |
| Single slotted slat             | 0.500     | 9.00     | 10.0                                  |
| Spoiler                         | 1.00      | 5.00     | 4.50                                  |

The contribution of the high lift devices,  $\Delta C_{L_f}$  was evaluated through ESDU 96003 and was then incorporated into ESDU 88040, to provide the roll derivative for the ailerons. As mentioned earlier, all analysis assumed a deflection of  $\pm 20^\circ$  excluding spoilers. The roll contribution from the spoilers was calculated using ESDU 14004. Presented in Table 43, are the inputs and results for ESDU 88040 including results from ESDU 70011 that were determined first.

Table 43 - Input and Output Data for ESDU 70011 and ESDU 88040

| ESDU 70011 |                 |          |                  |                                |          |             |
|------------|-----------------|----------|------------------|--------------------------------|----------|-------------|
| INPUTS:    | M               | 0.760    | OUTPUTS:         | $\beta \text{AR}$              | 6.20     |             |
|            | AR              | 9.54     |                  | $\text{AR tan}(\Lambda_{1/2})$ | 4.43     |             |
|            | $\Lambda_{1/4}$ | 27.0     |                  | $\frac{dC_L}{d\alpha}$         | 5.96     |             |
|            | $\lambda$       | 0.400    |                  |                                |          |             |
| ESDU 88040 |                 |          |                  |                                |          |             |
| INPUTS:    | Re              | 5.86E+07 | $\gamma'$        | 2.00                           | OUTPUTS: | Roll moment |
|            | M               | 0.760    | $\eta_i$         | 0.620                          |          |             |
|            | AR              | 9.54     | $\eta_0$         | 0.920                          |          |             |
|            | $\lambda$       | 0.400    | $J_\delta$       | 1.40                           |          |             |
|            | $\Lambda_{1/2}$ | 24.9     | $J_f$            | 18.0                           |          |             |
|            | $\Lambda_h$     | 20.0     | $\delta_t$       | -2.00                          |          |             |
|            | $c_d/c$         | 0.320    | $C_L$            | 0.670                          |          |             |
|            | t/c             | 0.140    | $\Delta C_{L_f}$ | 0.960                          |          |             |
|            | $\tau$          | 14.0     | $\zeta'$         | 20.0 and -20.0                 |          |             |

$\gamma'$ , the angle between the chord and camber line was assumed to be  $2^\circ$ . It was also assumed by Aero 5 that  $J_\delta$ ,  $J_f$  and  $\delta_t$  would be assumed to be 1.40, 18.0 and -2.00 respectively. These values were suggested by the ESDU 88040 as it was assumed to change the overall rolling moment insignificantly.

ESDU 70011 data was used to confirm the roll contribution that did not incorporate flaps in the analysis. This was done through ESDU data sheets 88013 and 88029. This yielded a rolling moment,  $\zeta' = -0.182 \text{ rad}^{-1}$ . This calculation can be found in Appendix 13.11. Therefore the assumptions made from ESDU 88040 were realistic due to the output result from Table 43 providing a greater negative roll moment of -0.202.

The contribution of the spoilers were calculated using ESDU 14004, which provided a rolling moment coefficient of -0.0275 at  $50^\circ$  deflection of the spoilers. This calculation can be found in Appendix 13.12. For stability it is required for the coefficient of roll to be negative (Raymer, 2012). The size of the spoilers were verified to be effective using Figure 7 in ESDU 14004, given the ratio of mid-span of the spoiler to the wing chord,  $\eta$  to be 0.284 and the height,  $h$  to be 0.5m.

To ensure the wing control surface sizing and locations were effective for control and stability, the method to evaluate lateral-direction control by Raymer (2012) was employed. Equation (54) below was provide by Raymer (2012) to determine the rolling moment coefficient. The calculation of each term can be found in Appendix 13.13.

$$C_l = C_{l\beta_w} + C_{l\delta_a} \delta a + C_{l\beta_v} \beta \quad (54)$$

$$C_l = -0.420 - 0.00823 * 0.349 - 0.0249 * 0.2 = -0.427$$

As it can be seen from the result, the aircraft provides a rolling moment of -0.427 which satisfies stability and the control surfaces provides and enforcement of the negative rolling moment.

The final geometry of the wing control surfaces can be seen laid out in Figure 40 on the wing planform section.

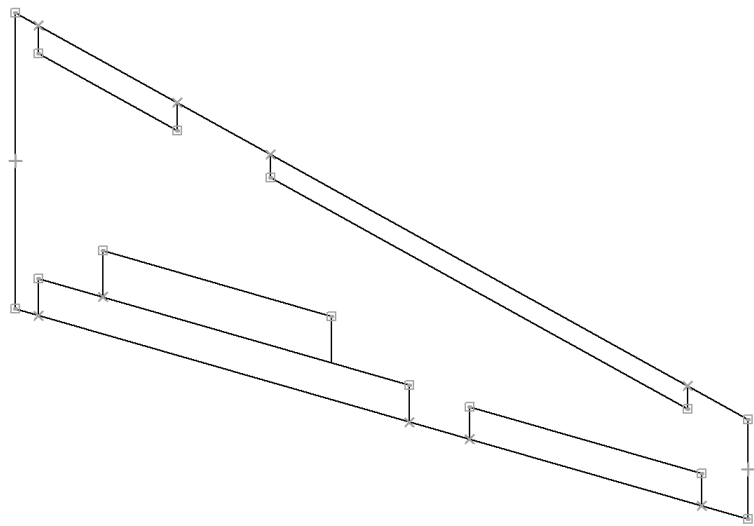


Figure 40 - Planform Diagram of Final Control Surfaces Placement

#### 5.5.4 Further Development and Improvements – PS

Constraints such as timescale and experience of Aero 5 meant that the sizing of control surfaces were conducted majorly through historical assumptions and the ESDU tools. A higher accuracy in the analysis of effectiveness of the control surfaces would have been achieved by using higher-end tools as well as using sizing matrix plots. Another consideration would be to evaluate the structural impact of the control surfaces on the tail, such as the mass contribution and iterate the control surface sizes based on this impact.

As it was also assumed that all the control surfaces were to be single sections, an improvement would be to break up some of the control surface and analyse the specific contributions of each part. For example, spoilers could be split into ground and flight spoilers, the flaps could be broken up and placed at intervals on the wing. It was also a consideration of Aero 5 to fully extend the slotted slat to the ends of the wing tip given time to consider the full aerodynamic impact.

#### 5.5.5 Tail Plane CAD – PS

Once the final dimensions of the elevator and the rudder were determined by Aero 5’s analysis, the CAD model for the horizontal and vertical tail plane were developed using the Solid Edge software. The CAD model of the vertical tail plane including the rudder is shown below in Figure 41 below and the model of the horizontal tail plane including the elevator is shown in Figure 42. As both parts of the tail had a symmetrical aerofoil, the thickness to chord ratio of 0.126 (from PDR Section 4.5) was used to create the geometry using dimensions from Sections 5.5.1 and 5.5.2 of this report. The loft function was used to create the 3D surface of the models.

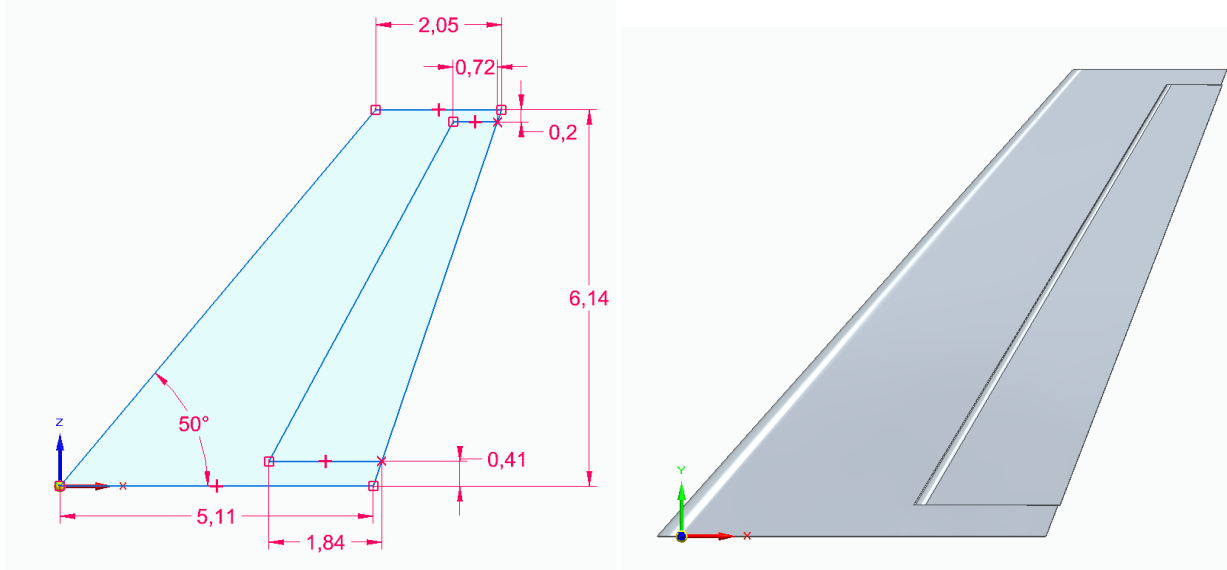


Figure 41 - Dimensioned and 3-D Model of the Vertical Tail

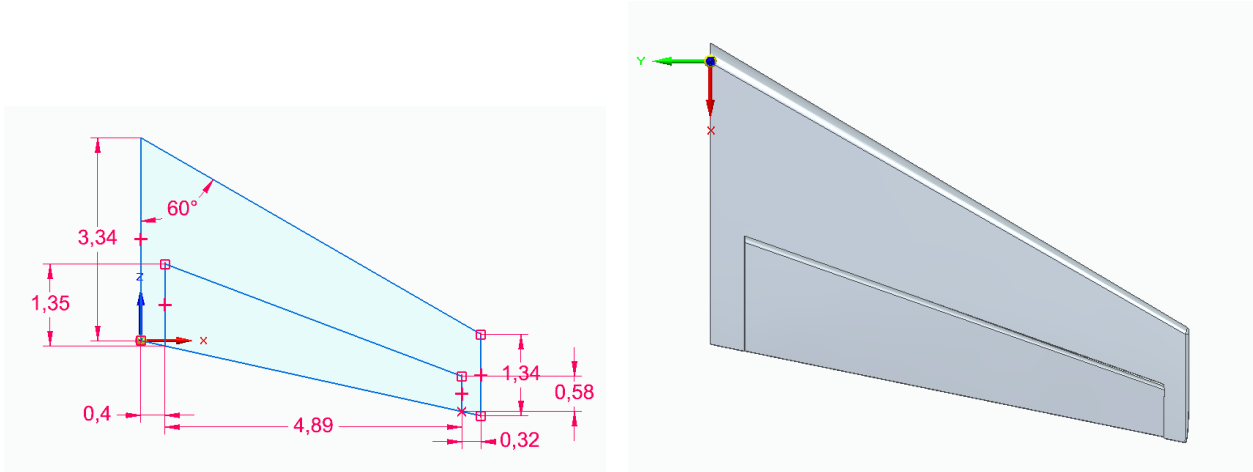


Figure 42 - Dimensioned and 3-D Model of the Horizontal Tail

## 5.6 Hinge Moments – BG

The control surfaces for the Aero 5 aircraft were designed and sized in order to maintain full control in pitch, roll and yaw throughout the flight envelope, with an appropriate safety margin. A hinge moment is the moment required to deflect a control surface and is a function of the control surface geometry, aircraft velocity, density and a non-dimensional hinge moment coefficient. Equation (55) shows how a hinge moment is calculated (Gilbey, 1989).

$$H = \frac{1}{2} \rho V^2 \bar{c}_f^2 s_f C_H \quad (55)$$

Where  $H$  is the hinge moment required to deflect the control surface,  $\rho$  is the local air density,  $V$  is the aircraft velocity,  $\bar{c}_f$  is the aerodynamic mean control chord aft of the hinge line,  $s_f$  is the span of the control surface and  $C_H$  is the non-dimensional hinge moment coefficient. Figure 43 (Gilbey, 1989) details the typical geometry of a control surface, including the location of the hinge line. According to Raymer (1992), the hinge line is usually located at a distance of  $0.2c$  from the leading edge, where  $c$  is the chord length of the control surface. The line AA' represents a cut through the control surface, perpendicular to the quarter chord sweep of the wing.

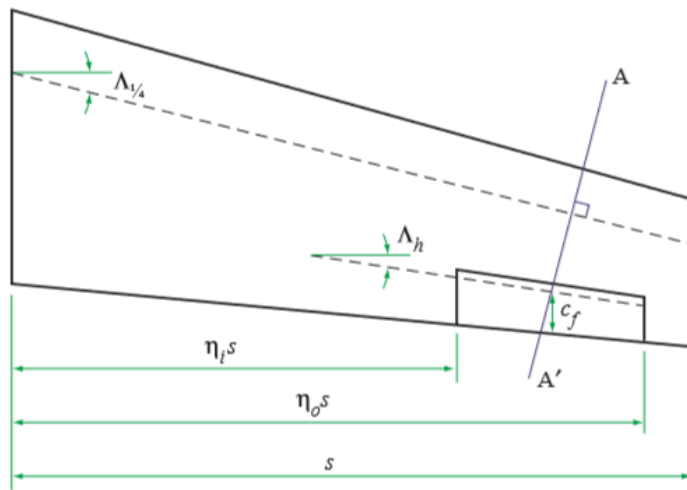


Figure 43 - Typical Control Surface Planform (Gilbey, 1989)

A fundamental part of the design of the control surfaces is to verify that they are able to maintain effectiveness in a gust load scenario, as specified by CS 24.415. Equation (56) is defined as part of CS 25.415, to calculate the hinge moment required to overcome a horizontal gust load ( $H_0$ ).

$$H_0 = \frac{1}{2} \rho V^2 c S K \quad (56)$$

Where  $\rho$  is local air density,  $V$  is the horizontal gust velocity,  $c$  is the mean aerodynamic chord of the control surface aft of the hinge line,  $S$  is the area of the control surface aft of the hinge line and  $K$  is a hinge moment factor for ground gusts. The value of  $K$  is unique for each control surface and is described in more detail in Table 44.

Table 44 - Values of  $K$

| Control Surface | $K$   |
|-----------------|-------|
| Aileron         | 0.500 |
| Elevator        | 0.750 |
| Rudder          | 0.750 |

To determine whether the Aero 5 aircraft control surfaces were sized appropriately the output of Equation (55) was compared against the output of Equation (56). Provided that the output of Equation (55) (with  $V$  being the minimum control speed, determined in Section 5.7.4), was greater than the output of Equation (56), the moment required to deflect the control surface would be sufficient to maintain effectiveness and control the Aero 5 aircraft in pitch, roll and yaw in a gust load scenario.

### 5.6.1 Process for Calculating Hinge Moments – BG

The basis of the hinge moment calculations was Section 21 of the ESDU Aerodynamic Series (Gilbey, 1989). The procedures outlined in these documents enabled the calculation of the hinge moment coefficient derivatives, as described in Equation (57) and Equation (58).

$$b_1 = \frac{\partial C_H}{\partial \alpha} \quad (57)$$

$$b_2 = \frac{\partial C_H}{\partial \delta} \quad (58)$$

Where  $b_1$  is the rate of change of the hinge moment coefficient with respect to the aircraft angle of attack and  $b_2$  is the rate of change of the hinge moment coefficient with respect to the control surface deflection.  $b_1$  and  $b_2$  were calculated separately for each control surface.

The hinge moment coefficient derivatives were calculated using the carpet plots and equations available in the ESDU Aerodynamic Series and this was implemented on a Microsoft Excel Spreadsheet. The following process described how the values of  $b_1$  and  $b_2$  were determined:

1. ESDU Wings 01.01.05 (Gilbey, 2007), ESDU Controls 01.01.03 (Gilbey, 1978), ESDU Controls 04.01.01 (Gilbey, 1989), ESDU Controls 04.01.02 (Gilbey, 1989) and ESDU Controls 04.01.03 (Gilbey, 1989) were used to determine section properties for the Aero 5 control surface design. After calculating the necessary section properties for the Aero 5 design, the process also required the calculation of a standard control surface section. A standard section is described in the ESDU documents as one that satisfies Equation (59).

$$\tan\left(\frac{\tau}{2}\right) = \frac{t}{c} \quad (59)$$

Where  $\tau$  is the trailing edge angle and  $t/c$  is the thickness to chord ratio for the aerofoil section. This stage of the calculation process was used to determine the hinge moment coefficient derivatives and lift curve slope derivatives for a two dimensional aerofoil section, in incompressible flow. During this stage of the calculation process factors such as flow transition and the effects of finite aspect ratio wings were also considered.

2. The second stage of the process was to apply a nose balance correction to the hinge moment coefficient derivatives calculated in Stage 1. It was assumed that all the control surfaces would be sealed and that the hinge line (about which the control surface pivots) was to be located at a distance of  $0.2c$  from the leading edge of the control surface (where  $c$  is the control surface chord length). The assumption that all the control surfaces would be sealed was made as ‘unsealing the gap between the nose of the control surface and the main aerofoil affects the control hinge moment coefficients’ (Gilbey, 1989) with a

tendency for the coefficients to ‘become more positive’. A more positive hinge moment coefficient would lead to a reduction in the effectiveness of the control surface.

3. The next stage of the calculation process used ESDU 70011 (Gilbey, 1989) to determine the lift curve slope for each control surface. This stage of the process also included a correction for the effects of compressible flow and taper ratio, in order to provide a more accurate estimation for the hinge moment coefficient derivatives. This part of the calculation also required a value for the hinge sweep, which was estimated based upon the suggestions made in ESDU 89009 (Gilbey, 1989).
4. The final stage of this process was to calculate the values of  $b_1$  and  $b_2$  using the carpet plots and equations defined in ESDU 89009. This involved using the data obtained in Steps 1 – 3 of this process. The hinge moment coefficient derivatives for each control surface are described in Table 45.

*Table 45 - Hinge Moment Coefficient Derivatives*

| Control Surface | $b_1$   | $b_2$  |
|-----------------|---------|--------|
| Aileron         | -0.0421 | -0.561 |
| Elevator        | -0.0171 | -0.470 |
| Rudder          | -0.0325 | -0.376 |

The data in Table 45 enabled the calculation of the hinge moment coefficient, using Equation (60). The value  $b_2$  was used to determine  $C_H$  as it would have a more significant impact on the subsequent calculation of  $H$  and result in a more accurate approximation of the hinge moment required to deflect each control surface. The values calculated for  $b_2$  are in agreement with the values presented in ESDU Controls 04.01.00 (Gilbey, 1989), as seen in Figure 44.

$$C_H = \int_{-\delta}^{+\delta} b_2 d\delta \quad (60)$$

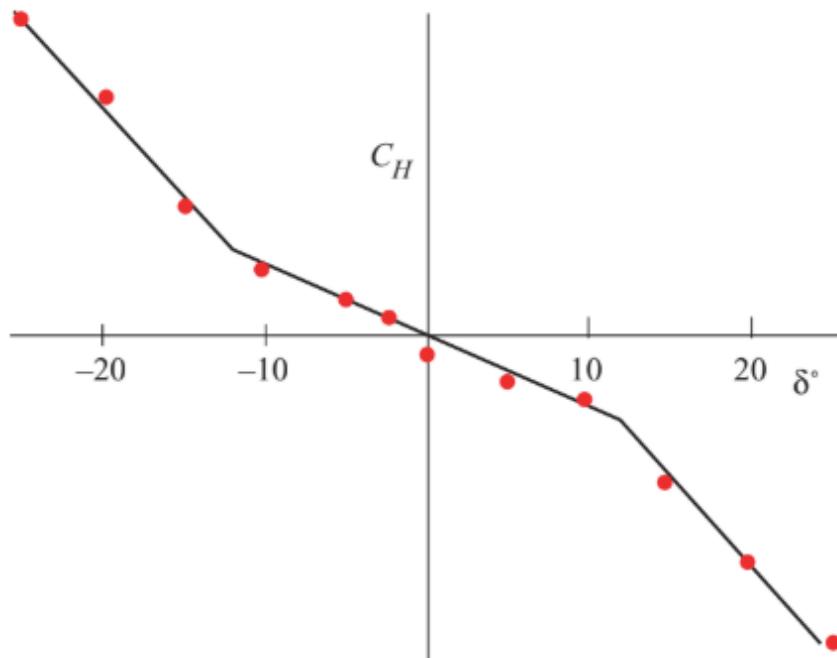


*Figure 44 - Typical Hinge Moment Coefficient vs.  $\delta$  Curve (Gilbey, 1989)*

The hinge moment coefficient was calculated based upon the maximum deflection of each control surface, which is defined in Section 5.5 as  $\pm 20^\circ$  for the elevator, rudder and aileron. The limits of the integral are defined as the maximum and minimum deflection for the control surface, as this ensured that the hinge moments calculated were large enough to maintain control of the aircraft when in a gust loading scenario. It was assumed that the relationship between  $C_H$  and  $\delta$  was linear, as the value of  $b_2$  calculated is described as a ‘mean value’ (Gilbey, 1989) for the range of control surface deflection. The calculated values of  $C_H$  are shown in Table 46.

Table 46 -  $C_H$  Values

| Control Surface | $C_H$  |
|-----------------|--------|
| Aileron         | -0.392 |
| Elevator        | -0.328 |
| Rudder          | -0.275 |

Prior to calculating the hinge moment for each control surface, the value of  $\bar{c}_f$  had to be calculated. ESDU 89009 (Gilbey, 1989) defines  $\bar{c}_f$  as:

$$\bar{c}_f = \int_{\eta_i}^{\eta_o} \frac{c_f^2}{\bar{c}_f} d\eta \quad (61)$$

Where  $\bar{c}_f$ , the geometric mean chord aft of the hinge line, is defined as:

$$\bar{c}_f = \int_{\eta_i}^{\eta_o} c_f d\eta \quad (62)$$

Where  $\eta_i$  and  $\eta_o$  are the inboard and outboard locations of the control surface with respect to the wing semi-span. The values of  $H$  for each control surface were then calculated, for the aircraft minimum ground control speed (using Equation (55)), and the results are shown in Table 47. Furthermore, the hinge moment required to maintain control effectiveness in a gust load case was calculated using Equation (56) and the results are shown in Table 47.

Table 47 - Comparison of  $H$  and  $H_0$

| Control Surface | $H$ (kNm) | $H_0$ (kNm) |
|-----------------|-----------|-------------|
| Aileron         | -1.01     | -0.94       |
| Elevator        | -1.97     | -1.64       |
| Rudder          | -3.58     | -3.50       |

Table 47 shows that the control surfaces satisfy CS 25.415, as the hinge moment produced by the aircraft at the minimum control speed is greater than the hinge moment required to maintain control effectiveness in a gust load condition. For the aileron and elevator, the values of  $H$  and  $H_0$  shown are the hinge moments per control surface (i.e. each aileron requires a hinge moment of 0.94kNm, to overcome a gust load at the minimum ground control speed).

## 5.6.2 Actuator Loads – BG

The final consideration for sizing the control surfaces and calculating the hinge moments for the Aero 5 aircraft were the actuator loads required to deflect the control surfaces. As stated in the Aero 5 PDR, Electro-Hydraulic Actuators (EHA) were selected to control the ailerons, elevators and rudder. The EHA was selected as the control method as it reduces weight and maintenance cost, whilst improving reliability when compared to a hydraulic actuator. As the exact location of each EHA has not been determined, it was not possible to determine the exact actuator load, however, the maximum hinge moment for each control surface has been determined. This will inform the exact actuator load when the EHA location is finalised.

The maximum hinge moment required was calculated using Equation (55), assuming cruise conditions and are shown in Table 48. The values of  $H_{Max}$  for the aileron and elevator have been calculated per control surface.

Table 48 - Maximum Hinge Moments

| Control Surface | $H_{Max}$ (kNm) |
|-----------------|-----------------|
| Aileron         | -5.35           |
| Elevator        | -18.9           |
| Rudder          | -10.4           |

The values in Table 48 consider the hinge moment required to deflect each control surface from the greatest positive deflection (+20°), to the greatest negative deflection (-20°). This deflection would not be expected during normal operation and hence the actual hinge moments required during flight would be significantly

lower. To ensure control effectiveness and aircraft safety the EHA for each control surface will be selected to produce the maximum hinge moment (including a suitable factor of safety), as per Table 48.

## 5.7 Take-off and Landing Considerations – BG

### 5.7.1 Take-off Considerations – BG

Further to the work carried out for the Aero 5 PDR, this section of the report will provide additional analysis regarding the performance of the Aero 5 aircraft during the take-off and landing phases. At the point of delivery of the Aero 5 PDR, the available information had been analysed and incorporated into the design. Since the successful delivery of the Aero 5 PDR, the Aero 5 design has included design decisions that resulted from the additional analysis described in this section of the report, that increase the fidelity of the Aero 5 design.

### 5.7.2 Drag at Take-off – BG

In the PDR, it was shown that for the One Engine Inoperable (OEI) case, the selected powerplant for the Aero 5 aircraft provided enough thrust to successfully take-off, as the thrust was greater than the total drag of the aircraft. This analysis has been progressed to determine the minimum drag speed of the Aero 5 aircraft during the take-off and climb phases.

The total drag that acts on an aircraft is a combination of the profile drag and the induced drag, as described by Equation (63) (Hancock, 2016).

$$Drag_{Total} = Drag_{Induced} + Drag_{Profile} \quad (63)$$

Equation (63) can be written as a function of velocity, as shown below in Equation (64), where  $\rho$  is the air density (as per the International Standard Atmosphere tables),  $V$  is the aircraft velocity,  $S_w$  is the wing reference area,  $C_{D0}$  is the profile drag coefficient (as determined in the Aero 5 PDR),  $k$  is a constant, defined by Equation (65) and  $W$  is the maximum take-off weight of the Aero 5 aircraft.

$$Drag_{Total} = \frac{1}{2}\rho V^2 S_w C_{D0} + \frac{kW^2}{\frac{1}{2}\rho V^2 S_w} \quad (64)$$

$$k = \frac{1}{\pi A Re} \quad (65)$$

In Equation (65),  $AR$  is the wing aspect ratio and  $e$  is the efficiency factor for the wing. It can be seen in Equation (64) that induced drag is proportional to the aircraft velocity squared, whereas profile drag is inversely proportional to the aircraft velocity squared. This implied that as the aircraft accelerates during the take-off phase, the induced drag will increase, whereas the profile drag will decrease. There will be a specific velocity at which the total drag is at a minimum, and this would be the optimum velocity to fly at during the climb phase. However, this may not be possible as the climb velocity is dictated by a requirement in the Customer Design Brief (CDB). The minimum drag speed occurs when the induced drag is equal to the profile drag and therefore the velocity at which the induced drag coefficient is equal to the profile drag coefficient. This is due to the fact that the profile drag coefficient is a fixed parameter but the induced drag coefficient depends upon the lift coefficient ( $C_L$ ), as shown in the relationship in Equation (66).

$$C_{Di} = \frac{C_L^2}{\pi A Re} = k C_L^2 \quad (66)$$

Using an Excel spreadsheet, the drag throughout the take-off phase was calculated as a function of the aircraft velocity and the results were plotted. Figure 45 shows the results of this analysis. It is worth noting that for the purposes of this analysis the drag acting on the aircraft was independent of the thrust produced by the aircraft. This implies that the Drag vs. Velocity curve will be the same for the OEI take-off case and the case where both engines are operational.

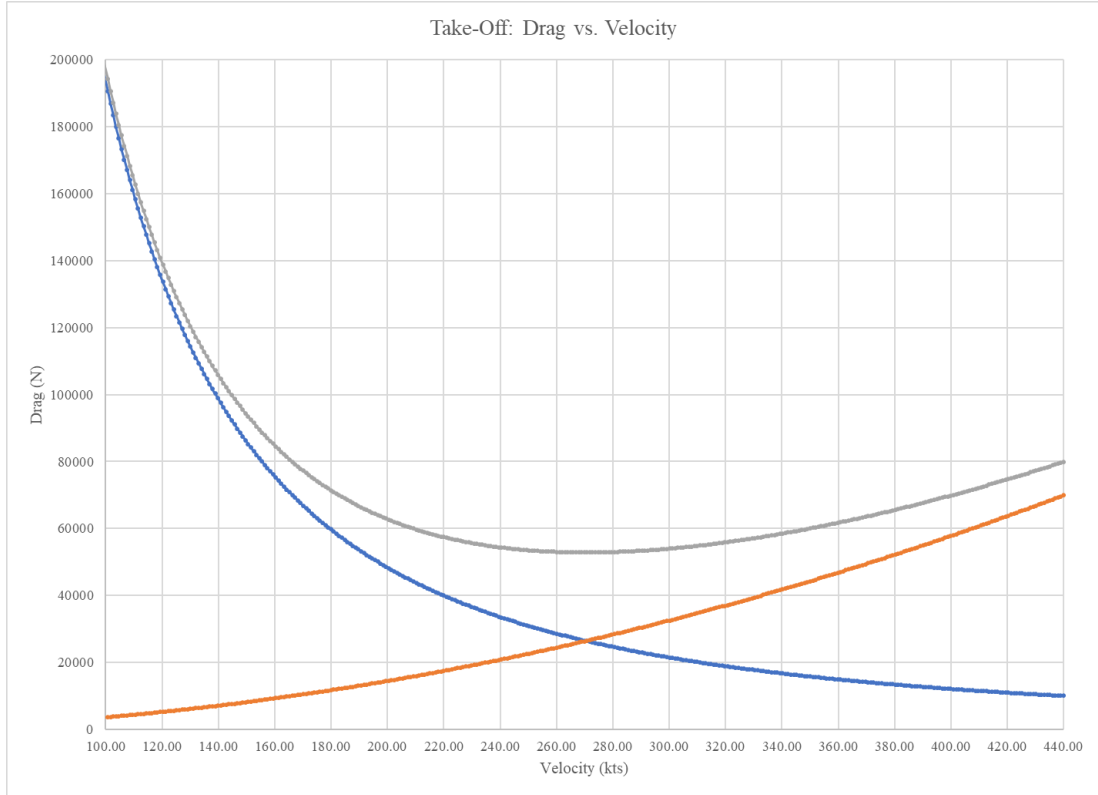


Figure 45 - Drag vs. Velocity at Take-Off

Figure 45 shows that the minimum drag speed for the take-off configuration is in the range 250kts to 290kts. It was possible, using Equation (67) (Hancock, 2016), to calculate the exact value of the minimum drag speed.

$$V_{minD} = \left( \frac{k}{C_{D0}} \right)^{\frac{1}{4}} \left( \frac{W}{\frac{1}{2} \rho S_w} \right)^{\frac{1}{2}} \quad (67)$$

Using Equation (67), the exact value of the minimum drag speed for the take-off condition was calculated to be 138 m/s (270 kts). Equation (67) also shows that the minimum drag speed varies with both aircraft weight and local air density. This implied that the minimum drag speed at cruise would be different to the minimum drag speed during the take-off and climb phases.

The CDB specifies that the climb velocity for the Aero 5 aircraft is to be 250 kts. The analysis described above and the results shown in Figure 45 indicate that the aircraft will be climbing at a velocity that is close to the velocity for minimum drag. This would improve the efficiency of the Aero 5 aircraft by reducing the overall fuel burn for a given flight. A reduction in fuel burn would also result in a reduction in DOC which is a key design driving requirement in the CDB.

### 5.7.3 Rate of Climb – BG

The rate at which an aircraft can climb was a critical factor that was considered during the design process of the Aero 5 aircraft. Specifically, the aircraft was sized and designed to be capable of climbing at the rate specified by CS 25.121, for the OEI scenario. The airworthiness specification describes a minimum gradient of climb at given stages of the typical flight path. The following analysis demonstrates that the Aero 5 aircraft has been sized to comply with CS 25.121, therefore proving that the aircraft would be operable if one of the engines were to fail. The analysis also determines the gradient and rate of climb for the scenario where both engines are fully operational.

The first step in calculating the rate of climb during the take-off phase was to determine the angle of climb of the aircraft. Hancock (2016) states that assuming a steady, climbing flight, the angle of climb can be determined from Equation (68).

$$\sin(\theta) = \frac{T - D}{W} \quad (68)$$

Where  $\theta$  is the angle of climb,  $T$  is the thrust,  $D$  is the total drag acting on the aircraft (as determined in Section 5.7.2) and  $W$  is the aircraft weight. As the total drag acting on the aircraft varies with the aircraft velocity, the angle of climb, and hence the rate of climb, would also vary with the aircraft velocity. The rate of climb is described as the vertical component of the aircraft velocity, as shown in Equation (69).

$$\text{Rate of Climb} = V_V = V \sin(\theta) \quad (69)$$

To fully satisfy CS 25.121, the gradient of climb needed to be determined, where the gradient of climb for a given velocity is defined as the ratio of the vertical velocity (rate of climb) to the horizontal velocity ( $V_H$ ). The horizontal velocity was calculated using Equation (70), and the gradient of climb could be determined using Equation (71).

$$V_H = V \sin(\theta) \quad (70)$$

$$\text{Gradient of Climb} = \frac{V_V}{V_H} \quad (71)$$

By plotting  $V_V$  against  $V_H$ , Figure 46 shows the variation in the gradient of climb for the Aero 5 aircraft with one engine inoperable, throughout the aircraft take-off path.

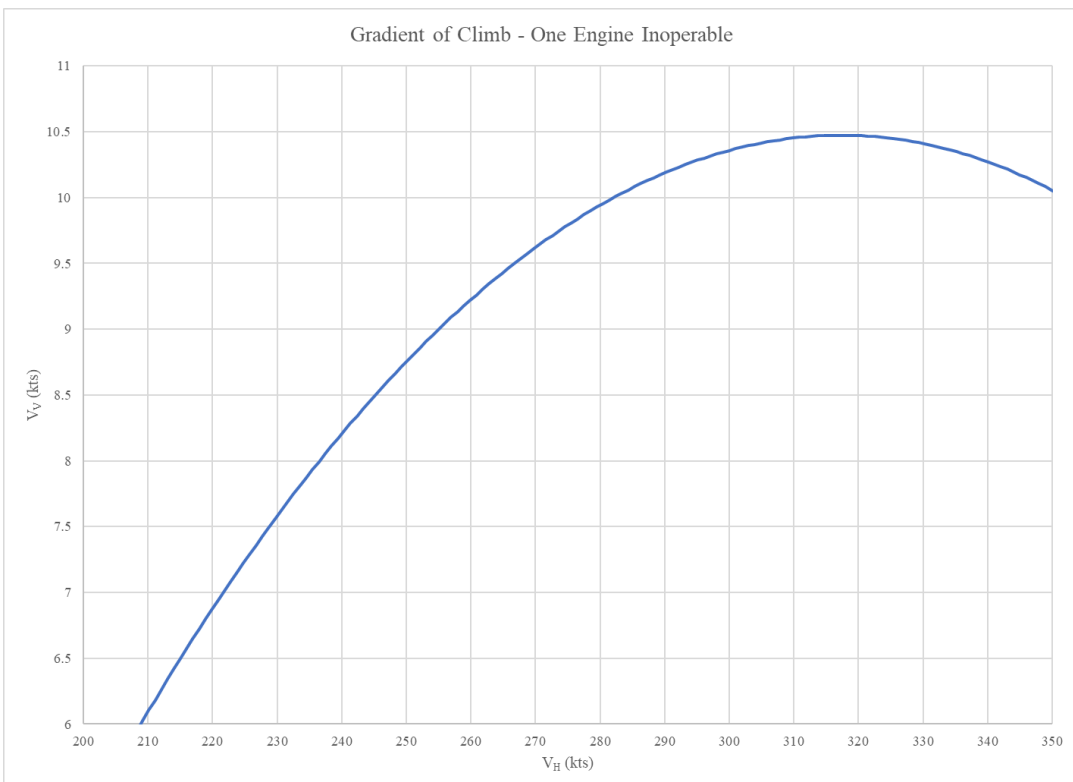


Figure 46 -  $V_V$  vs.  $V_H$  (OEI Case)

CS 25.121 specifies the minimum required gradient of climb for three different stages of the take-off phase with one engine inoperable. The three stages specified are '*Take-off; landing gear extended*', '*Take-off; landing gear retracted*' and '*Final take-off*', which are defined by CS 25.111. The first stage, where the landing gear is extended is described as the region of the take-off path from the instant the nose gear ceases to contact the runway, to 11m (35ft) above the take-off surface. CS 25.121 specifies that in the region of the take-off phase, 'the gradient of climb for a two-engined aeroplanes must be positive'. The second stage of the take-off phase is the distance over which the landing gear is retracted, which is described by CS 25.121 as being between 11m above the take-off surface, to 122m (400ft) above the take-off surface. In this region of the take-off phase the 'gradient of climb must be no less than 2.4% for two-engined aeroplanes'. The third stage of the take-off phase is the region, where the aircraft climbs from 122m (400ft) above the take-off surface to 457m

(1500ft) above the take-off surface (at this point the aircraft begins the climb phase of the flight path). For the final take-off phase, CS 25.121 specifies that ‘the steady gradient of climb may not be less than 1.2% for two-engined aircraft’.

Table 49 compares the gradient of climb at each take-off stage for both the OEI scenario and for the normal engine operation scenario. For the purpose of demonstrating compliance to this requirement, a conservative value of thrust (75% of maximum engine thrust – 103kN for the LEAP-1C) was chosen to determine the gradient of climb for the OEI scenario. This conservative value was selected to show that there is sufficient margin when demonstrating compliance to CS 25.121. For the ‘Both Engines Operational’ scenario, a value of 95% of the maximum thrust (261kN for the LEAP-1C) was used to calculate the gradient of climb. As the gradient of climb is a variable parameter, the values detailed in Table 49 are the maximum values calculated for each stage of the take-off phase.

*Table 49 - Angle of Climb and Gradient of Climb*

|                               | <b>OEI</b>                      |                          | <b>Both Engines Operational</b> |                          |
|-------------------------------|---------------------------------|--------------------------|---------------------------------|--------------------------|
|                               | Angle of Climb<br>(degrees) (°) | Gradient of<br>Climb (%) | Angle of Climb<br>(degrees) (°) | Gradient of<br>Climb (%) |
| <b>Landing Gear Extended</b>  | 2.08                            | 3.63                     | 10.8                            | 19.1                     |
| <b>Landing Gear Retracted</b> | 2.42                            | 4.22                     | 11.2                            | 19.7                     |
| <b>Final Take-Off</b>         | 2.73                            | 4.76                     | 11.5                            | 20.3                     |

Table 49 shows that the Aero 5 design is compliant to CS 25.121, for all stages of the take-off phase. A further consideration when determining the gradient of climb for the Aero 5 aircraft was the effect of ice accretion, in the situation where the anti-ice system fails. CS 25.121 specifies that for each of the stages of the take-off phase described in Table 49 the degradation of the gradient of climb is ‘greater than one-half of the applicable actual-to-net take-off flight path gradient reduction defined in CS 25.115(b)’. Table 55 (Section 6.4) describes the effect of ice accretion with respect to the rate of climb losses for the anti-ice system selected by Aero 5. When compared to the values specified by CS 25.115(b), it was determined that for loss of gradient of climb specified in Table 55, the Aero 5 aircraft is compliant to CS 25.115(b).

#### 5.7.4 Landing Considerations – BG

A key design consideration for the Aero 5 aircraft was the tail scrape angle. The definition and inclusion of the tail scrape angle was influenced by the predicted pitch of the aircraft during landing. This pitching angle was determined using analysis similar to that described in Section 5.7.3. However, there were additional factors that also had to be accounted for during the design process.

The definition of the tail scrape angle was dependent on the landing velocity of the aircraft, which in turn depended on the stall speed of the aircraft when in the landing configuration. The stall speed during landing was calculated using Equation (72) (Hancock, 2016).

$$V_{Stall} = \sqrt{\frac{2W}{\rho S_w C_{Lmax}}} \quad (72)$$

Where  $W$  is the weight of the aircraft at landing,  $\rho$  is the density (sea level),  $S_w$  is the wing area and  $C_{Lmax}$  is the lift coefficient when the aircraft is in the landing configuration. For the purpose of calculating  $V_{Stall}$  in the landing configuration, the aircraft weight was calculated using Equation (73).

$$W_{Landing} = W_{MTOW} - Weight\ of\ Fuel\ Used \quad (73)$$

For the purpose of calculating the stall speed at landing, a value of 2.1 was assumed for  $C_{Lmax}$ , based on historical data (Roskam, 1997). The stall speed at landing was calculated as 69.3 m/s (136 kts). The typical relationship between stall speed in the landing configuration and the landing speed is given in Equation (74) (Hancock, 2016):

$$V_{Landing} = 1.3V_{Stall} \quad (74)$$

The landing speed of the Aero 5 aircraft was determined as 90.0 m/s (176 kts). This value was used to calculate the maximum pitch of the aircraft at the point of making contact with the runway. The angle of pitch at the point of landing was calculated using Equation (68). Typically during landing, aircraft engines are idle, hence to calculate the pitch angle, idle thrust was assumed. The maximum angle of pitch during landing was calculated as being 13°, therefore informing the minimum required tail scrape angle for the Aero 5 aircraft. Based upon supervisor recommendation and typical values (Oza, 2019), as well as incorporating a suitable factor of safety into the aircraft design, a tail scrape angle of 15° was chosen. As a consequence of defining the tail scrape angle, the aircraft nose angle also had to be selected, so as to not impair pilot visibility during landing. Again, based upon supervisor recommendation (Oza, 2019), an aircraft nose angle of 13° was selected, which agrees with the values used for competitor aircraft.

Another important factor based upon the landing configuration of the Aero 5 aircraft was the selection of the minimum control speed for the aircraft whilst airborne and whilst on the ground. This was an important consideration, as it would affect the calculation of the hinge moments required to deflect the aircraft control surfaces. It was determined that the minimum control speeds should be less than the stall speed of the aircraft whilst in the landing configuration. In the scenario where the aircraft stalled, the ability to retain control of the aircraft to recover from stall was considered a critical safety feature of the design. This would also ensure that the aircraft control surfaces were sized and designed appropriately. The relationship between the stall speed in the landing configuration and the minimum control speeds are shown in Equation (75) and Equation (76).

$$V_{Minimum\ Control,\ Airborne} = 0.85V_{Stall} \quad (75)$$

$$V_{Minimum\ Control,\ Ground} = 0.80V_{Stall} \quad (76)$$

The relationships described in Equation (75) and (76) are supported by Hancock (2016). The minimum control speed whilst airborne was calculated to be 58.9 m/s (115 kts) and the minimum control speed whilst on the ground was calculated to be 55.4 m/s (108 kts).

## 5.8 Aero 5 Aircraft Flight Envelope – SH

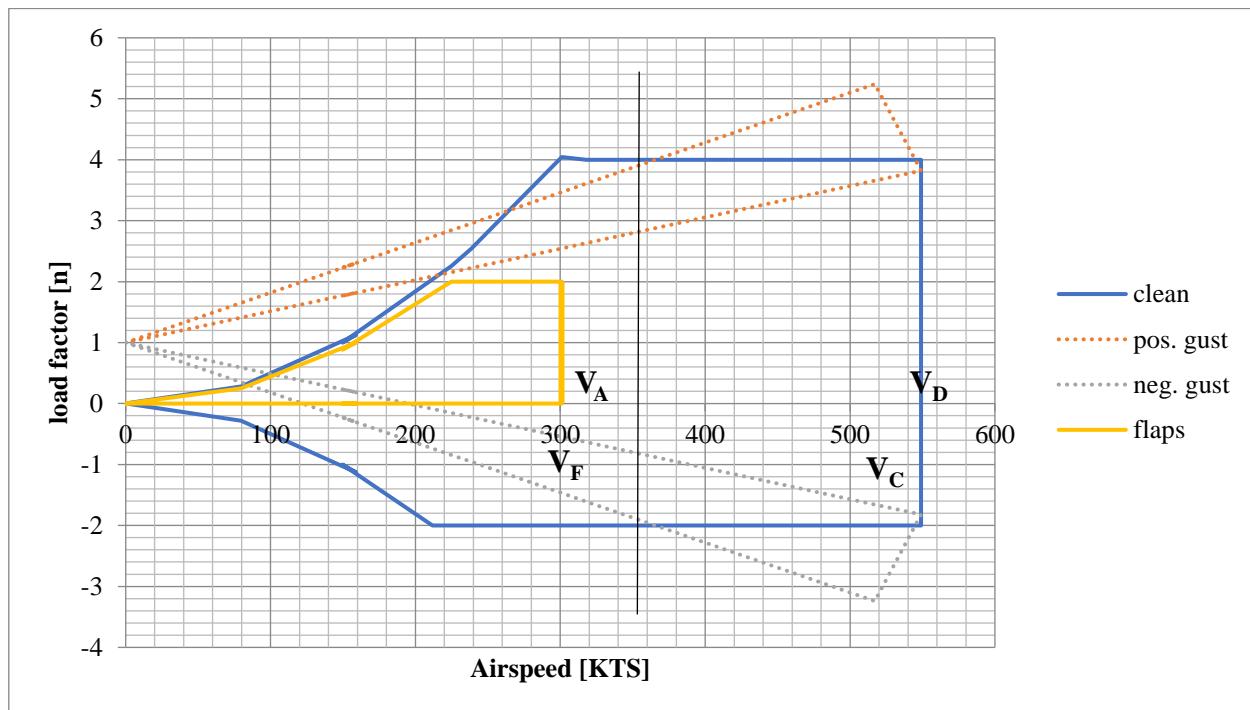


Figure 47 - Aero 5 Aircraft Flight Envelope

Figure 47 was created using the EASA flight envelope guide document (EASA.EUROPA.EU, 2019), using the supporting equations and flight envelope tools. The EASA document adheres to relevant compliances and

certification programmes in accordance with the regulatory frameworks that are addressed in the referenced document.

The structure of the flight envelope was influenced by the following speeds: stall speed  $V_s$ , flaps extended stall speed  $V_{so}$ , design manoeuvring speed  $V_A$ , flaps maximum operating speed  $V_F$ , design cruise speed  $V_C$ , design dive speed  $V_D$ . Additional speed calculations have been omitted for the sake of brevity. The formerly listed speeds were either extracted from the PDR or was achieved through consultation with the relevant parties involved or calculated using the equations in the EASA guidance document (EASA.EUROPA.EU, 2019).

## 5.9 Additional CAD Components – TL, AM

### 5.9.1 Nacelle – AM

Figure 48 shows the aircraft nacelle, that acts as a placeholder for the LEAP-1C engine in the Aero 5 CAD models.

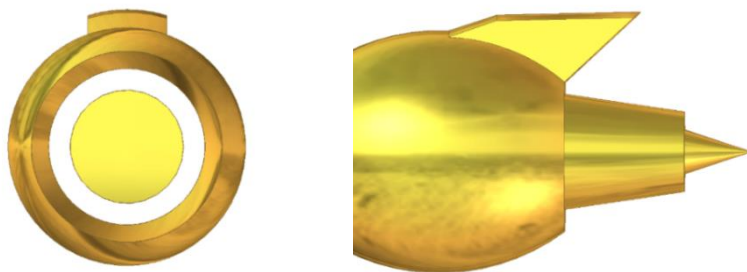


Figure 48 - Front and Side View of Aero 5 Nacelle

### 5.9.2 Passenger Seats – TL

Figure 49 shows an isometric view of the passenger seats used for the Aero 5 aircraft.



Figure 49 - Front and Rear Isometric View of the Aero 5 Passenger Seats

### 5.9.3 Aircraft Cabin – TL, KO

To make the assembly easier, a separate assembly of the cabin was made, prior to assembling the entire aircraft as a CAD model. This included the overhead compartments, cabinets, lavatories, galley and the floor. The cabin assembly is shown in Figure 50.

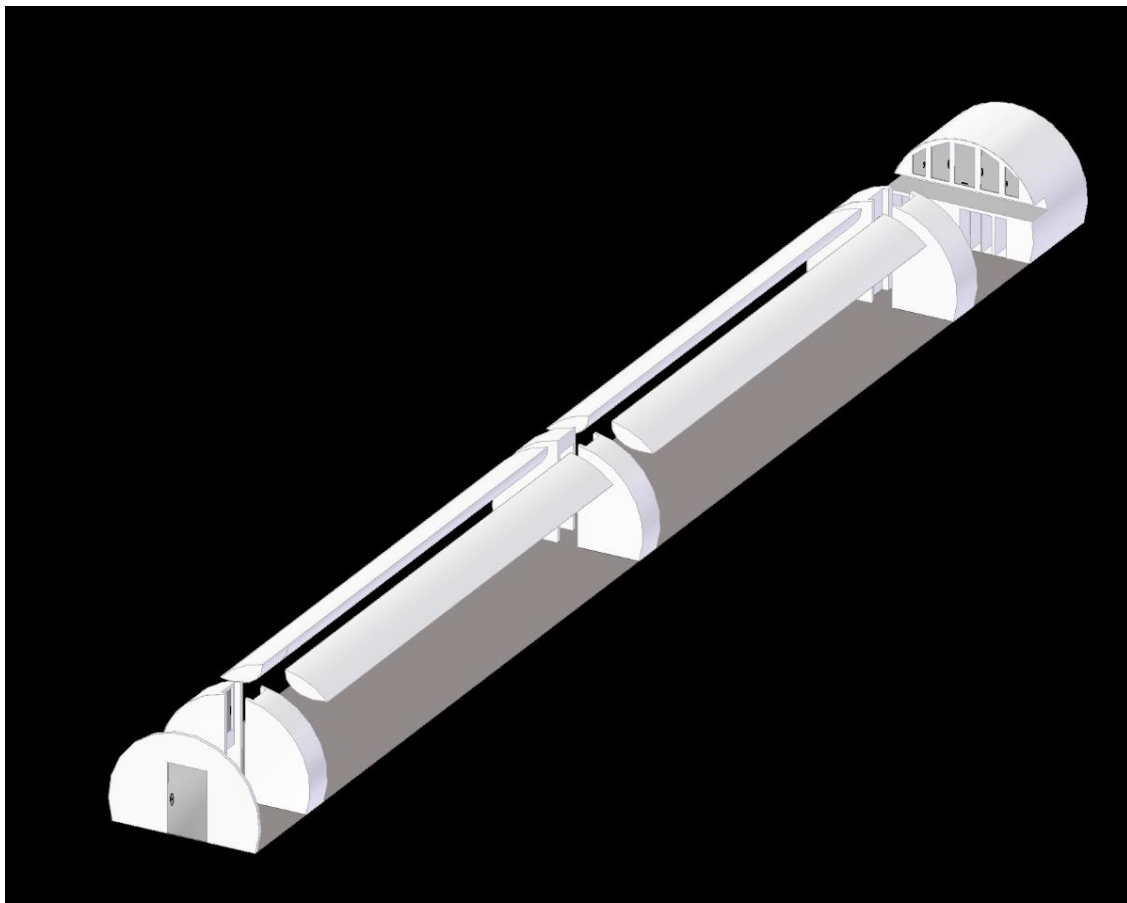


Figure 50 - Isometric View of Cabin Assembly

#### 5.9.4 Pilot Seat and Attendant Seat – TL

Figure 51 shows an isometric view of the Pilot Seat and Attendant Seat used for the Aero 5 aircraft.

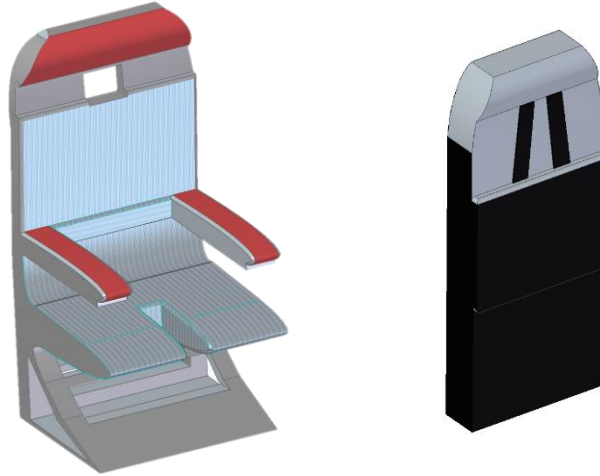


Figure 51 - Isometric View of Pilot Seat (Left) and Attendant Seat (Right)

#### 5.10 Full Aircraft CAD – TL, PS, KO

The complete aircraft was assembled using Solid Edge ST10 GB Metric Assembly mode, and met the dimensions defined by Aero 5 in the PDR and this document, if superseded. Figure 52 shows a plan view of the full aircraft assembly. Figure 53 shows an isometric view of the full aircraft assembly and Figure 54 shows an isometric view of the full aircraft assembly with the cabin shown. These figures include the fuselage, empennage, nose cone, wings and high lift devices. Components such as the landing gear were not designed as the team intend to procure these, and not manufacture them.

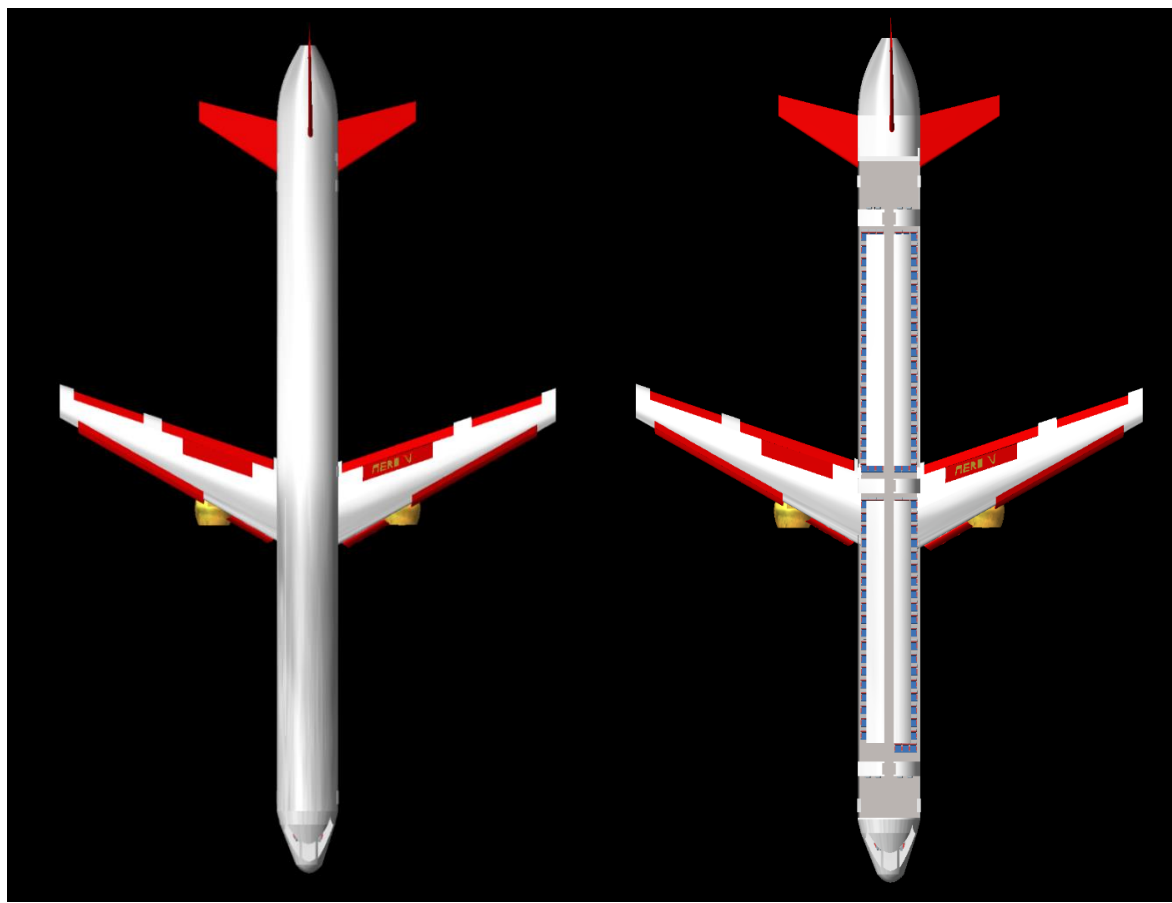


Figure 52 - Plan View of Aero 5 Aircraft Assembly



Figure 53 - Isometric View of Aero 5 Aircraft

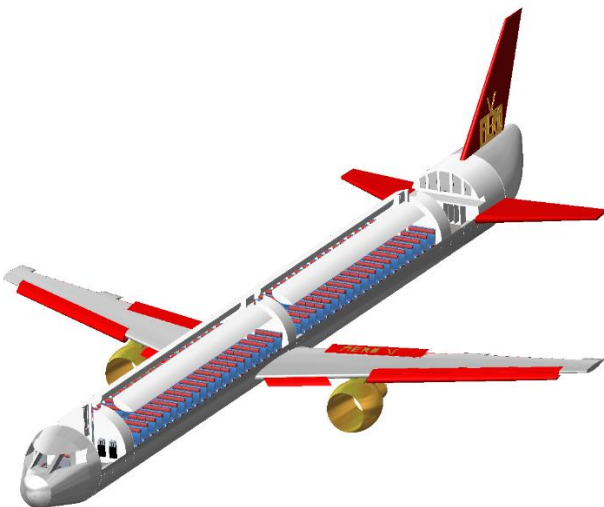


Figure 54 - Isometric View of Aero 5 Aircraft (with Cabin Shown)

## 5.11 Aircraft Centre of Gravity – SH

The structural analysis of the aircraft provided mass estimates for the primary internal structures of the fuselage and wing. However, due to the limited detail and availability of time, not all mass fractions could be captured and portrayed to a satisfactory degree of accuracy. Therefore, to determine the new CG for the matured CDR version of the Aero 5 aircraft, the mass forecast method which solved for the CG documented in PDR Section 4.2-4.3 was updated with new mass fractions and refined conservatism factors for more realistic mass fractions as well as presently available structural data from the technical analysis conducted for the CDR. Using the updated dimensions from the CAD developed for the CDR, new moment arm dimensions were added into the spreadsheet to place a CG position for the new aircraft geometry. The primary dimensions showing the largest change from the PDR were the new tailplane dimensions, as they had to be resized to better provide for the expected specifications.

The updated mass fractions can be seen in Appendix 13.8. The concluding iterative dimensional data for the CDR can be seen in Table 44 which tracks an updating record of the Aero 5 CG for the matured aircraft design. For clarity and to better show the numerical deviations, certain columns of the table have been adjusted to show values beyond 3 significant figures to easier highlight the iterative changes. From Table 44 it is evident that the CG analysis with the incorporation of dimensional data from the CAD model and the higher fidelity mass fractions have moved the CG position for both full and empty configurations further outboard relative to the nose-cone datum line. Each row in Table 44 shows an iteration of the CDR CAD model CG and corresponds to the affiliated row iteration number in Appendix 13.8.

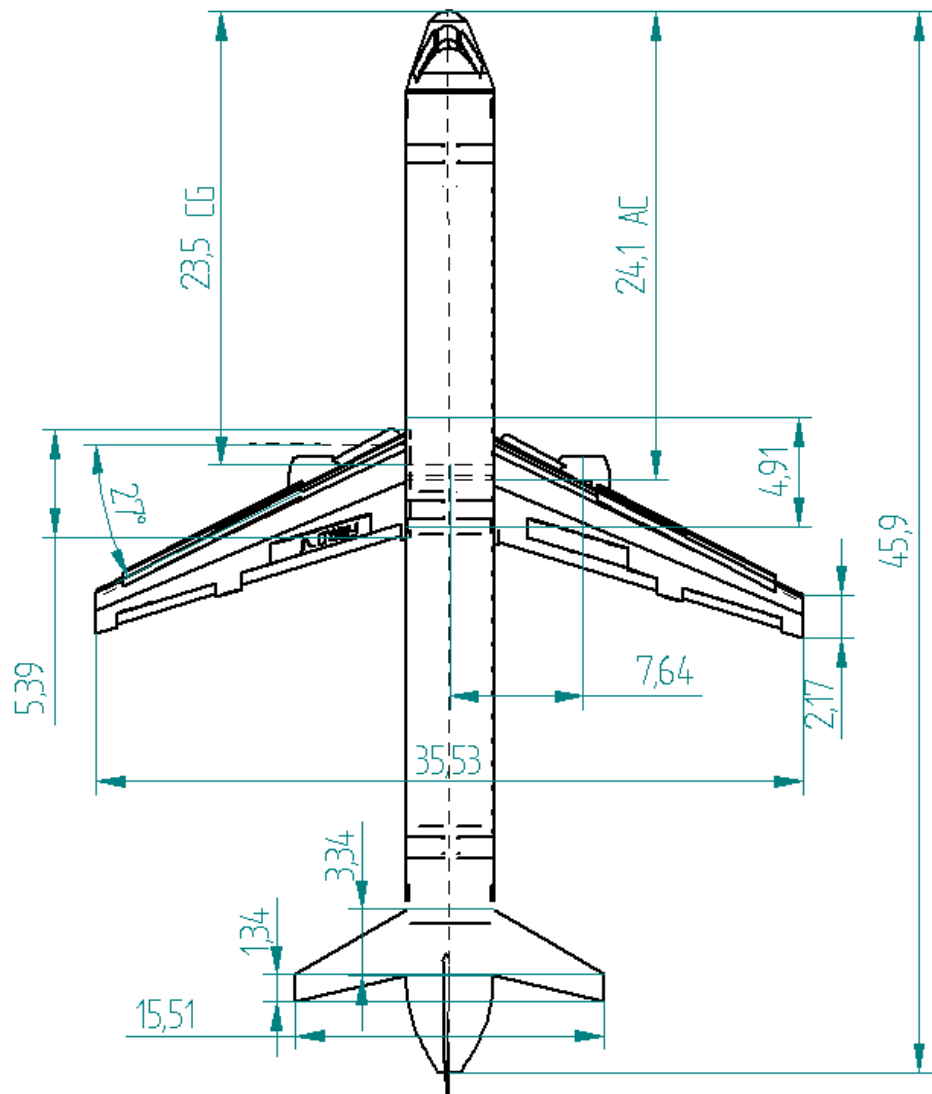
Table 44 - Summary of CG Data and other Dimensional Data

| Mean Aerodynamic Chord Length (m) | Static stability Margin (In terms of MAC) | CG position, CDR (full) (m) | CG position, CDR (empty) (m) | CG shift (empty and full) (m) | CG position, PDR (full) (m) | CG position, PDR (empty) (m) | Change in CG (empty) (%) |
|-----------------------------------|---|-----------------------------|------------------------------|-------------------------------|-----------------------------|------------------------------|--------------------------|
| 4.00                              | 0.150                                     | 23.357                      | 23.937                       | 0.580                         | 21.826                      | 22.236                       | 9.761                    |
| 4.00                              | 0.150                                     | 23.361                      | 23.939                       | 0.577                         | 21.496                      | 21.826                       | 0.005                    |
| 4.00                              | 0.150                                     | 23.391                      | 23.979                       | 0.588                         | 21.452                      | 20.917                       | 0.168                    |
| 4.00                              | 0.150                                     | 23.411                      | 24.005                       | 0.594                         | 21.658                      | 21.648                       | 0.109                    |
| 4.00                              | 0.150                                     | 23.432                      | 24.031                       | 0.599                         | 21.532                      | 21.491                       | 0.110                    |
| 4.00                              | 0.150                                     | 23.455                      | 24.061                       | 0.606                         | 21.574                      | 21.558                       | 0.123                    |
| 4.00                              | 0.150                                     | 23.476                      | 24.089                       | 0.613                         | 21.674                      | 21.624                       | 0.116                    |
| 4.00                              | 0.150                                     | 23.506                      | 24.130                       | 0.624                         | 21.655                      | 21.628                       | 0.169                    |

# AERO 5

## AIRCRAFT

### TOP-VIEW



| Aircraft Property                          | Distance or size (m) |
|--|----------------------|
| Centre of Gravity (CG)                     | 23.5                 |
| Aerodynamic Centre (AC)                    | 24.1                 |
| Wing Span                                  | 35.5                 |
| Horizontal Tailplane Root Chord            | 3.34                 |
| Horizontal Tailplane Tip Chord             | 1.34                 |
| Horizontal Tailplane Span                  | 15.5                 |
| Total Aircraft Length                      | 45.9                 |
| Landing Gear Track                         | 4.19                 |
| Engine Placement<br>(From fuselage centre) | 7.64                 |
| Wing Root Chord                            | 5.39                 |
| Wing Tip Chord                             | 2.17                 |

Figure 55 - Aero 5 Aircraft Plan View (with CG and AC)

## **6. Aircraft Systems – YA, MK**

### **6.1 Avionics Systems – YA, MK**

#### **6.1.1 Navigation Systems – YA**

The navigation system was defined as a safety critical system in the PDR. If it fails, the pilot will not be able to determine the position of the aircraft, consequently losing the aircraft or rendering it unable to land. Therefore, the navigation system was analysed to apply redundancy technology to minimise and reduce the frequency of total failure of the system. It was important to understand how each component in the navigation system could fail and how it would affect the whole system overall.

Firstly, the Global Positioning System (GPS) failures are caused by one or more component failures. As mentioned in the PDR, the GPS consists of two major components. The first component is the display where its failure is caused by one of the following two reasons:

- Component failure: this failure could be caused by the failure of the electrical connections, the diodes, or any other electrical component.
- Insufficient power: this failure is caused by the cables malfunctioning and not delivering enough power to the GPS display.

The second component of the GPS is the ADS-B transponder where its failure is caused by one of the following reasons:

- Insufficient power: the same reasons as mentioned for the display.
- Mode A: this type of code failure occurs when the GPS does not identify other aircraft around the local system.
- Mode C: this is an information failure only, where the GPS displays the wrong altitude or does not display any data about the altitude at all.
- Mode S: this is a 24-bit address failure which would result in an unidentified aircraft being present on the display or a wrong track correlation.

Secondly, the inertial reference system failures are caused by the ring laser gyroscope failures. The ring laser gyroscope measures the acceleration in each direction and determines the position of the aircraft based on the position the pilot has entered before taking-off. The ring laser gyroscope has two modes of failure; storage failure and operational failure. Storage failure is caused by one of the following four reasons:

- Loss of helium-neon gas: this failure is due to the diffusion or failure in containing the gas in a specific space.
- Contamination: this may arise from the penetration of water vapour which is mainly caused by exposure to humidity. This is minimized by using a package and storage container design. The average rate of this failure is around once every year (Air force avionics laboratory, 1973).
- Mirror degradation: long-term deterioration of mirror filtering and optics due to cracks and changes in optical properties. This failure mode is insignificant provided that the gyro is maintained routinely.
- Dimensional stability: this failure is caused by stresses forming in materials. It is a fatigue failure.

Moreover, operational failures are caused by one of the following four reasons:

- Accelerated gas loss: the gas losses occur due to their ionisation caused by the strong electric field.
- Electric failure: this failure could be caused by the failure of the electrical connections, the diodes one of the photodiodes or any other electrical component. This failure is really rare, with a probability to fail of only 0.01% every 1000 hours which gives a mean time between failures (MTBF) of around  $10^7$  hours which equates to once every 1000 years. This was longer than the expected lifetime of the whole aircraft, therefore, this failure was not taken into consideration.
- Mirror degradation: long-term deterioration of mirror filtering and optical due ion bombardment.
- Environmental failure: the environment causes structural failures and dimensional stability failures. Structural failure is due to breakage, slippage or separation of components under forces caused by aircraft operation. The dimensional stability failure is an intermittent failure due to distortion of structural components under the forces of aircraft operation.

Finally, radio aids failure is caused by one or more component failures. As mentioned in the PDR, the radio aids consist of 3 major components. However, all the major components of the radio aids system have the same causes of failure. For the radio aids system to fail all components would have to breakdown, but for each component to fail one of the following causes would have to occur:

- Radio interference: interference can make communication difficult or even impossible which is due to the fact that several airports use the same communication frequency.
- Malfunction: this is due to airborne equipment malfunction where the pilot selects a new frequency but the equipment does not respond to the change, so the pilot is unable to transmit or receive on this frequency.
- Mis-management: this is due to the process of changing frequency if the pilot selects the wrong frequency. This failure is a short-term failure which can be solved during flight.
- Insufficient power: the same reasons as mentioned above.

All the failure sources for the navigation system are summarised in the fault tree analysis, which can be seen in Figure 56.

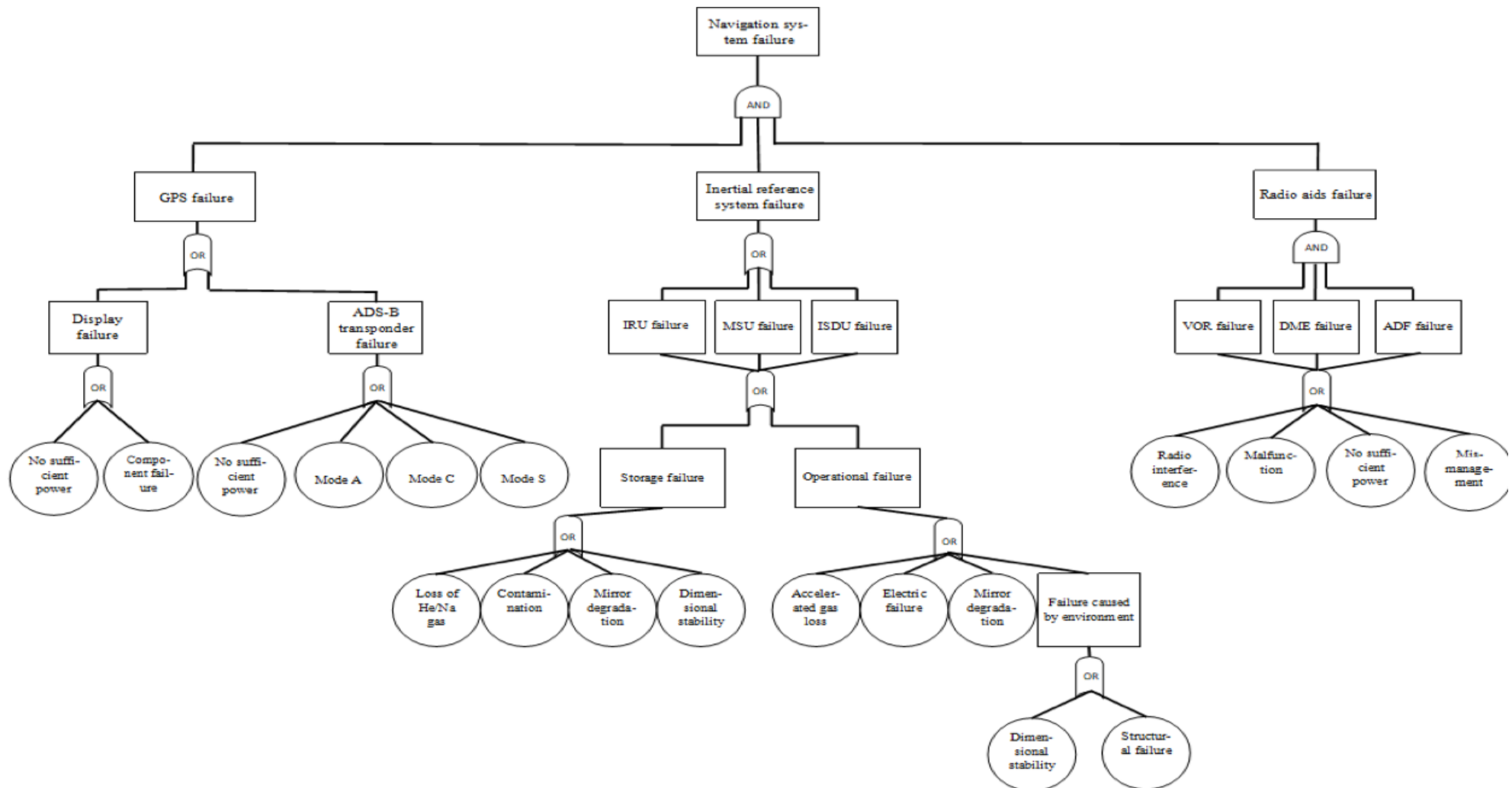


Figure 56 - Navigation System Fault Tree Analysis

The navigation system will only fail if the GPS, IRS and radio aids all fail at once. The acceptable rate of failure for the navigation system is once every 5 years, which corresponds to the D-check schedule. The failure rate will be analysed for each component for each system.

Firstly, for GPS, display failures are mainly caused by electric failures. The failure rates caused by electric failure are around 0.01% every 1000 hours which is a very rare event. Therefore, the display was not considered in the analysis. However, the ADS-B transponder has three different modes of failure and only one needs to occur for the ADS-B transponder to fail. Therefore the sum of all three failure rates will be the failure rate of the ADS-B transponder. Mode A failure has the highest failure rate at 6% every 400 hours, compared with mode C at 5.8% every 400 hours and mode S at 2.2% every 400 hours (Talotta, 1997). Therefore, the ADS-B transponder failure rate is 14% every 400 hours. This means that the MTBF is 2857 hours and converting that to years means that the ADS-B transponder fails 3.1 times every year. The acceptable failure rate was once every 5 years or in other words 0.2 times each year. Safety Integrity Levels (SIL) are determined by the risk reduction factor (RRF), which is calculated using the Equation (77).

$$RRF = \frac{\text{actual failure rate per year}}{\text{acceptable failure rate per year}} \quad (77)$$

The RRF for the GPS is 15.5. From the RRF value, the SIL was calculated. Table 51 shows the SIL for each range of RRF that will be used to determine the SIL for each aircraft system.

*Table 51 - SIL as a Function of RRF (Yoset, 2017)*

| SIL level | Risk reduction factor RRF |
|-----------|---------------------------|
| 1         | $10^1 - 10^2$             |
| 2         | $10^2 - 10^3$             |
| 3         | $10^3 - 10^4$             |
| 4         | $10^4 - 10^5$             |

As the RRF for the GPS is 15.5, the SIL of the GPS is 1. This means that the system is already redundant and no other component should be added.

Secondly, the IRS system has various failure modes, each with their own failure rates. For the IRS to fail, only one failure mode has to happen. Therefore, the failure rate of the IRS would be the sum of all the failure rates of each failure mode. The failure rate of each failure mode is displayed in Table 52.

*Table 52 - Failure Rates for IRS Failure Modes (Air Force Avionics Laboratory, 1973)*

| Failure mode                             | Failure rate (% every 1000hours) |
|--|----------------------------------|
| Loss of helium-neon gas                  | 3.98                             |
| Contamination                            | 16.3                             |
| Mirror degradation (storage failure)     | 0.533                            |
| Dimensional stability                    | 2.17                             |
| Electric failure                         | 0.010                            |
| Accelerated gas loss                     | 4.39                             |
| Mirror degradation (operational failure) | 0.989                            |
| Environmental failure                    | 2.27                             |
| <b>Total</b>                             | <b>30.6</b>                      |

From Table 52, the total failure rate of the IRS is 30.6% every 1000 hours. This means that the MTBF is 3270 for the IRS, or in other words, the IRS fails 2.7 times a year. However, the acceptable failure rate is 0.2 per year as mentioned above. This means that the RRF for the IRS is 13.5 and therefore the IRS has an SIL level of 1. This means that the system is already redundant and no other components should be added.

Finally, radio aids have three failure modes. However, the radio aids failure rate was already calculated by A. Ballantyne and R. Dexter in their Advances in aeronautical sciences book to be 1.6% for every 5 hours of flight. (Ballantyne and Dexter, 1958). Assuming the Aero 5 aircraft will travel 20 hours per day, the MTBF is 313 and this means that the radio aids will fail around 23.4 times per year. With the acceptable rate of failure is 0.2 per year, this means that the RRF for the radio aids is 117. This means that the radio aids have a SIL of level 2. However, the radio aids are already a redundant component of the navigation system which will only be used only if the GPS and the IRS both fails. Also, the radio aids have 3 different independent components,

where if one fails the radio aids would still function. It was concluded that the navigation system has different redundant components and it is highly reliable, therefore no other component needs to be added.

### 6.1.2 Flight Management System – YA

The flight management system was defined as a normal function system in the PDR. If it fails the pilot would have to fly the aircraft manually without any data available about the aircraft performance and operations. Therefore, the flight management system was analysed to apply redundancy technology to minimise and reduce the frequency of total failure of the system. To be able to do that it is important to understand how each component in the flight management system could fail and how will that affect the whole system overall.

Firstly, the first component of the flight management system is the navigation system which was analysed in Section 6.1.1. The second component of the flight management system is the flight management computer which calculates the aircraft performance and operations and sends the data to the automatic flight control system. This component has two failure modes:

- Hard failures: this failure mode is mainly caused by the inactivation of the flight management computer (FMC) by the pilot or an electric failure in one of the electrical components in the FMC.
- Soft failures: this a failure mainly caused by is a software error which could be caused by random disturbances or interference.

Secondly, the automatic flight control system receives data from the flight management computer and sends information about how to adjust the control surfaces as electrical signals to the actuators at each control surface, which is adjusted to provide the expected response. This component has four failure modes:

- Autopilot channels inactivation: on the autopilot, there are three channels; the inclined channel which controls the ailerons, the course channel which controls the elevators, and the pitch channel which controls the rudder. This failure happens when the pilot forgets to activate one or more of the channels.
- Yaw damping inactivation: this is the device used to damp the rolling and yawing oscillations. It is a yaw-rate sensor and a processor that provides a signal to the FMC to adjust the actuator connected to the rudder. This failure happens when the pilot forgets to activate the sensors.
- Gliding landing system inactivation: this is the device used to calculate the aircraft glide path while tracking the aircraft position. It adjusts the control surfaces and the engine thrust to flare manoeuvre to land automatically. This failure happens when the pilot forgets to activate the system.
- Electrical failure: this failure happens when one or more of the electrical components fail.

Finally, the Electronic Flight Instrument System (EFIS) which are mainly instruments that help the pilot to navigate by displaying airspeed, altitude, vertical speed and other parameters. This system has different failure modes which are:

- Component failure: the PFD is the Primary Flight Display which is a combination of all flight instruments such as altitude indicator, airspeed indicator and the aircraft heading, which is sufficient for a functioning EFIS. The PFD will fail due to an electrical component failure.
- Software failure: the PFD uses aircraft data to calculate important parameters to display for the pilot. However, when it fails a bold red ‘x’ is displayed in place of the parameter which the PFD failed to calculate. This failure is because the instrumentation sensors rely on uninterrupted 12VDC or 24VDC. Any interruptions in the power supply will disrupt the system and cause erratic indications or the bold red ‘x’ to appear. Those are due to a failure in the electrical system or lightning strikes (which is further discussed in Section 6.8).

The three components of the flight management system are dependent on the need for information from the FMC to control the control surfaces. Therefore, the flight management system will fail if one or more component fails.

Firstly, for the FMC, the failure rate is once in ten years which is lower than the acceptable rate discussed in Section 6.1.1 (Navigation System). Therefore, a SIL analysis could not be done. However, an FMC failure during flight will add difficulty to the controllability of the aircraft which will put the safety of the aircraft at risk. So, it has been decided to add another FMC which will add 11kg and require 300 W. This means that the flight management system has become a dual system. For a dual system to fail the failure will have to be

caused by a failure in the electrical system, where not enough power is delivered to the FMC. This adds a redundancy level which makes the FMC N+1 redundant.

Secondly, for the automatic flight control system, the failure modes cannot be prevented. If it fails the pilot has to control the aircraft manually. The automatic flight control system only simplifies the pilot's job. If it fails, it will not put the aircraft at risk. The pilot is already trained to fly the aircraft manually. Therefore, nothing will be added to the automatic flight control system.

Finally, for the electronic flight instrument systems, the PFD is the main component and it has two failure modes. If it fails during flight, there is no way to fix it while airborne. Therefore, a backup system will be added in the aircraft. The backup system will include an attitude indicator which indicates the aircraft orientation relative to Earth's horizon, an altitude indicator which indicates the altitude of the aircraft, an airspeed indicator which indicates the airspeed of the aircraft in knots and the vertical speed indicator which indicates the rate of climb or descent of the aircraft. The PFD could fail from an electrical system failure, so it has been decided to use conventional indicators. These conventional indicators do not require any power however they add mass. The airspeed indicator adds 453g, the vertical speed indicator adds 366g, the altitude indicator will add 1.58kg and the attitude indicator will add 820g. This means that the backup system will add 3.22kg. To conclude, the components added to the flight management system add 14.3kg and requires 300 W. The system is now more reliable and more redundant, which will deliver the required results during flight.

### 6.1.3 Communications Systems – MK

The communication system is required for the pilot to be able to communicate with air traffic control. The PDR lists the system as normal function rather than safety critical since the failure of the system will not directly endanger the lives of the crew and passengers.

The communication system consists of a number of subsystems. The first of these is the air-ground voice communication subsystem.

Modes of failure for the voice communication equipment include:

- Aircraft radio equipment malfunction
- Ground equipment malfunction
- Stuck microphone selector

These failure modes can result in communication impairment or loss of communication entirely. Duplicate radio equipment should be integrated into the aircraft in order to provide redundancy. Other possible failure modes for the voice communication system include radio interference and blocked transmissions.

In the event of complete communication loss, other systems, like the ADS-B IN subsystem that receives air-to-air information from other aircraft will allow the aircraft to continue to avoid collisions. Further information about the ADS-B subsystem can be found in Section 6.1.1 this document.

Loss of communications will occur in the event of loss of either or both of the following subsystem functions (Pettit, 2001):

- Voice communications
- Tracking signal

Loss of voice communications can occur due to failure of:

- Communications Radio (MTBF = 900)
- Communications Antenna (MTBF = 1200)
- Alternator (MTBF = 7600)

Loss of tracking signal can occur due to failure of:

- Transponder (MTBF = 1700)
- Transponder Antenna (MTBF = 9500)
- Alternator (MTBF = 7600)

Since each subsystem can fail as a result of any of the lower level failure events, the calculations will use the lowest MTBF in order to assess the SIL. This is a simplification due to the fact that weightings of the different failure modes are not known. The use of this assumption will result in an overestimate of the RRF which is

more desirable than an underestimate since it will add further redundancy, rather than making the system unsafe. Taking the overall communication system MTBF to be 900, a failure rate of 9.73 per year can be calculated. This give an RRF of 48.7, corresponding to SIL1. This calculation, as well as the level of redundancy across the communications and navigation system, suggests that the system is sufficiently redundant.

#### 6.1.4 Weather and Traffic Systems – MK

The weather and traffic system was defined in the PDR as a normal function system. The purpose of the system is to warn the pilot of potential hazardous weather including rainfall, hail, and snow, and to warn the pilot of close proximity to the ground and to other aircraft. Failure of the system to warn the pilot of dangerous conditions can result in collisions.

The weather part of the weather and traffic system consists solely of a weather radar.

A report from the School of Aeronautics at Northwestern Polytechnical University in China looks at the different failure modes of the Airborne Weather Radar (WXR) and analyses the safety of the system through failure mode, effects and criticality analysis (FMECA). Failure modes addressed in this report include:

- Failure of the MF unit in generating a local signal.
- Failure of the local oscillation channel unit to transmit a local signal.
- Failure of the signal generation unit to generate transmit signal.
- Failure of transmit channel unit to transmit signal.
- Failure of amplification unit to amplify signal.
- Failure of FM signal generation circuit to generate the FM signal.

The results of the FMECA show that the most critical mode of failure for the WXR is failure of the FM signal generation circuit in generating the FM signal.

The traffic system consists of an enhanced ground proximity warning system (EGPWS) and traffic radar.

One failure mode of the EGPWS is a false warning of close proximity to the ground which can occur as a result of failure of the components, computer and sensors. This type of failure shall not have an occurrence probability greater than  $10^{-4}$  per hour.

The probability of total EGPWS failure including signal failure and for the EGPWS itself was calculated by Honeywell using component failure rates. This probability was found to be  $1.767 \times 10^{-4}$  per flight. The Aero 5 aircraft is expected to carry out approximately 1460 flights per year (PDR Section 6.4). This gives a probability of failure of 0.258 per year. Using the allowable failure rate of 0.2 per year based on the 5-year maintenance plan, an RRF of 1.290 was calculated. The minimum RRF for SIL1 is 10 therefore this system is very safe and addition of further redundancy is not required.

The traffic radar or traffic collision avoidance system (TCAS) warns the pilot of proximity to other airborne aircraft. ICAO Annex 10 Vol. IV states that all systems must be compliant with TCAS II version 7.1.

A report from EUROCONTROL assesses the safety risks associated with failure of the TCAS II version 7.0 system. Based on data from recent years, this report updated the failure rate of the system and found a value of  $7.9 \times 10^{-9}$  per flight hour. With the estimated 3840 flight hours per year for the Aero 5 aircraft (PDR Section 6.4), this figure can be used to find a failure rate of  $3.034 \times 10^{-5}$  per year. This gives an RRF of  $1.517 \times 10^4$  which is also smaller than the minimum RRF for SIL1.

TCAS II Version 7.1 addresses the main issues faced by TCAS II version 7.0 including multiple failures of pilots to correctly respond to the alert “Adjust vertical speed, adjust”, as well as failure of the system to reverse a Resolution Advisory when multiple aircraft are converging and remain within 100 feet. These corrections mean that the system is likely to have a failure rate even lower than given above.

#### 6.2 Flight Data Recorder – YA

The crash protected flight recorder system was defined as a normal function system in the PDR, however, Aero 5 has reconsidered the system and found it to be a safety critical system. This decision was made because the crash protected flight recorder system records parameters during flight which could prevent engine failure or other system related failures during flight by using data collected from previous flights. Therefore, the crash protected flight recorder system will be analysed to apply redundancy technology to minimize and reduce the frequency of total failure of the system. To be able to do that, it was important to understand how each

component in the crash protected flight recorder system could fail and how would that affect the whole system overall.

In the crash protected flight recorder system, there are two independent components which are the flight data recorder (FDR) and the cockpit voice recorder (CVR). However, in the PDR, Aero 5 had decided to use a new technology which combines those two components into one for volume, mass and power consumption reasons. The combined component could fail for several reasons which are:

- High-intensity fire: if the aircraft crashes, the fuel could burn and explode which could start a fire at more than 1000°C, however at this temperature the fire would not last long as everything will burn quickly.
- Low-intensity fire: if the aircraft crashes, a fire could emerge with a lower temperature that will last longer.
- Impact shock: when the aircraft crashes with the ground, the FDR and CVR combination will hit the ground and any part inside the aircraft at a high velocity.
- Water immersion: the FDR and CVR combination could last in seawater for a until it is recovered found. Seawater could corrode the system; potentially corrupting the data.
- Fluid immersion: same as water immersion failure, the FDR and CVR combination could last in a fluid-like fuel, oil or other aircraft fluids for a long time and it will fail in a similar manner to the water immersion failure.
- Hydrostatic pressure: if the aircraft crashes into water, the FDR and CVR combination will sink into water; where it could face high pressures.
- Penetration: from the crash sharp objects with high acceleration could penetrate the FDR and CVR combination and destroy them.
- Static crush: if the aircraft crashes, a heavy object could fall on the FDR and CVR combination which could crush it.
- Corrosion: the electrolytic capacitors in the FDR and CVR combination begin to emit electrolytic fluid that corrodes the power supply board.

The crash protected flight recorder system will fail if only one of those failure modes occur. However, due to regulations made by European organisation for civil aviation equipment in EUROCAE-ED56, the manufacturers are required to test the FDR and CVR combination for most of those failures. The manufacturers have to follow the following criteria in designing the FDR and CVR combination:

- High-intensity fire: the FDR and CVR combination must survive a fire with a temperature 1100°C covering 100% of the system for 30 minutes
- Low fire intensity: the FDR and CVR combination should survive at least 10 hours in a temperature of 260°C (this test mostly occurs in an oven)
- Impact shock: the FDR and CVR combination has to survive a 3400 Gs impact for 10 milliseconds
- Water immersion: the FDR and CVR combination has to survive 30 days in sea water.
- Fluid immersion: the FDR and CVR combination has to survive in aircraft fluids (fuel, oil, etc) for at least 24 hours.
- Hydrostatic pressure: the FDR and CVR combination has to survive in a pressure equivalent to 20000ft of depth in sea water.
- Penetration resistance: the FDR and CVR combination has to survive a test where a 500lb object is dropped from 10ft with a ¼ inch diameter contact point.
- Static crush: the FDR and CVR combination has to survive under a 5000 pounds mass for 5 minutes on each axis.

Providing these regulations are implemented correctly, the crash protected flight recorder system will survive the crash. Furthermore, the corrosion failure mode is an electrical fatigue failure which cannot be prevented. However, due to regulations outlined in ICAO Annex 6 Chapter 6, CS 25.1457 and CS 25.1459, the aircraft is required to have a combination of FVR and CVR. This prevents the total loss of the information during a flight. If one fails, the other will function normally meaning the system has N+1 redundancies. To conclude, the chosen crash protected flight recorder system in the PDR is a reliable and redundancy protected system which will deliver the results required during any flight under any failure mode.

### 6.3 Environmental Control System – YA

The environmental control system is defined as a safety critical system in the PDR. Depending on the altitude, if the environmental control system fails, the aircraft will lose its oxygen concentration required for a person to breathe normally, which will lead to loss of intellectual ability followed by unconsciousness which will result in respiratory and heart failure. From 10000ft the effects become progressively more severe with increasing altitude. Therefore, the environmental control system will be analysed to apply redundant technology to minimize and reduce the frequency of total failure of the system. To be able to do that it is important to understand how the environmental control system could fail and how will that affect the aircraft's flight.

The first failure that could occur to the environmental control system is depressurisation. The aircraft has to maintain the cabin's pressure between 78kPa and 85 kPa. With this range of pressure, the aircraft is able to deliver an acceptable concentration of oxygen which is physiologically suitable. Three failure modes could cause depressurisation.

- Structural failure: with increasing altitude, the ambient pressure decreases, which means the absolute amount of oxygen available reduces. Maintain a pressure difference between the outside and the inside of the aircraft stresses the structure of the aircraft which causes the first failure mode. The stresses in the aircraft structure could cause a window, door or pressure bulkhead failure. Also, the structural failure could occur from an in-flight explosion from a system failure, dangerous cargo or explosive device.
- Deliberate act: the aircraft pilot could consider depressurising the aircraft as a last measure. This could occur for example in a way of cleaning the cabin from smoke.
- Pressurisation failure: this could occur from a malfunction of some part of the pressurisation system such as the outflow valve, or from a wrong system control input.

The second failure that could occur to the environmental control system is temperature control failure. The aircraft is supposed to maintain a cabin temperature between 18°C and 26°C. The heat exchanger bleeds air at high temperature and high pressure. The heat exchanger cools the air to the acceptable temperature using ram air. The temperature control failure occurs due to heat exchanger failure, which could be one of the following failure modes:

- Leakage: this failure is caused by an escape of air flow in the heat exchanger. This results in mass flow reduction where it could happen on the hot side of the heat exchanger or the cold side of the heat exchanger.
- Blocking: this failure is caused by an obstruction in the heat exchanger pipes. This results in heat transfer coefficient reduction where it could happen on the hot side of the heat exchanger or the cold side of the heat exchanger.
- Fouling: this failure is caused by a build-up layer of dirt on the tube surfaces of the heat exchanger. This causes a reduction in the value of the effective flow area.

The environmental control system could fail under any of those failure modes. To have a reliable control system, the aircraft should be able to land safely under any of those failures. So those failure modes will be analysed to address their severity and add any backup system if needed to keep the passengers safe until the aircraft lands.

Firstly, the depressurization of the aircraft could cause harm to the passengers and the crew members in less than a minute if there was no backup for the pressure control system. The human body could survive the low pressure in an altitude of 35000 ft or above, however, low oxygen concentration may lead to death in extreme cases. So in the case of depressurisation, the aircraft should provide emergency oxygen. There are three different considerations to choose from. The three different emergency consideration are presented in Table 53.

Table 53 - Oxygen Emergency System Considerations

| Types of Oxygen Emergency | Description  | Advantages   | Disadvantages  |
|---------------------------|--|--|--|
| Bottled Gas               | The oxygen is stored into tanks in a gaseous state. The only oxygen containers that meet the requirements is the aviator's grade breathing oxygen (ABO), which has an oxygen purity of 99.5% | <ul style="list-style-type: none"> <li>- Easily stored</li> <li>- Storing oxygen as gas is more economical it can be stored in high-pressure tanks and low-pressure tanks</li> </ul>   | <ul style="list-style-type: none"> <li>- It is really heavy</li> <li>- Requires a lot of space.</li> <li>- Inflammable</li> <li>- Dangerous</li> </ul>   |
| Bottled Liquid            | Oxygen could be stored and serviced to the aircraft in a liquid state. At very low temperatures oxygen becomes liquid and requires less volume   | <ul style="list-style-type: none"> <li>- It has an expansion ratio of 900 to 1</li> <li>- Requires less weight. It weights around a fifth of what ABO weights</li> <li>- Requires a third of what ABO requires in volume.</li> </ul> | <ul style="list-style-type: none"> <li>- Has to be stored at a temperature of almost -130°C</li> <li>- It will explode if it comes into contact with any petroleum products</li> <li>- If it comes with exposed skin it will cause severe frostbite</li> <li>- Inflammable</li> <li>- Dangerous</li> </ul> |
| Sodium Chlorate Candles   | The sodium chlorate candles release oxygen when ignited at a heat around 170°C. It gives the highest quantity of oxygen relative to its weight and size.                                     | <ul style="list-style-type: none"> <li>- It has an expansion ratio of 600 to 1 relative to ABO</li> <li>- It requires even less weight than LOX</li> <li>- Requires less volume</li> </ul>   | <ul style="list-style-type: none"> <li>- Once the chemical reaction has started, it cannot be stopped</li> <li>- It creates heat, so precautions have to be made to avoid a fire hazard</li> </ul>   |

The sodium chlorate candles are the best option, they require the least weight and volume. They are the less dangerous option. The aircraft is required to supply oxygen for the passengers for a range of 10 to 20 minutes which is the time that the aircraft needs to descend to 10000ft where the passengers can breathe normally without the pressurisation of the aircraft. Using sodium chlorate candles, where 2.2kg supplies the oxygen needed by one person for 24 hours (Martinez, 2019). This means that 30.6g will supply enough oxygen for one person for 20 minutes. The aircraft is designed to accommodate 240 passengers, 5 crew members and 2 pilots. For the crew members and the passengers, 7.5kg of sodium chlorate will supply enough oxygen for 20 minutes. For the pilots, the emergency oxygen is required to last for 2 hours. So for 2 hours, it requires 184g of sodium chlorate to supply enough oxygen for one person. So, for 2 pilots it requires 368g. This means that 7.9kg of sodium chlorate will meet all the requirements. Some metal peroxide is added to the sodium chlorate to prevent any possible chlorine gas formed to reach the passengers. To achieve that, it requires 5% of metal peroxide to be added relative to the mass of sodium chlorate required. This means an additional 400g will be added to the system. So the total weight is around 8.3kg. This oxygen emergency backup system does not require any power, the candles are ignited when the passengers pull a pin in their masks.

Secondly, temperature control failure will cause discomfort and minor health problems. To prevent any blockage, leaking or fouling, the pilot should perform a check before take-off. From the flight management computer, the pilot should check the parameters  $\gamma_n$  where n goes from 1 to 4 and each  $\gamma$  indicates the cause of a temperature control failure represented in Table 54.

Table 54 - Heat Exchanger Parameters Indications (Lu, 2015)

| Heat Exchanger Parameters | Indication   |
|---------------------------|--|
| $\gamma_1$                | A decrease in $\gamma_1$ indicates a blocking in the cold part of the heat exchanger           |
| $\gamma_2$                | A decrease in $\gamma_2$ indicates a leaking or fouling in the cold part of the heat exchanger |
| $\gamma_3$                | A decrease in $\gamma_3$ indicates a blocking in the hot part of the heat exchanger            |
| $\gamma_4$                | A decrease in $\gamma_4$ indicates a leaking or fouling in the hot part of the heat exchanger  |

If a temperature control failure occurs during flight, from these parameters the pilot could adjust the mass flow in the heat exchanger to adjust the temperature of the cabin to an acceptable value. The temperature control system does not need any backup system, it is already reliable and redundant. To conclude, the environmental control system is a reliable and redundant system which will deliver the results required during any flight under any failure mode.

#### 6.4 Ice Protection System – YA

The ice protection system is defined as a safety critical system in the PDR. If it fails, ice accumulates on the wing which leads to aerodynamic penalties. Also, the control surface hinges could freeze, meaning the pilot loses control of the control surfaces which could lead to a crash, as was the case for the Embraer EMB-500 Phenom crash in December 2014 in Gaithersburg, Maryland. Therefore, the ice protection system was analysed to apply redundancy technology where it was necessary to prevent total failure and reduce the failure rate of the ice protection system. To be able to do that it was important to understand how each component in the ice protection system could fail and how the overall system is affected.

The ice protection system contains electric components such as the power control modules and master control unit, where they are embedded in carbon nanotube layers which are embedded mainly in the wing, horizontal and vertical stabilisers. When the ice protection system is turned on, current runs in the carbon nanotube layer where the electrical energy is transformed into thermal energy and heats up the wing surfaces. For the ice protection system to fail, one or more of the failure modes have to happen:

- Human failure: this failure mode is caused by the pilot's failure to turn on the ice protection system which was the cause of the crash mentioned above.
- Insufficient power: this failure is caused by delivering an electrical power smaller than the minimum amount required to heat up the surfaces to a temperature that melts or evaporates the accumulating ice. This failure is divided into four different levels, where each level has different degrees of aerodynamic losses. The different levels are represented in Table 55.

Table 55 - Effect of Insufficient Power on Aircraft

| Aircraft Effect | Speed Losses       | Power Increase Required | Rate of Climb Losses       | Effects on Control Surfaces                 | Vibration on Controls |
|-----------------|--------------------|-------------------------|----------------------------|---|-----------------------|
| Level 1         | Less than 10 knots | Less than 10%           | No effect or less than 10% | No effect                                   | No effect             |
| Level 2         | 10-19 knots        | 10-19%                  | 10%-19%                    | No effect                                   | No effect             |
| Level 3         | 20-39 knots        | 20-39%                  | 20% or more                | Unusually slow responses from control input | Slight vibration      |
| Level 4         | 40 or more knots   | Not able to anti-ice    | Not able to climb          | Little or no response from control input    | Intense vibration     |

- The ice accumulated affects the aircraft speed, performance and the control surfaces. Therefore, as seen in Table 55 an increase of power in the ice protection system is required by the pilot, which depends on the level of the effects and losses of speed and rate of climb on the aircraft.

- Electric component failure: this failure is caused by a failure in one or more electrical components. The power control modules are responsible for heating a specific zone on the wing surface. Each power control module is linked to a single heating zone which is embedded in each of the wings in a symmetrical manner. If one power control module fails, asymmetrical heating will arise which will destabilise the aircraft during flight because ice accumulation will be different on each side of the wing. Therefore, the wings will not have the same aerodynamic characteristics. Moreover, the master control unit is responsible for implementing the ice protection control by the pilot. If it fails, the pilot will lose control over the ice protection system.

The ice protection system will fail if any of the failure modes occur. The acceptable failure rate for the ice protection system is once every five years, which corresponds to the D-check schedule. The failure rate will be analysed for each component for each system unless a different method is more suitable to prevent the modes of failure.

Firstly, the human failure mode does not depend on the system, it is a failure mode caused by a human factor. This failure mode cannot be measured in a failure rate nor in SIL. However, it could be prevented by adding an alarm system in the cockpit to notify the pilot that they forgot to activate the ice protection system that will always remind them before take-off. The alarm system was chosen for the aircraft needs around 1kW and weights 5kg (Martens, 2005). This alarm system could also be used for different alerts for the aircraft,

Secondly, insufficient power failure mode is also a human factor failure mode. This is a failure mode where the pilot did not adjust the power input in the ice protection system to properly deal with the weather conditions. This failure mode cannot be measured in a failure rate nor in SIL. However, it can be prevented as the electrical components have built-in sensors which detect the temperature of the control surfaces with ice accumulation. With, the alarm system added for the human factor failure mode and the sensors, the ice protection system will alert the pilot when the ice protection system requires more power and therefore prevent the aircraft from any aerodynamic penalties related to this failure mode.

Finally, the electrical component has a very low failure rate. The power control modules have a failure rate of 1% every 1000 hours, and the master control unit has a failure rate of 0.4% every 1000 hours (Stonestreet, Kraus and Genereux, 2012). This means it has an MTBF of 71000 hours. The failure rate was determined as 0.13 times per year, which is the equivalent of failing once every 7.7 years. This failure rate is lower than the acceptable rate which means that a SIL cannot be given to the electrical components, as there is no risk related to that failure mode. However, as the ice protection system is a safety critical system, precautions should be taken to prevent that a failure occurs during flight. As mentioned above, the failure of one power control module will destabilise the aircraft. Therefore, the power control modules will be arranged in such a way where both wings are symmetrical and connected. Which means if one power control module fails the mirrored one on the other wing half will shut down to prevent any asymmetrical heating.

Furthermore, each power control module contains the ability to provide fault isolation without affecting the non-affected zones, which provides an N+1 redundancy (Stonestreet, Kraus and Genereux, 2012) and high system availability. Also, another master control unit will be added that will only activate if the other one fails which will enable the aircraft to continue its flight without endangering the lives of everyone onboard. To conclude, with the alarm system added and the power control module arrangement which will help the aircraft to continue its flight and land safely under any failure mode and then be fixed when it lands. Therefore, the ice protection system is now redundancy protected and a highly reliable system.

## 6.5 Fuel Systems – MK

The fuel system is a safety critical system and its operation is required to deliver fuel to the engines and APU. The fuel system consists of tanks, pipes, and valves. Any of these components could fail in a number of ways, some of which are addressed in this section.

The tanks can either fail due to leakage or rupture. The symptoms for these failure modes would be loss of fuel from the system, restricted fuel flow to the engine, and a lowered pressure at the engine feed line inlet.

The pipes can fail by leakage, rupture, or blockage (partial or full). Blockage would result in the symptom of increased pressure at the engine feed line inlet, as well as reduced fuel flow to the engine. Pipe leakage and rupture will show the same symptoms as tank leakage and rupture.

Rupture or leakage in the fuel tanks, engines, or anywhere in between will result in a loss of fuel. Shutting down the affected engine can resolve the issue of fuel leak for that engine.

The pumps can fail due to leakage, or mechanically, on or off. Pump failure can be identified by a loss of fuel flow to the engine and a low engine feed line inlet pressure. To ensure that the fuel system can still operate in the case of pump failure, the fuel tanks will have multiple pumps built in for redundancy. It is unlikely that multiple pumps will fail at one time.

Valves can fail by becoming stuck, opening or closing at incorrect pressure, leakage, or blockage (partial or full). Multiple valves as well as regular cleaning and maintenance will add redundancy and reduce the rate of this failure mode

Fuel freezing can cause failure in the aircraft fuel system. If the fuel reaches its freezing point, it will become unusable. This failure would most likely occur with the fuel located in the wing tanks. If the fuel temperature indicator shows it to be close to its freezing point, the pilot can either descend to warmer air, increase flight speed (therefore increasing total air temperature), or relocate the fuel to a tank with higher temperature fuel.

The fuel tanks must be managed appropriately to avoid fuel imbalance. A fuel imbalance can occur in the event of fuel leak or engine failure and would result in difficulty in controlling the aircraft. Where possible, fuel should be shared equally between wing fuel tanks via the pipes connecting the tanks.

ICAO Annex 6, Chapter 4 states that flight of an aircraft shall only be commenced if the aircraft is carrying enough fuel to safely complete the planned mission, as well as a reserve of fuel in case of emergencies. The text also outlines the method to determine minimum required fuel for the flight. Amendment 36 to Annex 6 addresses fuel management and outlines the conditions in which the pilot should declare minimum fuel.

## **6.6 Hydraulics Systems – MK**

Since control surfaces in the aircraft will be actuated using the electrical system, the hydraulic system will be used solely to extend and retract the landing gear, as well as in braking.

Failure of the hydraulic system can occur due to pump failure. This will result in a loss of pressure in the system. Pressure loss can also be a result of fluid loss from the system. Other possible failure modes include overheating of the system or contamination of the hydraulic fluid.

Fluid contamination can be avoided by using an approved hydraulic fluid type that must not be mixed with any other fluid types. The filters built into the hydraulic system will aid in the prevention of fluid contamination. Guidelines will be provided by the manufacturers as to how regularly the filters should be cleaned and replaced.

There are two main methods for redundancy in the hydraulic system. The first of these is the use of multiple pressure systems. The hydraulic system in the aircraft will be driven by multiple pumps in case of failure of one pump. Failure of pumps would occur independently therefore it is highly unlikely that both pumps would fail at the same time.

The second main redundancy method makes use of multiple hydraulic systems. In aircraft where control surfaces are actuated by the hydraulic system, different control surfaces are actuated by different hydraulic systems however the Aero 5 aircraft uses the electrical system to actuate control surfaces and will therefore not need the complexity of multiple hydraulic systems.

If the hydraulic system required to extend the landing gear fails, a handle can be pulled to mechanically release the landing gear, allowing the main gears and nose gear to fall under the force of gravity and then be locked into place.

A precalculated value (Pettit, 2001) for failure rate of the hydraulic system of  $1.15 \times 10^{-4}$  per year has been used to calculate an RRF of  $5.75 \times 10^{-4}$ . This is an extremely small RRF considering that the minimum RRF for SIL1 is 10.

Since the hydraulic system has mostly been replaced by the electrical system, and due to the redundancy already built into the system, and this low RRF, the hydraulic system seems to be sufficiently safe.

## **6.7 Fire Protection System – MK**

The fire protection system is a safety critical system as stated in the PDR. The PDR identified the number and location of accessible manual fire extinguishers in accordance with FAA AC 20-42D – Hand Fire Extinguishers for Use in Aircraft.

Remote extinguishers in engines, APU, and cargo compartment release extinguisher agent through valves. These extinguishers have multiple separate valves in case one becomes inoperable.

These remote extinguishers and detectors are powered by the Hot Battery Bus and can therefore be used when the rest of the aircraft is powered off. This eliminates the risk of electrical failure in the case of a remote fire. The engine fire detection uses two loops, both of which must detect a fire before the warning is given and the extinguisher is activated. If one loop fails, it will be switched off and the remaining loop will operate independently.

Electrical failure is not a problem with cabin and cockpit fires since fire suppression is provided manually by the crew via handheld extinguishers located throughout the cabin and in the cockpit and detection is carried out by the crew since human ability to detect smoke or flames is sufficient.

Fire within the aircraft can be one of the most hazardous events in flight. Even with appropriate fire protection and suppression carried out, the aircraft should plan to make a safe landing as soon as possible.

A precalculated rate of occurrence for loss of aircraft due to failure to extinguish a nacelle fire of  $4.92 \times 10^{-8}$  per flight hour (Gann, 2007) has been used to calculate an SIL value for this particular failure mode due the criticality of this event. Using Aero 5's predicted flight hours of 3840 per year (PDR Section 6.4), this figure gives a failure rate of  $1.89 \times 10^{-4}$  per year. This failure rate gives an RRF of  $9.45 \times 10^{-4}$ , much lower than the minimum RRF for SIL1 suggesting that this is an extremely rare event. The use of two engines contributes to the rarity of loss of aircraft due to engine fire since one engine should still be operable in the event of one engine loss.

## 6.8 Electrical Systems – YA

The electrical system is defined as a safety critical system in the PDR. If it fails the aircraft will not have enough power to supply to the other systems and the passenger's safety will be at high risk. Therefore, the electrical system will be analysed to apply redundant technology to minimise and reduce the frequency of total failure of the system. To be able to do that it is important to understand how each component in the electrical system could fail and how that will affect the whole system overall. A fault tree analysis was made for the electrical system to comprehend the failure modes for each component, which could be seen in Figure 57.

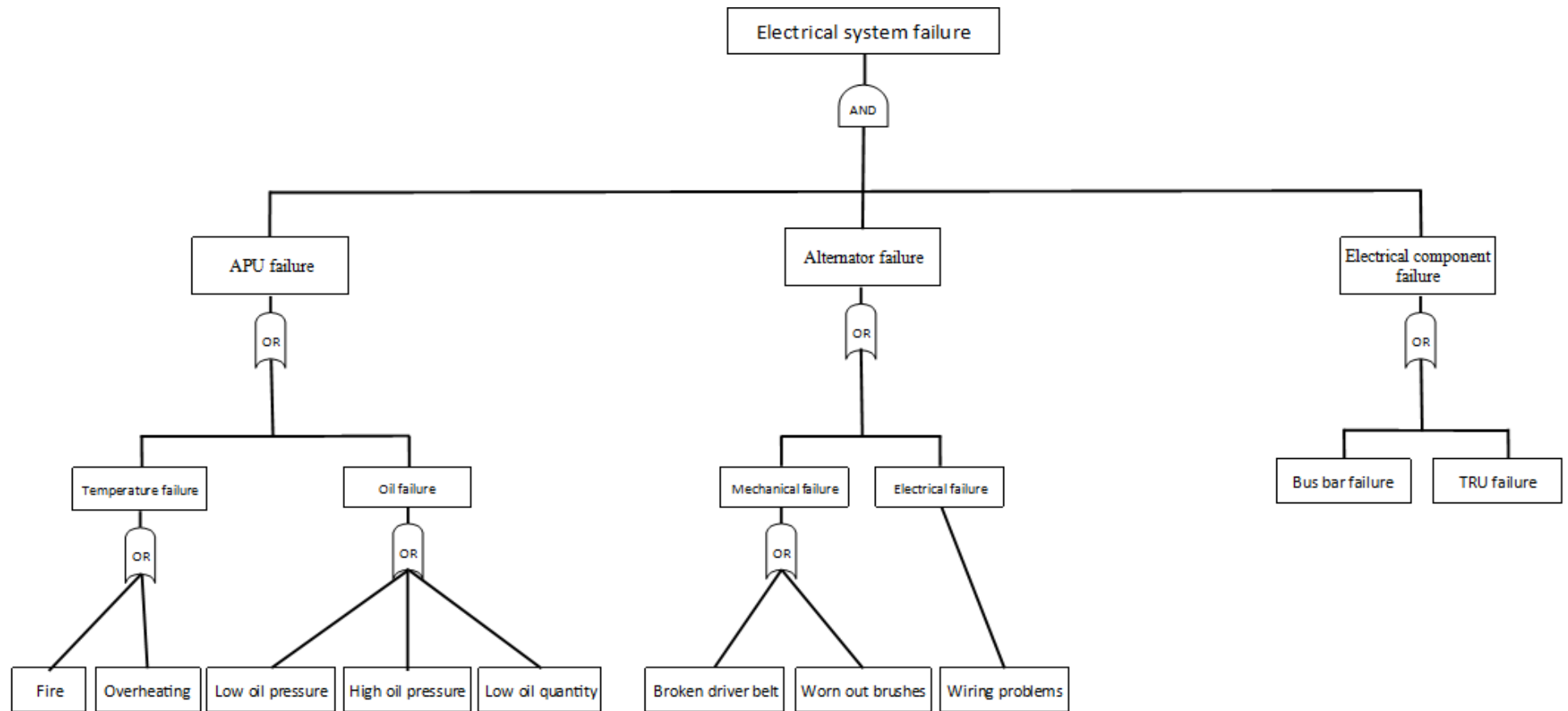


Figure 57 - Electrical System Fault Tree Analysis

The electrical system consists of an APU, alternators and electrical components that transmit power to the other systems. The APU is used for the start-up of the engines and provides backup power in case of an alternator failure. From Figure 57, it could be seen that the APU could fail by one of the following failure modes:

- Fire: fire in the air is one of the most hazardous situations that the aircraft could face during flight. Not only the power generated by the APU will be lost, but the aircraft integrity is also at risk. The fire could damage the fuselage or the empennage. The heat of the fire could cause deformation which could compromise the structural integrity of the aircraft leading to loss of some aircraft systems or even loss of control.
- Overheating: during flight the inlet door of the APU is closed, which could cause heat to build-up. A case study on Boeing 787 found that if an APU overheats, it takes around 20 minutes for the rotor shaft to bow, and the shaft takes around 2 hours to straighten up.
- Low oil pressure: the oil protects the APU and prevents any damage from any mechanical rubbing. If the oil pressure is too low the APU will shut down automatically.
- High oil temperature: as the oil is an important component in the APU if its temperature gets too high, the APU shutdowns automatically.
- Low quantity of oil: If the oil quantity is too low, the APU could still run for around 30 minutes and then it will automatically shut down.

The second component of the electrical system that can be seen is the alternators. Each engine consists of an alternator to generate electrical power. The alternators are the first source of electrical power on the aircraft. From Figure 57, it could be seen that the alternators could fail by one of the following failure modes:

- Broken driver belt: the driver belt takes rotational power from the main crankshaft pulley, which transfers it to the alternator pulley. If the belt is broken, cracked or worn out, the alternator will not produce any electrical power.
- Worn out brushes: the brushes are the first component that transform the AC voltage produced by the alternators to DC voltage. When the brushes are worn out the alternators will not be able to produce any DC voltage.
- Wiring problems: the wires transfer the produced power from the alternators to the systems. If it fails the systems will not receive any electricity and they will not function.
- Engine failure: in case of an engine failure, the alternator will not be able to produce any electrical power.

The final component of the electrical system are the electrical components that transmit, transform and transfer power from the alternators to the other systems. From Figure 57, it could be seen that the electrical components could fail by one of the following failure modes:

- Transformer-rectifier unit (TRU) failure: the TRU transforms AC voltage to DC voltage. It is a backup for the failure of the brushes in the alternators.
- Bus bar failure: the purpose of the bus bar in the electrical system is to conduct a substantial amount of electric current to the system. If it fails, a low or high amount of current would be delivered to the systems, where the systems will fail in both cases.

The alternators are the main source of electrical power in the aircraft. The best way to extend the life of an alternator on the aircraft is by paralleling the two alternators. This divides the workload on both the alternators. The aircraft requires around 400 kW, where each alternator produces 250kW. So dividing the workload means that each alternator should only produce 200kW. However, in case of an alternator failure, the APU is used to provide electrical power. The APU chosen in the PDR could produce up to 250kW. In case of an APU and one alternator failure, the aircraft is still able to produce enough power for all the systems to function normally excluding the environmental control system. Therefore, the aircraft will deploy an emergency oxygen system until it descends to an altitude it does not need an environmental control system, which around 10000ft. The electrical system is built with different TRU and bus bar failure which gives an extra redundancy to the system. To conclude the electrical system is able to provide enough power for all the other systems to function normally, it is also reliable and redundant which will make it provide the results required during a flight.

### 6.8.1 Electrical Systems Architecture – MK

Figure 58 shows a plan view of the Aero 5 aircraft complete with labels showing the locations of the various components of the aircraft systems addressed in this section. Each number label in Figure 58 matches up with a specific system or subsystem component or group of components in Table 56.

*Table 56 - Systems and Subsystems as Labelled on Figure 58*

| Number Label | System/Subsystem                                       |
|--------------|--|
| 1            | Flight Management System                               |
| 2            | Navigation System                                      |
| 3            | Communication System                                   |
| 4            | Crash Protected Flight Recorder                        |
| 5            | Weather and Traffic System                             |
| 6            | Ice Protection System                                  |
| 7            | Environmental Control System (ECS)                     |
| 8            | Fuel System  |
| 8a           | Fuel Tanks   |
| 8b           | Engines  |
| 9            | Fire Protection System                                 |
| 9a           | Hand extinguishers                                     |
| 9b           | Remote extinguishers and detectors (Engines)           |
| 9c           | Remote extinguishers and detectors (APU)               |
| 9d           | Remote extinguishers and detectors (Cargo compartment) |
| 10           | Hydraulics   |
| 11           | Electrical System                                      |
| 11a          | APU  |
| 11b          | Generators   |

The locations shown for the ECS are the locations of the A/C packs and the hydraulics location represents the location of the hydraulic reservoir.

More detailed descriptions of the locations of each system component with necessary justification can be found in the individual system sections in this document as well as in Section 5 of the PDR.

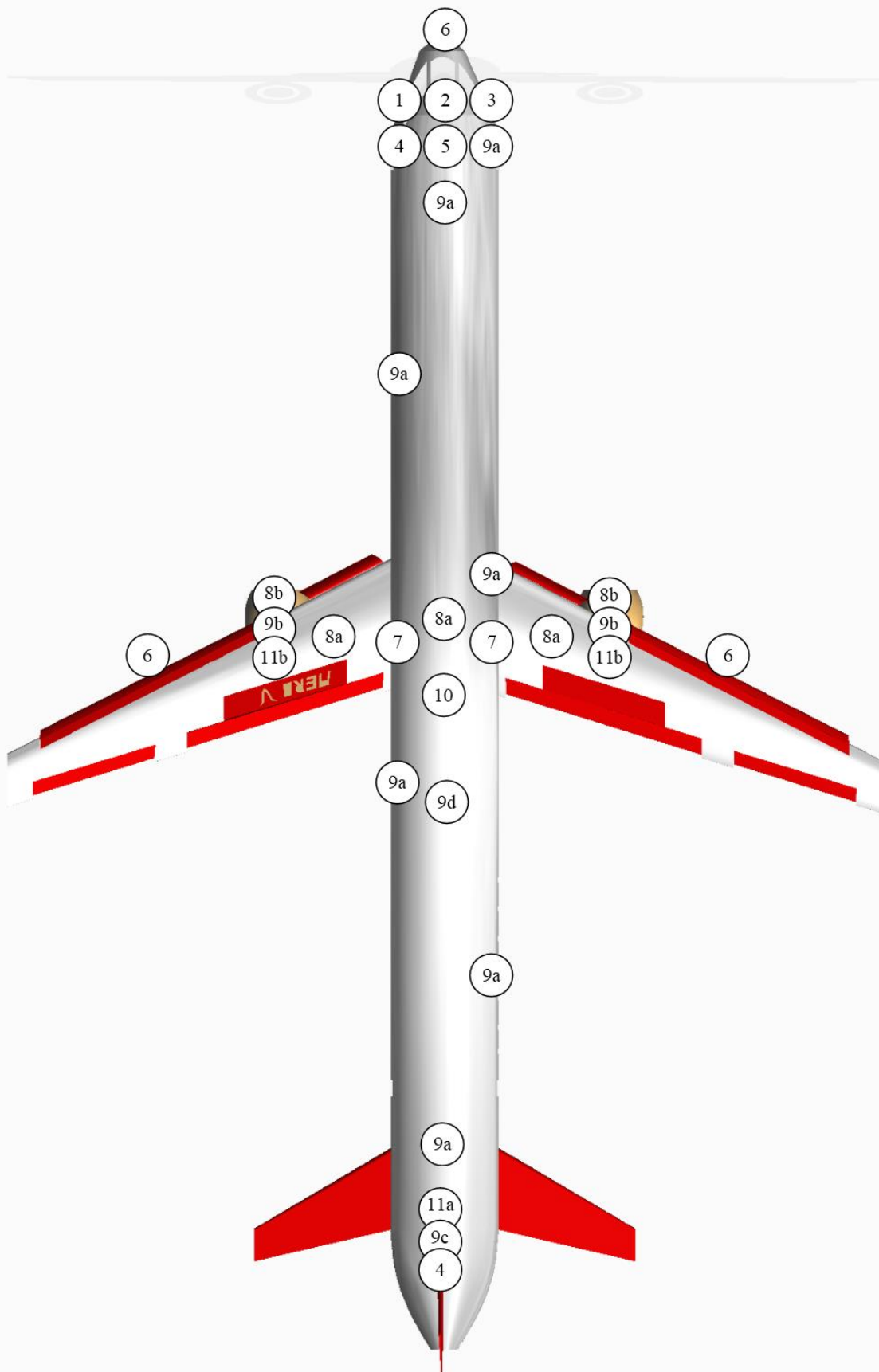


Figure 58 - Systems Architecture Map

## 7. Interface List – TL

Table 57 - Interface List

| Component 1              | Component 2              | Interface Type | Implementation Approach   | Constraints or Issues   |
|--------------------------|--------------------------|----------------|---------------------------|---|
| <b>Wing &amp; Engine</b> |                          |                |                           |   |
| Stringers                | Skin                     | Structural     | Rivet                     | Must take out larger sections than needed in repairs due to permanent fixture caused by rivets      |
| Spars                    | Ribs                     | Structural     | Bolts & washer, pivot pin | Concentration of stress at bolt, cracking, fracture, fatigue  |
| Fowler flap              | Trailing spar            | Mechanical     | Hinge                     | Stress load whilst deployed for increase lift, negative effect on aerodynamics if connection is bad |
| Aileron                  | Trailing spar            | Mechanical     | Hinge                     | Stress load whilst aircraft is in roll  |
| Krueger flap             | Leading spar             | Mechanical     | Hinge                     | Stress load whilst deployed for increase lift, negative effect on aerodynamics if connection is bad |
| Slats                    | Leading Spar             | Mechanical     | Hinge                     | Stress load whilst deployed for increase lift, negative effect on aerodynamics if connection is bad |
| Spoilers                 | Skin                     | Mechanical     | Hinge                     | Stress load whilst deployed for increase drag, negative effect on aerodynamics if connection is bad |
| Spars                    | Wing box                 | Structural     | Bolts & washer            | Concentration of stress at bolt, cracking, fracture, fatigue  |
| Engine                   | Nacelle                  | Structural     | Pin joints                | Vibrations over many cycles can loosen connections  |
| Nacelle                  | Pylon                    | Structural     | Pin joints                | Vibrations over many cycles can loosen connections  |
| Pylon                    | Leading & trailing spars | Structural     | Pin joints                | Vibrations over many cycles can loosen connections  |
| Alternator               | Engine                   | Structural     | Bolts & washer            | Concentration of stress at bolt, cracking, fracture, fatigue  |
| Main landing gear        | Lower wing surface       | Mechanical     | Struts                    | Concentrated point load can cause fatigue or fractures  |
| <b>Fuselage</b>          |                          |                |                           |   |
| Stringers                | Skin                     | Structural     | Rivet                     | Must take out larger sections than needed in  |

|                           |                           |            |                                     |  |
|---------------------------|---------------------------|------------|-------------------------------------|--|
|                           |                           |            |                                     | repairs due to permanent fixture caused by rivets  |
| Bulkhead                  | Longerons                 | Structural | Bolts & washer                      | Concentration of stress at bolt, cracking, fracture, fatigue from repeat cycles of pressurisations           |
| Nose (front fuselage)     | Cabin (main fuselage)     | Structural | Bolts, washer & lugs                | Concentration of stress at bolt, cracking, fracture, fatigue   |
| Empennage (rear fuselage) | Main fuselage             | Structural | Bolted bulkhead                     | Concentration of stress at bolt, cracking, fracture, fatigue   |
| Nose landing gear         | Nose (Front fuselage)     | Mechanical | Struts                              | Concentrated point load can cause fatigue or fractures   |
| Vertical tail-plane       | Rudder                    | Mechanical | Hinge                               | Stress load whilst aircraft is in yaw  |
| Horizontal tail-plane     | Elevator                  | Mechanical | Hinge                               | Stress load whilst aircraft is in pitch  |
| Vertical tail-plane       | Empennage (rear fuselage) | Structural | Bolts & washer                      | Concentration of stress at bolt, cracking, fracture, fatigue   |
| Horizontal tail-plane     | Empennage (rear fuselage) | Mechanical | Pivot fixing and hydraulic actuator | Load cycle causing fatigue   |
| APU                       | Empennage (rear fuselage) | Structural | Bolts & washer                      | Concentration of stress at bolt, cracking, fracture, fatigue   |
| Undercarriage             | Main fuselage             | Structural | Bolts & washer                      | Concentration of stress at bolt, cracking, fracture, fatigue.<br>Vibrations from flight can cause loosening. |
| Wing box                  | Main fuselage             | Structural | Rivets, bolts & washer              | Bending stress, stress concentration around connection area  |
| Exits                     | Main fuselage             | Mechanical | Bolts & washer                      | Possibility of not being air tight, stress concentration from pressure change of cabin                       |
| Windows                   | Main fuselage             | Structural | Bolts & washer                      | Glass can crack and delaminate by pressurisation cycles  |
| <b>Cabin</b>              |                           |            |                                     |  |
| Carpet                    | Floor                     | Structural | Epoxy glue and screws               | Needs regular maintenance to ensure safety and hygiene   |
| Passenger seats           | Floor                     | Structural | Bolts & washer onto railing         | Interchanging layouts can cause abrasive wear if not lubricated well   |
| Lavatory                  | Floor                     | Structural | Bolts & washer                      | Vibrations from flight can cause loosening   |

|                              |                           |            |                |   |
|------------------------------|---------------------------|------------|----------------|---|
| Galley                       | Floor                     | Structural | Bolts & washer | Vibrations from flight can cause loosening.                   |
| Overhead compartment storage | Overhead compartment door | Mechanical | Hinge          | Heavy loads and cause stress concentration                    |
| Overhead compartment unit    | Main fuselage             | Structural | Bolts & washer | Heavy loads and cause stress concentration                    |
| Attendant seats              | Wall                      | Structural | Bolts & washer | Concentration of stress at bolt, cracking, fracture, fatigue. |

## 8. Risk Management – YA, AS, AM

### 8.1 Risk identification – YA

As this is the final stage of the design process, the risk assessment was made to mitigate more detailed risks than the PDR and the PDS. The aim of this risk assessment was to focus on risks raised mainly from the manufacturing and operation process of the project. In Table 61 different risks were assessed and six were chosen to be analysed and mitigated. The six chosen risks were human safety, foreign object damage (FOD), precision of installation, structural failure, engine failure and aircraft systems failure.

#### 8.1.1 Human Safety – AM

Almost all the risks evaluated involved the safety of humans. However, in this section, the general risks were considered to reduce inconvenient incidents. Different phases of the project involve possible potential health related risks. During the design phase, the engineers have the potential to face the risk of being overloaded with tasks, hence there is a probability of mental breakdowns. In the manufacturing process, the manufacturing engineers may be exposed to hazardous substances such as inhaling carbon particulates and during flights, there are possibilities that the passengers or cabin crew can trip on obstacles on the floor.

#### 8.1.2 Foreign Object Damage (FOD) – AS

This is the one of the biggest problems in aviation that can reduce the safety factor during flight that could lead to catastrophic failure. It can be only specifically mitigated using the precise control measure methodology. Theoretically, the damage level is based on the high severity and destruction level that can occur during flight, which can potentially cause loss of human life.

These risks occur in certain environments such as taxiways, aerodrome gates, hangars, during flight and hence the largest consequences include flight delay, cancellation, scheduling issues and customer satisfaction. This assessment focuses on FOD classification and the associated risks and countermeasures.

In the general definition of FOD, it includes debris, particle or any foreign object surrounding the aircraft that can potentially cause damage either in the external or internal system. In the most serious case, it can be justified as a harmful object that could severely injure someone or damage the aircraft itself.

There are some articles from the Federal Aviation Administration (2010) that distinguish FOD in many forms. FOD can be placed in various classes such as metal, stone, miscellaneous and birds. However, they also stated that during air crash investigations over 60% of the evidence showed that they were made by metal, 18% from rubber material and the rest from miscellaneous objects, as shown in Table 58.

Table 58 - Sources of FOD (FAA, 2010)

| Types of FOD                        | Sources  |
|-------------------------------------|--|
| Personnel                           | Caused by poor quality of working by the maintenance                   |
| Airport infrastructure              | Sign, pavements and lights   |
| Environment                         | Wildlife, extreme temperature, humidity and precipitation              |
| Airfield equipment during operation | Operational transport vehicles, construction and maintenance equipment |
| Aircraft and engine fastener        | Nuts, bolts and washers  |

|                              |  |
|------------------------------|--|
| Aircraft parts               | Fuel cap, oil stick, trapdoor and tyre fragments         |
| Flight belongings            | Passengers luggage's and any other belongings            |
| Runway and taxiway materials | Tarmac chunks, big particle of dust, and joint materials |

The vulnerable location for FOD is the aircraft engine, as it intakes any object within a certain radius. This can cause technical problems if the debris damages the turbine blade depending on the size and hardness of the debris material. The debris cannot be extracted through the engine as this would cause engine intake flow disruption in the initial stage or if large enough, it would lead to engine failure.

Maragakis (2008) from the European Aviation Safety Agency (EASA) informed that between 1999-2008, 44% of FOD cases were bird strikes which caused serious damage to the engine section. The severity level has been classified based upon the turbine blade condition which is listed on the Table 59.

*Table 59 - Turbine Blade Severity Level Indicator (Maragakis, 2008)*

| Severity Level | Action Needed   |
|----------------|---|
| Minor          | No action is required   |
| Moderate       | 1 <sup>st</sup> stage repair is required                            |
| Severe         | 2 <sup>nd</sup> stage repair is required                            |
| Very Severe    | Whole blade replacement is required if it is not possible to repair |

Another major debris that plays a significant role in increasing casualties is tyre debris. A tyre bursting can lead to damage to the aircraft. The tyre treads from the landing gears can detach which can create a chain reaction through third body wear. Usually, this occurs during take-off and landing.

The worst-case scenario could happen during the flight when debris causes another piece of debris to damage the aircraft frame. Consequently, this could damage the wing structure, leading to aerodynamic losses which would mean the aircraft would be difficult to control.

There is a crucial condition when the FOD penetrates the fuselage area which can lead to rapid depressurisation causing fatal decompression sickness and suffocation to the whole cabin.

### **8.1.3 Accuracy of Installation – AM**

Accuracy of installation was stated as one of the top risks as it has a high probability to occur and will greatly delay certification. If the problem is identified during the assembling process, it would require the design and manufacturing of the component to be re-evaluated. As a result, the certification process will be delayed and the cost to manufacture would increase and negatively impact the DOC. However, if the installation issues are not addressed, the probability of losing the aircraft through catastrophic failure is high.

### **8.1.4 Structural Failure – AS**

Structural risk and reliability analysis is the engineering approach used to check the aircraft structural integrity whilst in service. Inevitable environmental defects such as corrosion, material fatigue and debris can damage the aircraft structure. A safety factor of 1.5 was applied in this project to mitigate the likelihood of a structural failure.

It is not possible to prevent all damage that occurs as a result of natural factor defects, due to extreme conditions, volatile environments and high humidity. The lifetime of the structure can be determined based on how well the material resists the deleterious environment. The analysis also includes where the critical concentration point load is located.

For example, the internal structure is expected to use a material with good corrosion resistance. Corrosion of the aircraft skin, that occurs as a result of the humid environment causes the material to lose its strength and degrade the performance. This can lead to permanent material loss, cracking and catastrophic failure.

Material fatigue is the condition in which the direct load is sustained continuously at a specific point, decreasing structure lifetime. Growth of fatigue cracks starts from material defects which can result from the manufacturer or poor quality of machining. However, this mostly happens due to the corrosion development in the later life of the aircraft when it reaches a certain point in its flight cycle.

White (2006) explained that the material fatigue assessment can be calculated using probabilistic fracture mechanics. The specialist engineering discipline focuses on crack growth behaviour with different sizes and the load which can affect the crack growth and the residual strength. In the critical concentration point load, the largest possible crack can be found by analysing the data from the crack distribution using the mathematical model theory.

Failure probability is obtained by combining all the probabilities, assuming a load greater than the failure load to account for the worst-case scenario. The behaviour of the failure can be expressed by the type of distribution in the Table 60.

*Table 60 - Distribution of the Random Variables (White, 2006)*

| Distribution | Behaviour of Failure                     |
|--------------|--|
| Normal       | Cumulative process of random amounts     |
| Log normal   | Multiplication process of random amounts |
| Exponential  | Random failure                           |
| Gamma        | Multiple random failure                  |

From the obtained material data, the variables of the material can be plotted and refer to the failure behaviour distribution. As a final result, typical criteria for each are  $10^{-3}$  for failure probability and  $10^{-7}$  for single flight. Furthermore, the crack grows over the time and thus, the total probability of failure usually increases proportionally with the growth of the crack.

### 8.1.5 Engine Failure – AM

Engines are a major component in an aircraft providing the thrust demand of the aircraft. The Aero 5 aircraft was designed to operate for an OEI case. However, the scenario where both engines fail was considered a high ranking risk because the severity was high enough to outweigh the likelihood of the occurrence of both engines failing. A double engine failure case has a high probability of resulting in a catastrophic outcome.

### 8.1.6 Aircraft Systems Failure – YA

The aircraft consists of multiple systems where each system has a specific task. Together, all the systems ensure a safe and comfortable flight for the passengers, in addition to reducing the workload for the pilot. The failure of any of these systems puts the safety of the Aero 5 aircraft at risk. In Section 8.3.6 the mitigation process that is required to ensure the function of the aircraft systems with the lowest failures possible is outlined. In case of any failure the mitigation process will discuss how to continue the flight safely.

## 8.2 Qualitative Risk Assessment – YA

In this section, the impact of severity of each risk and their probability of occurrence is assessed. This is shown in Table 61, the updated risk registers and the matrix supporting it in Appendix 13.9.

*Table 61 - Updated Risk Register*

| Risk                      | Risk Category    | Probability   | Impact      | Risk Score | Risk Ranking |
|---------------------------|------------------|---------------|-------------|------------|--------------|
| Human safety              | Manufacture risk | Very unlikely | Severe      | 6          | 5            |
| FOD                       | Operational risk | Unlikely      | Significant | 6          | 6            |
| Accuracy of installation  | Manufacture risk | Unlikely      | Severe      | 7          | 1            |
| Structural failure        | Operational risk | Unlikely      | Severe      | 7          | 4            |
| Engine failure            | Operational risk | Unlikely      | Significant | 7          | 3            |
| Aircraft systems failure  | Operational risk | Unlikely      | Severe      | 7          | 2            |
| Turbulence and quick drop | Operational risk | Possible      | Minor       | 5          | 9            |
| Hazardous fluid           | Disposal risk    | Possible      | Moderate    | 6          | 7            |
| Battery disposal          | Disposal risk    | Possible      | Moderate    | 6          | 8            |

From Table 61 the nine risks were assessed that could arise during different life cycle stages of the Aero 5 aircraft which are; manufacture, operation, and disposal. It was found that precision of installation was the risk with the greatest threat, as it has the most severe impact and the highest probability of occurrence. However, all the different risk still imposes a threat to the Aero 5 aircraft, therefore the highest 6 risks in the ranking from Table 61 were chosen to be analyzed and mitigated in Section 8.3.

### 8.3 Mitigation and Contingency – YA, AS, AM

#### 8.3.1 Human Safety – AM

During the design phase the only humans involved in the project are the engineers. Considering the health-related risks, the project tasks should be distributed evenly across the team members. During the manufacturing process, the engineers must be equipped with appropriate safety equipment to protect against the hazardous substances they are exposed to.

For the mitigation plan, the affected person must be treated along with all the engineers working in the manufacturing department. Finally, during the flight, the floor must be free of obstacles and if there are any in the path of passengers or the cabin crew, it must be indicated through a sign. In the case that anyone on the aircraft gets injured, first aid must be given. Hence the cabin crew must be trained to provide medical assistance.

#### 8.3.2 FOD – AS

FOD prevention can be achieved by having a good implementation of the safety systems, as well ensuring that it is managed appropriately. In order to do that, human factors play the biggest role in this because they are responsible for maintaining and enforcing the safety culture. This behaviour and manner to enhance self-strong discipline and the awareness of responsibility about the possible hazards is critical to the risk mitigation.

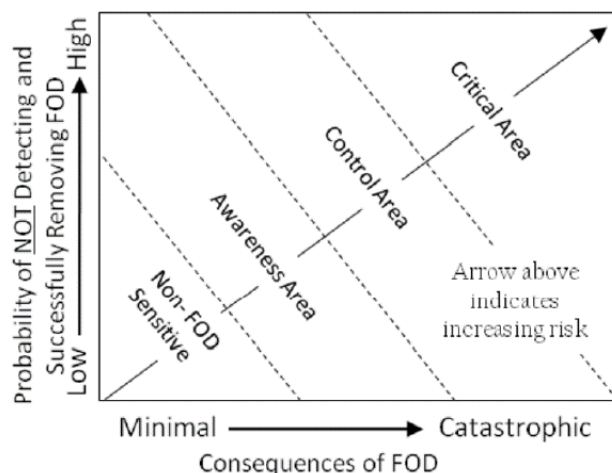


Figure 59 - FOD Probability Association with Consequence Assessment (NASA, 2010)

Figure 59 shows the FOD designation area as a risk indicator by NASA (2010). It is measured by FOD sensitive areas by combining two risk factors, probability (Y-axis) and consequences (X-axis). The sensitive area is the area where FOD is unlikely to damage the aircraft, implying it is a low risk.

The awareness area signifies there is an increased risk, since the damage tendency may become complicated and disrupt flight operation. On the other hand, the likelihood of the risk occurring is again increased in the control and critical area. If a risk was classified in this section, the FOD would have a high probability of not being detected, which would lead to potentially catastrophic aircraft failure.

High awareness when on the airfield and of the surrounding environment is essential during taxiing, take-off and landing. The airport management plays an important role here because they must be responsible for the clean environment on the runway to avoid FOD occurrences. Moreover, an air survey could also be applicable to mitigate the likelihood of a possible bird strike. In conclusion, it is unlikely to eliminate the possibility of FOD but, if the programme is successfully implemented, it will reduce the likelihood of occurrence in the future.

#### 8.3.3 Accuracy of Installation – AM

In the case of improper engine installation, the certification process will be delayed, hence the design calculations must be evaluated before manufacture and assembly. For the contingency plan, the interface

should be carefully designed to reduce the complexity of installation and the aircraft components must be tested as part of the process following the installation. The installed components of the aircraft must go through testing process once installed to ensure that the installation process has been carried out without any errors.

#### **8.3.4 Structural Failure – AS**

In order to prevent structural failure, the accuracy of analysis must be enhanced by evaluating the reliability of the structure itself. During the preliminary design, the material must be chosen wisely according to the function it is required for. Whilst the structure is designed to be as lightweight as possible, the safety factor is a top priority. For instance, in the main structure, moisture resistance is preferable for the internal structure covered by the aircraft skin to prevent corrosion. Another example is the use of a high strength material for the bulkhead to prevent excessive bending stresses.

Another factor that needs to be considered is the flight cycle. A maintenance programme is mandatory for every aircraft. This includes using Non-Destructive Techniques (NDT) to inspect the aircraft structure for cracks. In general, this is the most common technique to investigate the possibility of material cracks.

In conclusion, the innovation of material is also an option for the future by increasing the use of composite materials which are very durable and light. This has motivated the aircraft manufacturer to implement composite materials into aircraft structure. However, it is not valid with extreme temperature conditions due to the fact that composites have poor thermal resistance and this is especially problematic for internal engine parts.

#### **8.3.5 Engine failure – AM**

In the case of double engine failure, the aircraft loses its source of thrust. Hence when encountering this risk, an emergency landing at the nearest airport must be considered. This requires the pilot to be well experienced and hence for the mitigation plan, the piloting crew must be trained to work under pressure and to able to communicate clearly with the nearest airport if an emergency landing needs to be requested. The engine must also go through frequent inspection for component failure to identify the onset of any problems.

#### **8.3.6 Aircraft Systems Failure – YA**

To mitigate the aircraft systems failures, each system is different, however there is a general process that should be applied for all systems. The goal in each analysis is to understand all the failure modes for the system being analysed, with that being the first step of the process. After understanding how each component fails, a probability of failure should be calculated. From that probability, it should be analysed if the system could still function normally with that component failure. If the system would have an overall failure with the component failure, then redundancy technology should be applied, where the component should be doubled in the system. The analysis should make sure that the aircraft can fly safely with any component failure in any system, if it cannot accomplish that then the system is not reliable, and it should be redesigned with the addition of extra redundancy components.

## **9. Work Breakdown Structure and Schedule – BG, MK**

### **9.1 Work Breakdown Structure (WBS) – BG, MK**

The Activity List was updated regularly during the time between PDR and CDR to include the new lower level tasks identified by Aero 5. Treating the Activity List as a live document allowed Aero 5 to keep track of the work completed over the break following PDR submission. Aero 5 met after the submission of the PDR to discuss the next steps leading up to the start of Semester 2 to ensure that all team members had an appropriate and equal work load, including a technical element, for the following weeks. These plans were outlined in the Activity List. Teams were allocated at this time to ensure that all components of the CDR were covered or had a plan in place to be worked on at a later date. The fluidity of the teams and sub-teams had been working well so far in the project hence this flexibility was maintained. This proved useful in being able to create contingency for tasks and in re-balancing work load where appropriate.

The revised Activity List was then used to update the WBS Tree that is shown in Figure 60. The main top level tasks have not changed since the PDR. The second level has seen the addition of Programme Management tasks including Configuration Management, Change Requests, and Future Improvements. Aircraft Design tasks include Structure and CAD, and Systems tasks including Systems Architecture and Fault Tree Analysis. Many lower level tasks were also added in order to keep track of work load and create an updated Top Level Schedule as seen in Figure 61.

### **9.2 Schedule – BG, MK**

Throughout the design project, Aero 5 utilised a live Gantt Chart to represent the top level project schedule. An extract of the final schedule is shown in Figure 61, which focuses on the Aircraft Structures aspect of the design process. Aero 5 found that the use of a live document, allowed the team to constantly maintain focus on the most significant tasks at any given moment during the design process. The critical paths for the design project are represented on the schedule in dark blue, and were fundamental to the successful delivery of the Aero 5 CDR. The schedule also details the duration of each task, as well as the dependency of certain tasks on others, which enabled Aero 5 to understand the order of the project workload and the impact of successfully completing a task on time. To ensure that each individual task was managed appropriately, the schedule was divided into ‘half-week’ increments, to align with the bi-weekly team meetings held by Aero 5. This allowed tasks to be completed in advance of each meeting, which maintained a constant and effective work pace throughout the design process. Aero 5 aimed to include in the schedule all tasks that are relevant to the requirements outlined in the Customer Design Brief (CDB) and appropriate airworthiness regulations, as well as the activities that support the successful completion of these tasks.

Figure 60 - Aero 5 Work Breakdown Structure

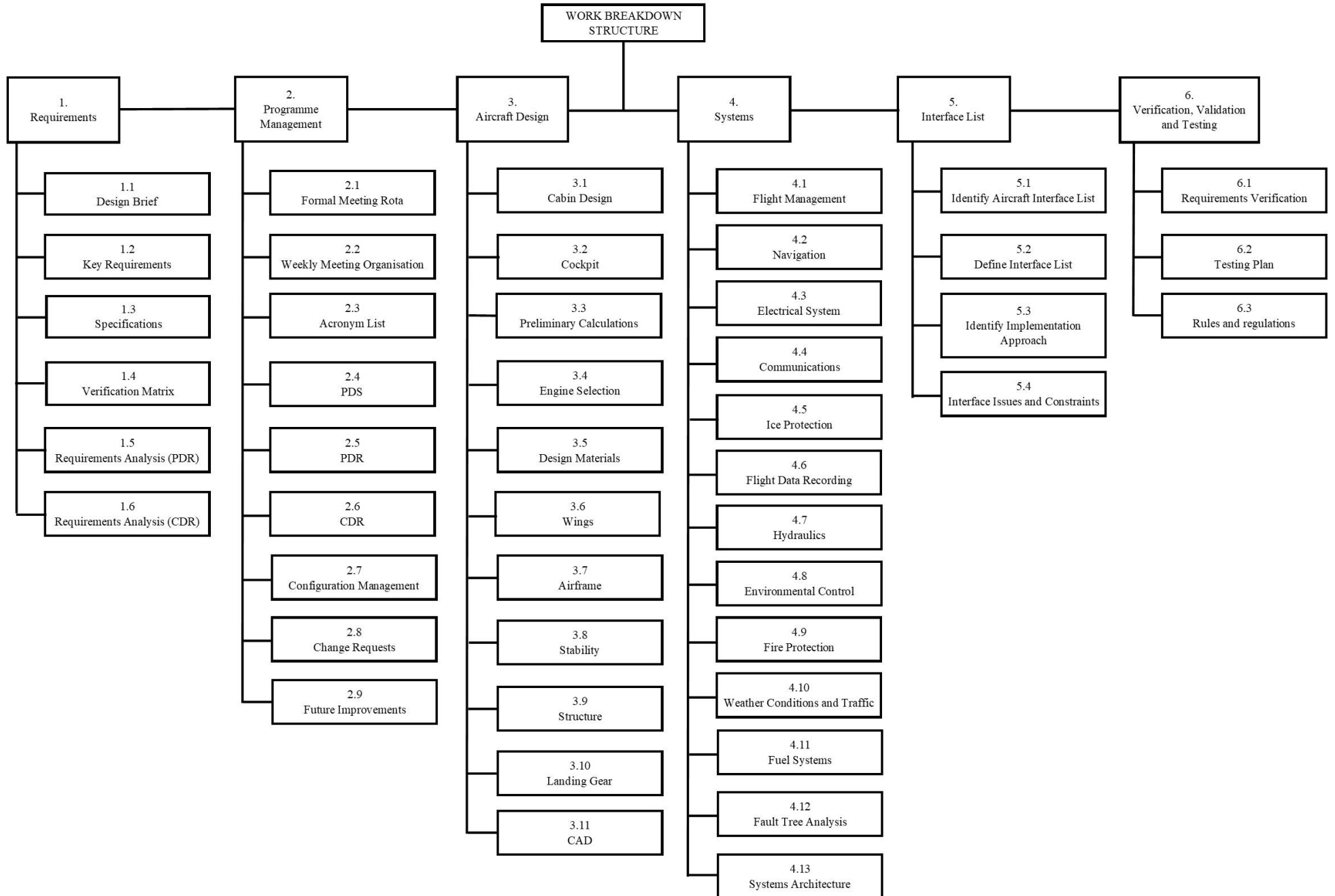


Figure 61 - Top Level Schedule Extract

| WBS I.D. | WBS Activity                         | Owner(s)                   | Duration | Week 1 |   | Week 2 |   | Week 3 |   | Week 4 |   | Week 5 |   | Week 6 |   | CDR | Week 7 |   | Presentation |
|----------|--------------------------------------|----------------------------|----------|--------|---|--------|---|--------|---|--------|---|--------|---|--------|---|-----|--------|---|--------------|
|          |                                      |                            |          | T      | F | T      | F | T      | F | T      | F | T      | F | T      | F |     | T      | F |              |
| 3.9      | Aircraft Structure                   | LM, KO, SH, AS, PS, BG, TL | 5.5      |        |   |        |   |        |   |        |   |        |   |        |   |     |        |   |              |
| 3.9.1    | Fuselage Design                      | LM, KO                     | 4.0      |        |   |        |   |        |   |        |   |        |   |        |   |     |        |   |              |
| 3.9.1.1  | Bending and Shear Analysis           | LM                         | 1.5      |        |   |        |   |        |   |        |   |        |   |        |   |     |        |   |              |
| 3.9.1.2  | Structural Design and Optimisation   | LM                         | 2.5      |        |   |        |   |        |   |        |   |        |   |        |   |     |        |   |              |
| 3.9.1.3  | CAD                                  | KO                         | 2.0      |        |   |        |   |        |   |        |   |        |   |        |   |     |        |   |              |
| 3.9.2    | Wing Design                          | SH, AS, PS, BG, TL         | 5.5      |        |   |        |   |        |   |        |   |        |   |        |   |     |        |   |              |
| 3.9.2.1  | Bending and Shear Analysis           | SH, AS                     | 2.0      |        |   |        |   |        |   |        |   |        |   |        |   |     |        |   |              |
| 3.9.2.2  | Structural Design and Optimisation   | SH, AS                     | 2.0      |        |   |        |   |        |   |        |   |        |   |        |   |     |        |   |              |
| 3.9.2.3  | Control Surface Placement and Sizing | PS                         | 2.0      |        |   |        |   |        |   |        |   |        |   |        |   |     |        |   |              |
| 3.9.2.4  | Hinge Moment Calculations            | BG                         | 2.0      |        |   |        |   |        |   |        |   |        |   |        |   |     |        |   |              |
| 3.9.2.5  | CAD                                  | TL                         | 4.0      |        |   |        |   |        |   |        |   |        |   |        |   |     |        |   |              |
| 3.9.3    | Empennage Design                     | PS, BG, KO                 | 4.0      |        |   |        |   |        |   |        |   |        |   |        |   |     |        |   |              |
| 3.9.3.1  | Control Surface Placement and Sizing | PS                         | 2.5      |        |   |        |   |        |   |        |   |        |   |        |   |     |        |   |              |
| 3.9.3.2  | Hinge Moment Calculations            | BG                         | 3.0      |        |   |        |   |        |   |        |   |        |   |        |   |     |        |   |              |

## **10. Configuration Management – BG**

During the conceptual design phase there were many aspects of the Aero 5 design that were subject to change, in order to optimise the design and deliver an appropriate aircraft design. As such, there were often small design changes that affected other design components, and consequently required continuous updates to keep the Aero 5 team at the same design baseline. Through effective and constant communication, this agile design process was adequately managed through to the successful delivery of the Aero 5 PDR.

The delivery of the PDR signified the point at which the Aero 5 design was ‘frozen’. This implied that the conceptual design submitted and described in the PDR was to be the design baseline moving forward for the project. Ideally, the design submitted for PDR would remain unchanged, but become more detailed and refined for the CDR delivery. As with many engineering projects there were unavoidable changes, indicating that a reliable configuration control process was required.

Aero 5 employed a Change Request (CR) system, to account for all design changes that were made after the PDR delivery and prior to the CDR delivery. If a change was required, the engineer responsible for the change first discussed the change with the Aero 5 team and described the reasons as to why it was required. At this stage, the responsible engineer filled out a CR form, to provide more detail about the design modification. The CR form included a description of the components affected by the proposed change, the justification for making the change, the actions that would result from making the change, the impact to other systems and the project schedule if the change was made and the impact to the design and to the schedule if the change was not made. Appendix 13.1 contains the major change requests that were raised by Aero 5. In addition to this, a CR tracker was created and treated as a live document to ensure that all potential changes were being managed appropriately throughout the design process.

As well as design changes, there were other aspects of the design process that required configuration control. One of these key aspects was the CAD modelling that was carried out to provide a visual representation of the Aero 5 aircraft. Firstly, as there was a minimum of three engineers developing CAD models at any one time, it was crucial that the same software and the same version of that software was being used. This would allow a successful assembly and integration of the constituent parts of the CAD model for the Aero 5 design. The version of CAD used for the duration of the Aero 5 project was Solid Edge ST10. Furthermore, a technique was employed wherein a new version file was saved each time a CAD model was updated. This created a map of the progress that had been made with regard to the Aero 5 CAD model, as well as providing design security in case an issue arose with the CAD files. If a file became corrupt, the previous iteration of the design would have been saved as a separate file, allowing the progress to be recovered in a short amount of time.

Another aspect of the configuration control process for the Aero 5 design was the risk register. This was also treated as a live document and was updated at any point where a design change, schedule update or newly discovered risk was raised. By treating the risk register as a live document Aero 5 were able to fully understand the most pertinent risks to the project at a given point of the schedule. The configuration control of the risk register mitigated the duplication of risks, as they were all logged and managed in one location, as well as keeping track of the most severe risks for the duration of the project. The most severe risks to the project, at the point of delivery of the CDR, are discussed in detail in Section 8 of this report.

The final aspect of configuration control that was considered for the Aero 5 project was another live document, the action list. By maintaining an up to date document that tracked all actions raised throughout the project, Aero 5 were able to progress according to the schedule. In addition, the action tracker was a useful tool that enabled Aero 5 to understand areas of the project that required further attention. The action tracker detailed all actions that had been raised, the date the action was raised, the engineer responsible for the closure of the action, the date the action was due to be closed and the actual date the action was closed. An extract of the Aero 5 action tracker is shown in Appendix 13.2.

## **11. Conclusions and Further Improvements – BG**

### **11.1 Design Conclusions – BG**

Since the delivery of the Aero 5 PDR, the design has been refined and more detail has been added, with a particular focus on the airframe structure. Throughout the design focus, the Aero 5 design has focused on satisfying the requirements specified in the CDB, whilst striving to produce an innovative and creative design solution. The key design drivers were a 15% reduction in DOC when compared to the 2015 state of the art, high operational reliability and aircraft commonality. Aero 5 have satisfied these requirements, whilst remaining compliant to the appropriate airworthiness specifications.

The common fuselage design proposed in the Aero 5 PDR for both the 190 passenger, 2-Class layout and the 240 passenger, 1-Class high density layout has been developed, in detail, in this critical design review, to provide a lightweight composite structure that satisfies the appropriate requirements whilst providing a suitable factor of safety. Structural analysis has also been completed for the aircraft wings, again to ensure a lightweight structure that provides optimal performance. The design of the aircraft control surfaces has been progressed and analysis has proved that the sizing of the control surfaces proposed by Aero 5 satisfies the appropriate airworthiness requirements and enables full control of the aircraft within the flight envelope. All of these design decisions were made with the project driving requirements in mind and hence the design has been optimised for performance and to satisfy the customer requirements.

The project cost analysis has shown that, compared to the 2015 state of the art, the Aero 5 project will achieve an 18.8% reduction in DOC. Since the delivery of the PDR, the project cost has been updated and Aero 5 expect to breakeven after the sale of the 13<sup>th</sup> aircraft. As stated in the PDR, by the 2027 entry into service date, Aero 5 expect to own 1/6<sup>th</sup> of the short range civil aviation market, with a predicted 2,443 aircraft orders and 1,529 successful aircraft deliveries.

### **11.2 Project Conclusions – BG**

Throughout the group design project Aero 5 faced several challenges, that resulted in some key learning experiences. Firstly, and perhaps most importantly, Aero 5 learned the importance of teamwork and effective communication when working collaboratively. From an early stage in the project design process, Aero 5 identified the need for constant and concise communication between all team members, which ensured that the project was progressing appropriately, whilst remaining on schedule. Aero 5 ensured that there were multiple ways of contacting each team member (through email or instant messaging groups), as well as holding bi-weekly meetings to keep the Aero 5 team up to date with each team members work. Additionally, Aero 5 learnt the importance and effectiveness of working in sub-teams (for example, the Empennage sub-team) whilst maintaining communication between sub-teams, as without effective communication interface issues could arise.

Another key learning point from the group design project was the importance of a project schedule and workload prioritisation. By planning when certain design activities should be completed, Aero 5 were able to complete each work stream within a suitable time frame, so as to not affect the overall project duration. Furthermore, Aero 5 learnt that schedules are not fixed, and can be treated as live documents. For example, if Aero 5 underestimated the duration of a task, the responsible engineer would inform the team and an alternative deadline was discussed, ensuring that all affected team members understood why the schedule was being modified and that the impact on succeeding tasks was minimised. For Aero 5, a critical way of keeping the project on track was ensuring that for each meeting, a concise but informative set of minutes were distributed within the team and that any actions raised were being worked by the responsible engineer. An action tracker was set up to record any actions raised, and to confirm that all actions were completed within the required time frame. Aero 5 found that the action tracker was a key part of ensuring that tasks were completed within suitable timeframes and that no individual part of the project was behind schedule.

Arguably the most significant thing that Aero 5 learnt from the design project was the importance of requirements, and using project requirements to inform certain areas of work within the project. Aero 5 learnt that well-defined top level requirements are fundamental in a successful project, as well as ensuring that the project was not over constrained. Further to this, Aero 5 learnt the importance of requirement traceability – being able to relate system and subsystem level requirements to the requirements defined by the customer. Aero 5 also learnt that the ability to trace requirements from a subsystem level to a customer level enabled more effective design decisions, as each design choice was in response to a system, and consequently a customer requirement. This process also provided Aero 5 with an appreciation of the systems engineering process used in industry, which was considered by all team members an invaluable learning experience.

Aero 5 also learnt that as with many projects, there were conflicting requirements that need to be managed and aggregated appropriately. An example of this from the Aero 5 design project was the requirement to achieve a 15% reduction in DOC compared to the 2015 state of the art and to produce an innovative, low risk design. These requirements conflicted as new and innovative designs heavily reduced DOC. However, the uncertainty in design fidelity and lack of experimental or test data meant that innovative design choices often became too high risk to include in the Aero 5 design for the given entry into service target date.

If Aero 5 were to undertake the project again, there are certain areas of the project that would be completed differently, either as a result of the key learning points outlined previously, or as a way to improve the final design. Firstly, Aero 5 would have a different approach to the powerplant selection. Instead of selecting a placeholder engine to inform the aircraft sizing, and allowing for possible future derivatives of that engine, Aero 5 would determine the optimal fan size and bypass ratio for the given specification, and if necessary elect to use a bespoke engine that was designed to optimise the performance of the Aero 5 aircraft. The process Aero 5 used to select the aircraft powerplant over constrained the design at an early stage of the project and limited some of the design choices that were required at later stages in the project.

There were some other design areas which, given more time, Aero 5 would have improved in the following ways. Firstly, Aero 5 could have considered more extensive and innovative design alternatives during the preliminary design phase. This would have allowed Aero 5 to compare the suitability of each configuration to the design brief, which would have provided the optimal design solution.

Secondly, a greater number of factors would have been considered for the placement of the landing gear to improve the fidelity and accuracy of the design. Aero 5 considered the aircraft systems as another area of potential improvement, as with more time, a greater analysis of the technical systems could have been completed, which would provide more accurate mass, placement and power requirement estimates in addition to providing an emphasis on passenger safety when designing aircraft systems.

Finally, if more time were available to Aero 5 during the design process, the team would aim to provide more detail with regard to the aircraft structure and aircraft performance estimates. This would be achieved by carrying out more iterations in calculations in order to provide higher fidelity data. An example of this could be dividing the aircraft into more sections to obtain a more accurate bending moment diagram to form the basis of the fuselage structural analysis. Additionally, instead of using arbitrary length ratios to produce stringer cross-sections, a more in depth analysis could be completed to optimise the second moment of area for a given cross-section, and then size the stringers accordingly. Another area where Aero 5 could improve the design would be to provide further performance estimates, for example, the minimum drag speed for the take-off configuration is known, however, the minimum drag speed for the cruise configuration could also be determined to improve the overall fidelity and accuracy of the design.

Overall, Aero 5 have learnt an incredible amount from this design project and regard the project as an invaluable learning experience. The importance of effective communication and teamwork was a fundamental learning point, as well as gaining an appreciation of the aircraft design process used in industry and the significance of the systems engineering process.

## 12. References

- Abbott, I. and von Doenhoff, A., 1959 – ‘Theory of Wing Sections’, Appendix II, Published by Dover Publications Inc. Published in New York.
- Airbus, 2011. Airbus Newsroom. [Online]
- Airbus, 2018. Aircraft Characteristics: Airport and Maintenance planning A350, France: Airbus S. A.S.
- Airbus, 2019. Aircraft Characteristics Airport and Maintenance Planning, France: Airbus S.A.S.
- Airfoiltools.com. (2018). NASA SC(2)-0710 AIRFOIL (sc20710-il). [online] Available at: <http://airfoiltools.com/airfoil/details?airfoil=sc20710-il> [Accessed 27 Nov. 2018]
- Airfoiltools.com. (2019). NASA SC(2)-0714 AIRFOIL (sc20714-il). [online] Available at: <http://airfoiltools.com/airfoil/details?airfoil=sc20714-il> [Accessed 15 Mar. 2019].
- Allan, J. (1997). *ESDU 74011*. [ebook] IHS ESDU. Available at: [https://www.esdu.com/cgi-bin/ps.pl?sess=unisurrey\\_1190317115834bhz&t=pdf&p=esdu\\_74011a](https://www.esdu.com/cgi-bin/ps.pl?sess=unisurrey_1190317115834bhz&t=pdf&p=esdu_74011a) [Accessed 13 Mar. 2019].
- Anon, (1983). Cockpit Voice Recorder Systems. [online] Available at: <https://publicapps.caa.co.uk/docs/33/CASPEC11.PDF> [Accessed 2 Mar. 2019].
- Anon, (2019). [online] Available at: <http://www.acpsales.com/upload/Mechanical-Properties-of-Carbon-Fiber-Composite-Materials.pdf> [Accessed 10 Mar. 2019].
- ARFF website, <http://www.arff.info>, 2006.
- Available at: <https://www.airbus.com/newsroom/news/en/2011/03/the-largest-composite-fuselage-panel-for-airbus-a350-xwb-completes-its-curing-process.html> [Accessed 20 February 2019].
- Babcock, G. (1973). RF Cleaning ring-laser gyro. [online] Available at: <https://apps.dtic.mil/dtic/tr/fulltext/u2/911373.pdf> [Accessed 13 Feb. 2019].
- Brady, C. (2000). 737 Electrics. [online] Available at: <http://www.b737.org.uk/electrics.htm> [Accessed 11 Mar. 2019].
- CFM (2015). CIT Selects CFM56-5B for new A321 aircraft. [online] Available at: <https://www.cfmaeroengines.com/press-articles/cit-selects-cfm56-5b-for-new-a321-aircraft/791/> [Accessed 15 Mar. 2019].
- Civil Aviation Authority, 1976. Ground Proximity Warning Systems. Specification No. 14, Issue 2.
- Composite Material Handbook (2002). Depart of Defense Handbook, pp.29-30.
- Core.ac.uk. (2019). [online] Available at: <https://core.ac.uk/download/pdf/82723892.pdf> [Accessed 9 Mar. 2019].
- Cunbao, M., Zi, G. & Lin, Y., 2011. Safety analysis of airborne weather radar based on failure mode, effects and criticality Analysis. Procedia Engineering, Issue 17, pp. 407 - 414.
- DEPARTMENT OF DEFENSE (2019). COMPOSITE MATERIALS HANDBOOK VOLUME 2. POLYMER MATRIX COMPOSITES MATERIALS PROPERTIES. COMPOSITE MATERIALS HANDBOOK. [online] DEPARTMENT OF DEFENSE, p.388. Available at: <https://snebulos.mit.edu/projects/reference/MIL-STD/MIL-HDBK-17-2F.pdf> [Accessed 7 Mar. 2019].
- Doornbos, P. (2018). Airbus A320 Specs - Modern Airliners. [online] Modern Airliners. Available at: <http://www.modernairliners.com/airbus-a320-introduction/airbus-a320-specs/> [Accessed 15 Mar. 2019].
- Dovey, J. (2003). *ESDU 96003*. [ebook] IHS ESDU. Available at: [https://www.esdu.com/cgi-bin/ps.pl?sess=unisurrey\\_1190317115834bhz&t=pdf&p=esdu\\_96003e](https://www.esdu.com/cgi-bin/ps.pl?sess=unisurrey_1190317115834bhz&t=pdf&p=esdu_96003e) [Accessed 13 Mar. 2019].
- Dubois, T. (2018). APUs Getting More Attention From MRO Providers. [online] Available at: <https://www.mro-network.com/engineering-design/apus-getting-more-attention-mro-providers> [Accessed 11 Mar. 2019].
- EASA (2012). CODAMEIN Composite Damage Metrics and Inspection. EASA.2010.C13. [online] Hamburg: Bishop GmbH - Aeronautical Engineers, pp.23-38. Available at: [https://www.easa.europa.eu/sites/default/files/dfu/CODAMEIN\\_Report\\_20120312\\_highres.pdf](https://www.easa.europa.eu/sites/default/files/dfu/CODAMEIN_Report_20120312_highres.pdf) [Accessed 20 Feb. 2019].
- EASA, 2011. CS-25 Large Aeroplanes Amendment 11, s.l.: EASA.
- EASA.EUROPA.EU, 2019. Flight Envelope - EASA, s.l.: EASA.
- Engineering ToolBox, 2012. Euler's Column Formula, s.l.: s.n.

EUROPEAN ORGANISATION FOR THE SAFETY OF AIR NAVIGATION, 2010. Collision risk due to TCAS safety issues, Brussels: EUROCONTROL.

Experimental Aircraft Info, n.d. Hydraulic Principles. [Online] Available at: <https://www.experimentalaircraft.info/articles/hydraulic-principles.php> [Accessed 27 February 2019].

FAA, (2010) *Airport Foreign Object Debris (FOD) Management* (U.S Department of Transport)

Federal Aviation Administration. (2014). [online] Available at: [https://www.faa.gov/pilots/safety/pilotsafetybrochures/media/Oxygen\\_Equipment.pdf](https://www.faa.gov/pilots/safety/pilotsafetybrochures/media/Oxygen_Equipment.pdf) [Accessed 6 Mar. 2019].

Flower, J. and Batt, C. (2014). *ESDU 14004*. [ebook] IHS ESDU. Available at: [https://www.esdu.com/cgi-bin/ps.pl?sess=unisurrey\\_1190317115834bhz&t=pdf&p=esdu\\_14004](https://www.esdu.com/cgi-bin/ps.pl?sess=unisurrey_1190317115834bhz&t=pdf&p=esdu_14004) [Accessed 13 Mar. 2019].

Foreman, C. (2016). Aircraft Structures ENG2096: Aircraft Structure & Materials. Guildford: University of Surrey, pp.20-30.

Foreman, C., 2016. Aircraft Structures & Materials, Guildford: University Of Surrey.

Gann, R. G., 2007. Advanced Technology for Fire Suppression in Aircraft, Washington DC: Special Publication (NIST SP) - 1069.

Gilbey, R. (1978). *ESDU Controls 01.01.03*. [ebook] IHS ESDU. Available at: [https://www.esdu.com/cgi-bin/ps.pl?sess=unisurrey\\_1190317115834bhz&t=pdf&p=esdu\\_aeroc010103b](https://www.esdu.com/cgi-bin/ps.pl?sess=unisurrey_1190317115834bhz&t=pdf&p=esdu_aeroc010103b) [Accessed 13 Mar. 2019].

Gilbey, R. (1992). *ESDU 88013*. [ebook] IHS ESDU. Available at: [https://www.esdu.com/cgi-bin/ps.pl?sess=unisurrey\\_1190317115834bhz&t=pdf&p=esdu\\_88013b](https://www.esdu.com/cgi-bin/ps.pl?sess=unisurrey_1190317115834bhz&t=pdf&p=esdu_88013b) [Accessed 13 Mar. 2019].

Gilbey, R. (1992). *ESDU 88040*. [ebook] IHS ESDU. Available at: [https://www.esdu.com/cgi-bin/ps.pl?sess=unisurrey\\_1190317115834bhz&t=pdf&p=esdu\\_88040c](https://www.esdu.com/cgi-bin/ps.pl?sess=unisurrey_1190317115834bhz&t=pdf&p=esdu_88040c) [Accessed 13 Mar. 2019].

Gilbey, R. (2015). *ESDU Controls 08.01.01*. [ebook] IHS ESDU. Available at: [https://www.esdu.com/cgi-bin/ps.pl?sess=unisurrey\\_1190317115834bhz&t=pdf&p=esdu\\_aeroc080101b](https://www.esdu.com/cgi-bin/ps.pl?sess=unisurrey_1190317115834bhz&t=pdf&p=esdu_aeroc080101b) [Accessed 13 Mar. 2019].

Gilbey, R. and Wood, S. (2014). *ESDU 87008*. [ebook] IHS ESDU. Available at: [https://www.esdu.com/cgi-bin/ps.pl?sess=unisurrey\\_1190317115834bhz&t=pdf&p=esdu\\_87008i](https://www.esdu.com/cgi-bin/ps.pl?sess=unisurrey_1190317115834bhz&t=pdf&p=esdu_87008i) [Accessed 13 Mar. 2019].

Gilbey, R., 1978 – ‘IHS ESDU Aerodynamic Series, Section 20: Controls – Lift, Pitching Moment, Rolling Moment, Drag, ESDU AERO C01.01.03’. Available via HIS ESDU Aerodynamics Design Collection. (Accessed on 01/03/2019).

Gilbey, R., 1989 – ‘IHS ESDU Aerodynamic Series, Section 21: Controls – Hinge Moment, ESDU 89009’. Available via HIS ESDU Aerodynamics Design Collection. (Accessed on 03/03/2019).

Gilbey, R., 1989 – ‘IHS ESDU Aerodynamic Series, Section 21: Controls – Hinge Moment, ESDU AERO C04.01.01’. Available via HIS ESDU Aerodynamics Design Collection. (Accessed on 02/03/2019).

Gilbey, R., 1989 – ‘IHS ESDU Aerodynamic Series, Section 21: Controls – Hinge Moment, ESDU AERO C04.01.02’. Available via HIS ESDU Aerodynamics Design Collection. (Accessed on 02/03/2019).

Gilbey, R., 1989 – ‘IHS ESDU Aerodynamic Series, Section 21: Controls – Hinge Moment, ESDU AERO C04.01.03’. Available via HIS ESDU Aerodynamics Design Collection. (Accessed on 02/03/2019).

Gilbey, R., 2007 – ‘IHS ESDU Aerodynamic Series, Section 8: Aerofoils at Subcritical Speeds – Pressure Distribution, Lift, Pitching Moment, Aerodynamic Centre, AERO W01.01.05’. Available via HIS ESDU Aerodynamics Design Collection. Accessed on 01/03/2019.

Hale, J., 2006. Boeing 787 from the ground up. Aeromagazine, pp. 17-23.

Hancock, P., 2016 – ‘Aircraft Performance’, ENG2091: Aerodynamics and Flight Mechanics. Available via SurreyLearn. (Accessed on 06/03/2019).

Hancock, P., 2016 – ‘Climbing Flight’, ENG2091: Aerodynamics and Flight Mechanics. Available via SurreyLearn. (Accessed on 07/03/2019).

Hancock, P., 2016 – ‘Induced Drag’, ENG2091: Aerodynamics and Flight Mechanics. Available via SurreyLearn. (Accessed on 06/03/2019).

Hancock, P., 2016 – ‘Landing’, ENG2091: Aerodynamics and Flight Mechanics. Available via SurreyLearn. (Accessed on 07/03/2019).

Hariram, S., Philipp, P. & Dummeyer, D., QTR\_04 2010. Fire Protection: Engines and Auxiliary Power Units. AERO.

Holt, J. M. (.), 1996. Structural Alloys Handbook, West Lafayette: Purdue University.

Honeywell (2019). Spectra Fiber | Honeywell Spectra®. [online] Available at: <https://www.packagingcomposites-honeywell.com/spectra/product-info/spectra-fiber/> [Accessed 11 Mar. 2019].

Honeywell International Inc., 2009. Failure Modes, Effects, and Safety Analysis For Installations Of The MK XXII Enhanced Ground Proximity Warning System, Redmond, Washington: s.n.

Honeywell, 2008. 131-9[A] Auxiliary Power Unit, Phoenix: Honeywell Aerospace.

HOOU, 2019. Mass and Centre of Gravity, Hamburg: HOOU.

International, C., 2016. EASA TYPE-CERTIFICATE DATA SHEET, Paris: EASA.

Kaur, R. (2014). Spars and Stringers - Function and Designing. International Journal of Aerospace and Mechanical Engineering, [online] 1(1). Available at: <http://www.ijamejournals.com/pdf/Spars%20and%20Stringers-%20Function%20and%20Designing.pdf> [Accessed 28 Feb. 2019].

Kelly, E. & L.M., B., 2006. Aircraft Fuel System Diagnostics Using Digraphs. Loughborough, Proceedings of the 19th International COMADEM (Condition Monitoring and Diagnostic Engineering Management).

Khella, M., Martin, T., Pearson, J. & Dixon, R., 2010. Systems Approach for Health Management Design: A Simple Fuel System Case Study. Loughborough, 5th International Conference on System of Systems Engineering.

Kundu, A. K., 2010. Undercarriage. In: Aircraft Design. New York: Cambridge University Press, p. 194.

Leoviriyakit, K., 2019. Aircraft Operating Economics. Surrey: Airbus.

Lindeman, T., Basic airframe of a passenger jet, The Washington Post, April 17, 2006.

Ma, J., Lu, C. and Liu, H. (2015). Fault Diagnosis for the Heat Exchanger of the Aircraft Environmental Control System Based on the Strong Tracking Filter. [online] Available at: <https://journals.plos.org/plosone/article?id=10.1371/journal.pone.0122829> [Accessed 6 Mar. 2019].

Maragakis (2009) *Bird Population Trends and Their Impact on Aviation Safety 1999-2008* (European Aviation Safety Agency)

Martinez, I. (2019). Aircraft Environmental Control. [online] Available at: <http://webserver.dmt.upm.es/~isidoro/tc3/Aircraft%20ECS.pdf> [Accessed 6 Mar. 2019].

McKenzie, S. (2014). Common Failures of the Cockpit Voice Recorder (Black Box) | Duncan Aviation. [online] Available at: <https://www.duncanaviation.aero/intelligence/2014/April/common-failures-of-the-cockpit-voice-recorder-black-box> [Accessed 2 Mar. 2019].

Meier, N. (2005). Civil Turbojet/Turbofan Specifications. [online] Jet-engine.net. Available at: <http://www.jet-engine.net/civtfspc.html> [Accessed 15 Mar. 2019].

Mouritz, A. (2012). Introduction to aerospace materials. Oxford: Woodhead Publishing.

NASA (2010) *FOD Prevention Program* (National Aeronautics and Space Administration)

Nickles, G. et al., 2001. A Descriptive Model of Aircraft Inspection Activities, Clemson: Clemson University.

Niu, M. C.-Y., 1995. Airframe Structural Design. 8th ed. Hong Kong: Commilit Press Ltd..

NTSB. (2016). NTSB Finds Failure to Use De-Ice System Caused 2014 Crash of Embraer Jet. [online] Available at: <https://www.ntsb.gov/news/press-releases/Pages/PR20160607.aspx> [Accessed 13 Mar. 2019].

Office of Aviation Research Washington, D. 2., 2003. Metallic Materials Properties Development and Standardization (MMPDS), Washington: Federal Aviation Administration.

Ostrower, J., Breaking: Structural flaw halts production of Alenia 787 sections, [www.freerepublic.com](http://www.freerepublic.com), 2009

Oza, K., ‘Semester 2, Week 4 Minutes – 1st March 2019’, Aero 5 Group Project. Available via SurreyLearn.

Parks, E., 2002. Boeing 737-300/400 Notes, s.l.: s.n.

Patents.google.com. (2019). US20090212155A1 - Engine pylon made from composite material - Google Patents. [Online] Available at: <https://patents.google.com/patent/US20090212155> [Accessed 9 Mar. 2019].

Pathirana, Y. and profile, V. (2019). Integral Fuel Tanks. [online] Aviamech.blogspot.com. Available at: <https://aviamech.blogspot.com/2011/04/integral-fuel-tanks.html> [Accessed 11 Mar. 2019].

Pettit, D. & Turnbull, A., 2001. General Aviation Aircraft Reliability Study, Hampton, Virginia: NASA.

Raymer, D., 1992 – ‘Aircraft Design: A Conceptual Approach’, Chapter 16 ‘Stability, Control and Handling Qualities’, Published by American Institute of Aeronautics and Astronautics Inc. Published in Washington, DC.

- Robins, A., 2018 – ‘Isentropic Flow Tables’, ENG3167: Aerodynamics. Available via SurreyLearn. (Accessed on 08/03/2019).
- Robins, A., 2018 – ‘Trans-Hypersonics’, ENG3167: Aerodynamics. Available via SurreyLearn. (Accessed on 08/03/2019).
- Roskam, J., ‘Airplane Aerodynamics and Performance’, Chapter 3. Published by Design, Analysis and Research Corporation. Published in Kansas, USA.
- Safran Aircraft Engines, 2018. Commercial Engines, s.l.: Safran.
- SKYbrary, 2017. Air Ground Communication. [Online] Available at: [https://www.skybrary.aero/index.php/Category:Air\\_Ground\\_Communication](https://www.skybrary.aero/index.php/Category:Air_Ground_Communication) [Accessed 4 March 2019].
- SKYbrary, 2017. Engine Fire Protection. [Online] Available at: [https://www.skybrary.aero/index.php/Engine\\_Fire\\_Protection](https://www.skybrary.aero/index.php/Engine_Fire_Protection) [Accessed 25 February 2019].
- SKYbrary, 2018. Aircraft Fuel Systems. [Online] Available at: [https://www.skybrary.aero/index.php/Aircraft\\_Fuel\\_Systems](https://www.skybrary.aero/index.php/Aircraft_Fuel_Systems) [Accessed 27 February 2019].
- SKYbrary, 2018. Hydraulic Systems. [Online] Available at: [https://www.skybrary.aero/index.php/Hydraulic\\_Systems](https://www.skybrary.aero/index.php/Hydraulic_Systems) [Accessed 27 February 2019].
- SKYbrary, 2019. Airborne Collision Avoidance System (ACAS). [Online] Available at: [https://www.skybrary.aero/index.php/Airborne\\_Collision\\_Avoidance\\_System\\_\(ACAS\)](https://www.skybrary.aero/index.php/Airborne_Collision_Avoidance_System_(ACAS)) [Accessed 4 March 2019].
- Skybrary. (2016). Aircraft Electrical Systems. [online] Available at: [https://www.skybrary.aero/index.php/Aircraft\\_Electrical\\_Systems](https://www.skybrary.aero/index.php/Aircraft_Electrical_Systems) [Accessed 11 Mar. 2019].
- Skybrary. (2017). Communication Equipment Technical Problems. [online] Available at: [https://www.skybrary.aero/index.php/Communication\\_Equipment\\_Technical\\_Problems](https://www.skybrary.aero/index.php/Communication_Equipment_Technical_Problems) [Accessed 13 Feb. 2019].
- Skybrary. (2017). Flight Data Recorder (FDR) - SKYbrary Aviation Safety. [online] Available at: [https://www.skybrary.aero/index.php/Flight\\_Data\\_Recorder\\_\(FDR\)](https://www.skybrary.aero/index.php/Flight_Data_Recorder_(FDR)) [Accessed 2 Mar. 2019].
- Skybrary. (2018). Loss of Cabin Pressurisation - SKYbrary Aviation Safety. [online] Available at: [https://www.skybrary.aero/index.php/Loss\\_of\\_Cabin\\_Pressurisation](https://www.skybrary.aero/index.php/Loss_of_Cabin_Pressurisation) [Accessed 6 Mar. 2019].
- Skybrary. (2019). Aircraft Ice Protection Systems - SKYbrary Aviation Safety. [online] Available at: [https://www.skybrary.aero/index.php/Aircraft\\_Ice\\_Protection\\_Systems](https://www.skybrary.aero/index.php/Aircraft_Ice_Protection_Systems) [Accessed 4 Mar. 2019].
- Stanford, B. K., 2014. Optimal Topology of Aircraft Rib and Spar Structures under, Stanford: NASA.
- Stecki, J. S., Conrad, F. & Oh, B., 2002. Software Tool for Automated Failure Modes and Effects Analysis (FMEA) of Hydraulic Systems. s.l., Fifth JFPS International Symposium.
- Stonestreet, A., Genereux, D. and Kraus, H. (2012). Electrothermal wing ice protection system. [online] Available at: <https://patents.google.com/patent/US8820683> [Accessed 4 Mar. 2019].
- Tiwary, T. (2018). What is the advantage of I section beams than any other beams? [online] Available at: <https://www.quora.com/What-is-the-advantage-of-I-section-beams-than-any-other-beams> [Accessed 11 Mar. 2019].
- Viquerat, A., 2019 – ‘Shear Flow’, ‘Advanced Stress Analysis ENG3172’. Available via SurreyLearn. Accessed on 06/03/2019.
- Wencheng, L. (2011). Principles for determining material allowable and design allowable values of composite aircraft structures. Procedia Engineering, 17, pp.279-285.
- Wencheng, L. (2011). The 2nd International Symposium on Aircraft Airworthiness (ISAA 2011) Principles for determining material allowable and design allowable values of composite aircraft structures. [online] Core.ac.uk. Available at: <https://core.ac.uk/download/pdf/82723892.pdf> [Accessed 11 Mar. 2019].
- White, P. (2006). Review of Methods and Approaches for the Structural Risk Assessment of Aircraft. [ebook] Victoria: Defence Science and Technology Organisation, pp.2-4. Available at: <https://apps.dtic.mil/dtic/tr/fulltext/u2/a462955.pdf> [Accessed 14 Mar. 2019].
- Wide-body aircraft, [http://en.wikipedia.org/wiki/Wide-body\\_aircraft](http://en.wikipedia.org/wiki/Wide-body_aircraft), 2011

## 13. Appendices

### 13.1 Change Requests

#### 13.1.1 Change to Horizontal and Vertical Tail Plane Areas – PS

| Change Request - 1   |   |
|--|---|
| Change Request Title   | Change in Vertical and Horizontal Surface Areas |
| Date Raised  | 05/02/2019                                      |
| Owner  | Preeti Singh                                    |
| Change Request Details   |   |
| Components Affected  | Aircraft Empennage                              |
| Expected Cost Impact   | Change not expected to impact cost.             |
| Expected Schedule Impact   | Change not expected to impact schedule.         |
| Reason for Change  |   |
| <i>Why do the items listed above require changing?</i>   |   |
| <p>To start control surface sizing, it was required to recalculate the surface areas of the tail plane, from using the moment arm calculated from the wing AC. This was due to the variable nature of the CG location, which was used to calculate the initial tail surface areas. Using this moment arm provided Aero 5 with a more accurate surface area to then move on to sizing control surfaces.</p> |   |
| Recommended Action   |   |
| <i>How will the issue(s) identified be resolved?</i>   |   |
| <p>The sizing iterations mentioned by Aero 5 in the PDR will be iterated again but utilising the moment arm from the wing AC location.</p>   |   |
| Impact to Other Systems  |   |
| <i>How will the change affect other aspects of the design?</i>   |   |
| <p>This change would affect the CG, drag and the sizing iteration.</p>   |   |
| Impact if Change not Approved  |   |
| <i>What are the consequences of not approving this change?</i>   |   |
| <p>If the change is not incorporated into the design, it may affect aspects of stability due to the varying nature of the CG location and sizing the empennage based on one CG location.</p>   |   |

### 13.1.2 Moveable Tail Plane – BG

| <b>Change Request - 2</b>  |   |
|--|---|
| Change Request Title   | Incorporation of Moveable Tail Plane    |
| Date Raised  | 28/02/2019                              |
| Owner  | Barney Green/Preeti Singh               |
| <b>Change Request Details</b>  |   |
| Components Affected  | Aircraft Empennage                      |
| Expected Cost Impact   | Change not expected to impact cost.     |
| Expected Schedule Impact   | Change not expected to impact schedule. |
| <b>Reason for Change</b>   |   |
| <p><i>Why do the items listed above require changing?</i></p> <p>Prandtl-Glauert analysis of the Aero 5 aircraft tail plane in the cruise condition has shown that during cruise, the flow over the horizontal tail plane will be in the transonic regime, and hence there will be areas of supersonic flow over the horizontal tail plane. This will cause a strong interaction between the flow and the boundary layer, which could cause flow separation. This would result in the elevator losing effectiveness during cruise.</p> <p>By including a moveable horizontal tail plane, the effective angle of incidence will be able to be adjusted during flight to maintain fully subsonic flow over the horizontal tail plane and hence retain elevator effectiveness throughout the flight path.</p> |   |
| <b>Recommended Action</b>  |   |
| <p><i>How will the issue(s) identified be resolved?</i></p> <p>Aero 5 aim to resolve the above issue by modifying the design of the horizontal tail plane from a fixed tail plane to a moveable tail plane.</p>  |   |
| <b>Impact to Other Systems</b>   |   |
| <p><i>How will the change affect other aspects of the design?</i></p> <p>This change is not expected to affect any other aspects of the design. The dimensions of the horizontal tail plane will not change, neither will the dimensions of the aircraft empennage.</p>  |   |
| <b>Impact if Change not Approved</b>   |   |
| <p><i>What are the consequences of not approving this change?</i></p> <p>If the change is not incorporated into the design, it will not be possible to control the aircraft in pitch during cruise.</p>  |   |

### 13.1.3 Addition of Spoilers – PS

| <b>Change Request - 3</b>   |   |
|---|---|
| Change Request Title  | Incorporation of Spoilers on the Wing       |
| Date Raised   | 22/02/2019                                  |
| Owner   | Preeti Singh                                |
| <b>Change Request Details</b>   |   |
| Components Affected   | Aircraft Wings                              |
| Expected Cost Impact  | Additional Manufacturing Costs for the Wing |
| Expected Schedule Impact  | Change not expected to impact schedule.     |
| <b>Reason for Change</b>  |   |
| <i>Why do the items listed above require changing?</i>  |   |
| The configuration and the sizing of the control surfaces of the wing showed Aero 5 that additional roll control was required. This would satisfy the stability conditions required for manoeuvrability.   |   |
| It was found that spoilers would be a beneficial addition to the wing design, primarily to provide roll control.  |   |
| <b>Recommended Action</b>   |   |
| <i>How will the issue(s) identified be resolved?</i>  |   |
| Aero 5 aims to include spoilers as part of the wing control surfaces.   |   |
| <b>Impact to Other Systems</b>  |   |
| <i>How will the change affect other aspects of the design?</i>  |   |
| This change is expected to have minimal effect on other aspects of the design. It will contribute to the effectiveness of the wing control surfaces.  |   |
| <b>Impact if Change not Approved</b>  |   |
| <i>What are the consequences of not approving this change?</i>  |   |
| If this change is not approved, it would be required to incorporate a larger aileron surface or the aircraft would have ineffective roll control. Larger aileron surface would require further analysis and high-lift systems would also be affected due to the surface area available to incorporate them. |   |

### 13.1.4 Updated Engine Mounting Location – AM

| <b>Change Request - 4</b>   |  |
|---|--|
| Change Request Title  | Engine location in the spanwise direction from the wing root (from 6.47 to 4.19) |
| Date Raised   | 27/02/2019   |
| Owner   | Aanantha Murugavel   |
| <b>Change Request Details</b>   |  |
| Components Affected   | Wing Loading.  |
| Expected Cost Impact  | No expected impact to project cost.  |
| Expected Schedule Impact  | Time required to recalculation shear force and bending moment along the wing     |
| <b>Reason for Change</b>  |  |
| <i>Why do the items listed above require changing?</i>  |  |
| The previously calculated engine location based on approximated value for the rudder dimensions and the assumption that the length of the wing is 18m but in the actual distance between the wing root and the tip is 15.82m. |  |
| <b>Recommended Action</b>   |  |
| <i>How will the issue(s) identified be resolved?</i>  |  |
| The engine location will be recalculated using a value of 15.82m from the wing root to the wing tip.  |  |
| <b>Impact to Other Systems</b>  |  |
| <i>How will the change affect other aspects of the design?</i>  |  |
| The components on the wing need to be adjusted according to the engine location.  |  |
| The wing loading is affected since the shear force and bending moment calculations are based on the engine location.  |  |
| <b>Impact if Change not Approved</b>  |  |
| <i>What are the consequences of not approving this change?</i>  |  |
| Inaccurate values used in the generation of aircraft wing bending moment diagrams and shear force diagrams.   |  |

## 13.2 Aero 5 Action Tracker Extract – BG

*Table 62 - Aero 5 Action Tracker Extract*

| Aero 5 Action List |             |                      |   |            |              |
|--------------------|-------------|----------------------|---|------------|--------------|
| Action ID          | Date Raised | Action Owner         | Action  | Due Date   | Closure Date |
| 23                 | 16/11/2018  | KO, BG               | Calculate the drag profile for a swept wing configuration.                      | 23/11/2018 | 22/11/2018   |
| 24                 | 16/11/2018  | YA, LM               | Put the aircraft systems in a triage  | 23/11/2018 | 22/11/2018   |
| 25                 | 23/11/2018  | ALL                  | Look at PDR marking scheme  | 30/11/2018 | 30/11/2018   |
| 26                 | 23/11/2018  | AS                   | Look at more modern aerofoils   | 27/11/2018 | 26/11/2018   |
| 27                 | 23/11/2018  | BG                   | Resize wing (plan time for sizing sub-team to meet and do this)                 | 30/11/2018 | 30/11/2018   |
| 28                 | 23/11/2018  | TW                   | Check that DOC is being met   | 30/11/2018 | 30/11/2018   |
| 29                 | 23/11/2018  | MK                   | Find more accurate data for reduction in weight due to use of carbon composites | 27/11/2018 | 27/11/2018   |
| 30                 | 07/12/2018  | LM                   | Find out plural of aircraft   | 14/12/2018 | 12/12/2018   |
| 31                 | 07/12/2018  | SH                   | Put updated risk and assessment and verification in main text of PDR            | 08/12/2018 | 10/12/2018   |
| 32                 | 07/12/2018  | ALL                  | Rewording in PDR to expect a different outcome in CDR                           | 08/12/2018 | 08/12/2018   |
| 33                 | 07/12/2018  | SH                   | Scale C.G. diagram up   | 08/12/2018 | 08/12/2018   |
| 34                 | 07/12/2018  | KO                   | Plot $C_L$ vs $C_D$ , make sure not American plot                               | 08/12/2018 | 08/12/2018   |
| 35                 | 07/12/2018  | BG                   | Finish collation of PDR   | 08/12/2018 | 09/12/2018   |
| 36                 | 07/12/2018  | ALL                  | Proof read  | 09/12/2018 | 09/12/2018   |
| 37                 | 08/02/2019  | LM, KO, AS, TL       | Determine the interface between the wing and the fuselage.                      | 15/02/2019 | 15/02/2019   |
| 38                 | 15/02/2019  | SH, TL, AM, AS       | Wing spar depths and locations need to be determined                            | 22/02/2019 | 19/02/2019   |
| 39                 | 15/02/2019  | BG, PS               | Determine minimum control speed   | 22/02/2019 | 20/02/2019   |
| 40                 | 15/02/2019  | YA                   | Fault Tree Analysis for a safety critical system                                | 22/02/2019 | 21/02/2019   |
| 41                 | 22/02/2019  | Dr M Placidi, LM, MK | Find FAA materials document   | 01/03/2019 | 01/03/2019   |
| 42                 | 22/02/2019  | YA, MK               | Fault Tree Analysis for Electrical System                                       | 08/03/2019 | 11/03/2019   |

### 13.3 DOC – PS, KO

Table 63 - DOC Spreadsheet Sheet 1

| Financial Costs            | Inputs     |                       |  |  |
|----------------------------|------------|-----------------------|--|--|
| Gate to Gate time          | 2.13       |                       |  |  |
| Available time of aircraft | 4000       | hr/year               |  |  |
| Block Time                 | 2.13       |                       |  |  |
| Turnaround Time            | 0.42       | assumed due to engine |  |  |
| Utilisation                | 1568.62745 | # trips per year      |  |  |
| Engine SFC                 | 1972.8     |                       |  |  |
| Block Fuel                 | 926.197183 | kg                    |  |  |
|                            |            |                       |  |  |
| Total investment           | 124400000  | \$                    |  |  |
| MSP                        | 1.08E+08   | \$                    |  |  |
| Airframe Spares            | 8000000    | \$                    |  |  |
| Spare propulsion units     | 8400000    | \$                    |  |  |
| Engine price               | 14000000   | \$                    |  |  |
| Number of Engines          | 2          |                       |  |  |

Table 64 - DOC Spreadsheet Sheet 2

|                      |            |         |                      |
|----------------------|------------|---------|----------------------|
| Depreciation         | 3172.2     | \$/trip | for a 25-year period |
| Interest             | 3965.25    |         |                      |
| Insurance            | 4.1310E+02 |         |                      |
|                      |            |         |                      |
|                      |            |         |                      |
| Total financial cost | 7550.55    |         |                      |

Table 65 - DOC Spreadsheet Sheet 3

|                   |                            |                    |            |
|-------------------|----------------------------|--------------------|------------|
| Maintenance costs | Maintenance costs          | 667392944.7        |            |
|                   | Airframe Maintenance (AMC) | 667392508.4        |            |
|                   |                            | Airframe price     | 80000000   |
|                   |                            | airframe materials | 666880000  |
|                   |                            | airframe labour    | 512508.386 |
|                   |                            | Airframe weight    | 38300      |
|                   |                            | labour rate        | 66         |
|                   |                            |                    |            |
|                   | Engine Maintenance (EMC)   | 436.3511115        |            |
|                   |                            | labour             | 25.6836038 |
|                   |                            | material           | 42.9250616 |
|                   |                            | bypass ratio       | 11         |
|                   |                            | c1                 | 0.94692115 |
|                   |                            | c3                 | 0.666      |
|                   |                            | NC                 | 3          |
|                   |                            | static thrust      | 13.8       |
|                   |                            | c2                 | 1.38491553 |
| Flight Costs      |                            | OPR                | 40         |
|                   |                            |                    |            |

|  |                    |             |     |  |
|--|--------------------|-------------|-----|--|
|  | Flight costs       | 3470.324848 |     |  |
|  | Total crew costs   | 1704        |     |  |
|  | Cockpit Crew (CPC) | 809.4       |     |  |
|  | Cabin Crew (CAC)   | 894.6       |     |  |
|  | NCAB               | 7           |     |  |
|  | Navigation charges | 674.138176  |     |  |
|  | study length       | 926         | km  |  |
|  | MTOW               | 106         |     |  |
|  | landing fee        | 636         |     |  |
|  | fuel cost          | 456.186672  |     |  |
|  | block fuel         | 2037.6338   | lbs |  |
|  | fuel price         | 1.5         |     |  |
|  |                    |             |     |  |
|  |                    |             |     |  |

**Equations used:**

$$\text{Airframe Materials} = \text{AFP} \times (4.2 + 2.2 \times (t - 0.25))$$

$$\text{Airframe Labour} = \left( 0.09 \times \text{AFW} + 6.7 - \left( \frac{350}{\text{AFW}+75} \right) \right) \times (0.8 + 0.68 \times (t - 0.25)) \times R$$

Engine Maintenance Costs:

|                  | Turbojet or Turbopropfan                                    | Turboprop or Propfan   |
|------------------|---|--|
| <b>Labour:</b>   | $LT = 0.21 \times C1 \times C3 \times (1+T)^{0.4} \times R$ | $LT = 0.152 \times C3 \times (1+N)^{0.4} \times R$ [Core]<br>$LP = 0.072 \times B \times (1+N/2)^{0.4} \times R$ [Props] |
| <b>Material:</b> | $MT = 2.56 \times (1+T)^{0.8} \times C1$<br>$(C2+C3)$       | $MT = 1.65 \times (1+N)^{0.8} \times (C2+C3)$<br>[Core]<br>$MP = 0.56 \times (1+N/2)^{0.8} \times B$ [Props]             |
| <b>Total:</b>    | $EMC = NE \times (LT + MT) \times (tf+1.3)$                 | $EMC = NE \times (LT+MT) \times (tf+1.3)$<br>$+ NE \times (LP+MP) \times (tf+0.5)$                                       |

$$C1 = 1.27 - 0.2 \times BPR^{0.2}$$

$$A = 8.5 \times (N / 3 \times P + 28)^{0.5} + 0.9$$

$$C2 = 0.4 \times (OPR / 20)^{1.3} + 0.4$$

$$B = (0.05 \times P + 0.6) \times (0.4 \times (D / A) + 0.6)$$

$$C3 = 0.032 \times NC + 0.57$$

Crew Costs:

$$\text{Cockpit Crew Cost} = 380 \times \text{Block Time}$$

$$\text{Cabin Crew} = 60 \times \text{NCAB} \times \text{Block Time}$$

$$\text{Navigation Charges} = 0.5 \times \text{Study Length} \times (\text{MTOW} / 50)^{1/2}$$

$$\text{Landing Fees} = 6 \times \text{MTOW}$$

$$\text{Fuel Cost} = (\text{Block Fuel} / 6.7) \times \text{Fuel Price} \#$$

## 13.4 Project Cost – PS, KO

Table 66 - Project Cost Calculation

| <b>Financial Costs</b>      |  | <b>Inputs</b>            |                  |
|-----------------------------|--|--------------------------|------------------|
| Gate to Gate time           |  | 2.13                     |                  |
| Available time of aircraft  |  | 4000                     | hr/year          |
| Block Time                  |  | 2.13                     |                  |
| Turnaround Time             |  | 0.42                     |                  |
| Utilisation                 |  | 1568.62745               | # trips per year |
| Engine SFC                  |  | 4160                     |                  |
| Block Fuel                  |  | 1953.05164               | kg               |
|                             |  |                          |                  |
| Total investment            |  | 134130000                | \$               |
| MSP                         |  | 1.18E+08                 | \$               |
| Airframe Spares             |  | 9830000                  | \$               |
| Spare propulsion units      |  | 6000000                  | \$               |
| Engine price                |  | 10000000                 | \$               |
| Number of Engines           |  | 2                        |                  |
| Depreciation                |  | 5700.525                 | \$/trip          |
| Interest                    |  | 4275.39375               |                  |
| Insurance                   |  | 4.5250E+02               |                  |
| <b>Total financial cost</b> |  | 10428.41625              |                  |
| Maintenance costs           |  | 820684259                |                  |
|                             |  | 820683874.8              |                  |
|                             |  | Airframe price           | 98300000         |
|                             |  | airframe materials       | 819428800        |
|                             |  | airframe labour          | 1255074.76       |
|                             |  | Airframe weight          | 93900            |
|                             |  | labour rate              | 66               |
|                             |  |                          |                  |
|                             |  | Engine Maintenance (EMC) | 384.2084398      |
|                             |  | labour                   | 24.1099591       |
|                             |  | material                 | 36.3001729       |
|                             |  | bypass ratio             | 5.7              |
|                             |  | c1                       | 0.98672714       |
|                             |  | c3                       | 0.666            |
|                             |  | NC                       | 3                |
|                             |  | static thrust            | 10.4             |
|                             |  | c2                       | 1.38491553       |
| Flight Costs                |  | OPR                      | 40               |
|                             |  |                          |                  |
|                             |  | <b>Flight costs</b>      | 4301.087882      |
|                             |  | total crew costs         | 1448.4           |
|                             |  | Cockpit Crew (CPC)       | 809.4            |
|                             |  | Cabin Crew (CAC)         | 639              |
|                             |  | NCAB                     | 5                |
|                             |  | Navigation charges       | 858.737073       |

|  |  |              |            |        |
|--|--|--------------|------------|--------|
|  |  | study length | 926        | k<br>m |
|  |  | MTOW         | 172        |        |
|  |  | landing fee  | 1032       |        |
|  |  | fuel cost    | 961.950809 |        |
|  |  | block fuel   | 4296.71362 | lbs    |
|  |  | fuel price   | 1.5        |        |

## 13.5 Fuselage Structure – LM

### 13.5.1 Fuselage Weight Distribution – LM

*Table 67 - Fuselage Weight Distribution*

|    |   |   |       |
|----|---|---|-------|
|    | 4 x Attendant inc/baggage<br>4 x HD seats<br>2 x Type A Emergency exit<br>9 x Full trolley<br>Fixed equipment<br>Catering<br>*600 x stringers | 85/attendant<br>10/seat<br>12/m/door<br>35/trolley<br>1/pax<br>8/pax<br>*0.122kg/Stringer | *3626 |
| 11 | Empennage   | 16658   | 16658 |

\*Stringer amount and mass needed after first iteration.

### 13.5.2 Bending Moment Diagram (Iteration 1) – LM

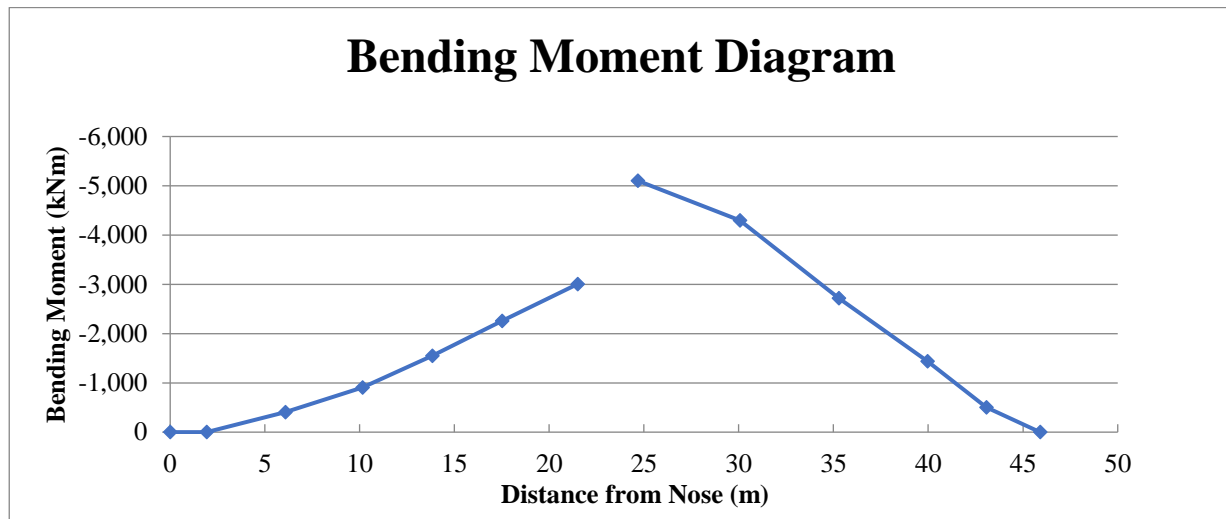


Figure 62 - Bending Moment Diagram after First Iteration

### 13.5.3 Shear Force Diagram (Iteration 1) – LM

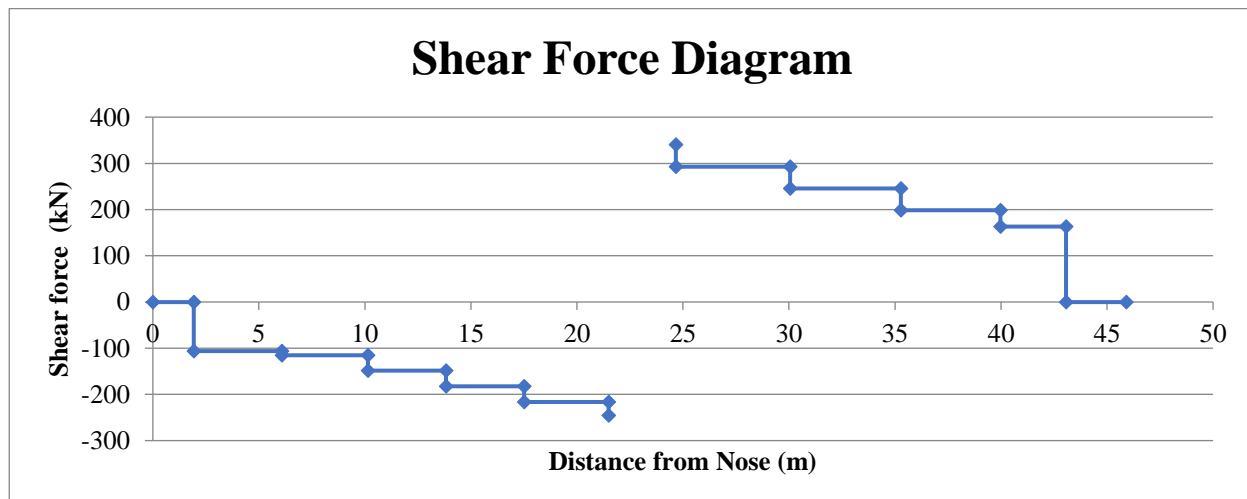


Figure 63 - Shear Force Diagram after First Iteration

### 13.5.4 Initial Boom Area Calculations – LM

Table 68 - Initial Boom Area Calculations

| Section | $\pm$ Max y (m) | Total I <sub>xx</sub> (m <sup>4</sup> ) | Max M(x) (kNm) | $\pm$ Max Stress divided by B (N/mm <sup>2</sup> ) | Allowable stress (MPa) | Boom Area (B) |
|---------|-----------------|---|----------------|--|------------------------|---------------|
| 1       | 2.19            | 173                                     | -205           | -2590  | 94.0                   | 27            |
| 2       | 2.19            | 173                                     | -633           | -7980  | 94.0                   | 85            |
| 3       | 2.19            | 173                                     | -1260          | -15900   | 94.0                   | 169           |

|    |      |     |       |        |      |     |
|----|------|-----|-------|--------|------|-----|
| 4  | 2.19 | 173 | -1900 | -24000 | 94.0 | 255 |
| 5  | 2.19 | 173 | -2670 | -33700 | 94.0 | 358 |
| 6  | 2.19 | 173 | -3380 | -42600 | 94.0 | 453 |
| 7  | 2.19 | 173 | -5100 | -64300 | 94.0 | 684 |
| 8  | 2.19 | 173 | -4300 | -54100 | 94.0 | 576 |
| 9  | 2.19 | 173 | -2720 | -34400 | 94.0 | 364 |
| 10 | 2.19 | 173 | -1440 | -18100 | 94.0 | 193 |
| 11 | 2.19 | 173 | -506  | -6380  | 94.0 | 68  |

### 13.5.5 Initial Buckling Length Data – LM

Table 69 - Initial Buckling Length Data

| Section | Buckling length (mm) |
|---------|----------------------|
| 1       | 17                   |
| 2       | 234                  |
| 3       | 317                  |
| 4       | 442                  |
| 5       | 588                  |
| 6       | 754                  |
| 7       | 726                  |
| 8       | 631                  |
| 9       | 510                  |
| 10      | 382                  |
| 11      | 55                   |

### 13.6 Wing Design Material Data – SH

Table 70 - Wing Design Material Data

| Physical Properties:<br>Aluminium 7075-T6 | Metric           |
|---|------------------|
| Density                                   | <u>2.81 g/cc</u> |
| Ultimate Tensile Strength                 | <u>572 MPa</u>   |
| Tensile Yield Strength                    | <u>503 MPa</u>   |
| Elongation at Break                       | <u>11 %</u>      |
| Elongation at Break                       | <u>11 %</u>      |
| Modulus of Elasticity                     | <u>71.7 GPa</u>  |

| Physical Properties:<br>Aluminium 2024-T4 | Metric           |
|---|------------------|
| Density                                   | <u>2.78 g/cc</u> |
| Ultimate Tensile Strength                 | <u>469 MPa</u>   |
| Tensile Yield Strength                    | <u>324 MPa</u>   |
| Elongation at Break                       | <u>19 %</u>      |
| Elongation at Break                       | <u>20 %</u>      |
| Modulus of Elasticity                     | <u>73.1 GPa</u>  |

| Physical Properties:<br>Titanium Ti-6Al-4V (Grade 5), Annealed | Metric           |
|--|------------------|
| Density  | <u>4.43 g/cc</u> |
| Ultimate Tensile Strength                                      | <u>950 MPa</u>   |
| Tensile Yield Strength   | <u>880 MPa</u>   |

|                       |                  |
|-----------------------|------------------|
| Elongation at Break   | <u>14 %</u>      |
| Elongation at Break   | <u>36 %</u>      |
| Modulus of Elasticity | <u>113.8 GPa</u> |

Referenced from Metallic Materials Properties Development and Standardisation (MMPDS) (Office of Aviation Research Washington, 2003) and Structural Alloys Handbook (Holt, 1996).

### 13.7 MATLAB Code for Fuel Tank Dimension Calculations – AM

```

clear;clc;
% the coordinates of the chosen airfoil:
%Chord (root)
x_top = [3829.74,3775.8,3721.86,3667.92,3613.98,3560.04,3506.1,3452.16,3398.22,3344.28,3290.34,3236.4,3182.46,3128.52,3074.58,3020.64,2
y_top = [283.185,289.6578,295.5912,301.5246,306.9186,312.3126,317.1672,322.0218,326.337,330.6522,334.9674,338.7432,342.519,345.7554,348
x_bottom = [10.768,26.97,53.94,107.88,161.82,215.76,269.7,323.64,377.58,431.52,485.46,539.4,593.34,647.28,701.22,755.16,809.1,863.04,91
y_bottom = [-58.09338,-89.43252,-120.8256,-159.6624,-186.093,-206.0508,-222.7722,-236.7966,-249.2028,-260.5302,-270.2394,-279.4092,-288
%{
%chord(tip)
x_top = [1553.76,1532.18,1510.6,1489.02,1467.44,1445.86,1424.28,1402.7,1381.12,1359.54,1337.96,1316.38,1294.8,1273.22,1251.64,1230.06,1
y_top = [110.7054,113.295,115.8846,118.2584,120.6322,122.7902,124.9482,126.8904,128.8326,130.559,132.2854,134.0118,135.5224,137.033,138
x_bottom = [258.96,280.54,302.12,323.7,345.28,366.86,388.44,410.02,431.6,453.18,474.76,496.34,517.92,539.5,561.08,582.66,604.24,625.82,
y_bottom = [-118.4742,-121.2796,-123.8692,-126.4588,-128.8326,-130.9906,-132.9328,-134.875,-136.6014,-138.3278,-139.8384,-141.349,-142.
%}
n_xtop = numel(x_top);
n_xbottom = numel(x_bottom);
n_ytop = numel(y_top);
n_ybottom = numel(y_bottom);

% the area enclosed by the aerofoil(considering trapezoidal rule):
darea_top = [];
area_top = 0;
for i = 1:(n_xtop-1)
    area_1 = 0.5*abs(y_top(i)+y_top(i+1))*abs(x_top(i+1)-x_top(i));
    darea_top(end+1) = area_1;
    area_top = area_top + area_1;
end

darea_bottom = [];
area_bottom = 0;
for j = 1:(n_xbottom-1)
    area_2 = 0.5*abs(y_bottom(j)+y_bottom(j+1))*abs(x_bottom(j+1)-x_bottom(j));
    darea_bottom(end+1) = area_2;
    area_bottom = area_bottom + area_2;
end

% Chord-wise centre of area from the leading edge:
% considering negligible difference in the neighbouring y-coordinates:
dtx_bar = [];
dbx_bar = [];
for k = 1:(n_xtop-1)
    dtx_bar1 = 0.5*(x_top(k+1) - x_top(k));
    dtx_bar(end+1) = dtx_bar1 + x_top(k);
end
for l = 1:(n_xbottom-1)
    dbx_bar1 = 0.5*(x_bottom(l+1) - x_bottom(l));
    dbx_bar(end+1) = dbx_bar1 + x_bottom(l);
end

ax = 0;
ax_2 = 0;
for m = 1:numel(darea_top)
    ax = ax + (darea_top(m)*dtx_bar(m));
end
for n = 1:numel(darea_bottom)
    ax_2 = ax_2 + (darea_bottom(n)*dbx_bar(n));
end
x_bar_top = ax/area_top;
x_bar_bottom = ax_2/area_bottom;

% overall centre of area:
x_bar = ((area_top*x_bar_top)+(area_bottom*x_bar_bottom))/(area_top + area_bottom);
total_area = area_top + area_bottom;
disp(['centre of area from the leading edge: ', num2str(x_bar), 'mm']);
disp(['Total area: ', num2str(total_area), 'mm^2']);

```

## 13.8 CDR Mass Fraction Iterations – SH

Table 71 - Mass Fraction Iterations

| Iteration Counter (CDR) | MTOW Kg    | MZMF (Max zero fuel weight) Kg | ETOW (Structural Weight) Kg | Fuel Weight Kg | Payload Weight Kg | Engine Weight Total Kg | Wing Weight (Total) Torenbee k method Kg | Horizontal Tail Kg | Vertical Tail Kg | Aircraft Systems & Equipment Kg | Landing Gear Kg | Nose Gear Kg | Fuselage Cabin Mass Kg | Engine Install Weight |
|-------------------------|------------|--------------------------------|-----------------------------|----------------|-------------------|------------------------|--|--------------------|------------------|---------------------------------|-----------------|--------------|------------------------|-----------------------|
| 17                      | 106383.630 | 90872.119                      | 30339.515                   | 15511.511      | 26331.300         | 7870.000               | 10299.739                                | 970.941            | 788.674          | 16221.414                       | 4787.263        | 1595.754     | 28685.991              | 10679.590             |
| 18                      | 106490.014 | 90978.503                      | 30339.515                   | 15511.511      | 26331.300         | 7870.000               | 10419.690                                | 970.941            | 788.674          | 16237.193                       | 4792.051        | 1597.350     | 28685.991              | 10679.590             |
| 19                      | 106437.886 | 90926.375                      | 30339.515                   | 15511.511      | 26331.300         | 7870.000               | 10522.519                                | 970.941            | 788.674          | 16229.461                       | 4789.705        | 1596.568     | 28685.991              | 10679.590             |
| 20                      | 106443.205 | 90931.694                      | 30339.515                   | 15511.511      | 26331.300         | 7870.000               | 10631.587                                | 970.941            | 788.674          | 16230.250                       | 4789.944        | 1596.648     | 28685.991              | 10679.590             |
| 21                      | 106447.460 | 90935.949                      | 30339.515                   | 15511.511      | 26331.300         | 7870.000               | 10740.548                                | 970.941            | 788.674          | 16230.881                       | 4790.136        | 1596.712     | 28685.991              | 10679.590             |
| 22                      | 106438.949 | 90927.439                      | 30339.515                   | 15511.511      | 26331.300         | 7870.000               | 10848.077                                | 970.941            | 788.674          | 16229.619                       | 4789.753        | 1596.584     | 28685.991              | 10679.590             |
| 23                      | 106436.822 | 90925.311                      | 30339.515                   | 15511.511      | 26331.300         | 7870.000               | 10956.316                                | 970.941            | 788.674          | 16229.303                       | 4789.657        | 1596.552     | 28685.991              | 10679.590             |
| 24                      | 106382.566 | 90871.055                      | 30339.515                   | 15511.511      | 26331.300         | 7870.000               | 11058.545                                | 970.941            | 788.674          | 16221.256                       | 4787.215        | 1595.738     | 28685.991              | 10679.590             |

### 13.9 Pitching Moment Coefficient Calculation – PS

From Raymer (2012), the following Equation (78) was adapted to determine the pitching moment coefficient.

$$C_{m_{cg}} = C_L(\overline{X_{cg}} - \overline{X_{acw}}) + C_{m_w} + C_{m_{w\delta f}}\delta_f + C_{m_{fus}} - \eta_h \frac{S_h}{S_w} C_{L_h}(\overline{X_{ach}} - \overline{X_{cg}}) \quad (78)$$

Where  $C_L(\overline{X_{cg}} - \overline{X_{acw}})$  was simply the coefficient of lift of 0.67 multiplied by the difference of the fractional lengths of the CG and the wing AC,  $(\overline{X_{cg}} - \overline{X_{acw}}) = -0.05$ . This gives the first term as -0.0335.

$C_{m_w}$  was determined by Equation (79) below (Raymer, 2012).

$$C_{m_w} = C_{m0_{airfoil}} \left( \frac{AR \cos^2(\Lambda)}{AR + 2 \cos(\Lambda)} \right) \quad (79)$$

Aerofoil data for NASA SC(2)-0714 was used to determine the  $C_{m0_{airfoil}}$ , which was given to be -0.14 at zero incidence (Airfoiltools.com, 2019). From which the following result was obtained, with  $AR = 9.54$  and  $\Lambda = 27^\circ$ .

$$C_{m_w} = -0.14 \left( \frac{9.54 * \cos^2(27)}{9.54 + 2 * \cos(27)} \right) = -0.0937$$

$C_{m_{w\delta f}}$  was determined by Equation (87) below (Raymer, 2012).

$$C_{m_{w\delta f}} = -\frac{\partial C_L}{\partial \delta_f} (\overline{X_{cp}} - \overline{X_{cg}}) \quad (80)$$

Where  $\frac{\partial C_L}{\partial \delta_f} = 3.5$  given by figure 16.6 (Raymer, 2012), using the ratio of the chord of flaps to the wing chord,  $\frac{c_f}{c} = 0.2$  and  $\frac{t}{c} = 0.14$ . The fractional distance  $(\overline{X_{cp}} - \overline{X_{cg}})$  was calculated to be 0.341. This gives the following result.

$$C_{m_{w\delta f}} = -3.5 * 0.341 = 1.19$$

$C_{m_{fus}}$  was determined by the following Equation (81) (Raymer, 2012).

$$C_{m_{fus}} = \frac{K_{fus} W_f^2 L_f}{c S_w} \quad (81)$$

Where  $K_{fus}$  was determined from figure 16.14 (Raymer, 2012) to be 0.03.  $W_f = 4.37$  the fuselage diameter,  $L_f = 45.8$  the length of the aircraft,  $c = 4.01$  and  $S_w = 136$ . This results in the following value.

$$C_{m_{fus}} = \frac{0.03 * 4.37^2 * 45.8}{4 * 136} = 0.0482$$

The final term,  $\eta_h \frac{S_h}{S_w} C_{L_h}(\overline{X_{ach}} - \overline{X_{cg}}) = 0$ , this was assumed for simplicity as the horizontal tail plane was a symmetrical aerofoil shape with a movable surface.

### 13.10 Yawing Moment Coefficient Calculation – PS

From Raymer (2012), the following Equation (82) was used determine the yawing moment coefficient.

$$C_n = C_{n\beta_w}\beta + C_{n\delta_a}\delta_a + C_{n\beta_{fus}}\beta + C_{n\beta_v}\beta - \frac{T\overline{Y_p}}{qS_w} - \frac{D\overline{Y_p}}{qS_w} \quad (82)$$

Where,

$$C_{n\beta_w} = C_L^2 \left\{ \frac{1}{4\pi AR} - \left[ \frac{\tan(\Lambda)}{\pi AR(AR + 4 * \cos(\Lambda))} \right] \left[ \cos(\Lambda) - \frac{AR}{2} - \frac{AR^2}{8\cos(\Lambda)} + \frac{6(\overline{X_{acw}} - \overline{X_{cg}})\sin(\Lambda)}{AR} \right] \right\}$$

Which gives  $C_{n\beta_w} = 0.0143$ .

$C_{n\delta_a}$  was calculated from Equation (83) below,

$$C_{n\delta_a} = -0.2C_L C_{l\delta_a} \quad (83)$$

Where,  $C_{l\delta_a} = \frac{2K_f \left( \frac{\partial C_L}{\partial \delta_f} \right) Y_i S_i \cos(\Lambda_h)}{S_w b}$ ,  $K_f$  can be found from figure 16.7 (Raymer, 2012) and  $\frac{\partial C_L}{\partial \delta_f}$  can be found from figure 16.6 (Raymer, 2012).  $Y_i = 14.5$ ,  $S_i = 3$ ,  $\Lambda_h = 20^\circ$  and  $b = 36$  were the values used to produce  $C_{l\delta_a} = 0.0614$  and hence  $C_{n\delta_a} = -0.00823$ .

$C_{n\beta_{fus}}$  was determined from Equation (84) below.

$$C_{n\beta_{fus}} = -1.3 \frac{\text{fuselage volume}}{S_w b} \left( \frac{D_f}{W_f} \right) \quad (84)$$

Where  $\frac{D_f}{W_f}$  is the ratio of the depth of the fuselage (length) to the width. This gives the following value.

$$C_{n\beta_{fus}} = -0.183$$

$C_{n\beta_v}$  was calculated using Equation (85).

$$C_{n\beta_v} = C_{F\beta_v} \frac{\partial \beta_v}{\partial \beta} \eta_v \frac{S_v}{S_w} (\bar{X}_{acv} - \bar{X}_{cg}) \quad (85)$$

Where,  $\frac{\partial \beta_v}{\partial \beta} \eta_v = 0.724 + \frac{3.06 \frac{S_{vs}}{S_w}}{1 + \cos(\Lambda)} - 0.4 \frac{Z_{wf}}{D_f} + 0.009 AR = 1.07$ . This gives the following result assuming  $C_{F\beta_v} = 0.288$ .

$$C_{n\beta_v} = 0.978$$

As D=T was assumed,  $-\frac{T\bar{Y}_p}{qS_w} - \frac{D\bar{Y}_p}{qS_w} = 2 * \frac{T\bar{Y}_p}{qS_w}$

$$\frac{T\bar{Y}_p}{qS_w} = \frac{137 * 1.44}{31.3 * 136} = 0.0464$$

### 13.11 Rolling Moment Calculation – PS

Hand calculation of the rolling moment due to ailerons (without flaps):

ESDU 88013 document was used to provide the equations and information required to complete this analysis. Equation (86) below gave the rolling moment equation used.

$$L'_\xi = L_\xi \cos(\Lambda_h) \quad (86)$$

Where  $\Lambda_h$  is the hinge sweep angle, and  $L_\xi$  is given by Equation (87) below.

$$L_\xi = -0.5 \bar{\eta} \left( \frac{\partial C_L}{\partial \delta} \right) (\Phi_{\xi_i} - \Phi_{\xi_o}) \quad (87)$$

Where  $\bar{\eta} = 0.5(\bar{\eta}_i + \bar{\eta}_o) = 0.5(0.62 + 0.94) = 0.78$  is the ratio of the distance to the mid-span of the aileron to the span of the wing, the part span contribution  $(\Phi_{\xi_i} - \Phi_{\xi_o})$  can be found using  $K1 - k2$ .

$K1$  and  $k2$  can be found in figures 4c and 5 with the inboard and outboard,  $\bar{\eta}_i$  and  $\bar{\eta}_o$ , respectively and using  $AR \tan\left(\frac{\Lambda_1}{2}\right) - 8\lambda = 1.23$ .

This resulted in  $\Phi_{\xi_i} = K1(\text{inboard}) - k2(\text{inboard}) = 0.27 - 0.08 = 0.19$  and  $\Phi_{\xi_o} = K1(\text{outboard}) - k2(\text{outboard}) = 0.075 - 0.018 = 0.057$ .

To determine  $\frac{\partial C_L}{\partial \delta}$  the Equation (88) below was used.

$$\frac{\partial C_L}{\partial \delta} = \left[ \frac{\frac{\partial C_L}{\partial \delta}}{\frac{\partial C_L}{\partial \alpha}} \right] \frac{\partial C_L}{\partial \alpha} (1 - k_1 k_2) \quad (88)$$

From figure 1 in the ESDU document,  $\left[ \frac{\frac{\partial C_L}{\partial \delta}}{\frac{\partial C_L}{\partial \alpha}} \right]$  was determined to be 0.68. From figure 2 of the same document,  $k_1 = 0.22, k_2 = 0.36$  were determined using  $\left( \frac{t}{c} \right) \sec \Lambda_{\frac{1}{2}} = 0.154$ .

Substituting into the equation above, gives

$$\frac{\partial C_L}{\partial \delta} = 0.68 * 5.96 (1 - (0.22 * 0.36)) = 3.758$$

From which the rolling moment can be calculated.

$$L_\xi = -0.5 \bar{\eta} \left( \frac{\partial C_L}{\partial \delta} \right) (\Phi_{\xi_i} - \Phi_{\xi_o}) = -0.5 * 0.78 * 3.758 * (0.19 - 0.057) = -0.195$$

$$L'_\xi = L_\xi \cos(\Lambda_h) = -0.195 \cos(20) = -0.182 \text{ rad}^{-1}$$

### 13.12 Roll Contribution of Spoilers – PS

Hand calculation of roll contribution of spoilers:

ESDU 14005 was used to evaluate the sizing to the spoilers to ensure it provides stability in roll.

Equation (89) below was used to calculate the roll moment coefficient.

$$(C_{ls})_{ss} = \psi_{ps} (C_{ls})_{ss} \quad (89)$$

Where  $(C_{ls})_{ss}$  is given by Equation (90) below and  $\psi_{ps}$  is given by the inboard and outboard  $\eta$  values.

Given  $\bar{\eta}_i = 0.127$  and  $\bar{\eta}_o = 0.44$ ,  $\psi_i = 0.06$  and  $\psi_o = 0.4$  can be determined from figure 5a in the ESDU document. This give the part-span values as  $\psi_{ps} = 0.4 - 0.06 = 0.34$ .

$$(C_{ls})_{ss} = \frac{\Delta C_{lsF}}{4} k_a \bar{\eta}_{plan} \quad (90)$$

Table 6.2 in the ESDU document gives  $\Delta C_{lsF} = -0.783$  at  $50^\circ$ , and figure 3 gives  $k_a = 0.94$ .

To get  $\bar{\eta}_{plan}$  from figure 6d,  $AR \sqrt{1 - M^2 \cos^2(\Lambda_{\frac{1}{4}})}$  was calculated to be 7.02. This gave  $\bar{\eta}_{plan} = 0.439$ .

These values were substituted into Equation (91) above to give,

$$(C_{ls})_{ss} = \frac{\Delta C_{lsF}}{4} k_a \bar{\eta}_{plan} = \frac{-0.783}{4} * 0.94 * 0.439 = -0.0808 \quad (91)$$

Hence providing the rolling moment as,

$$(C_{ls})_{ss} = \psi_{ps} (C_{ls})_{ss} = 0.34 * -0.0808 = -0.275$$

### 13.13 Rolling Moment Coefficient Calculation – PS

The rolling moment coefficient Equation (92) below was given by Raymer (2012).

$$C_l = C_{l\beta_w} + C_{l\delta_a} \delta a + C_{l\beta_v} \beta \quad (92)$$

Where,

$$C_{l\beta_w} = \left( \frac{C_{l\beta_{wing}}}{C_L} \right) C_L + (C_{l\beta})_\Gamma + C_{l\beta_{wf}}$$

and,

$$C_{l\beta_v} = -C_{F\beta_v} \frac{\partial \beta_v}{\partial \beta} \eta_v \frac{S_v}{S_w} \bar{Z}_v$$

$\frac{C_{l\beta_{wing}}}{C_L} = -0.18$  was determined from figure 16.21 (Raymer, 2012).

Where,

$$(C_{l\beta})_\Gamma = -\frac{C_{L\alpha}\Gamma}{4} \left[ \frac{2(1+2\lambda)}{3(1+\lambda)} \right] = -0.0128 \text{ for a dihedral angle, } \Gamma \text{ of } 5.11^\circ, \lambda = 0.4 \text{ and } C_{L\alpha} = 0.67.$$

And,

$$C_{l\beta_{WF}} = -1.2 \frac{\sqrt{AR} Z_{WF}(D_f + W_f)}{b^2} = -0.286.$$

From these values,  $C_{l\beta_w} = -0.420$  was calculated.

$C_{l\beta_v}$  was calculated using  $C_{F\beta_v} \frac{\partial \beta_v}{\partial \beta} \eta_v \frac{S_v}{S_w}$  values and  $C_{l\delta_a}$  term have been calculated previously in Appendix 13.10, which gave  $C_{l\beta_v} = -0.0249$ .

Substituting into Equation (92), gives  $C_l = -0.427$

### 13.14 Updated Risk Matrix – YA

Table 72 - Updated Risk Matrix

| -               | Negligible 1 | Minor 2               | Moderate 3                            | Significant 4           | Severe 5  |
|-----------------|--------------|-----------------------|---------------------------------------|-------------------------|---|
| Very Likely 5   | -            | -                     |                                       |                         |   |
| Likely 4        | -            | -                     | -                                     | -                       |   |
| Possible 3      | -            | -Turbulence and Drops | -Battery Disposal<br>-Hazardous Fluid | -                       | -   |
| Unlikely 2      | -            | -                     | -                                     | -FOD<br>-Engine Failure | -Accuracy of Installation<br>-Structural Failure<br>-Aircraft Systems Failure |
| Very Unlikely 1 | -            | -                     | -                                     |                         | -Human Safety   |

### 13.15 Team Member Contributions – All

Table 73 - Team Member Contributions

| Team Member        | Contributions                               |
|--------------------|---|
| Youssef Abouelmagd | Aircraft Systems                            |
|                    | Navigation System Fault Tree Analysis       |
|                    | Risk Management                             |
| Barney Green       | Prandtl-Glauert Theory                      |
|                    | Hinge Moment Calculation and Actuator Loads |

|                    |  |
|--------------------|--|
|                    | Drag at Take-Off and Minimum Drag Speed                |
|                    | Rate of Climb  |
|                    | Minimum Control Speed                                  |
|                    | Landing Calculations and Tail Scrape Angle Calculation |
|                    | Configuration Management                               |
|                    | Change Request Process                                 |
|                    | WBS and Activity List                                  |
|                    | Schedule   |
|                    | Action List  |
|                    | Conclusion   |
|                    | Editing, Compiling and Formatting                      |
|                    | Proof Reading  |
| Salman Habib       | Introduction   |
|                    | Requirements and Verification                          |
|                    | Powerplant Selection                                   |
|                    | Static and Gust Load Case                              |
|                    | Spar Sizing  |
|                    | Rib Boom Idealisation                                  |
|                    | Mass Fraction Iterations                               |
|                    | Aircraft Flight Envelope                               |
|                    | Aircraft CG  |
|                    | Proof Reading  |
| Megan Keeping      | Aircraft Systems                                       |
|                    | Electrical System Fault Tree Analysis                  |
|                    | Electrical Systems Architecture                        |
|                    | WBS and Activity List                                  |
|                    | Schedule   |
| Tak Li             | Wing CAD   |
|                    | Cabin Seat CAD   |
|                    | Pilot and Attendant Seat CAD                           |
|                    | CAD Assembly   |
|                    | Interface List   |
| Luca Moscattini    | Requirements and Verification                          |
|                    | Fuselage Structural Analysis                           |
|                    | Stringer Design and Lay Up                             |
|                    | Buckling Analysis                                      |
| Aanantha Murugavel | Nacelle CAD  |

|               |  |
|---------------|--|
|               | Engine Mounting                        |
|               | Wing Box                               |
|               | Wing Fuel Tanks                        |
| Kusha Oza     | Fuselage CAD                           |
|               | Nose CAD                               |
|               | CAD Assembly                           |
|               | Empennage CAD                          |
|               | Stringer and Frame CAD                 |
|               | Aircraft Maintenance and Manufacture   |
|               | Wing Fuselage Interface                |
|               | Business Case                          |
|               | Executive Summary                      |
|               | DOC                                    |
|               | Proof Reading                          |
| Preeti Singh  | Control Surface Sizing                 |
|               | Aircraft Stability                     |
|               | Vertical and Horizontal Tail Plane CAD |
|               | Frame Analysis                         |
|               | Minimum Control Speed                  |
|               | Business Case                          |
|               | DOC                                    |
|               | Proof Reading                          |
| Andre Sunaryo | Wing Structure                         |
|               | Stringer Boom Idealisation             |
|               | Risk Management                        |
| Tomas Webster | DOC                                    |

### 13.16 Rendered CAD Images



Figure 64 - "Soar to the Sky"



Figure 65 - "Beyond the Clouds"



Figure 66 - "Over the City"